THE ROLE OF CLUSTERS IN GAS-SOLIDS REACTORS

AN EXPERIMENTAL STUDY

R.H. Venderbosch

THE ROLE OF CLUSTERS IN GAS-SOLIDS REACTORS

AN EXPERIMENTAL STUDY

PROEFSCHRIFT

ter verkrijging van de graad van doctor
aan de Universiteit Twente, op gezag van
de rector magnificus, prof. dr. F.A. van Vught
volgens besluit van het College voor Promoties
in het openbaar te verdedigen op
donderdag 19 februari 1998
te 16.45 uur.

door
Robertus Hendrikus Venderbosch
geboren op 1 augustus 1966
te Utrecht

Dit proefschrift is goedgekeurd door de promotor

prof. dr. ir. W.P.M. van Swaaij

en de assistent-promotor

dr. ir. W. Prins

THE ROLE OF CLUSTERS IN GAS-SOLIDS REACTORS

AN EXPERIMENTAL STUDY

R.H. Venderbosch

Referent: dr. ir. J.H.A. Kiel

The research in this thesis was financially supported by the Dutch Ministry of Economic Affairs through the Netherlands Energy Research Foundation ECN.

Venderbosch, R.H.

The role of clusters in gas-solids reactors: an experimental study

Thesis Twente University

ISBN 9036510945

Printed by Print Partners Ipskamp, Enschede, The Netherlands

CONTENTS

GENERAL INTRODUCTION

Background

The production of electricity in Integrated Gasification Combined Cycle (IGCC) power plants has been the subject of considerable research over the past decades throughout the whole world. Since 1994 a IGCC demonstration plant of 250 MW(el) is operated at Buggenum, the Netherlands. Due to environmental legislation and the specifications of the process equipment (for example the gas turbine), it is necessary to reduce dust and gaseous pollutants (amongst which H_2S and COS) down to very low concentration levels. A system study, initiated by the Netherlands Agency for Energy and the Environment (NOVEM) concluded that the application of a dry gas cleaning process at a high temperature level (> 623 K) improves the overall efficiency of the IGCC plant significantly, if compared to an installation with conventional wet gas cleaning. One of the major process steps involved in dry gas cleaning is the high temperature (> 625 K) and high pressure (> 20 bar) desulfurization, that is the removal of H_2S and COS from the hot coal gas.

Pioneering work on high-temperature desulfurization was mainly concerned with sorbent development and characterization (reactivity, capacity, regenerability, and possible deactivation) in small cyclic (isothermic) operated packed bed reactors. Usually, in these reactors relatively large particles (> 1 mm) are applied, at higher conversion rates giving rise to the presence of diffusional resistances inside the particle. The desulfurization rate on iron-oxide based sorbents is shown to be very high, especially when fresh sorbent particles are used (Van der Ham *et al.*, 1994), and consequently small particles (< 200 μm) are preferred. Nowadays the research interest has shifted from sorbent development towards the development of continuous processes. A high temperature desulfurization process, considered by the Energy Research Foundation (ECN) in Petten, the Netherlands, includes the use of a very promising, newly developed sorbent. It is based on mixture of iron-oxide and molybdenum oxide on amorphous aluminium phosphate carrier material, with an average diameter of 169 μm. Fluidized bed type reactors are preferred as possible large-scale reactors in a continuous process, because an easy transport of solid material between reactor and regenerator is possible.
Bubbling fluid bed technology is well known and widespread through industry. The solids mixing in these reactors is very good, and bed-to-wall heat transfer rates are high, which is especially attractive when large heat effects are involved. A major drawback of a bubbling fluid bed, however, is the possible by-passing of reactant gas through rising bubbles. Although little pertinent conversion data are available, the general idea in the literature is that severe gas by-passing can be avoided in high-velocity fluid beds (the turbulent fluid bed, the fast fluid bed or pneumatic conveying; Van Deemter, 1980). At the same time, the reactor diameter is reduced for the same gas through-put, which is attractive for high-pressure application.

The efficiency of gas-solids contacting in a chemical reactor is especially important when a high degree of conversion is required. Non-idealities at the scale of the reactor, like dispersion or back-mixing of reactant gas, and by-passing of the solids through channels or bubbles, may reduce the overall conversion significantly. At the same time, the contact efficiency becomes a crucial factor in case of a high local reaction rate, when the effects of internal and external diffusion limitations are emerging.
The high temperature desulfurization of coal gas over solid sorbent particles is a typical example of a process for which a conversion close to one is required, because no slip of H_2S is allowed. Moreover, the rate of the desulfurization reaction is extremely high for the iron-

oxide based particles to be used.

Considering the requirements of the high-temperature desulfurization system (high H_2S removal degree, rapid reaction, continuous operation, necessary sorbent regeneration, high gas flow rates, high pressure) a reactor system based on high-velocity fluidization of fine sorbent particles (Geldart's type A) seems to be attractive. For instance a combination of a riser for adsorption and a turbulent fluid bed for regeneration, just like in the Fluid Catalyst Cracking (FCC) installations of the petroleum industry, may be possible.

Scope of this work

Little is known about the scaling up of high-velocity fluidized bed reactors for rapid reaction and high conversion. Besides, conversion data for such reactors are scarcely available in the literature and difficult to interpret in terms of contacting efficiency. Because of the current interest in electricity generation by high efficiency gasification of sulfur containing coal, ECN in Petten is considering the construction of a pilot plant facility for continuous desulfurization of coal gas. The results of conversion measurements in such a facility should then be interpreted in a proper way to allow their utilization in subsequent scale-up considerations and procedures. This problem was addressed by initiating a Ph.D. research project at the University of Twente, meant to investigate the contacting efficiency in several gas-solids reactors at a laboratory scale. A key issue was to find a representative model reaction which is applicable at elevated temperatures and can be used to determine the contacting pattern in a reliable way. If such a model reaction can also be used to establish the contacting efficiency in large scale installations under practical conditions, it should be possible to predict the conversion performance on basis of the intrinsic reaction kinetics measured in an ideal reactor.

The results of the lab-scale work are presented in this thesis. It has been observed in our work that for the extremely high reaction rates considered (especially in case of desulfurization with *fresh* sorbent material), the contact pattern in all reactor types examined is far from ideal. Part of the reactant gas appears to pass along the solids without any contact and reaction, because the fine particles considered tend to form agglomerates due to hydrodynamical factors and intra-particle forces. By applying the selected model reaction, these agglomerates have been demonstrated to exist even for the small laboratory reactors used in this work. This model reaction, viz. the oxidation of carbon monoxide over a platinum catalyst, shows an extremely large change in reaction order upon shifting from reaction-kinetics to mass transfer controlled conditions, and provides a strong tool in the interpretation of conversion measurements. CO conversion measurements have been carried out in a small packed bed, in a bed fluidized at velocities up to and beyond the transition to the turbulent regime, and in a riser reactor. Also on basis of the related hydrodynamics, it could be shown that the formation of agglomerates is an important phenomenon for all these reactors. Even in the packed bed, intra-particle forces and channel formation due to small variations in the bed porosity, are a cause of particle clustering for the fine particles of this study (small values of the Reynolds number; see also Schlünder, 1977)

Before presenting any results and the outline of this thesis into more detail, it may first be useful to clarify the term 'contact efficiency', defined to characterize the non-ideal contact pattern.

Definition of contact efficiency

Various peculiar phenomena are reported in the literature for gas solids reactors in which

small particles are processed. These phenomena include commonly accepted observations like:

- the surprisingly low values of Sh and Nu numbers for mass and heat transfer observed for all gas-solids reactor types (d_p<200 μm or Re<1, see Van der Ham *et al.*, 1994),
- the existence, apart from the bubbling bed, of a homogeneous and a turbulent fluidization regime for Geldart's type A particles,
- the relatively low values of the Bo numbers for axial dispersion in packed beds of small particles (d_p<500 μm; Moulijn and Van Swaaij, 1976),
- packed bed conversion rates which are sometimes lower than observed for a bubbling bed at similar conditions (Geldart type A particles; Hermann, 1991),
- a significantly reduced gas-to-solids momentum transfer rate in fast fluidized beds and riser reactors, resulting in an increased solids hold-up and slip velocities much higher than the terminal falling velocity of the individual particles.

All these phenomena can be understood in terms of non-ideality of the gas-solids distribution structure and the related contacting. For risers, for instance, it is nowadays generally accepted that the reduced momentum transfer rate is caused by the fact that the particles are not transported as individual particles, but enclosed in particle agglomerates.

In case of a chemical reaction, the imperfect contact between the gas and solids can also be noticed from a reduced conversion in comparison to what is expected for ideal contacting. The non-ideality of the gas-solids contacting is then reflected by the value of the contact efficiency parameter η, which (for a first order reaction) is defined by:

$$\eta = \frac{k_{ov}}{k_p \eta_p} = \frac{\text{apparent conversion rate constant}}{\text{theoretical maximum conversion rate constant}} \qquad (1)$$

In this definition, the conversion rate constants are based on the volume of active solid material. In fact, the contact efficiency η indicates the effects of other conversion-rate controlling resistances than those inside or around the single particle. The extreme values of the theoretical maximum conversion rate constant are given by the (known) intrinsic reaction kinetics (η_p=1) on the one hand, and by the diffusion rate through the boundary layer around the solid particle on the other ($k_p\eta_p=k_g a$, with a representing the specific surface area of the particle, and η_p being the particle effectiveness factor).

Experimental evidence for clusters in a riser reactor

Apart from any hydrodynamic evidence (chapter 3), the existence of particle clusters in a fast fluid bed or a riser reactor, can also be demonstrated by conversion experiments. Two additional mass transfer resistances are created by the presence of clusters. One is related to the transfer of reactant from the main gas bulk to the cluster surface, and the other to the transport by diffusion inside such a cluster. Figure 1 (taken from chapter 4) illustrates the situation that conversion rates are dominated by the gas-to-cluster mass transfer, and subsequent diffusion through the cluster in parallel with a) single particle reaction controlled by the catalyst reactivity or b) single particle reaction controlled by particle boundary layer diffusion.

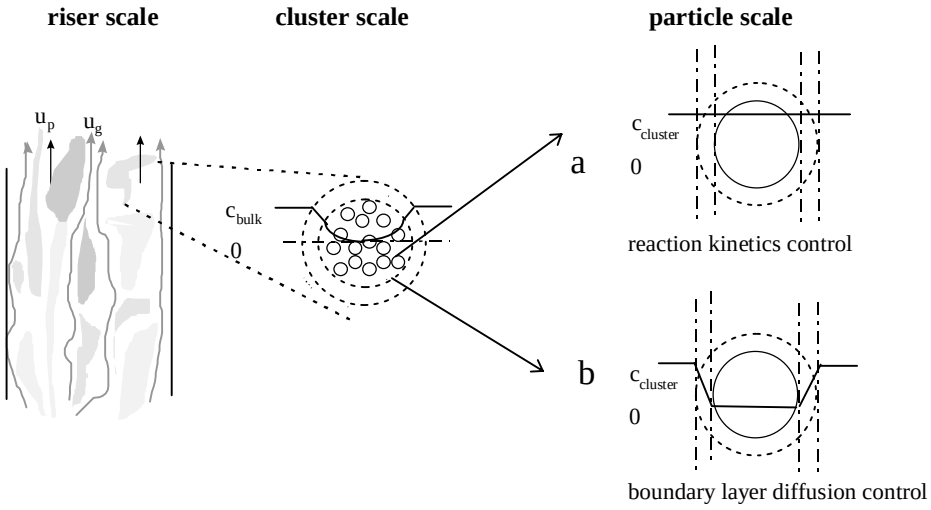

Figure 1. Possible local concentration profiles due to cluster formation for (a) particle reaction controlled by the intrinsic reaction kinetics, and (b) particle reaction controlled by boundary layer diffusion.

From CO conversion measurements, carried out in a small riser reactor for mass transfer controlled conditions and a diluted catalyst system, apparent Sh^0 numbers can be derived from the apparent reaction rate constant evaluated with a plug flow model for a first order reaction. In figure 2, this Sh^0 number is plotted as a function of the solids hold-up for a superficial gas velocity of 2.5 m/s, and a dilution ratio of n_d=2500. At low solids concentrations, Sh^0 approaches the value predicted by the Ranz and Marshall (1952) equation for ideal contacting, which is plotted as a closed symbol on the y-axis. Obviously, the maximum conversion rate constant obtained at low solids hold-ups in this riser set-up is determined by the external mass transfer resistance located in the boundary layer around the individual particle. However, for higher solid hold-ups, the observed Sherwood numbers decrease significantly, approaching a more or less constant value, which is a factor 4 to 10 lower than the ones predicted for ideal contacting. In chapter 4 it has been explained that this decrease can not be attributed to an increasing effect of possible axial dispersion of the gas at the higher conversion degrees. More probably, the decrease in Sh^0 with a factor 4 to 10 is caused by shielding of the active particles, as a consequence of cluster formation.

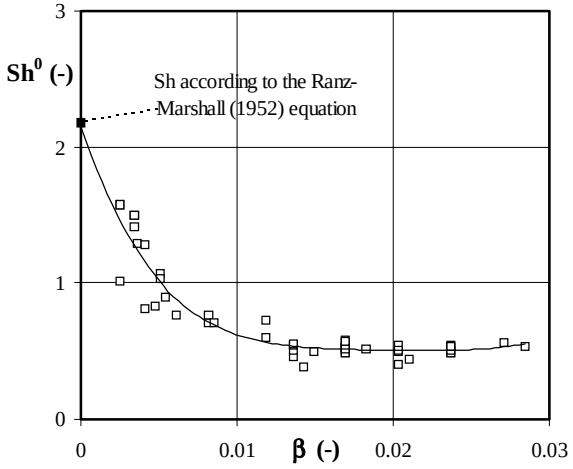

Figure 2. Apparent Sherwood number as a function of the solids hold-up. Results of mass transfer controlled CO oxidation experiments in a riser reactor (see chapter 4) at T=775 K, u_g=2.5 m/s, τ=0.3 s, $0.5< k_p\beta/(1+n_d) <5\ s^{-1}$, and n_d=2500. The solid line only indicates the trend. A closed symbol on top of the y-axis represents the Sh value derived from the Ranz and Marshall (1952) equation for ideal gas-solids contacting.

Possible causes of contact efficiency loss in packed beds

The interpretation of conversion data in terms of gas-solids contacting efficiency (equation 1) is not always straightforward. This can be illustrated nicely by comparing the results of two simple conversion calculations for a first order reaction in a packed bed of very fine particles. In the first case it is supposed that these particles are compacted to relatively large, spherical pellets of a certain diameter d, to be contacted by a gas in plug flow. These pellets can then be considered to represent particle agglomerates or clusters; they are supposed to be ideally contacted by the gas, by which the contact efficiency of the packed bed reactor becomes equal to the pellet's effectiveness factor: $\eta=\eta_p$.
In the second case it is assumed that all the fine particle themselves are perfectly contacted by the gas, while complete mixing of the reactant gas is now supposed to cause the apparent loss in contact efficiency.

The first calculation is based on solution of the mass balance over the volume of a pellet, in which reaction and diffusion take place in parallel. If boundary layer diffusion is neglected, an expression can be obtained for the pellet's effectiveness factor as a function of the Thiele modulus ϕ.

$$\eta = \frac{1}{3\phi^2}\left(\frac{3\phi_p - \tanh(3\phi)}{\tanh(3\phi)}\right) \qquad (2)$$

In this equation $\phi=(d/6)\sqrt{(k_r/(\beta D))}$, with k_r representing the reaction rate based on the reactor volume, β the average solids concentration in the reactor, d the pellet diameter, and D the effective diffusion coefficient inside the pellet. The conversion efficiency is plotted in figure 3 (solid line) as a function of the reaction number $N_r=k_rH/u_g$ for the conditions mentioned in the legends. It can now be considered also to represent the (pellet-bed) contact efficiency versus the non-dimensional reactivity.

The second calculation appears to yield a very similar result. The dashed curve in figure 3 represents the extreme case of an ideally stirred gas phase, and perfect contact between the gas and all the fine particles constituting the pellets of the previous calculation. In this case the apparent loss in contact efficiency can be derived as:

$$\eta = -\frac{1}{N_r}\ln\left(\frac{1}{1+N_r}\right) \qquad (3)$$

In figure 3, also the contact efficiency η derived from equation 3, is plotted versus N_r.

The objective of the comparison made in figure 3 is merely to show that it is difficult to distinguish whether diffusion through agglomerates or gas mixing is the main reason for any loss of contact efficiency observed in conversion experiments. For all values of the reaction number N_r, there is a strong similarity between the two curves. It should be noticed however that, although a certain degree of axial dispersion in the packed bed is possible, the assumption of ideal mixing of reactant is quite unrealistic.

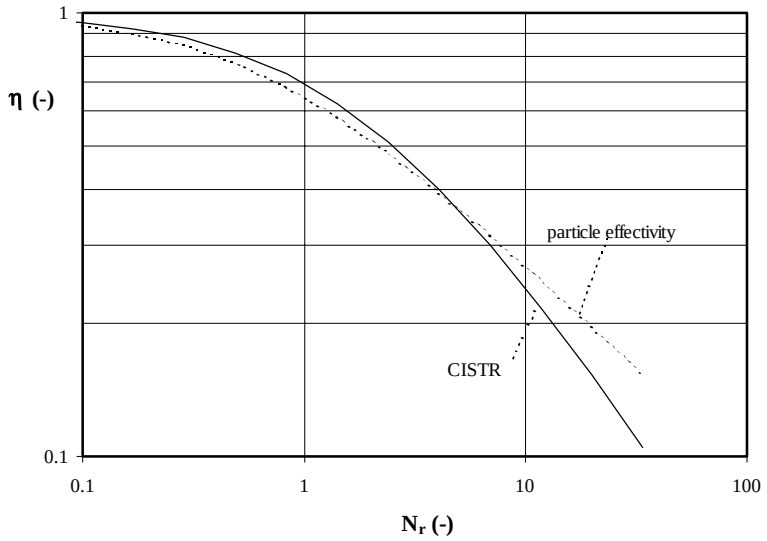

Figure 3. Apparent contact-efficiency η as a function of the non-dimensional reactivity, for a first order reaction in a packed bed of fine particles. Two different situations are considered. The first one assumes plug flow for the gas and efficiency loss due to internal diffusion limitation inside agglomerates of fine particles (dashed curve, equation 2). In the second situation the efficiency loss is caused by the assumed ideal mixing of reactant gas (solid curve, equation 3) which is supposed to be in perfect contact with all the fine particles (no agglomerates). Conditions: d=700 μm, $D=3\cdot10^{-5}$ m^2/s, $H/u_g=10^{-3}$ s and β=0.4.

Experimental evidence for clusters in a packed bed reactor

Just like for the riser reactor (figure 2), the presence of clusters could also be demonstrated for a small packed bed reactor on basis of CO oxidation experiments. Hereafter, the important role of cluster formation will be illustrated by comparing the experimental conversion data with predictions from reactor equations in a plot of the non-dimensional outlet concentration against the superficial gas velocity (figure 4).
In first instance the two curves for a first order reaction, perfect contact between gas and solids, and either plug flow or ideal mixing for the gas, have been drawn in the figure. Two additional curves (dashed lines) have been added to the diagram of figure 4. The first one has been constructed for the plug flow model with axial dispersion for a Péclet number that can be calculated from Wen and Fan's (1975) empirical equation:

$$\text{Pé} = \left(\frac{0.5}{1 + \frac{3.8}{\text{Re}_p \, \text{Sc}}} + \frac{0.3}{\text{Re}_p \, \text{Sc}} \right)^{-1} \frac{H}{d_p} \qquad (4)$$

and the other one is derived on basis of a constant Péclet number reported by Moulijn and Van Swaaij (1976) for a bed of small particles (d_p=100 μm; Pé=7).

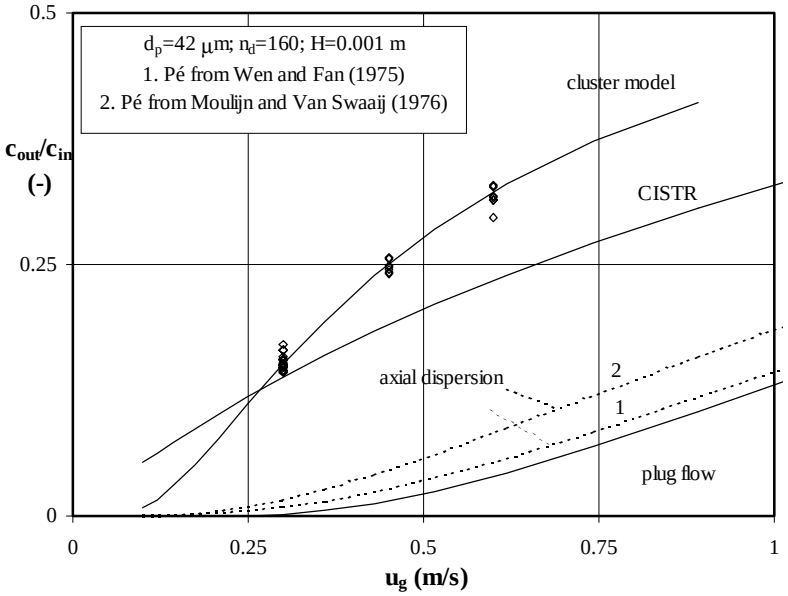

Figure 4. The experimentally observed non-dimensional outlet concentration c_{out}/c_{in} versus u_g for CO oxidation experiments in the packed bed (chapter 2; d_p=42 μm, $k_p\beta/(1+n_d)$=2000 s^{-1}, and $1<H/u_g<3$ ms. Indicated as solid lines are the curves for ideal contacting and plug flow behaviour of the gas, and ideal contacting plus ideal mixing of the gas. The dashed lines are obtained from a plug flow plus axial dispersion model (with Péclet numbers derived from Wen and Fan (1975, curve 1) and a Péclet number reported by Moulijn and Van Swaaij (1976 curve 2)). The fifth curve with data points has been calculated with the cluster model of appendix II.

The experimental CO conversion data are indicated in the figure as symbols. Apparently, none of the ideal contacting curves in figure 4 predicts the experimentally determined outlet concentrations very well; they are even higher than for the extreme case of perfect contacting and ideal mixing of the gas phase. The observed high values of c_{out}/c_{in} clearly indicate that other mass transfer resistances are causing a reduced contact efficiency, and it is postulated here that these additional resistances are closely associated with the occurrence of particle agglomerates or clusters.

As mentioned before, the existence of particle clusters are ascribed to a (local) non-uniform distribution of solids and voids in the bed, in the range of low Reynolds number causing large variations in the local superficial gas velocity over the bed volume (see also Martin, 1980). The consequences of agglomerates have now been illustrated for a packed bed of fine particles and a first order chemical reaction. In figure 4, an additional curve is presented, which is constructed on basis of the cluster model, developed in this study and described in appendix II. Apparently, this curve predicts the measured outlet concentrations quite accurately. The effective size of the cluster, as represented by the diameter ratio d_{cl}/d_p, depends on the applied superficial gas velocity. For the particles used in this work, this diameter ratio ranges from 18 down to 10 as u_g varies from 0.3 to 0.6 m/s (chapter 2).

For the small particles (Geldart's type A) and the high volumetric conversion rates applied in this work, the occurrence of particle clusters in gas-solids reactors are shown to be the main cause of a reduced contact efficiency, a conclusion which is supported by re-evaluation of various literature publications. These clusters are created by the combination of hydrodynamic factors and inter-particle forces. Their size is determined by particle properties, operating parameters and reactor geometry, and appears to be crucial in understanding the gas-solids contacting behaviour. As an important conclusion of this thesis, the contact-efficiency parameter η, as defined by equation 1, is shown to be strongly dependent on the local reaction rate. The latter fact is not always recognized in the

literature. The main reason is that inside agglomerates of particles, the conversion occurs then parallel rather than purely in series with mass transfer

At present, the agglomerates is risers can only be demonstrated to exist and their dimension and flow structures cannot yet be calculated on the forehand. With the advance of CFD modelling, clusters with their associated flow fields may be accessible for CFD calculations. Recently, Hoomans *et al.* (1998) calculated clusters by CFD modelling for risers, applying a mixed Langrangian / Eulerian calculation scheme. Before these type of calculations can be used for development and design, their is still a long way to go. The same holds for the clusters in packed bed of small particles, where possibly also particle-particle forces have to be taken into account to understand the complex geometrical structure.

Outline of this thesis

As stated before, in the present thesis, clusters are suggested to be a major cause for the contacting loss in gas-solids contactors of fine particles. This will be verified by applying a non linear fast reaction system, which allows evaluation of the type of contacting pattern that occurs in gas-solids reactors. The thesis consists of four main parts. First, a part where a model reaction is introduced and tested, a second in which the conversion experiments conducted in the packed bed regime are discussed, a third in which hydrodynamic and conversion results are presented for the riser regime, and finally a part that is dedicated to high velocity fluid beds such as the turbulent fluid bed. The emphasis is put on experimental tests. Related theory models are included in a number of separate appendices.

The CO oxidation reaction over a platinum catalyst, to be used as a gas-solids contacting test reactor is discussed in detail in **chapter 1**. The reason for the application of this stable and very rapid reaction is that it shows some additional advantages over other model reactions (like the absence of side reactions). Besides, it provides an extra indicator for distinguishing between reaction-kinetics and mass transfer controlled reaction, viz. by a changing value of the observed effective reaction order in CO. The derived intrinsic reaction rate equation is evaluated for much higher temperatures in **appendix I**.

The conversion in a small scale packed bed reactor for different reaction regimes is reported in **chapter 2** for three average particles sizes varying from d_p=42 to 75 μm. From these experiments, mass transfer numbers are derived and interpreted by accounting for the shielding of active particles (particle clustering). Solids dilution is used to suppress the effect of particle clustering, which is shown to be an important cause for the low contact efficiency in packed beds of all-active particles. A quantitative approach is based on the cluster model, outlined in **Appendix II**. Depending on the applied particle size and gas velocity, the effective cluster size varied from 7 to 18 times the particle diameter, values which are comparable with those reported in, or re-evaluated from the literature.

The presence of particle cluster in risers is generally accepted in the literature. Nevertheless, this type of reactor is often stated to offer excellent contacting between the gas and the solids. Clusters in riser can be recognized by investigating the hydrodynamics (f.i. by determining the solids concentrations and slip velocities), as well as by performing conversion experiments. First, in **chapter 3** the flow properties of various powder types (Geldart's classification AC to BA) in a small scale riser set-up (ID 13 mm) at ambient conditions are presented. Especially for A-powders, cluster formation is shown to be an important phenomenon in explaining the high solids concentrations in the riser. Indirect evidence for clusters is moreover obtained by showing that a small fraction of relatively heavy tracer material was transported at the same velocity as the bed material.

Then, conversion experiments were carried out in the riser. For **chapter 4**, the CO oxidation reaction over the platinum catalyst at mass transfer controlled conditions was applied to study the effect of the local catalyst activity (varied by dilution with inert solids) on the conversion rate in the so-called developed region of the riser. The local reactivity appeared to be an important parameter, because the conversion rate per unit catalyst volume decreases significantly as a consequence of local depletion of reactant. In **Appendix III** the results of the hydrodynamics of chapter 3, and the conversion results of chapter 4, are interpreted. By applying the earlier discussed cluster model, values could be derived for the apparent cluster size and its density. It appeared that the derived cluster diameter d_{cl} (varying from 30 to 70 times the particle diameter) does not depend very much on the average solids concentration β in the riser. The cluster becomes denser ($0.05<\beta_{cl}<0.5$) when the riser solids concentration is increased. Re-interpreted results from other investigators showed similar effects, and also that effective cluster sizes are larger in larger riser set-ups.

The high velocity fluid bed (a.o. the turbulent fluid bed) is supposed to offer unique properties for gas-solids reactions. Most of these advantages are directly related to the use of small particles, but also to the increased solids hold-up in the freeboard of the reactor. The ECN in Petten identified the high-velocity fluid beds (for example the turbulent bed) as promising reactor for the desulfurization of the coal gas, and especially for the regeneration (oxidation) of the sulfided material. Because little information is available on the gas-solids contacting of high velocity fluid beds, even not on a small scale as used in bench-scale or small pilot plant, we extended our experiments also to this regime.
Prior to the presentation of the desulfurization results, carried out close to the turbulent fluid bed regime, **chapter 5** discusses the characterization of the various fluidization regimes, and the determination of the axial porosity profile for various particles in relation to the superficial gas velocity.
Then, the CO oxidation was conducted near and in the turbulent bed regime and results are reported in **chapter 6**. In this chapter, additional data for mass transfer in the turbulent fluid bed regime, and the effects of dilution of the active material, will be presented. The conversion data will be interpreted in terms of the apparent mass transfer number, the contact efficiency, the two-phase model and the cluster model.

The results of the desulfurization of coal gas using the new sorbent material in the turbulent fluid bed regime are summarized in **chapter 7**. First, the sorbent material is investigated in terms of stability, regenerability and reactivity over more than 40 cycles. Then, the desulfurization efficiencies at the early stage of the break-through curve results are interpreted in terms of the apparent mass transfer number, the conventional two-phase model, the contact efficiency and the cluster model.

NOTATION

d	pellet diameter	m
d_p	particle diameter	m
D	molecular diffusion coefficient	$m^2 s^{-1}$
H	Height of the bed	m
k_{ov}	apparent reaction rate	s^{-1}
k_p	intrinsic reaction rate constant on catalyst volume	s^{-1}
k_r	reaction rate constant based on reactor volume	s^{-1}
n_d	dilution ratio	-
N_r	reaction number $k_r H/u_g$	-
Pé	Péclet number	-
Re_p	Reynolds number $\rho_g u_g d_p/\eta_g$	-
Sc	Schmidt number $\eta_g/(\rho_g D)$	-

Sh^0	observed Sherwood number $k_{ov}d_p^2/(6D)$	-
T	operating temperature	K
u_g	superficial gas velocity	$m\ s^{-1}$
β	average solids concentration in the reactor	-
ϕ	Thiele modulus	-
η	contact effectivity defined by equation 1	-
η_p	particle effectiveness factor for at bulk conditions	-
ρ_g	gas density	$kg\ m^{-3}$

REFERENCES

Geldart D., 1973, Types of gas fluidization, *Powder Technol.*, 7, 285

Herrmann E., 1991, *Katalysierte Stickoxidreduktion in der stationären und zirkulierenden Wirbelschicht*, thesis University of Karlsruhe, Germany

Jiang P., Bi H., Jean R.-H., Fan L.-S., 1991, Baffle effects on performance of catalytic circulating fluidized bed reactor, *A.I.Ch.E.J.*, **37**, 1392

Hoomans B., Kuipers J.A.M., Van Swaaij W.P.M., 1998, *personal communications*

Kuipers J.A.M., Van Swaaij W.P.M., 1997, Application of computational fluid dynamics to chemical reaction engineering, *Rev. Chem. Engng.*, 13(3)

Kunii D., Levenspiel O., 1991, *Fluidization Engineering*, Butterworth-Heinemann, Boston

Martin H., 1980, Low Péclet number particle-to-fluid heat and mass transfer in packed beds, *Chem. Engng. Sci.*, **33**, 913

Moulijn J.A., Van Swaaij W.P.M., 1976, The correlation of axial dispersion data for beds of small particles, *Chem. Engng. Sci.*, **31**, 845

Ranz W.E., Marshall Jr. W.R., 1952a, Evaporation from drop: part I, *Chem. Eng. Prog.*, **48**, 141

Ranz W.E., Marshall Jr. W.R., 1952b, Evaporation from drop: part II, *Chem. Eng. Prog.*, **48**, 173

Rietema, 1991, *The dynamics of fine powders*, Elsevier Applied Science, London

Schlunder E.U., 1977, On the mechanism of mass transfer in heterogeneous systems- in particular in fixed beds, fluidized beds and on bubble trays, *Chem. Engng. Sci.*, **32**, 845

Van Deemter J.J., 1980, Mixing patterns in large-scale fluidized beds, in *Fluidization*, edited by Grace J.R. and Matsen J.M., Plenum Press, New York, 69

Van der Ham A.G.J., Prins W., Van Swaaij W.P.M., 1994, Regenerative, high temperature desulfurization of coal gas in a circulating fluidized bed, in *Circulating Fluidized Bed Technology IV*, Pennsylvania, Engineering Foundation, 657

CHAPTER 1

PLATINUM CATALYZED OXIDATION OF CARBON MONOXIDE AS A MODEL REACTION IN MASS TRANSFER MEASUREMENTS

ABSTRACT

The oxidation of CO with oxygen over a Pt/γ-alumina catalyst is proposed as a model reaction to be used for the determination of mass transfer in packed and fluidized beds. It is applicable at relatively low temperatures (< 800 K) and for very small particles (< 100 μm).

In the present work, the kinetics for this reaction have been investigated in a small fixed bed facility (average particle diameter 54 μm) for various reactant concentrations, temperatures and superficial gas velocities. As a result the Langmuir-Hinshelwood kinetics (E_a=75.4 kJ/mole) appeared to describe the experimental results better than a power law expression (E_a=90.6 kJ/mole).

Three temperature regimes can be identified upon interpretation of experimental results with a suitable single particle model: a reaction rate controlled regime (I) at relatively low temperatures, characterized by a reaction order for oxygen of plus one and a carbon monoxide reaction order of minus one, an intermediate temperature interval (regime II) for which the reaction rate is controlled by both mass transfer and kinetics, and where the apparent reaction order in CO decreases to values considerably lower than minus one, and the high temperature regime (III) where mass transfer resistances are dominant, and the apparent reaction orders in O_2 and CO are changed to values of zero and plus one respectively.

In case of carbon monoxide oxidation over a platinum catalyst, the observed orders in O_2 and CO provide an extra instrument to recognize the prevailing conversion rate controlling phenomenon, apart from known indicators like the observed activation energy value or the influence of hydrodynamic conditions. As a consequence, the reliability of mass transfer measurements is significantly improved. This has been verified by the application in mass transfer measurements for a packed bed and for a riser system.

1 INTRODUCTION

Mass transfer from the bulk of the fluid to the particle interface in gas-solids systems has been the subject of many studies during the last decades. Mass transfer coefficients have been measured for many types of gas-solids contactors, including the packed bed (amongst many others Resnick and White, 1949), the bubbling fluidized bed (a.o. Hsiung and Thodos, 1977), turbulent (Kumar *et al.*, 1993) and fast fluidized beds (e.g. Van der Ham *et al.*, 1991, 1994; Vollert and Werther, 1994). Comparison of data obtained for the various reactor types is possible in the well-known diagram of Sherwood (related with the Nusselt number through the Chilton-Colburn analogy) versus the Péclet number ($u_g d_p/D$, or $u_g d_p/a$ for heat transfer). For similar particles, Sherwood numbers ($k_g d_p/D$) for fast fluidized beds appear to fit into the band of literature data for fluidized and packed beds (Kunii and Levenspiel, 1990; Van der Ham *et al.* 1991, 1994).

Usually, physical or chemical-reaction systems are used to derive the mass transfer coefficients, like f.i. the vaporization of solid materials or various adsorption methods. Examples are the naphtalene adsorption on FCC catalyst by Van der Ham *et al.* (1991), the adsorption of nitrogen oxide on a Hopkalit catalyst by Vollert and Werther (1994), and the

H_2S absorption on iron-oxide (Van der Ham *et al.*, 1994).
In the present work it will be shown that for a wide range of conditions the oxidation of CO over a platinum based catalyst has several advantages as a model reaction in mass transfer measurements over the above mentioned systems. It provides a unique additional property to determine whether mass transfer is really dominant.

1.1 Oxidation of carbon monoxide

The oxidation of carbon monoxide over noble metal catalysts has been extensively studied for many years, because the reaction with palladium or platinum metal as a catalyst is widely applied in automobile catalytic exhaust converters. This oxidation reaction then occurs at temperatures below 475 K. In table I various kinetic rate expressions for the oxidation reaction over a Pt/γ-alumina catalyst proposed in literature are given. The derived reaction rate expressions vary somewhat. In general a Langmuir-Hinshelwood mechanism (LH) is assumed, while sometimes a power-law reaction order expression, $R(c)=k_p c^a c_{O2}^{\ b}$, has been proposed. Such a power-law expression can of course be derived from the LH mechanism at particular conditions. According to this LH mechanism, carbon monoxide and oxygen are both adsorbed at the surface of the catalyst, where the reaction towards carbon dioxide takes place. The following reaction rate expression is adopted from Voltz *et al.* (1973):

$$R(c) = \frac{k_p^o \exp(-\frac{E_a}{RT}) \cdot c \cdot c_{O_2}}{(1 + K_a^o \exp(-\frac{\Delta H_a}{RT}) \cdot c)^2} \qquad (1)$$

where c and c_{O2} represent the CO and O_2 concentration respectively.
According to equation 1, the reaction must be first order in CO at extreme low values for the carbon monoxide concentration (viz. well below $5 \cdot 10^{-3}$ mole/m^3). However, at higher CO concentrations the apparent order in CO becomes negative. As confirmed experimentally by the authors and included in table I, the apparent reaction order in O_2 is positive over the total range of operating conditions (a value of +1 is usually observed). Values for the activation energies reported in the literature (table I) are widely spread. Low values are often ascribed to strong diffusional resistances (see e.g. Hlavácek and Votruba, 1974).
Considering the reaction rate equation, it is clear that a low value for the adsorption energy ΔH_a indicates that the influence of temperature on the resulting order in the CO-concentration is limited. When the values reported by Voltz *et al.* for the reaction rate constants and the activation- and adsorption energies are introduced, it appears that the order in the CO-concentration at high (775 K) and low temperatures (475 K) is almost the same. Extrapolation of the reaction rate equation 6a to a temperature level of almost 800 K, and comparison with a mass transfer rate at f.i. stagnant conditions (Sh = 2), indicates the possibility of mass transfer limitation even for very small particles (<100 μm), and especially at the lower carbon monoxide concentrations.

Table I. Reported kinetics for the CO-oxidation over Pt/γ-alumina.

investigators	reaction type	catalyst	T (K)	E_a (kJ/mole)	ΔH_a (kJ/mole)	order in CO	CO (vol.%)	O_2 (vol.%)
Voltz *et al.* (1973)	LH	2-3 mm spheres; Pt/alumina	500-650	104.4	8.0		0.7-4.0	3-10
Hlavácek and Votruba (1974)	LH[a]	3.4 mm spheres; Pt/alumina	300-600	52.4	-		3-4	
Nicholas and Shah (1976)	LH	0.27 wt.% Pt/ porous glass fibre	450-625	30	4.2		0.5-2	0.2-1
Hegedus *et al.* (1977)	LH	3.5-3.7 mm spheres; 0.06-0.089 wt.% Pt/alumina	450-550	62.85	8.4		0.2-0.4	2
Cant *et al.* (1978)	power law	0.15 mm spheres; 5 wt.% Pt/SiO_2	340-500	56	-	-0.2±0.2[b]	0.1-10	0.1-10
Oh and Cavendish (1982)	LH	monolith	300-700	104.4	8		1-2.5	3.5-5
Herskowitz and Kenney (1983)	LH	0.15-0.20 mm spheres; 0.825-1.17 wt.% Pt/SiO_2	400-450	100.2[c]	18.4[c]		1-6	1-4
Yu-Yao (1984)	power law	spheres; Pt/γ-alumina	400-800	92-125		-0.6 >n>-1	0.5	0.5
Subramaniam and Varma (1985)	LH	monolith; 0.1 wt.% Pt	540-753	121.2	8.4		0.1-2	0.1-2
Harold and Luss (1987)	LH	4 mm spheres; 0.3 wt.% Pt/alumina	300-525	55.4	6.53		0.6-8	
Psyllos *et al.*(1994)	LH	monolithic 1.36 wt.% Pt	400-510	56.1	7.5		3-3.3	1.6-2.1
Campman (1996)	power law	0.25-0.30 mm spheres; 0.398 wt.% Pt/alumina	463-503	112	-	-1	0.2-7.5	0.3-7.5

[a]power 1 in denominator [b]the order in CO tends to be more negative above 450 K [c]reference Harold and Luss (1987).
'LH' represents Langmuir-Hinshelwood kinetics (see equation 1), whereas power law indicates a n^{th} order reaction rate expression with orders n in the CO concentration

The above analysis leads to the following expectations. When going from a kinetically controlled reaction at low temperatures to mass transfer controlled reaction at the higher temperatures, a shift in the apparent order in CO will be observed, viz. from a negative value to plus one. Besides, where for kinetically controlled reaction a first order in the oxygen concentration is observed by all authors included in table I, the apparent order in oxygen (if present in excess) will change from +1 to 0 at mass transfer controlled conditions. Finally, upon arriving in the mass transfer controlled regime, the apparent activation energy should be decreased to a value in line with the temperature dependency of diffusional transport.

Obviously, the specific features of the CO oxidation over a platinum catalyst allow for verification whether mass transfer or kinetics is dominant in several distinct ways. A combination of observations enables the classification of the operation regimes with high confidence.

Apart from the special features outlined above, the oxidation of CO has some additional advantages over other model reactions:

- There are no side reactions: CO is oxidized exclusively to CO_2.
- The platinum-based catalyst is very stable towards the oxidation reaction.
- The catalyst can be prepared easily by impregnation on a suitable carrier material (see f.i. Li *et al.*, 1988).
- Because this reaction plays an important role in the catalytic control of automobile emissions, an enormous amount of information is available, for a wide range of conditions (see table I).

However, the catalytic oxidation of CO over platinum also introduces some difficulties. The observed negative order in CO, when coupled with intra-particle or external mass transfer resistances, can give rise to peculiar phenomena, such as particle effectiveness factors above unity, multiple steady state solutions and oscillations (Aris, 1975; Roberts and Satterfield, 1966; Hegedus *et al.*, 1977). Therefore, conclusions with respect to mechanisms and rate equations of CO oxidation over platinum catalysts in the literature can be somewhat conflicting (see e.g. Voltz *et al.*, 1973 and Yu-Yao, 1984). Beusch *et al.* (1972) and Hegedus *et al.* (1977) showed already that the observed multiplicities of steady states for a negative order reaction in a porous catalyst can be interpreted by diffusion-reaction interferences. It occurs at relatively high reactant concentrations (negative reaction order in CO), in the intermediate temperature range where intra-particle mass transfer and kinetics are interfering (Beusch *et al.*, 1972). However, this phenomenon can be excluded for the regime of complete external mass transfer control, prevailing at high temperatures.

1.2 Present work

The work presented here is part of a larger research project meant to investigate the gas-solids contacting in packed and (bubbling, turbulent or fast) fluidized bed reactors. The oxidation reaction of CO over Pt/γ-alumina seems to be an appropriate system to investigate this gas-solids contacting at mass transfer controlled conditions, allowing verification via the apparent activation energy and the apparent orders in the reactant concentration.
In the following theoretical section, the influence of external and intra-particle mass transport limitations on the particle effectiveness factor and the apparent reaction order will be first discussed more generally, on basis of single particle modelling for simple (positive) power law kinetics. Then, the single particle model is applied for the observed Langmuir Hinshelwood type of reaction kinetics according to equation 6a (see section 4). This equation has been derived for the low temperature regime of $T < 550$ K, and will be extrapolated towards higher temperatures in the single particle model calculations.
After the presentation of (the results of) the reaction rate measurements, it is demonstrated that, for CO oxidation, experimental verification whether mass transfer is really dominant is

quite simple.

2 THEORY

2.1 Single particle analysis for (positive) power law kinetics

For conversion of a gaseous reactant inside a porous catalyst particle (pseudo-homogeneous and spherical), the steady state differential mass balance is given by:

$$\frac{\partial}{\partial r}\left(r^2 D_p \frac{\partial c}{\partial r}\right) - r^2 R(c) = 0 \qquad (2a)$$

where R(c) is the specific conversion rate, D_p the intra-particle effective diffusion coefficient, and r radial position in the particle. The boundary conditions are:

$$r = 0\,;\, \frac{\partial c}{\partial r} = 0 \;\text{ and }\; r = R_p\,;\, D_p \frac{\partial c}{\partial r} = k_g (c_\infty - c_i) \qquad (2b)$$

Integration of equation (2) yields the radial concentration profile as a solution. Usually, the particle effectiveness factor is taken to be a representative indicator of the solution. It is the degree of catalyst utilisation, η_p, defined as the ratio between the observed reaction rate and the reaction rate when all concentration gradients due to external or internal mass transfer resistances are absent (viz. the reaction rate at bulk conditions).

Calculation of effectiveness factors for isothermal reactions obeying (positive) power-law kinetics, $R(c)=k_p c^n$, is relatively straightforward (e.g. Bischoff, 1965; Westerterp *et al.*, 1987; Froment and Bischoff, 1990). For a first order reaction and a constant diffusivity, it can be derived that:

$$\eta_p = \frac{\int_0^{V_p} R(c)\,dV_p}{R(c_\infty) V_p} = \frac{Bi_p}{3\phi_p^2}\left(\frac{3\phi_p - \tanh(3\phi_p)}{3\phi_p + (Bi_p - 1)\tanh(3\phi_p)} \right) \qquad (3)$$

As indicated above, this expression includes the effects of external mass transfer limitations. Rewriting to a form analogous to Froment and Bischoff (1990) yields:

$$\frac{1}{\eta_p} = \frac{1}{\eta_p^*} + \frac{3\phi_p^2}{Bi_p} \quad \text{with} \quad \eta_p^* = \frac{1}{3\phi_p^2}\left(\frac{3\phi_p - \tanh(3\phi_p)}{\tanh(3\phi_p)}\right) \qquad (4)$$

with $Bi_p = k_g d_p/(2D_p)$, and ϕ_p representing the Thiele modulus for the individual particle. This Thiele modulus is the ratio of the reaction rate at bulk conditions over the maximum diffusion rate inside the particle. In general:

$$\phi_p = \frac{d_p}{6}\sqrt{\frac{R(c_\infty)}{D_p c_\infty}} \qquad (4a)$$

but for a simple first order reaction this can be simplified to:

$$\phi_p = \frac{d_p}{6}\sqrt{\frac{k_p}{D_p}} \qquad (4b)$$

On basis of equation 4, the relation between the Thiele modulus ϕ_p and the effectiveness factor η_p can be plotted in a diagram. For n^{th} order kinetics, $R(c)= k_p c^n$, representative plots

for the effectiveness factor have been derived by Bischoff (1965). He showed that equation 4 gives a reasonable estimate for the effectiveness factor of any positive reaction order, if the proper Thiele modulus is used.

Table II. Parameters used for kinetic measurements and in the model simulations.

parameter	kinetic measurements	model simulation
d_p (μm)	54	65
c_∞ (mole/m^3)	0.2-0.5	0.02-0.2
c_{O2} (mole/m^3)	1.6-2.6	1.6-2.6
D_p (m^2/s)	-	10^{-5}
u_g (m/s)	0.5-0.9	-
T (K)	480-530	500-1000
Bi_p	-	0.1-10
ϕ_p	-	0.01-10
R(c)	-	equation 6a

In the present work, a numerical technique (finite-difference technique with a Newton-Raphson method) has been applied to solve equation 4 for arbitrary kinetics with respect to the carbon monoxide concentration (including LH kinetics). For the effective intra-particle diffusion coefficient a constant value of $D_p=10^{-5}$ m^{2}s^{-1} has been assumed throughout this paper, and the equations are solved for particles with an average particle diameter of d_p=65 μm (see also table II for the parameters used in the model simulations).

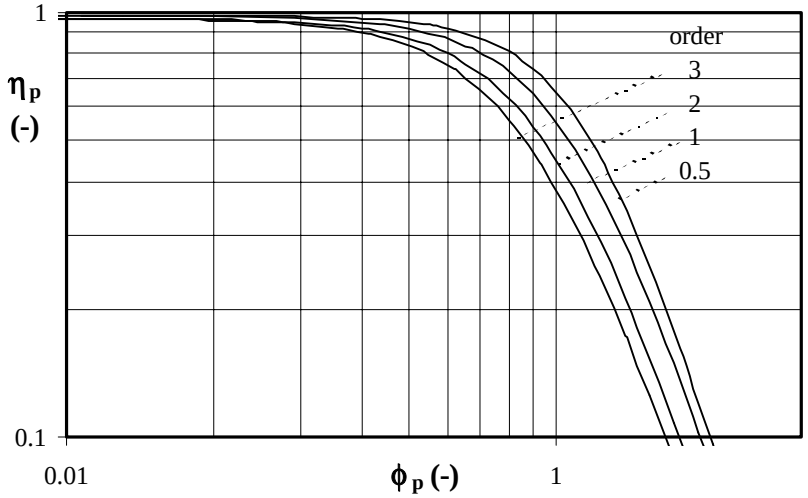

Figure 1. Particle effectiveness factor as a function of the Thiele modulus for various intrinsic reaction orders. $R(c)= k_p c^n$; Bi_p=10.

In figure 1 the numerically calculated effectiveness factor has been plotted against the corresponding Thiele modulus value for power law kinetics and various reaction orders: $R(c)= k_p c^n$ with n=0.5, 1, 2 and 3. A Biot number of 10 was taken as a representative value. The computed results presented in figure 1 are in good agreement with those derived from equation 4 (for Bi_p=10 and n=1), which confirms the validity of our numerical technique. In the low reaction rate region (ϕ_p<0.2), all curves in figure 1 approach the one for n=1. On the other hand, at high reaction rates (ϕ_p »1) all curves will eventually coincide, because an apparent first order reaction is obtained for complete external mass transfer limitation

If the reaction rate is plotted as a function of the (bulk) concentration of the reactant an apparent order in the reactant, m, can be derived by fitting the reaction rate to a function $R(c)=k_p^* c_\infty^m$ over the considered concentration range. This procedure has been applied for the concentration range from 0.2 to 2 mole/m^3, to construct figure 2. At low values of k_p the

order in the reactant is determined by the intrinsic reaction kinetics. Obviously, at high values for the kinetic rate constant all curves come together; as expected they approach eventually to the order of one, corresponding to complete external mass transfer limitation.

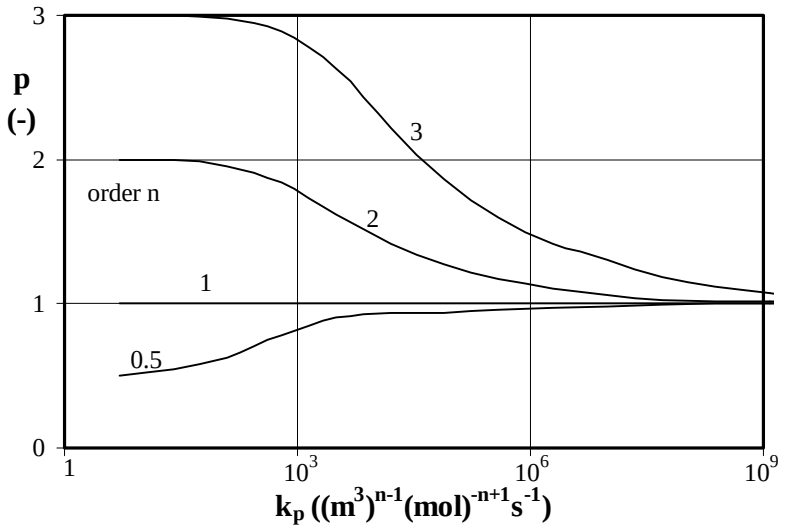

Figure 2. The apparent reaction order m, as a function of the kinetic rate constant for different intrinsic reaction orders. $R(c)= k_p^* c^n$; $Bi_p=10$.

2.2 Single particle analysis for Langmuir-Hinshelwood kinetics

An apparent negative order reaction (as from LH kinetics), when influenced by intra-particle and external diffusional resistances can lead to particle effectiveness factors above unity and multiple steady state solutions, at specific combinations of temperature and hydrodynamic conditions (Beusch *et al.*,1972; Hegedus *et al.*, 1977). In this work, relatively low temperatures (less than 525 K) were applied for the determination of reaction kinetics, as a regime where mass transfer resistances can be neglected. On the other hand, the identified specific conditions are also irrelevant for the application of the CO-oxidation under completely mass transfer controlled conditions.

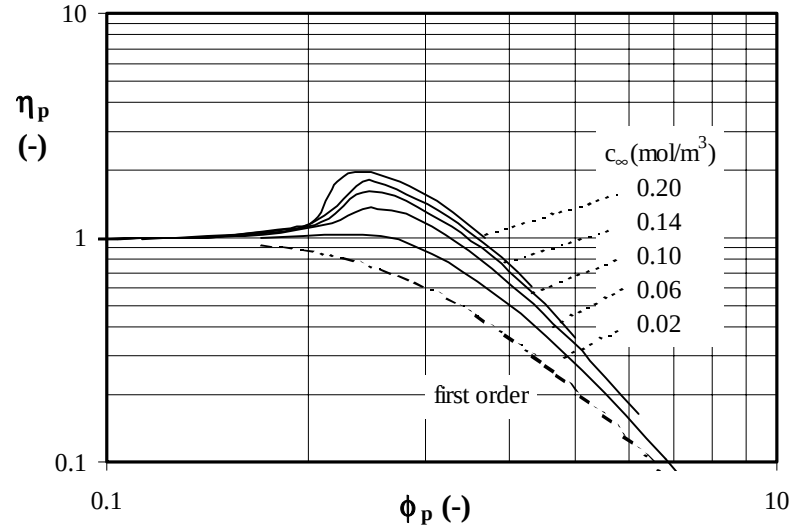

Figure 3. Effectiveness factor as a function of the Thiele modulus for the LH kinetics derived in this work (eq. 6a) at various CO inlet concentrations. $Bi_p=10$.

Equation 2 can be solved in combination with an expression for the Langmuir-Hinshelwood kinetics. As will be discussed in the experimental section, equation 6a gives a good estimation for the observed reaction kinetics. For the simulation conditions listed in table II, the particle effectivity, derived from the numerical model, is plotted as a function of the Thiele modulus in figure 3. Similar plots have already been presented by Roberts and Satterfield (1966), Aris (1975) and Morbidelli and Varma (1983). In the present work, the degree of catalyst utilisation, η_p, is defined as the ratio between the observed reaction rate, and the one occurring when all concentration gradients are absent (that is for bulk conditions prevailing at all radial positions). If negative order reactions are considered in combination with external or intra-particle mass transfer resistances, reactant concentrations at the active surface are substantially lower than in the gas bulk around the reacting particle. At such intermediate conditions, that is when reaction and mass transfer resistances are both reaction rate controlling ($0.4 < \phi_p < 1$), this can lead to effectiveness factors $\eta_p > 1$. As shown in figure 3, the effect is more pronounced at higher reactant bulk concentrations. Another peculiar phenomenon in this region for the Thiele modulus is, that at certain combinations of c_∞ and Bi_p, *three* solutions for the effectiveness factor can be obtained (Morbidelli and Varma, 1983). However, for the simulation conditions belonging to figure 3 this is not the case; a single unique solution has been obtained for all cases considered.

General agreement consists with respect to the asymptotic values for low and high Thiele moduli: for both extreme cases the particle effectivity approaches the solution for first order reaction (equation 4), represented by the dotted line.

In future work we intend to use the oxidation reaction of carbon monoxide under complete external mass transfer controlled conditions, where the observed reaction order in CO should reach a value of +1. In figure 4 the calculated reaction rate R(c) is plotted as a function of the reactant bulk concentration for various temperatures. It is roughly proportional to the reciprocal bulk concentration of CO at low temperatures (543 K), indicating an overall negative order. However, at 583 K the reaction rate first increases with c_∞, and then passes through a maximum at approximately c_∞=0.04 mole/m^3. At still higher temperatures this maximum shifts towards larger c_∞ values. Finally, a complete transition from the kinetically controlled to the mass transfer controlled regime rates takes place. At the highest temperatures (above 743 K), a reaction rate curve is obtained, which is close to the one derived for complete mass transfer limitation, over the entire c_∞-range.

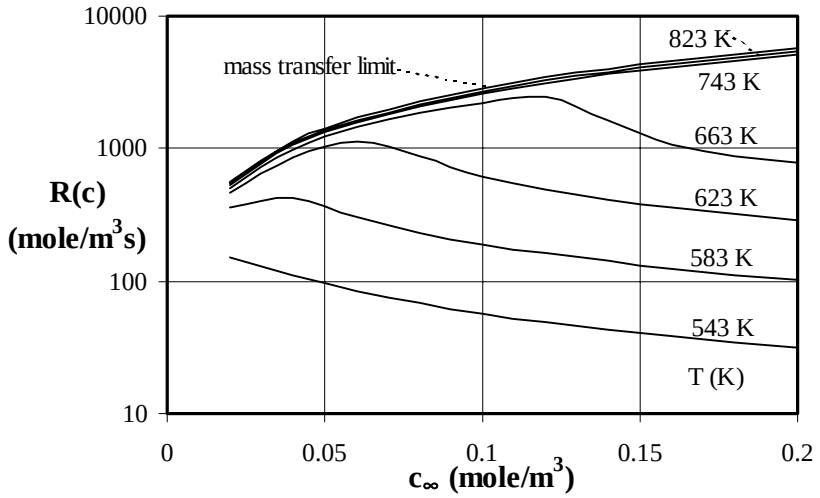

Figure 4. Calculated reaction rate as a function of the CO bulk concentration, for the LH kinetics of equation 6a, various temperatures, and Bi_p=1 (solid lines). Also indicated is the curve for mass transfer controlled conditions.

Just like in case of positive power law kinetics, the value for the apparent reactant order m can now be derived as the slopes of the curves presented in figure 4. The values of these slopes depend on i) the c_∞ interval for which m has been determined as the averaged slope, ii) the value of the Biot number, iii) the temperature. For figure 5a, m has been derived from curve sections in the bulk concentration interval 0.1-0.2 mole/m^3, and is plotted as a function of temperature for three different Biot numbers.
Figure 5b shows the effect of the bulk concentration interval selected for the determination of m explicitly.

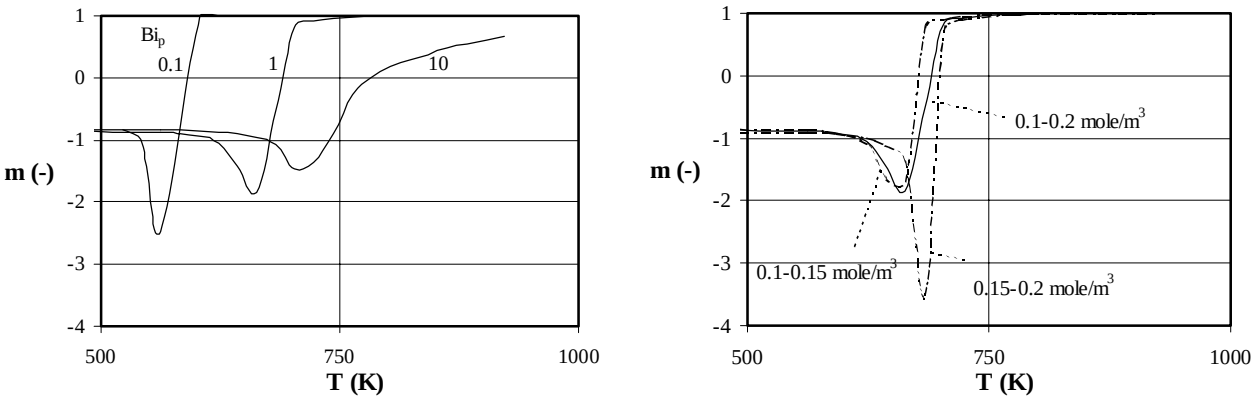

(a) (b)

Figure 5. Apparent reaction order of carbon monoxide, derived for 0.1< c_∞<0.2 mole/m^3 and three different Biot numbers (a), and for three different bulk concentration intervals and Bi_p=1 (b), as a function of the reaction temperature.

Generally, at low temperatures a negative order of approximately -1 is found, that is the one calculated from the LH rate equation 6a. If the temperature is increased the observed order becomes significantly lower than -1. As explained before (see figure 3), at conditions where mass transfer limitations become notable, the particle effectiveness factor can exceed the value 1. When the *apparent* reaction rate is plotted as a function of the bulk concentration (like in figure 4), the slope of the curve is, for those specific conditions, steeper than for a similar *intrinsic* reaction curve. Accordingly, the apparent order in carbon monoxide m will become smaller than -1.

If Bi_p=0.1, this phenomenon takes place at temperatures around 540 K, leading to a minimum in the apparent reaction order of approximately -2.5. On the other hand, for Bi_p>10 (when the influence of external mass transfer limitation is much smaller) the minimum reaction order is considerably higher and found around 700 K. In all simulated cases, the reaction order becomes positive again at high temperatures, eventually yielding m=1 when complete external mass transfer limitation is reached.
Figure 5b shows that the course of the reaction order curves is strongly affected by the interval over which the apparent order is derived. Obviously, the transition from reaction rate control to external mass transfer control is not only determined by the Biot number and the temperature, but also by the absolute value of the CO bulk concentration.

3 EXPERIMENTAL CONDITIONS

For both, the measurements of the reaction kinetics and those of mass transfer rates, a platinum-based catalyst has been used. It has a high reactivity and stability towards the oxidation of carbon monoxide. Besides, when γ-alumina (3912P; Engelhard) is used as a carrier material, it can be applied in future experiments as a fluid bed material. A 0.5 wt.% platinum/γ-alumina catalyst is prepared by an impregnation method using an aqueous

solution of H_2PtCl_6. A certain size range with an average particle diameter of 54 μm is obtained by sieving. The catalyst was activated by a mixture of CO, O_2 and balance N_2 (at a temperature of 725 K) before it was used in the experiments.

For the measurement of the intrinsic reaction kinetics, the oxidation of carbon monoxide is carried out in a down-flow operated small-scale packed bed facility. It consists of i) a gas mixing section to provide the required gas mixture for the oxidation reaction, ii) a heated packed-bed reactor section, and iii) an analysis set for continuous CO and CO_2 monitoring with two Maihak analysers. The packed bed column is a 0.5 m long and 0.0078 m I.D. quartz tube, with a glass wool plug at approximately 0.4 m from the top to support the catalyst bed. It is positioned in a 0.75 m high and 0.10 m I.D. fluidized bed of sand, which is surrounded by an electric oven. In this way isothermal operation of the packed bed was realized at temperatures ranging from 450 to 525 K. The gas flow through the bed is controlled by Brooks mass flow controllers, and ranges from 0.023 to 2.3 Nl/min. Thermocouples are used to measure the temperatures of the fluidized bed, the inlet of the reactor, and the reactor outlet.

The reaction rate experiments have been performed at relative high gas velocities of 0.5 to 0.9 m/s; higher gas velocities should be avoided to keep the pressure drop over the packed bed negligible. Lower gas velocities were not allowed because that would result in too high conversions (close to 1) and inevitable errors in the analysis of the reaction gas. Low CO concentrations and low conversions were applied to ensure isothermal conditions ($\Delta T_{ad} \approx 80^{o}C$ per vol.% CO). CO inlet volume fractions ranged from 0.2 to 0.4 mole/m^3 (at 475 K corresponding with 0.8 to 1.6 vol.%), while the conversion was always kept below 25%. The O_2-fractions were varied from 1.6 to 2.6 mole/m^3. The range of operating conditions applied is summarized in table II. In all experiments, the packed bed reactor had a three layer structure: one layer (≈2 mm) of 50 mg active material and two similar layers of 50 mg inert material, positioned just above and below the active layer. Whereas the top layer was meant for stabilizing (and heating) of the inlet gas flow, the bottom layer should prevent the penetration of catalyst in the glass wool plug. In all cases γ-alumina was used as the inert material. Before any further measurements, a blank experiment was carried out to check whether conversion over the 'inert' material occurs. It was found that in the range from 450 to 775 K the γ-alumina is indeed inactive with respect to the oxidation of CO. The packed bed conversion of CO can be used to evaluate an apparent reaction rate, R(c), defined on basis of the catalyst volume. The following relation, obtained from the mass balance for a plug flow reactor, is valid if the conversion of CO remains well below 20%:

$$\frac{\partial c}{\partial x} = -R(c)\frac{4M_{cat}}{\rho_p u_g \pi D_r^2} \qquad (5)$$

M_{cat} represents the mass of active catalyst in the reactor, R(c) the reaction rate in mole/(m^3s).

Table III. Side-effects in the evaluation of fixed bed measurements.

criterion	phenomenon to be neglected	reference	This study
$\frac{D_r}{d_p} > 10$	gas by-passing flow maldistribution	a.o. Burban *et al.*, 1990	> 150
$\frac{L}{d_p}\frac{u_g d_p}{D}\ln\left(\frac{1}{1-\xi}\right) > 1$	back-mixing	Petersen, 1965	> 5
$\left\lvert\frac{R(c)\cdot d_p^2}{4c_\infty D}\right\rvert \cdot (n-\gamma\cdot\beta) < 1$	particle mass and heat transport limitation	Weisz and Hicks, 1962	< 0.07

Criteria given by Burban *et al.* (1990), Petersen (1965) and Weisz and Hicks (1962), are used to verify that various phenomena possibly disturbing the measurements and their interpretation, could be neglected (see table III).

Measurements to determine mass transfer have been carried out in a similar packed bed (I.D. 0.0113 m), as well as in a small riser facility (I.D. 0.015 m) adopted from Van der Ham *et al.* (1994). Details of these two experimental facilities will be presented in chapter 2 and 4 of this thesis.

4 RESULTS OF THE KINETIC MEASUREMENTS

The kinetic measurements have been carried out at relatively low temperatures (480 to 530 K) while varying the gas velocity, the oxygen concentration, and the carbon monoxide concentration. Based on table I, a Langmuir-Hinshelwood expression for the kinetics of the oxidation reaction has been adopted. The experimental data are analyzed using a downhill simplex minimisation method, leading to the following rate expression:

$$R(c) = \frac{4.267\cdot 10^{11}\exp\left(-\frac{75.41\cdot 10^3}{RT}\right)\cdot c\cdot c_{O_2}}{\left(1+43.06\exp\left(\frac{3.127\cdot 10^3}{RT}\right)\cdot c\right)^2} \qquad (6a)$$

A comparison with the data listed in table I shows that the activation and adsorption energies are in close agreement with values reported by some of the quoted authors.

Results of a few typical conversion experiments are shown in figure 6: the conversion drops at an increasing carbon monoxide concentration c_{in} (a), but increases at higher oxygen inlet concentrations $(c_{O2})_{in}$ (b). These observations lead to a negative apparent order in CO, and a positive one in O_2. Because the adsorption energy is low (see Voltz *et al.*, 1973), it is indeed likely that the reaction has a negative order in the CO concentration, if the reaction proceeds according to LH kinetics.

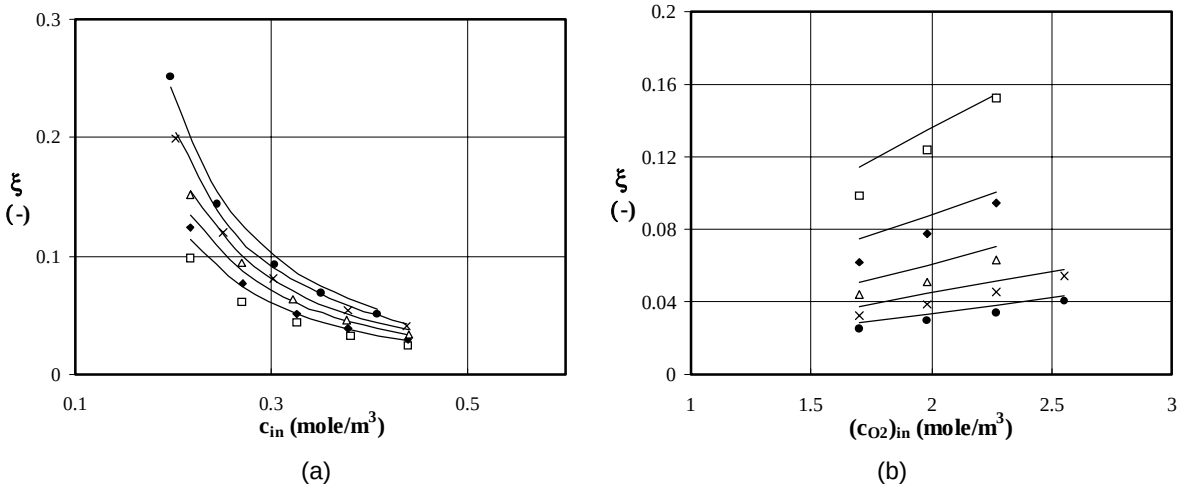

Figure 6. Observed conversion as a function of the reactant inlet concentrations c_{in} and $(c_{O2})_{in}$. The lines indicate the conversion calculated from equation 5 on basis of the reaction rate expression 6a. T=510 K; u_g=0.64 m/s. Legends: a) □ $(c_{O2})_{in}$ =1.74 mole/m^3; ♦ $(c_{O2})_{in}$ =1.98 mole/m^3; Δ $(c_{O2})_{in}$ =2.27 mole/m^3; x $(c_{O2})_{in}$ =2.56 mole/m^3; • $(c_{O2})_{in}$ =2.84 mole/m^3; b) □ c_{in}=0.22 mole/m^3; ♦ c_{in}=0.27 mole/m^3; Δ c_{in}=0.32 mole/m^3; x c_{in}=0.38 mole/m^3; • c_{in}=0.49 mole/m^3.

In figure 7, a comparison is made between the experimentally obtained conversion and the one derived from equations 5 and 6a. It shows that the agreement between the derived reaction rate expression and the experimental results is good. In the applied temperature and concentration range, the apparent orders in oxygen and carbon monoxide can also be derived from a power law expression. Equation 6b shows the results of such an interpretation.

$$R(c) = 2.15 \cdot 10^{10} \exp\left(-\frac{90.6 \cdot 10^3}{RT}\right) \cdot c^{-1} \cdot c_{O_2} \qquad (6b)$$

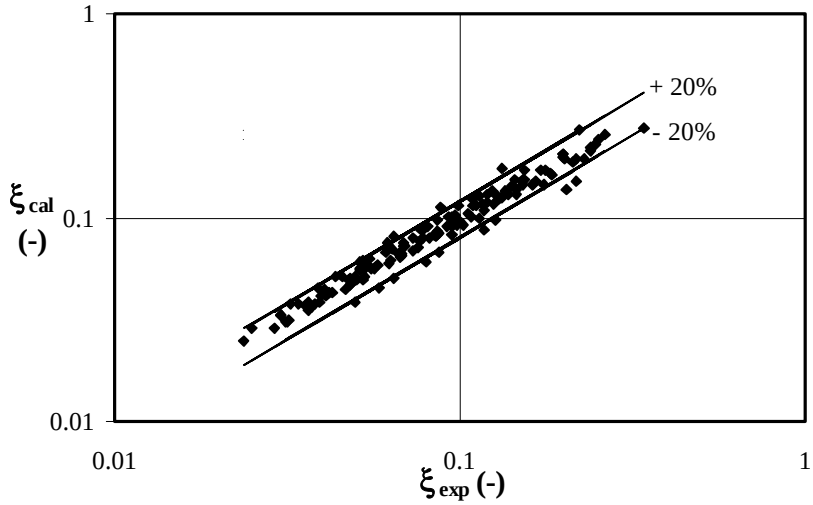

Figure 7. Parity plot for the extent of conversion of carbon monoxide to carbon dioxide over a γ-alumina catalyst, impregnated with platinum. The calculated conversions are derived from equations 5 and 6a (plug flow and LH kinetics, respectively).

The orders found are +1 and -1 for O_2 and CO respectively, and E_a was determined to be 90.6 kJ/mole. Both, the activation energy and the apparent orders in CO and O_2, are in very good agreement with the results obtained by other authors (see for example Yu Yao, 1984). However, it should be noticed that the LH kinetics describe the experimental results

considerably better than such a power law expression.

From equation 6a, the temperature at which the reaction is expected to be dominated by external mass transfer can be estimated. At low CO inlet concentrations this occurs at temperatures > 750 K (see also figure 4).

5 EXPERIMENTAL VERIFICATION OF THE CHANGING REACTION ORDER IN CARBON MONOXIDE

At this point we should emphasize that the kinetic measurements were carried out for only a small temperature range (450-525K). The theoretical considerations are based on extrapolation of equation 6a towards much higher temperatures. The objective was to show that mass transfer controlled conditions can be recognized by a shift in the observed order in the reactant concentrations, and by the decrease in the influence of temperature on the reaction rate (the apparent activation energy). Besides, interferences between reaction kinetics and intra-particle mass transfer are characterized by an apparent order in the carbon monoxide concentrations notably lower than -1. Experimental results obtained for different types of gas-solids contactors, but with similar particles, can now be compared with the theoretical simulations. In figure 8, the experimentally observed apparent reaction order in CO is compared with the calculated ones (solid line) presented in figure 5 for the case that Bi_p=1, which corresponds to the actual conditions (Sh≈1). The closed squares represent some of our results for the kinetic measurements in the small packed bed reactor (see section 2, I.D. 0.0078 m) used for this work.

The values represented by the open squares are derived from mass transfer measurements at higher operating temperatures in a similar packed bed (I.D. 0.0113 m), which required the dilution of our active material with inert γ-alumina (n_d=480). Details of the mass transfer measurements in this second packed-bed facility will be reported in chapter 2 of this thesis. Results of mass transfer measurements in a riser of a small circulating fluid bed set-up are also included (closed triangles). A more detailed report of this circulating fluid bed (cfb) study will be presented in chapter 4 of this thesis.

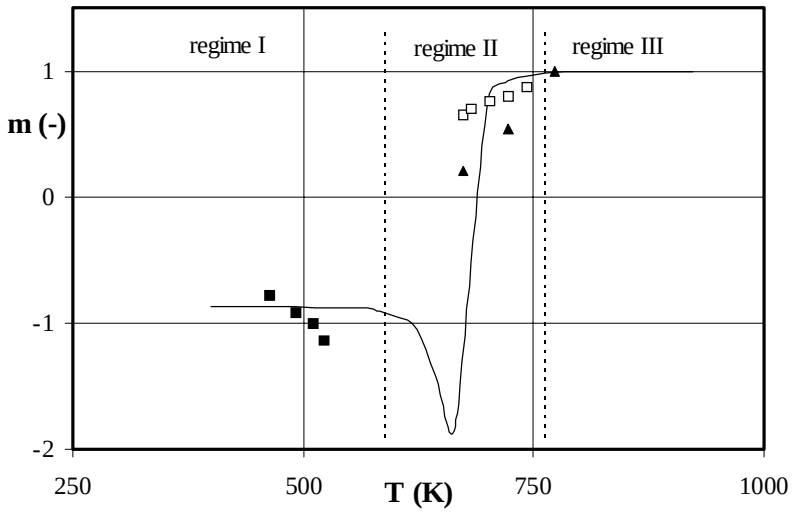

Figure 8. Reaction order of carbon monoxide as a function of the temperature. Comparison of simulated results (see also figure 5a, for Bi_p=1) with experimental data points for a packed bed and the riser of a circulating fluid bed. Legends: ■ packed bed measurements (0.0078 m. I.D.): $(c_{O2})_{in}$ = 1.1-2.0 mole/m^3 and u_g = 0.4-0.6 m/s; ▲ cfb-riser measurements (I.D. 0.015 m): n_d = 2500, $(c_{O2})_{in}$ = 1.1-1.4 mole/m^3, β = 2 vol.% and u_g = 3.5 m/s; □ packed bed measurements (I.D. 0.0113 m): n_d = 480, $(c_{O2})_{in}$ = 1.6 mole/m^3 and u_g = 0.3 m/s.

Similar to figure 5, three regimes can be identified in figure 8. The reaction rate controlled regime at low temperatures is characterized by negative carbon monoxide reaction orders (regime I). This has been confirmed by the reaction rate measurements of this study (around 500 K). The corresponding data points show a tendency to decrease with temperature which indicates already a beginning effect of mass transfer limitations. In regime II, the reaction rate is controlled by both, mass transfer and reaction kinetics. No pertinent experimental data are obtained in this intermediate regime between 525 K and 600 K. Measurement of reaction rates in the lower temperature range in this regime will be difficult anyway, because of the occurrence of multiplicities and possibly oscillations. Finally, regime III can be identified, where mass transfer resistances are really dominant. The data points in figure 8 referring to mass transfer experiments in a packed bed and the riser of a small cfb indeed show that the reaction order in CO is positive close to and in the regime III temperature interval. Observed values for the apparent activation energy in this regime are in line with the temperature dependency of diffusional transport.

For experiments in the mass transfer controlled regime, the active platinum material must be diluted with inert γ-alumina to avoid complete conversion of the reactant gas. As will be explained in the next chapters in a cfb riser, and to some extent also in packed beds of fine particles, mass transfer measurements are influenced by particle agglomeration. This effect can only be avoided by a strong dilution of the active particles with similar inert ones (n_d=480 for the packed bed experiments; n_d=2500 for the riser set-up). A full discussion of this subject matter is beyond the scope of this chapter.

6 CONCLUSIONS

The oxidation of CO over a Pt/γ-alumina at relatively low temperatures (< 800 K) is very attractive as a model reaction to investigate mass transfer in gas-solids reactors, because it provides an extra indicator for distinguishing between reaction rate and mass transfer controlled conditions. This indicator is the observed value of the reaction order in carbon monoxide

A reaction rate expression has been derived according to a Langmuir-Hinshelwood reaction scheme as far as a comparison is possible; the observed reaction kinetics are in good agreement with earlier published results. Extrapolation of the derived reaction rate expression indicates that at temperatures of 725-775 K, mass transfer controlled reaction will occur, even for very small particles (> 100 μm). By using a suitable single particle model, three operating temperature regimes can be identified:
i) a regime controlled by the intrinsic reaction kinetics (I), characterized by a negative carbon monoxide reaction order,
ii) a regime (II) in which the conversion is controlled by both mass transfer and reaction kinetics, and where the apparent reaction order in CO can be much lower than minus one,
ii) regime III, where mass transfer resistances are dominant and the apparent reaction order has a value of plus one.

Apart from this special feature, the CO oxidation over a platinum catalyst provides the following advantages over other model reactions: i) the reaction is simple, there are no side reactions, ii) the platinum-based catalyst is very stable towards the oxidation reaction, iii) the preparation of the catalyst is simple, and iv) for a wide range of conditions experimental data are available in the literature.

ACKNOWLEDGEMENT

We acknowledge the financial support of the Dutch Ministry of Economic Affairs through the Netherlands Energy Research Foundation ECN. We also thank M.G.B. Bloem, A. Groen and R. de Wit for their assistance in the experimental work. We are also indebted to J.H.A. Kiel for taking part in the discussions.

NOTATION

a	thermal diffusivity	$m^2 s^{-1}$
Bi_p	Biot number particle $k_g d_p/(2D_p)$	-
c	reactant concentration	mole m^{-3}
c_{in}	reactant inlet concentration	mole m^{-3}
c_{O2}	oxygen concentration	mole m^{-3}
$(c_{O2})_{in}$	oxygen inlet concentration	mole m^{-3}
c_∞	reactant bulk concentration	mole m^{-3}
c_i	reactant concentration at particle surface conditions	mole m^{-3}
d_p	average particle diameter	m
D_r	reactor diameter	m
D	molecular diffusion coefficient	$m^2 s^{-1}$
D_p	effective intra-particle diffusion coefficient	$m^2 s^{-1}$
E_a	activation energy defined by equation 1	J $mole^{-1}$
ΔH_a	adsorption energy defined by equation 1	J $mole^{-1}$
K_a^0	reaction constant defined by equation 1	m^3 $mole^{-1}$
k_p^0	reaction rate constant, defined by equation 1	m^3 $mole^{-1}$
k_g	gas-to-particle mass transfer coefficient	m s^{-1}
k_p	intrinsic reaction rate constant	$(m^3)^{n-1}(mol)^{n-1}s^{-1}$
k_p*	apparent reaction rate constant	$(m^3)^{m-1}(mol)^{m-1}s^{-1}$
L	length of reactor	m
m	apparent reaction order in reactant	-
M_{cat}	total amount of catalyst in reactor	kg
n	intrinsic reaction order in reactant	-
n_d	dilution ratio	-
Pé	Péclet number $u_g d_p/D$	-
R	gas constant	J $mole^{-1}$ K^{-1}
r	radial position inside the spherical particle	m
$R(c)$	molar rate of reaction per unit volume of catalyst	mole m^{-3} s
Re	Reynolds number $\rho_g u_g d_p/\eta_g$	-
Sc	Schmidt number $\eta_g/(\rho_g D)$	-
Sh	Sherwood number $k_g d_p/D$	-
T	operating temperature	K
u_g	superficial gas velocity	m s^{-1}
V_p	particle volume	m^3
x	non-dimensional reactor length	-
β	temperature factor	-
β	solids hold-up in a riser	-
ϕ_p	particle Thiele modulus by equation 4b	-
γ	non-dimensional adiabatic temperature rise	-
η_p	particle effectiveness factor for bulk conditions	-
η_p*	particle effectiveness factor for interface conditions	-

ρ_p	solids density	kg m^{-3}
ξ	conversion	-
subscripts		
cat	catalyst	
g	gas	
i	inert	
in	at reactor inlet	
p	particle	
r	reactor	
s	solid	

REFERENCES

Aris R., 1975, *The mathematical theory of diffusion and reaction in permeable catalysts*, Clarendon Press, Oxford

Beusch H., Fieguth P., Wicke E., 1972, Thermisch und kinetisch verursachte instabilitäten im reaktionsverhalten einzelner katalysatorkörner, *Chemie Ing. Techn.*, **44**, 445

Bischoff K.B., 1965, Effectiveness factors for general reaction rate forms, *A. I. Ch. E. J.*, **11**, 352

Burban P.M., Schuit G.C.A., Koch T.A., Bischoff K.B., 1990, Kinetics and characterization of bismuth molybdate catalysts, *J. Catal.*, **126**, 317

Campman M., 1996, *Kinetics of carbon monoxide oxidation over supported platinum catalysts: the role of steam in the presence of ceria*, thesis University of Eindhoven, the Netherlands

Cant N.W., Hicks P.C., Lennon B.S., 1978, Steady state oxidation of carbon monoxide over supported noble metals with particular reference to platinum, *J. Catal.*, **54**, 372

Froment G.F., Bischoff K.B., 1990, *Chemical reactor analysis and design*, John Wiley & Sons, New

Harold M.P., Luss D., 1987, Use of multiplicity features for kinetic modeling: CO oxidation on Pt/Al_2O_3, *Ind. Engng. Chem. Res.*, **26**, 2099

Hegedus L.L., Oh S.H., Baron K., 1977, Multiple steady states in an isothermal, integral reactor: the catalytic oxidation of carbon monoxide over platinum-alumina, *A. I. Ch. E. J.*, **23**, 632

Herskowitz M., Kenny C.N., 1983, Kinetics and multiple steady states, *Can. J. Chem. Engng.*, **61**, 194

Hlavácek V., Votruba J., 1974, Experimental study of multiple steady states in adiabatic catalytic systems, *Advances in Chemistry series, Chemical reaction Engineering II*, Evaston

Hsiung T.H., Thodos G., 1977, Mass-transfer in gas-fluidized beds: measurement of actual driving forces, *Chem. Engng. Sci.*, **32**, 581

Kumar H.B., Sublette K.L., Shah Y.T., 1993, Effect of high voidage on mass transfer coefficients in a fluidized bed, *Chem. Engng. Comm.*, **121**, 157

Kunii D., Levenspiel O., 1990, *Fluidization Engineering*, J. Wiley & Sons, New York

Li Y.-E., Boecker D., Gonzales R.D., 1988, CO oxidation on Pt/SiO_2 and Pd/SiO_2 catalysts: rapid FTIR Transient studies, *J. Catal.*, **110**, 319

Morbidelli M., Varma A., 1983, Isothermal diffusion-reaction in a slab catalyst with bimolecular Langmuir-Hinshelwood kinetics, *Chem. Engng. Sci.*, **38**, 289

Nicholas D.M., Shah Y.T., 1976, Carbon monoxide oxidation over a platinum-porous fiber glass supported catalyst, *Ind. Engng. Chem. Prod. Res. Dev.*, **15**, 35

Oh S.H., Cavendish J.C., 1982, Transients of monolithic catalytic converters: response to step changes in feedstream temperature as related to controlling automobile emissions, *Ind. Engng. Chem. Prod. Res. Dev.*, **21**, 29

Petersen E.E., 1965, *Chemical Reaction Analysis*, Prentice Hall, New Yersey, 194

Psyllos A., Papayannakos N., Philippopoulos C., 1994, CO oxidation in a Carberry reactor: manifestation of reaction kinetics by controlled reaction/transport, *J. Chem. Engng. Japan*, **27**, 693

Resnick W., White R.R, 1949, Mass transfer in systems of gas and fluidized solids, *Chem. Eng. Prog.*, **45**, 377

Roberts G.W., Satterfield C.N., 1966, Effectiveness factor for porous catalysts, *Ind. Engng. Chem. Fund.*, **5**, 317

Subramaniam B., Varma A., 1985, Reaction kinetics on a commercial three-way catalyst: the $CO\text{-}NO\text{-}O_2\text{-}H_2O$ system, *Ind. Engng. Chem. Prod. Res .Dev.*, **24**, 512

Van der Ham A.G.J., Prins W., van Swaaij W.P.M., 1991, Hydrodynamics and mass transfer in a regularly packed circulating fluidized bed, in *Circulating Fluidized Bed Technology III*, Pergamom Press, New York, 605

Van der Ham A.G.J., Prins W., van Swaaij W.P.M., 1994, Regenerative, high temperature desulfurization of coal gas in a circulating fluidized bed, in Circulating Fluidized Bed Technology IV, Pennsylvania, Engineering Foundation, 657

Vollert J., Werther J., 1994, Mass transfer and reaction behaviour of a circulating fluidized bed reactor, *Chem. Engng. Technol.*, **17**, 201

Voltz S.E., Morgan C.R., Liederman D., Jacob S.M., 1973, Kinetic study of carbon monoxide and propylene oxidation on platinum catalysts, *Ind. Engng. Chem. Prod. Res. Dev.*, **21**, 294

Weisz P.B., Hicks J.S., 1962, The behavior of porous catalyst particles in view of internal mass and heat diffusion effects, *Chem.Engng.Sci.*, **17**, 265

Westerterp K.R., van Swaaij W.P.M., Beenackers A.A.C.M., 1987, *Chemical reactor design and operation*, John Wiley & Sons, New York

Yu Yao Y.-F., 1984, The oxidation of CO and Hydrocarbons over noble metal catalysts, *J. Catal.*, **87**, 152

CHAPTER 2

INFLUENCE OF CATALYST DILUTION ON MASS TRANSFER IN PACKED BEDS OF FINE PARTICLES

ABSTRACT

In chapter 1, the oxidation of carbon monoxide over a Pt/γ-alumina catalyst was shown to have potential as an attractive model reaction for mass transfer measurements in packed and fluidized beds. The oxidation of carbon monoxide over a platinum catalyst allows for the verification whether mass transfer or kinetics is dominant in several distinct ways: the combination of these observations enables the classification of the reaction regimes with high confidence. In the present paper, this reaction has been applied in a small packed bed reactor (0.0113 m ID) of fine particles (42, 54 and 75 μm) at temperatures ranging from 675 to 750 K. It is demonstrated that mass transfer controlled reaction rates were obtained for CO and oxygen inlet fractions between 0.3 and 1 vol.%, and 7 and 10 vol.% respectively. From these measurements, mass transfer numbers could be derived.

Because solids dilution is thought to suppress the effect of particle clustering, which might be an important cause for contact-efficiency loss in packed beds of all-active particles, the ratio of active particles over inert (but similar) γ-alumina particles were varied. Results of the measurements indeed showed that the contacting efficiency is maximal at infinite dilutions; at 735 K it decreases roughly by a factor 2 upon decreasing the dilution ratio n_d from 480 to 80. With respect to the influence of particle diameter, it has been observed that the apparent rate constant k_{ov} decreases for larger particles due to the corresponding decrease of the specific surface involved, while the non-dimensional mass transfer number Sh^0 increases. This mass transfer number also increases when the applied superficial gas velocity is enlarged.

The results of the mass transfer measurements have been interpreted with a model, which accounts for the effects of particle clustering, and predicts the observed influence of the solids dilution ratio satisfactory. Depending on the applied particle size and gas velocity, the estimated size of the effective cluster varies from 7 to 18 times the particle diameter, values which are comparable with those presented by Moulijn and Van Swaaij (1976). Results of packed-bed mass transfer measurements by Bar-Ilan and Resnick (1957) and Hsiung and Thodos (1977b), re-evaluated on the basis of the proposed cluster model, show that the ratio of the effective cluster size over the particle diameter decreases from roughly 30 to 1 when the particle Reynolds number is increased from 0.1 to 1. The present results fit well into this band.

1 INTRODUCTION

During the last decades the dependence of mass and heat transfer coefficients on the molecular Péclet-number $Pé_m=Re\cdot Sc$ ($u_g d_p/D$ and $u_g d_p/a$ respectively) in packed bed reactors has been the subject of many studies. An extended review has been published by Dwivedi and Upadhyay (1977). In figures 1a and 1b, experimentally observed mass transfer numbers ($k_g d_p/D$) are plotted as a function of $Pé_m$ for gas-solids and liquid-solids systems at low Reynolds numbers (Re<10 for gas-solids and Re<1 for liquid-solids systems). The belonging tables I and II provide the most important experimental conditions of the work concerning mass transfer in gas-solids and liquid-solids system.

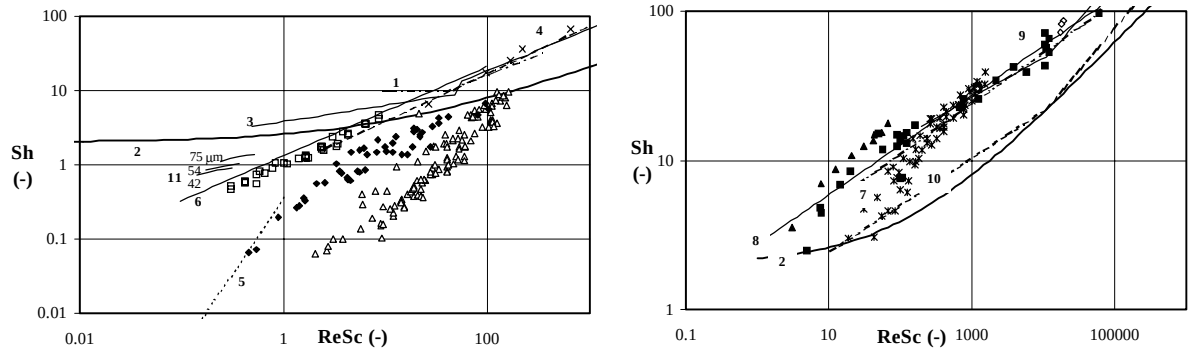

Figure 1. Mass transfer numbers in packed bed reactors versus the Péclet number for gas-solids (a) and liquid-solids (b) systems. The lines represent derived correlations. Legends: **1**. Hobson and Thodos (1951), 2. Ranz and Marshall (1952), **3**. Chu *et al.* (1953), **4**. Petrovic and Thodos (1968), **5**. Wakao and Tanisho (1974), **6**. Hsiung and Thodos (1977b), **7**. Williamson *et al.* (1963), **8**. Wilson and Geankoplis (1966), **9**. Upadhyay and Tripathi (1975), **10**. Kumar *et al.* (1977), **11**. this work for n_d=160 and d_p=42, 54 and 75 µm, Δ Resnick and White (1949), ♦ Bar-Ilan and Resnick (1957), □ Hsiung and Thodos (1977b), ◊ Upadhyay and Tripathi (1975), ■ Wilson and Geankoplis (1966), ★ Fedkiw and Newman (1982), ▲ Appel and Newman (1976).

Mass transfer rates have been investigated in all kinds of gas-solids contactors, amongst which the packed bed (for instance Resnick and White, 1949), and the bubbling (a.o. Hsiung and Thodos, 1977), turbulent (Kumar *et al.*, 1993) and fast fluidized bed (e.g. Van der Ham *et al.*, 1994; Vollert and Werther, 1994). Comparison of the data obtained is possible in the well-known diagram of the Sherwood number (interrelated with the Nusselt number by the Chilton-Colburn analogy) versus the $Pé_m$-number. Sherwood numbers ($k_g d_p/D$) for fluidized beds then appear to fit into the band of literature data for packed beds (Kunii and Levenspiel, 1991; Van der Ham *et al.* 1994). Roughly considered, it seems that the various mass transfer results reported show little correlation with the reactor type in which they were obtained.

Apart from this peculiar feature, other phenomena (in packed beds) can be observed. For $Pé_m$-values larger than 100, the trend of the Sherwood number has been more or less well established, but the values are consistently higher (about a factor 3) than those predicted by the well-known Ranz-Marshall equation (1952). At lower $Pé_m$-numbers, that is when lower fluid velocities and smaller particles are applied, the results obtained by various authors are widely differing. Packed bed experiments concerning mass transfer between particles and liquids (figure 1b) yield Sherwood numbers which are only slightly lower than those predicted by Ranz-Marshall, even for small $Pé_m$-numbers. For gas-solids systems (figure 1a), the mass transfer numbers are much lower for the same range of $Pé_m$-numbers ($Re \cdot Sc<100$). This could be related to the differences in fluid phase diffusivity. Gas phase diffusivities are orders of magnitude larger than liquid phase diffusivities (10^{-5} compared to 10^{-9} m^2/s). For the same particle size and fluid velocity, $Pé_m$ (liquid) is roughly 10^4 times larger than $Pé_m$ (gas). In gas-solids systems, the range of $Pé_m$-values where axial dispersion may influence mass or heat transfer measurement is reached easily. However, there may also be other causes for the small Sh numbers reported for the range of low $Pé_m$-values. Hereafter, relevant literature concerning this phenomenon will be discussed.

Table I. Experimental work on gas-solids mass transfer in packed beds for low Reynolds numbers (Re<10).

Authors	**Experimental method**	**material**	**d_p (μm)**	**ρ_p (kg/m^3)**	**Fluid**	**Sc**	**Re**	**correlation Sh**
Resnick and White (1949)	vaporization in a fluidized bed	naphtalene spheres	265..1030	1066	air/H_2/ CO_2	2.39 1.47 4.02	0.6..64	-
Hobson and Thodos (1951)	vaporization	porous spheres	9400	-	air/N_2/ CO_2 /H_2	0.607.. 5.056	8.55..327	$Sh = 10 \cdot Sc^{1/3}$ $Re < 10$ $Sh = 1.3 \cdot Re^{0.55} \cdot Sc^{1/3}$ $Re > 150$
Chu *et al.* (1953)	vaporization	regular shaped particles	693.. 14072	-	air	-	20..10^4	$Sh = 5.7 \cdot (1-\varepsilon)^{0.78} \cdot Re^{0.22} \cdot Sc^{1/3}$ $0.5 < Re < 15$ $Sh = 1.77 \cdot (1-\varepsilon)^{0.44} \cdot Re^{0.56} \cdot Sc^{1/3}$ $15 < Re < 5000$
Bar-Ilan and Resnick (1957)	vaporization	naphtalene spheres	370..8200	-	air	2..6	0.17..173	-
Petrovic and Thodos (1965)	vaporization	porous spheres	1831.. 9398	-	air	0.6..5.5	3..230	$Sh = \frac{0.357}{\varepsilon} \cdot Re^{0.641} \cdot Sc^{1/3}$ $3 < Re < 100$
Wakao and Tanisho (1974)	pulse response non-absorption	cylindrical and spherical catalyst particles	4660x 3080 710..1410	-	air in H_2	1.6	0.15..1.83	$Sh = 0.35 \cdot Re^2$
Wakao *et al.* (1976)	pulse response absorption	activated carbon spheres	2200	1100	air in H_2	1.6	0.099..0.96	-
Hsiung and Thodos (1977)	vaporization in a diluted bed	naphtalene spheres	248..2000	1040	air	2.5	0.1..100	$Sh = 1.33 \cdot Re^{0.6} \cdot Sc^{1/3}$ $0.1 < Re < 100$

Table II. Experimental work on liquid-solids mass transfer in packed beds for low Reynolds numbers (Re<1).

Authors	Experimental method	material	d_p (μm)	ρ_p (kg/m^3)	Fluid	Sc	Re	correlation Sh
Dryden *et al.* (1953)	dissolution	naphtol and benzoic acid spheres	6250	-	water	814..1147	0.0125..7.21	-
Selke *et al.* (1956)	ion exchange	spherical amberlite IR-120	420..850	1100	$AgNO_3$; $CuSO_4$	517..1125	2.74..124	-
Williamson *et al.* (1963)	dissolution	benzoic acid spheres	6000	-	water	-	0.08..120	$Sh = 2.40 \cdot \varepsilon^{0.66} \cdot Re^{0.34} \cdot Sc^{0.42} \quad 0.04 < Re < 60$ $Sh = 0.442 \cdot \varepsilon^{0.31} \cdot Re^{0.69} \cdot Sc^{0.42} \quad 60 < Re < 2500$
Wilson and Geankopolis (1966)	dissolution	benzoic acid spheres	6380	-	water & propylene glycol solution	950..70600	0.0016..55	$Sh = \frac{1.09}{\varepsilon} \cdot Re^{1/3} \cdot Sc^{1/3} \quad 0.0016 < Re < 55$ $Sh = \frac{0.250}{\varepsilon} \cdot Re^{0.69} \cdot Sc^{1/3} \quad 55 < Re < 1500$
Miyauchi *et al.* (1975)	pulse response	spherical sulfonic acid ion-exchange resin beads	870..1540	-	NaOH solution	510..649	-	$Sh = 16.7; \; Re \downarrow 0$ $Sh = 1.3 \cdot (Re\,Sc)^{1/3}$
Upadhyay and Tripathi (1975)	dissolution	benzoic acid spheres	5967..11968	1300	water	572..1350	0.405..11610	$Sh = 3.8151 \cdot (1-\varepsilon)^{0.7317} \cdot Re^{0.2683} \cdot Sc^{1/3} \quad Re < 1$ $Sh = 1.6218 \cdot (1-\varepsilon)^{0.4447} \cdot Re^{0.5553} \cdot Sc^{1/3} \quad Re > 1$
Appel and Newman (1976)	limiting current	stainless steel spheres	3970	-	ferro- and ferricyanide solution	1400	0.002..0.0294	-
Kumar *et al.* (1977)	dissolution	cylindrical pellets	538..1198	1300	water & 60% aqueous glycol solution	767..42400	0.01..600	$Sh = \frac{1}{\varepsilon}((0.12 \cdot (Gr \cdot Sc)^{1/4})^6 + (.05 \cdot (Re \cdot Sc)^{1/3})$ $Re < 10, \; 123 < Sc < 42000$ $Sh = \frac{1}{\varepsilon}((1.05 \cdot Re^{1/3})^6 + (0.525 \cdot Re^{0.56})^6)^{1/6} Sc^{1/}$ $0.001 < Re < 1, \; 42000 < Sc < 70600$ and $1 < Re < 2500, \; 123 < Sc < 70600$
Fedkiw and Newman (1982)	limiting current	stainless steel spheres	3175	-	copper sulfate solution	1900, 8880	0.00271..0.198	

2 LITERATURE RESULTS

According to some authors the most important reason for the anomaly in the results of mass or heat transfer measurements is the inadequate interpretation of experimental results, especially for conditions at which axial dispersion plays an important role. Results obtained at low $Pé_m$-numbers in liquid solids systems are usually obtained at low superficial liquid velocities, where axial dispersion is likely to play an important role. In gas-solids systems, the high gas phase diffusion coefficient may easily cause axial dispersion to become important (at low $Pé_m$-numbers). With some exceptions the influence of axial dispersion has always been neglected, which is a crucial omission at low $Pé_m$(Gunn and de Souza, 1974). The consequence of this can be even more serious when shallow beds are used to maintain a nearly constant driving force. As was shown by, amongst others, Fedkiw and Newman (1982), the error made at higher $Pé_m$-values is relatively unimportant.
Some other causes of the strongly decreasing Sherwood numbers at those low molecular $Pé_m$-numbers (« 10) have been identified for gas-solids packed bed systems. Kunii and Suzuki (1967) stated that channelling, or a local uneven contacting of fluids with solids, is responsible for the excessive decrease of the apparent heat and mass transfer coefficients. Nelson and Galloway (1975) on the other hand, postulated that the 'sink' infinitely far away from the particle surface (the essential boundary condition for a single sphere, resulting in the minimum value of 2 for the Sherwood and Nusselt numbers at low Reynolds numbers) is not valid for a particle embedded in a matrix of other particles, that are all participating in the mass or heat transfer process. They showed that, upon assuming that the boundary condition is valid at a certain *finite* distance from the particle surface, the theoretical limiting value for Sh/Nu at low $Pé_m$-numbers becomes zero. However, the theoretical results obtained in these two studies are trivial, because the derived linear correlation between Sh/Nu and $Pé_m$ followed from an incorrect definition of the driving force for mass or heat transfer: the initial driving force was used instead of the local driving force (Schlünder, 1977; Glicksman and Joos, 1980).

Another kind of explanation for the strong decrease in mass transfer numbers is also put forward: Schlünder (1977) explained the effect of low $Pé_m$ number by considering a bundle of parallel capillaries, with one large diameter tube embedded in a matrix of smaller tubes. He showed that the overall performance of such a non-uniform system is lower than that of a system, in which the non-uniformities in geometry are absent. Martin (1978) extended this idea by applying it to a packed bed, which was considered to consist of two regions: an annular outer region where the porosity was high and a central core with bulk porosity. He stated that the discrepancy between theory and experiments can be explained by such a simple model. However, an essential feature of his model is the existence of an *inactive* surface in the annular region, whose contribution should be fitted to the experimental data. An analytical model, accounting for axial dispersion, channelling, and inaccuracies in the experimental observations, was proposed by Glicksman and Joos (1980). They postulated that dispersion in the flow direction was the primary mechanism for the decline of the effective Sherwood or Nusselt numbers at low $Pé_m$ numbers. Tsotsas (1992) stated that the impact of flow maldistribution on mass and heat transfer numbers is low, except for the case of a large non-interacting and really inactive bypass, as is the case in the model of Kunii and Suzuki (1967).

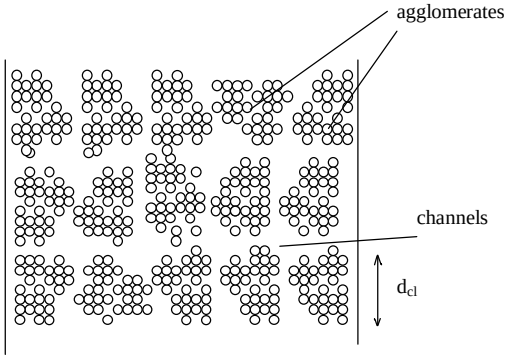

Figure 2. Representation of the agglomeration model, from Moulijn and Van Swaaij (1976).

More or less similar to their model, but based on own data and on literature data of axial dispersion of gases in packed beds with fine particles, Moulijn and Van Swaaij (1976) considered the packed bed to be composed of agglomerates of equal diameter, d_{cl} (see figure 2). By correcting the effective Bodenstein number at high $Pé_m$-numbers for the presence of agglomerates, equivalent agglomerate diameters were derived from own experiments and studies by various authors. As a general conclusion these authors showed that d_{cl} is inversely proportional to the particle diameter for particle diameters smaller than 500 μm, and they suggested that another factor for the low mass and heat transfer rates at low $Pé_m$-values, apart from the omission of axial dispersion, might be the occurrence of a non-uniform particle distribution. This phenomenon results in severe channelling of gas.

Our starting point is, that the strong decrease in the mass or heat transfer at low $Pé_m$-values should indeed be attributed to a large non-interacting bypass or shielding of active particles (particle clustering). The clustering of particles is probably due to inter-particle forces, and their effect is due to the flow properties at low Re-numbers as explained by Schlünder (1977). Several investigators give indirect evidence for the existence of such clusters in packed beds as well as in various fluidized beds. As explained before, it might be the cause for large axial dispersion coefficients in packed beds of fine particles. Furthermore, experimental work performed in packed beds by Hermann (1991) shows that conversion limitation due to gas by-passing the catalyst particles in a packed bed can even be more severe than in a bubbling bed (operated at u_g=0.08 m/s).
There are several indicators that inter-particle forces for small particles lead to deviating behaviour also in other gas-solids contactors. For example, Rietema and co-workers (1991) state that inter-particle forces (with elastic properties) are required to explain the homogenous fluidization regime of Geldart's type A-particles. It seems that clustering of particles in packed bed systems are important only if small particle diameters (d_p<500 μm) are considered (Moulijn and Van Swaaij, 1976).

3 THIS WORK: THE CLUSTER CONCEPT

In this work, a model is adopted, which is more or less similar to the agglomeration model proposed by Kunii and Suzuki (1967) and to the later models by Moulijn and Van Swaaij (1976) and Verver (1984). This model, the so-called cluster model, is based on the assumption that the packed bed consists of spherical agglomerates (or clusters of particles), surrounded by a flowing fluid; the transport of reactant inside such agglomerates is supposed to occur by molecular diffusion only.
The derivation of the cluster model is given in appendix II of this thesis. The following relations for the effectiveness factor of the particle cluster are obtained, assuming a first-order reaction mechanism:

$$\eta_{ov} = \left(\frac{1}{\eta_{cl}^{*}} + \frac{3\phi_{cl}^{2}}{Bi_{cl}} \right)^{-1} \left(\frac{1}{\eta_{p}^{*}} + \frac{3\phi_{p}^{2}}{Bi_{p}} \right)^{-1} \qquad (1)$$

where:

$$\frac{1}{\eta_{p}} = \frac{1}{\eta_{p}^{*}} + \frac{3\phi_{p}^{2}}{Bi_{p}} \text{ with } \eta_{p}^{*} = \frac{1}{3\phi_{p}^{2}} \left(\frac{3\phi_{p} - \tanh(3\phi_{p})}{\tanh(3\phi_{p})} \right)$$

$$\frac{1}{\eta_{cl}} = \frac{1}{\eta_{cl}^{*}} + \frac{3\phi_{cl}^{2}}{Bi_{cl}} \text{ with } \eta_{cl}^{*} = \frac{1}{3\phi_{cl}^{2}} \left(\frac{3\phi_{cl} - \tanh(3\phi_{cl})}{\tanh(3\phi_{cl})} \right)$$

$$\phi_{cl} = \frac{d_{cl}}{6} \sqrt{\frac{k_{cl}}{D_{cl}}} \quad Bi_{cl} = \frac{k_{g,cl} d_{cl}}{2D_{cl}} \quad \text{and} \quad \phi_{p} = \frac{d_{p}}{6} \sqrt{\frac{k_{p}}{D_{p}}} \quad Bi_{p} = \frac{k_{g} d_{p}}{2D_{p}}$$

$$k_{cl} = k_{p} \eta_{p} \frac{(1-\varepsilon_{cl})}{(1+n_{d})} \qquad (2)$$

The relation for the apparent reaction rate constant, k_{ov}, of an overall (close to) first order process can be derived from the appropriate mass balances for a plug flow reactor (PFR) or a model of a series of m continuously operated ideally stirred tank reactors (mCISTR's):

PFR:

$$k_{ov} = -\frac{u_{g} \pi D_{r}^{2} \rho_{p}}{4 M_{cat}} \ln\left(\frac{c_{out}}{c_{in}} \right) \qquad (3)$$

mCISTR's:

$$k_{ov} = -\frac{m u_{g} \pi D_{r}^{2} \rho_{p}}{4 M_{cat}} \left(1 - \left(\frac{c_{out}}{c_{in}} \right)^{-1/m} \right) \qquad (4)$$

M_{cat} represents the mass of active catalyst in the reactor, and c_{in} and c_{out} the in- and outlet concentrations of gaseous reactant.

The conversion of a model compound in the packed bed reactor can be used to evaluate the apparent reaction rate constant, k_{ov}, defined on basis of the catalyst volume. Its value can be compared with the one derived from our cluster model, adjusting the equivalent particle cluster size, d_{cl}. In appendix II of this thesis, the effects of cluster formation on the apparent rate constant have been shown in detail for a first order reaction. As a first result, the cluster model predicts that the apparent rate constant, k_{ov}, defined per unit volume of active catalyst, increases at higher dilution ratios, n_{d}. This is due to the reduction of the diffusional resistance in the particle cluster caused by a decreased cluster reactivity. In the extreme case of infinite dilution, the cluster effectivity approaches the value of 1. Another outcome of the model is concerned with the size of the clusters. The apparent rate constant k_{ov} decreases for larger clusters, that is at higher values for the ratio of cluster-over-particle diameter d_{cl}/d_{p}. This can be explained by the decreased mass transfer rate to and inside the cluster. To verify the validity of the cluster model the following conditions appear to be essential:

- The intrinsic reaction rate must be very fast, so that the overall rate is (preferably) mass transfer controlled.

- On basis of the observations made by Moulijn and Van Swaaij (1976) cluster formation in packed beds is likely to take place for small particle diameters (< 500 μm) only.
- One of the important parameters in the model is the dilution ratio n_d, the total volume of solids over the volume of active material. Unfortunately, the range of dilution ratios, which can be obtained in mass transfer experiments is limited, and dilution of active catalyst can have side-effects on the overall activity of the packed bed reactor; this will be discussed first.

4 SIDE-EFFECTS OF CATALYST DILUTION

The basic idea of this work is that the effects of channelling can be simulated by a model in which the packed bed is thought to consist of particle clusters with a stagnant gas phase representing the "dead zones" between channels. By the simulations reported in appendix II of this thesis, it is shown already that, in case of a mass transfer controlled reaction, dilution can have a strong effect on the packed bed conversion rate based on the active particle volume. Apart from this effect, a number of side effects are reported in literature which will be discussed hereafter, but shown to be unimportant for the present work.

Generally, three main effects of catalyst dilution have been reported: 1) a decrease of the effect of back-mixing, 2) (local) heat effects in the reactor, and 3) stochastical effects. They can play a serious role if results in an undiluted bed are compared with data obtained in a diluted bed:
ad 1) Due to a lower conversion per unit reactor length at higher dilution ratios the concentration gradient will be flattened, resulting in a decreasing driving force for the back-mixing of reactant. Ho and White (1991), and as a response Aris (1992), infer that, for a positive-order reaction, a fixed bed with back-mixing will yield a higher conversion if the bed is diluted with inert material, because at the same mass of active catalyst, addition of inert particles increases the bed height, and reduces the axial (and perhaps radial) concentration gradient. To ensure that back-mixing of the gaseous reactant does not affect the measurements, the criterion of Petersen (1965) must be verified.
ad 2) Dilution is obtained by adding inert material while keeping the number of active particles constant. It is obvious that any non-isothermicity will be suppressed by dilution. In case of an exothermic reaction this may result in lower conversions (at 750 K ΔT_{ad}=75 K/vol.%CO). In this work low inlet fractions of CO are used. Therefore heat effects remain small and the packed bed can be operated under (nearly) isothermal conditions.
ad 3) A too strong dilution can affect the extent of conversion by a corresponding change in the residence time distribution and/or in the distribution of catalytic activity. Besides, it can lead to gas by-passing the active solids in the packed bed. Van de Bleek *et al.* (1969) proposed a criterion for neglecting these dilution effects. However, Sofekun *et al.* (1994) showed that this dilution criterion is not valid for all reaction orders. They showed that the effect of dilution decreases and eventually vanishes, when the number of classes in a standard normal distribution (used for the statistical modelling) increases. They estimated the maximum effect of dilution by extrapolation to infinite dilution to be approximately 2.5% when a first-order reaction is applied. In the present study the possible effect of a non-uniform distribution of gas residence times and catalytic activities has been neglected.

5 EXPERIMENTAL CONDITIONS

5.1 Selection of the model reaction and belonging catalyst

Mass transfer controlled reaction rates can be observed using an appropriate (very fast) model reaction system. In chapter 1, the oxidation of CO over a Pt/γ-alumina catalyst was shown to be a promising model reaction, yielding the following kinetic reaction rate

expression (based on LH kinetics):

$$R(c) = \frac{4.27 \cdot 10^{11} \exp\left(-\frac{75.4 \cdot 10^3}{RT}\right) c \cdot c_{O_2}}{\left(1 + 43.1 \exp\left(\frac{3.13 \cdot 10^3}{RT}\right) c\right)^2} \quad (5)$$

Extrapolation of this reaction rate equation, to much higher temperatures indicated the possibility of mass transfer limitation for particles smaller than 100 μm, especially at low carbon monoxide concentrations.

On basis of this reaction rate equation, three possible regimes of operation could be identified. A kinetic reaction rate controlled regime, indicated by negative carbon monoxide reaction orders (regime I), a temperature interval where the reaction rate is controlled by mass transfer and kinetics, and where apparent reaction orders in CO can be even lower than -1 (regime II), and regime III, where mass transfer resistances are really dominant and the apparent reaction order is 1. Apparently, for this model reaction, the shift from a negative order reaction to a first order reaction when going to the mass transfer controlled regime, is a valuable extra tool that can be used to verify whether mass transfer resistance are actually dominant.

For the present work, three different size ranges of catalyst particles have been produced by sieving of the ground material, their average particle diameter being 42, 54 and 75 μm. Part of each size range was then provided with the Pt catalyst and activated at a temperature of 725 K over a mixture of CO, O_2 and balance N_2.

5.2 Experimental set-up

Specific details of the small-scale packed bed facility can be found in chapter 1 of this thesis. A 11.3 mm ID quartz tube was used as the reactor. In all experiments, the packed bed reactor had a three layer structure: one layer (≈ 2 mm) of 50 mg active+inert material and two similar layers of 50 mg inert material, positioned just below and above the active layer. Whereas the top layer was used for stabilising (and heating) of the inlet gas, the bottom layer should prevent the penetration of catalyst in the glass wool plug. The active particles are taken from the same batch of catalyst material as prepared in chapter 1. The influence of dilution of the active material has been determined at temperatures ranging from 675 to 750 K, CO inlet volume fractions ranged from 0.3-0.9 vol.% and O_2-fraction from 7-10 vol.%. The experiments were performed at three different gas velocities, 0.3, 0.45 and 0.6 m/s, and dilution ratios, n_d, varying from 80 to 480 m^3 inert material per m^3 catalyst. In a few separate experiments, it has been demonstrated that, in the temperature range from 480 to 800 K, the γ-alumina is inert with respect to oxidation of CO. In the same temperature range CO conversion due to homogeneous oxidation could not be detected either.

6 RESULTS

6.1 Effect of the O_2 and CO inlet fractions

At temperatures ranging from 675 to 750 K, experiments with platinum/γ-alumina (54 μm), diluted with inert γ-alumina have been performed.
As a first result, illustrated in figure 3, it appeared that at temperatures of about 750 K the observed packed-bed CO conversion is independent on the applied oxygen inlet fraction y_{O2} (7 to 10 vol.%), indicating zero-order in the oxygen concentration. However, at 680 K there

is a small effect of y_{O2} on the conversion noticeable, indicating a slight effect of the reaction kinetics on the conversion rate (at kinetically controlled reaction rates the apparent order in oxygen should be +1). Apparently, at temperatures ≥ 750 K mass transfer controlled conditions are reached completely.

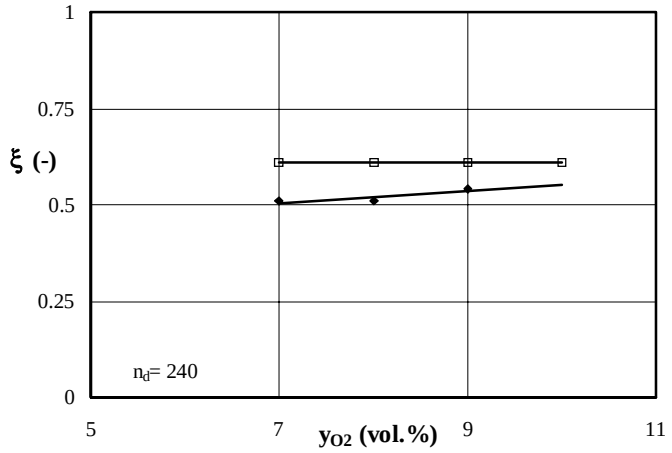

Figure 3. CO conversion versus the oxygen inlet concentration y_{O2}, measured at two operating temperatures T, a dilution ratio of n_d=240, and a superficial gas velocity of u_g =0.6 m/s, ♦T=680 K, □ T=750 K.

According to the kinetic rate expression (equation 5) the conversion should also decrease with y_{in}, the inlet fraction CO. For mass transfer controlled reaction, however, the effect of y_{in} on the observed conversion is not noticeable, because mass transfer is a first order mechanism. In figure 4 the experimentally observed conversion is plotted as a function of the CO inlet fractions for three temperatures and two dilution ratios, n_d=80 and n_d=240, while keeping the bed height constant.

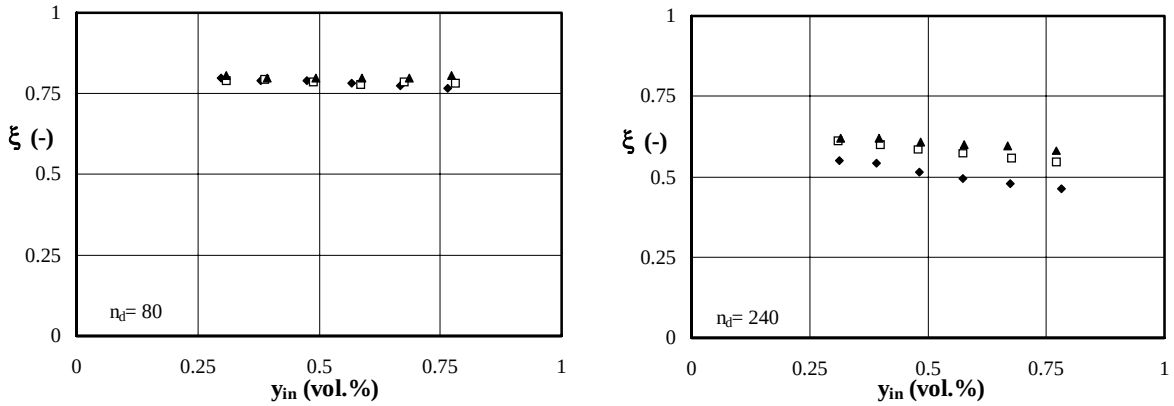

Figure 4. CO conversion versus the carbon monoxide inlet fraction y_{in} at three operating temperatures T and at dilution ratios of n_d=80 (a) and n_d=240 (b); u_g=0.6 m/s, ♦T=680 K, □ T=720 K, ▲ T=750 K.

At a relatively low value for the dilution ratio (n_d=80) the conversion of carbon monoxide is almost independent on the carbon monoxide inlet fraction y_{in}, and this clearly indicates a first order reaction in CO. At the higher dilution ratio of n_d=240, first lower CO conversions are obtained, which is likely as the amount of active material is decreased. Then, the conversion is almost independent on y_{in}<0.5 vol.% only at T=750 K. At the lower temperatures, and for

y_{in}>0.5 vol.%, the conversion is slightly decreasing with y_{in} indicating a reaction order in CO smaller than one. Apparently, upon increasing the fraction of active material (and increasing the inlet fraction CO) a conversion rate mechanism for which both, mass transfer and kinetics, are shown to be important (n_d=240) to one for which only the mass transfer is dominant (n_d=80). This conclusion is elucidated by considering the effect of the operating temperature in more detail.

6.2 Effect of operating temperature

The effect of the temperature becomes more pronounced at higher dilution ratios. Assuming plug flow behaviour of the gas, the apparent reaction rate constant k_{ov}, based on the active catalyst volume, can be estimated from equation 3. In an Arrhenius type of plot, the logarithmic value of this observed reaction rate constant (defined per unit volume of active catalyst), is presented as a function of the inverse temperature for different values of n_d and y_{in}=0.3 vol.%.

Figure 5 shows that larger dilution ratios result in higher values for the experimentally observed apparent rate constants, while the influence of the dilution ratio becomes somewhat less pronounced at higher y_{in}.

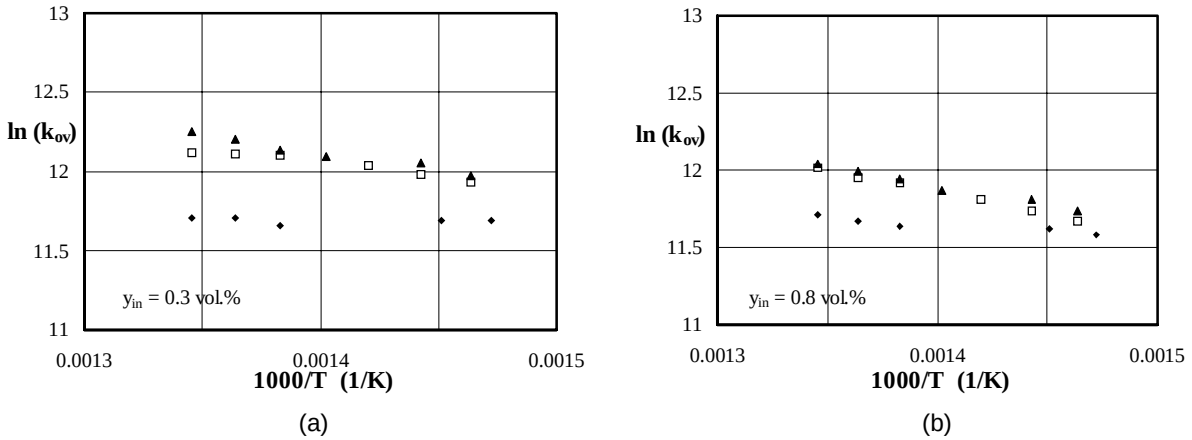

Figure 5. Dependence of the observed apparent rate constant k_{ov} (equation 3) on the operating temperature T and the dilution ratio n_d at a gas velocity of 0.6 m/s for y_{in}=0.3 vol.% (a) and y_{in}=0.8 vol.% (b) Legends: ♦ n_d=80, □ n_d=240, ▲ n_d=480.

These two effects can be analysed by means of a model incorporating particle clusters; intrinsic reaction kinetics are indeed expected to become noticeable at higher dilution ratios due to the increase of the cluster effectivity. The intrinsic reaction kinetics is minus first order in the carbon monoxide concentration (equation 5), and at relatively high y_{in} (with corresponding smaller values for the intrinsic conversion rate), the effect of the dilution ratio diminishes. Although at these CO inlet concentrations the influence of mass transfer limitation decreases, it still remains dominant. This conclusion is supported by considering the apparent activation energies: for example if n_d=240, the apparent activation energy increases from 13 kJ/mole at the CO inlet fraction of 0.3 vol.% to 24 kJ/mole at y_{in}=0.8 vol.%. Both values are close to the diffusional value of approximately 10 kJ/mole.
Herewith, it should be noticed that these observed reaction rate constants are calculated by assuming plug flow behaviour of the gas in the reactor and close to first order behaviour (equation 3). However, it can be shown that for all the experiments the mixers-in-series model (equation 4) already predicts the same relationship between the apparent rate constant and the dilution ratio when assuming that the number of tanks m≥2, indicating that the influence of axial mixing is not very important.

Summarising, at higher dilution ratios and y_{in}>0.5 vol.% two major effects are observed:

- the relative degree of conversion of carbon monoxide becomes gradually more dependent on the carbon monoxide inlet concentration (figure 4), and
- the effect of the temperature becomes more pronounced, resulting in apparent activation energies E_a significantly higher at higher n_d values.

Both effects are elucidated in figure 6.

These phenomena indicate that at higher dilution ratios, and for the higher inlet fractions of CO, the effect of the kinetics of the reaction becomes more important. Over the range of 0.3<y_{in}<0.9 vol.%, the apparent order of the reaction in the CO concentration shifts to values significantly smaller than +1, together with higher apparent activation energies. At higher dilution ratios (n_d>120), the conversion rate becomes dominated by a mechanism where both mass transfer and reaction are involved, whereas at the lower n_d-values only mass transfer is important. Over the inlet concentration range of 0.3<y_{in}<0.5 vol.% the apparent order is in the range of 0.95 to 1.

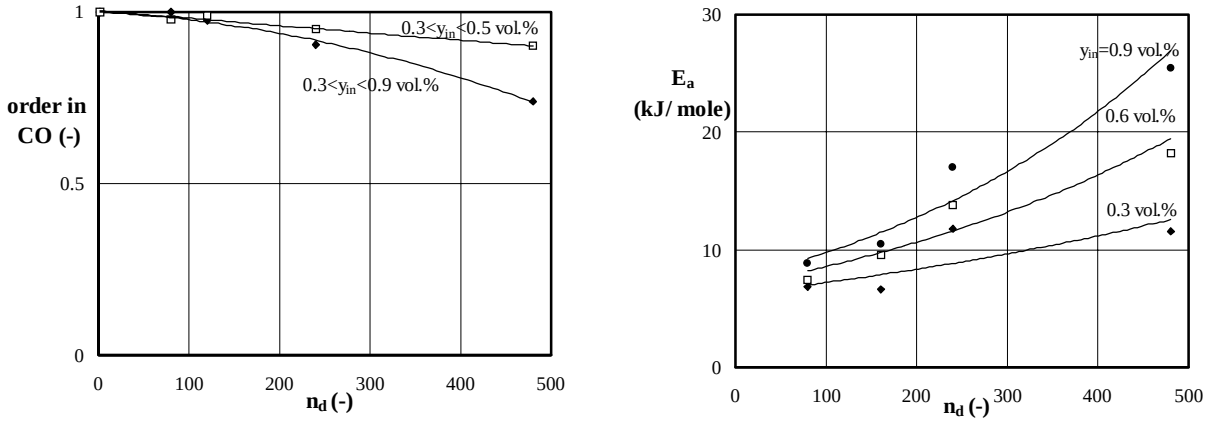

Figure 6. (a) The apparent order in the CO concentration versus n_d for the concentration interval 0.3<c_{in}<0.5 vol.% (□)and for 0.3<c_{in}<0.5 vol.% (♦) for T=750 K, and (b) the apparent activation energy versus the dilution ratio n_d at a superficial gas velocity of u_g =0.6 m/s, T=750 K and for y_{in}=0.3 (♦), 0.6 (□) and 0.9 vol.% (●).

These phenomena can not be explained on the scale of the single particle only, and the occurrence of clusters seems therefore a likely explanation. At still higher temperatures, the overall rate remain practically first order also at the higher dilution rates (see for example chapter 4), indicating that then also mass transfer on a particle scale is dominant.
At this point we should emphasise that the reproducibility of our conversion experiments is very good. In appendix I of this thesis, the reaction rate expression of equation 5 has been used to evaluate the effect of any reaction kinetics on the conversion rate for the individual particles. Although the correct trends are predicted by model calculations, and the intrinsic reaction rates based on equation 5 are predicted to have only a slight influence on the reaction rates, it appears that the actual intrinsic reaction rates are somewhat higher than predicted from an extrapolation of equation 5 to higher temperatures. The influence of the intrinsic reaction rate on the conversion is even less than can be estimated from equation 5.

6.3 Effect of dilution ratio

Both effects, the shift in the order in CO to +1 at the lower dilution ratios, and the corresponding decrease in the value for the activation energy, can be clarified further by plotting the experimentally observed apparent rate constant as a function of the dilution ratio.

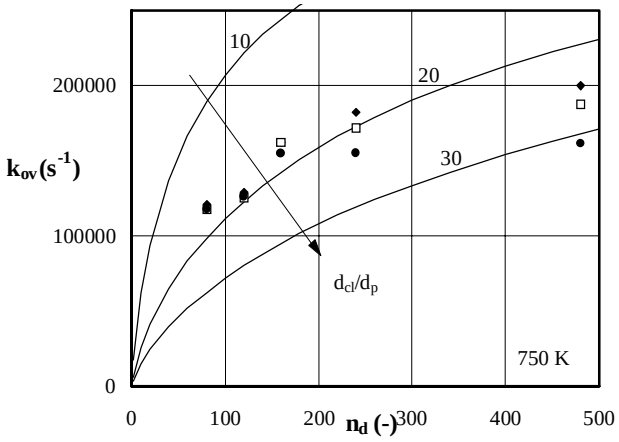

Figure 7. Dependence of the observed apparent rate constant k_{ov} (equation 3) on the dilution ratio n_d at the highest operating temperature T=750 K. The lines represent the calculated apparent rate constant assuming mass transfer limitation and different cluster over particle diameter ratios d_{cl}/d_p at a superficial gas velocity of u_g=0.3 m/s. Legends: ♦ y_{in}=0.3 vol.%, □ y_{in}=0.5 vol.%, ● y_{in}=0.8 vol.%.

In figure 7 the apparent rate constant (derived for a first order reaction, shown to be valid for y_{in}=0.3 vol.%) is shown as a function of the dilution ratio for different y_{in} values and at the highest operating temperature. The lines represent the mass-transfer limited reaction rate constant predicted by the cluster model for three cluster-to-particle diameter ratios at the applied superficial gas velocity of 0.3 m/s. The relations used for additional model input parameters are summarized in appendix II of this thesis.

The effect of diluting the active catalyst with inert material is evident: similar to the model calculations presented in appendix II, k_{ov} increases roughly by a factor of almost 2 at higher dilution ratios. It was shown earlier, that at lower temperatures (not shown) the influence of y_{in} is relatively large, due to the notable influence of the reaction kinetics and the belonging negative order in CO. At higher temperatures and relatively low dilution ratios, the effect of y_{in} vanishes, because mass transfer limitation is then completely controlling the conversion rate. Applying higher dilution ratios (n_d>240) the effect of the inlet fraction increases, even at this temperatures, and obviously, the effect of mass transfer becomes less pronounced. The predicted apparent rate constants agree well with experimental ones derived at low dilution ratios and low carbon monoxide inlet fractions (where mass transfer is dominant), if the cluster-to-particle diameter is taken to be approximately 15 to 20.

The deviation of experimental points from the predicted mass-transfer-control line at high values of the dilution ratio n_d in figure 7 is caused by two effects: 1) the increasing influence of the reaction kinetics, resulting in a reaction order <1, and 2) the diminishing effect of shielding of the active particles, when going to the higher n_d values. Apparently, in that very dilute regime the cluster model is no longer valid. The shift in rate-controlling mechanism is also illustrated by the increasingly negative influence of y_{in} on the experimental results. The best fit for the data points at low dilution ratios for the applied conditions is obtained for a d_{cl}/d_p ratio of 18, which is in very good agreement with the values derived by Moulijn and Van Swaaij (1976) from residence time distribution measurements (for 100 μm particles, ranging from 7 to 14 times d_p).

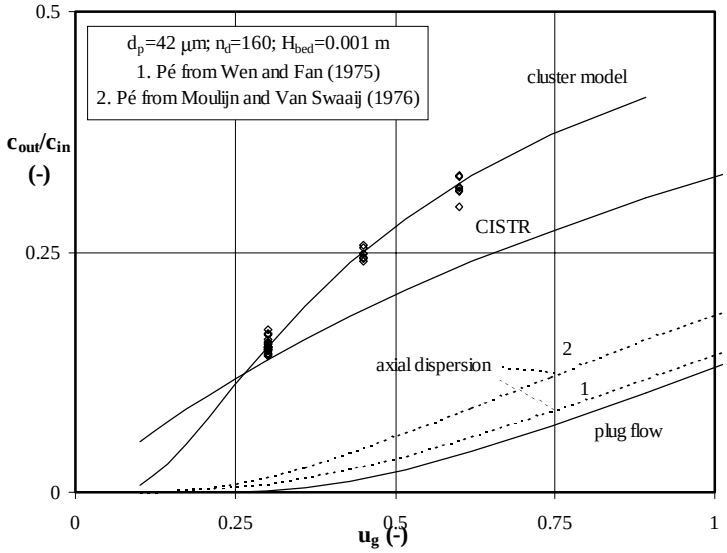

Figure 8. The experimentally observed non-dimensional outlet concentration c_{out}/c_{in} versus u_g for CO oxidation experiments in the packed bed (d_p=42 μm, $k_p\beta/(1+n_d)$=2000 s^{-1}, 1<τ<3 ms. Indicated as solid lines are the curves for ideal contacting and plug flow behaviour of the gas, and ideal contacting plus ideal mixing of the gas. The dashed lines are obtained from a plug flow plus axial dispersion model (with Péclet numbers derived from Wen and Fan (1975, curve 1) and a Péclet number reported by Moulijn and Van Swaaij (1976 curve 2)). The fifth curve presented has been calculated with the cluster model of appendix II.

This section is now completed with two additional remarks:

- One might believe that the observed strong decrease in k_{ov} as a function of n_d should be explained by the unjustified neglect of axial dispersion. From correlations in the literature (f.i. Wen and Fan, 1975) follow that for our conditions almost plug flow behaviour of gas is likely. The important role of cluster formation can be illustrated by comparing the experimental conversion data with predictions from ideal-reactor equations in a plot of the non-dimensional outlet concentration against the superficial gas velocity (figure 8). More details of figure 8 are presented in the introduction of this thesis. The slip of reactant can not be explained by an ideal contacting reactor, as being considered in the plug flow, the axial dispersion or ideally mixed tank model.
- At low dilution ratios, the effect of mass transfer becomes dominant, whereas at n_d>240 a combination of mass transfer and kinetics is likely to occur. We explained this observation also by the diminishing effect of mutual shielding of the active particles. On beforehand, it can also be explained by the corresponding average lower CO volume fractions in the bed. According to equation 5, this should yield higher reaction rates, and consequently more pronounced mass transfer controlled reaction rates. However, if this is the case, larger values for k_{ov} would be obtained at these lower dilution ratios. Hence, the opposite is true, as k_{ov} decreases at these lower dilution ratios, excluding this possibility.

6.4 Effect of average particle diameter and gas velocity

As already indicated by Moulijn and Van Swaaij, the cluster-over-particle diameter is a function of the average particle diameter, d_p. These authors did not determine the influence of gas velocity. In our opinion the particle diameter as well as the superficial gas velocity u_g (both represented by the particle Reynolds number) are important for the existence of effective particle clusters. Therefore the experiments under mass transfer controlled conditions were repeated for two other gas velocities (0.3 and 0.45 m/s), and for two other

particle sizes (42 and 75 μm). In all these experiments, the average particle diameter of the inert material was equal to the particle diameter of the active ones. Similar results as those presented in figure 4 to 7 were obtained for each combination of gas velocity and particle diameter: it is interesting to note that the effect of y_{in}, T and n_d became more pronounced at lower gas velocities and smaller particle diameters, indicating the increasing influence of mass transfer limitation. However, it is in contradiction with the general opinion that mass transfer limitation is less dominant when smaller particles are applied.

Figure 9 and 10 show the influence of the average particle diameter in plots of k_{ov} (a) and Sh^0 (b) against the dilution ratio n_d, and the superficial gas velocity u_g respectively. The belonging operating temperature is 745 K and the CO inlet fraction 0.3 vol.%. The apparent Sherwood number Sh^0 is calculated from the apparent kinetic rate constant, $k_{ov}=k_g a_p$, with the specific particle surface area equal to $6/d_p$:

$$Sh^0 = \frac{k_g d_p}{D} = \frac{k_{ov} d_p^2}{6D} \qquad (6)$$

D represents the bulk diffusion coefficient, that can be calculated with the correlation proposed by Fuller et al. (1962).

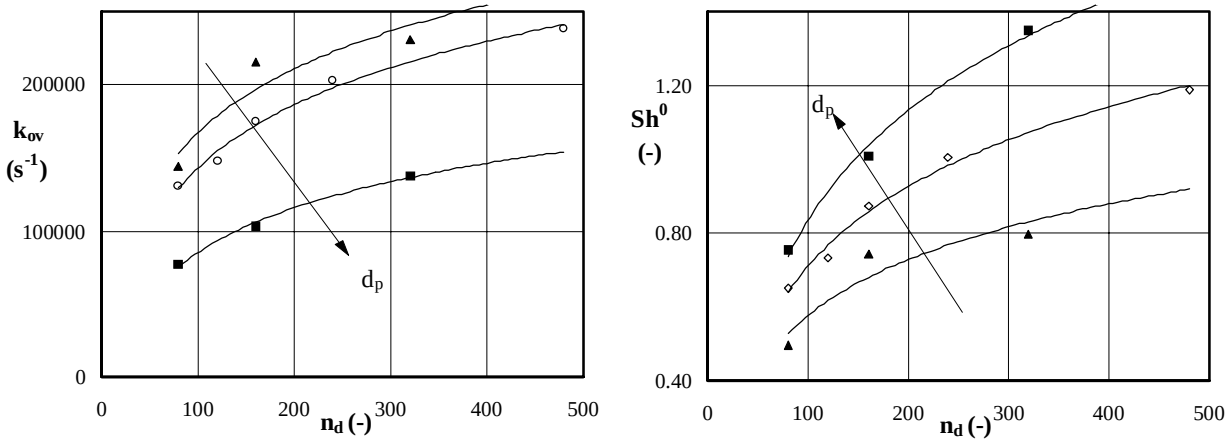

(a) (b)

Figure 9. (a) Dependence of the observed apparent rate constant k_{ov} (equation 3) and (b) the Sh^0 number (equation 6) on the dilution ratio n_d at a gas velocity of 0.3 m/s and an operating temperature T=745 K for different average particle diameters for the inactive as well as the active ones; ▲ d_p=42 μm, ◊ d_p=54 μm, and ■ d_p=75 μm. The solid lines indicate trends.

As expected, k_{ov} and Sh^0 increase with the dilution ratio (figure 9) and the gas velocity (figure 10). For the smaller particle diameters, a higher conversion rate constant is obtained due to the increase of the specific surface area of the particles. However, as shown in figure 9b an 10b the observed Sh^0 number increases with the particle diameter, obviously due to the formation of clusters of a smaller number of particles when larger particles are applied.

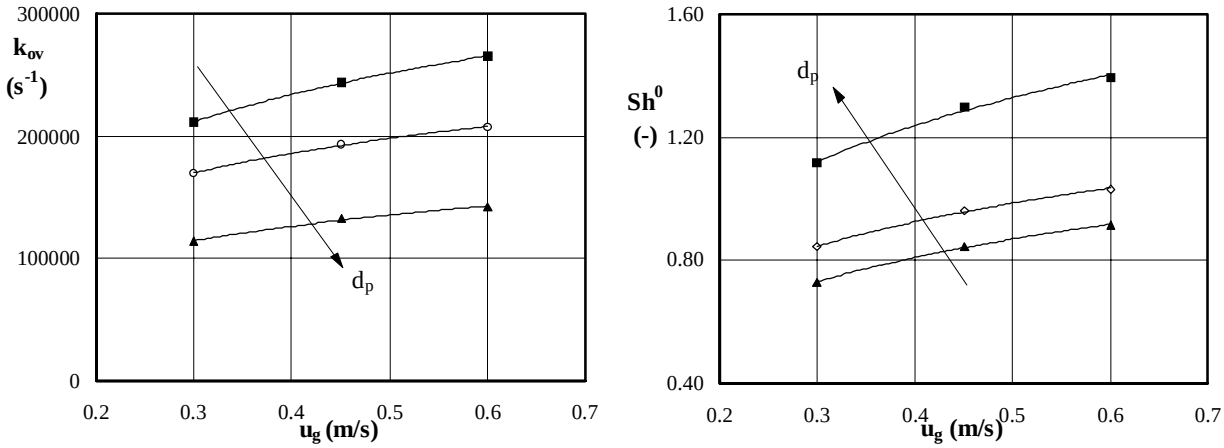

(a) (b)

Figure 10. Dependence of the observed apparent rate constant k_{ov} (equation 3) and the Sh^0 number (equation 6) on the gas velocity u_g at a dilution ratio n_d=160 and an operating temperature T=745 K for different average particle diameters; ▲ d_p=42 µm, ◊ d_p=54 µm, and ■ d_p=75 µm. The solid lines only indicate trends.

This conclusion is confirmed by calculating this effective cluster diameter from the cluster model. In figure 11 the cluster-over-particle diameter has been plotted for the three sizes of particles as a function of the particle Reynolds number at a dilution ratio n_d=160 and y_{in}=0.3 vol.%.

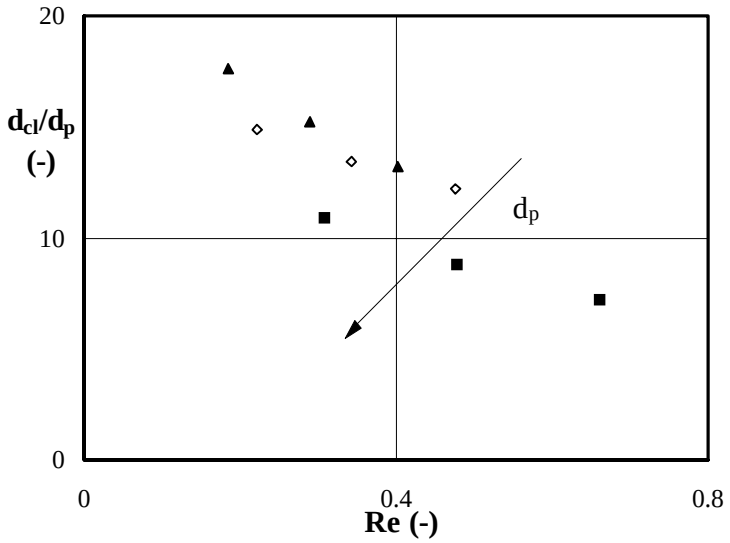

Figure 11. The equivalent effective cluster-over-particle diameter d_{cl}/d_p, derived from experimental results by applying the cluster model, versus the particle Reynolds number Re. Legends: ▲ d_p=42 µm, ◊ d_p=54 µm, and ■ d_p=75 µm.

The size of the clusters depend on both d_p and Re, and are due to both a solid mechanical and a fluid dynamical aspect. Apparently a more or less linear relationship exists between the observed cluster-over-particle diameter and particle Reynolds number. This indicates that $d_{cl} \propto 1/d_p^2$. In other words, the size of the agglomerate depends on the surface area of the single particle. Comparing the experimental results with those of the model simulations presented in appendix II, the conclusion can be drawn that the model qualitatively predicts the influence of the dilution ratio on the apparent rate constant quite satisfactory, if the

correct cluster-over-particle diameter is selected. Unfortunately, no other (cluster) data are available in literature than the ones provided by Moulijn and Van Swaaij. For comparison with previous work, mass transfer data published by other investigators should therefore be re-evaluated on basis of our cluster model.

7 COMPARISON WITH PREVIOUS WORK

According to Moulijn and Van Swaaij, particle clustering is likely for relatively small particles (<500 μm). Unfortunately, the amount of data obtained for such small particles is limited; in fact, only those reported by Bar-Ilan and Resnick (1957) and by Hsiung and Thodos (1977b) have been obtained in a packed bed for particles smaller than 500 μm, and can thus be used for the validation of the proposed cluster model. The latter authors studied the mass transfer in packed beds by using the naphthalene-air system. To avoid saturation of the gas phase Hsiung and Thodos diluted the bed with inert particles, and its influence can be taken into account in the cluster model.

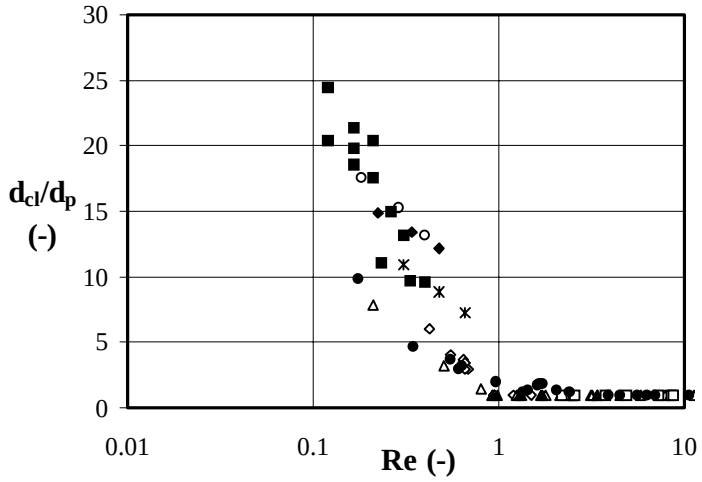

Figure 12. The equivalent effective cluster-over-particle diameter d_{cl}/d_p, derived from the cluster model plotted as a function of the particle Reynolds number Re. Legends: Hsiung and Thodos (1977b): ■ 246 μm, ◊ 345 μm, ▲ 490μm; Bar-Ilan and Resnick (1957): Δ 480 μm, □ 480 μm, ● 377 μm; this study: ★ 75 μm, ♦ 54 μm, ○ 42 μm.

Figure 12 shows the results of our cluster model re-evaluation for the data of the above two references. The calculated cluster-over-particle diameter d_{cl}/d_p is presented as a function of the particle Reynolds number for all particles smaller than 500 μm. Data of the present work (presented in figure 11) are included. This plot seems to indicate that for Reynolds numbers larger than 1 the cluster model is not appropriate anymore. This is confirmed by the fact that at these conditions the observed mass transfer coefficient approaches the one predicted by the original Ranz-Marshall equation.
A conclusion from the re-evaluation of literature data is that the cluster-over particle diameter depends indeed on the Reynolds number. Figure 12 also shows that the results of this work agree very well to those of Hsiung and Thodos (1977b) and Bar-Ilan and Resnick (1957), although these authors applied a different measuring technique and upstream instead of downstream as in this study. Similar to our data, as a rough estimation we can state that the size of the cluster $d_{cl} \propto 1/d_p^2$.

The absolute values for the mass transfer numbers, derived from this work are added in figure 1. The 3 curves shown (curve 11) represent the observed Sherwood number as a function of Péclet number at n_d=160 and T=750 K. As was concluded already, the apparent

Sherwood numbers are (much) higher than those from other studies, obviously due to the dilution of the active material. The same reason can be given for the high value for Sh, derived by Hsiung and Thodos (curve 6 in figure 1). These authors applied somewhat lower dilution ratios, ranging from $20<n_d<100$.

8 CONCLUSIONS

Gas-to-particle mass transfer controlled reaction rates of very small particles (<100 μm) can be measured by applying a new and simple model reaction, viz. the oxidation of carbon monoxide with oxygen over a Pt/γ-alumina catalyst. For CO inlet fractions in the order of 0.3 to 1 vol.% these conditions could be realised already at temperatures ranging from 675 to 750 K. The validity of mass transfer limitation could be checked easily because i) the apparent orders in CO and O_2 fractions shift from negative values and +1 respectively, to +1 and 0 upon transition from the kinetic controlled to the mass transfer controlled reaction rate regime, and ii) the observed apparent activation energy is low, which is in accordance with the temperature dependency of diffusion (approximately 10 kJ/mole). Both these observation are in agreement with the theoretical considerations presented in chapter 1.

Conversion experiments in a small packed bed set-up were carried out while diluting the active material (Pt on γ-alumina) with inert material (γ-alumina).
In summary, the following main observations of the experimental work concerning the catalyst dilution can be given:

- The apparent reaction order in the CO concentration and the apparent activation energies E_a are dependent on the dilution ratio n_d and carbon monoxide inlet fraction y_{in}. At an operating temperature > 730 K, low y_{in} (<0.5 vol.%) and low dilution ration ($n_d<240$) the influence of mass transfer becomes dominant. This effect can be noticed from a shift in the CO reaction order to +1 and a decrease in E_a to roughly 13 kJ/mole, which is close to the diffusional value of 10 kJ/mole.
- The apparent rate constant k_{ov} based on the volume of active catalyst is dependent on y_{in} and n_d. At lower temperatures and higher dilution ratios, k_{ov} decreases significantly with the CO inlet fraction. This effect diminishes, and eventually vanishes, when higher temperatures and/or lower dilution ratios are applied. The conversion rate constant per unit catalyst volume increases by roughly a factor 2 upon increasing the degree of dilution n_d from 50 to 500.
- The apparent Sherwood number increases with particle diameter, whereas k_{ov} decreases.
- At lower gas velocities and for smaller particle diameters, the above mentioned effects of y_{in}, T and n_d on k_{ov} becomes more pronounced, indicating the increasing influence of mass transfer limitation at these conditions.

In general, the effects of agglomeration of particles, or clustering, can be observed especially when the conversion rate is controlled by mass transfer to the cluster surface, that is at the highest temperatures applied and for $n_d<120$.

A cluster model, based on homogeneous distribution of active particles in an inert matrix, has been evaluated. The model takes into account the agglomeration of particles, and an equivalent cluster diameter can be calculated. The experimental results obtained for the diluted bed are explained quite well by the model; the decrease in the observed apparent rate constant k_{ov} with decreasing dilution is caused mainly by the influence of mass transfer from the bulk gas to the cluster surface. The calculated average cluster is in the range from 7 to 18 times d_p, decreasing with increasing gas velocity and particle diameter. These values are comparable with those given by Moulijn and Van Swaaij (1976). Earlier published data from Bar-Ilan and Resnick (1957) and Hsiung and Thodos (1977b) are re-evaluated by means of the cluster model. It is observed that for these data the equivalent cluster-over-

particle diameter is dependent on the particle Reynolds number. Although the authors applied a different measuring technique and mode of operation, the calculated cluster-over-particle diameters agreed very well with the present results. As a first approximation, the cluster diameter for small particles is proportional to $1/d_p^2$.

ACKNOWLEDGEMENT

We acknowledge the financial support of the Dutch Ministry of Economic Affairs through the Netherlands Energy Research Foundation ECN. We also acknowledge M.G.B. Bloem and R. de Wit for their assistance in the experimental and theoretical work.

NOTATION

a	thermal diffusivity	$m^2\ s^{-1}$
a_p	specific surface area of the particle	m^{-1}
Bi_{cl}	Biot number cluster $k_{g,cl}d_{cl}/(2D_{cl})$	-
Bi_p	Biot number particle $k_g d_p/(2D_p)$	-
c	carbon monoxide concentration	mole m^{-3}
c_{O2}	oxygen concentration	mole m^{-3}
c_{in}	reactant concentration inlet	mole m^{-3}
c_{out}	reactant concentration outlet	mole m^{-3}
D	molecular diffusion coefficient	$m^2\ s^{-1}$
D_{cl}	effective diffusion coefficient in cluster	$m^2 s^{-1}$
d_{cl}	cluster diameter	m
d_p	particle diameter	m
D_r	reactor diameter	m
E_a	activation energy	kJ/mole
k_g	gas-to-particle mass transfer coefficient	$m\ s^{-1}$
$k_{g,cl}$	gas-to-cluster mass transfer coefficient	$m\ s^{-1}$
k_{cl}	reaction rate constant per unit volume of cluster	s^{-1}
k_{ov}	apparent reaction rate constant	s^{-1}
k_p	intrinsic reaction rate constant	s^{-1}
m	number of tanks in series, defined by equation (4)	-
M_{cat}	total amount of catalyst in reactor	kg
n_d	dilution ratio	-
$Pé_m$	molecular Péclet number $u_g d_p/D$	-
R	gas constant	J $mole^{-1}K^{-1}$
$R(c)$	molar rate of reaction per unit volume of catalyst	mole $m^{-3}s^{-1}$
Re	Reynolds number $\rho_g u_g d_p/\eta_g$	-
Sc	Schmidt number $\eta_g/(\rho_g D)$	-
Sh	Sherwood number $k_g d_p/D$	-
Sh^0	apparent Sherwood number defined by equation 6	-
T	operating temperature	K
u_g	superficial gas velocity	$m\ s^{-1}$
y_{in}	inlet fraction CO	vol.%
y_{O2}	inlet fraction oxygen	vol.%
ΔT_{ad}	adiabatic temperature rise	K
ε_{cl}	cluster porosity	-
ϕ_{cl}	Thiele modulus of a spherical cluster in eq. (2)	-
ϕ_p	particle Thiele modulus by eq. (2)	-
η_{cl}	cluster effectiveness factor, defined by eq. (2)	-

η_{cl}^*	cluster effectiveness factor, defined by eq. (2)	-
η_g	gas viscosity	Pa s
η_{ov}	overall effectiveness factor, defined by eq. (1)	-
η_p	particle effectiveness factor, defined by eq. (2)	-
η_p^*	particle effectiveness factor, defined by eq.(2)	-
ρ_p	catalyst density	kg m^{-3}
ρ_g	gas density	kg m^{-3}
ξ	conversion	-

REFERENCES

Appel P.W., Newman J., 1976, Application of the limiting current method to mass transfer in packed beds at very low Reynolds numbers, *A.I.Ch.E. J.*, **22**, 979

Aris, R., 1992, Comments on Mitigation of Backmixing via Catalyst Dilution, *Chem. Engng. Sci.*, **47**, 507

Bar-Ilan M., Resnick W., 1957, Gas phase mass transfer in fixed beds at low Reynolds numbers, *Ind. Eng. Chem.*, **49**, 313

Van den Bleek C.M., Van der Wiele K., Van den Berg P.J., 1969, The effect of dilution on the degree of conversion in fixed bed catalytic reactors, *Chem. Engng. Sci.*, 1969, **24**, 681

Chu J.C., Kalil J., Wetteroth W.A., 1953, Mass transfer in a fluidized bed, *Chem. Eng. Prog.*, **49**, 141

Dwivedi P.N., Upadhyay S.N., 1977, Particle-fluid mass transfer in fixed and fluidized beds, *Ind.Engng. Chem. Process Des.Dev.*, **16**, 157

Fedkiw P.S., Newman J., 1982, Mass-transfer coefficients in packed beds at very low Reynolds numbers, *Int. J. Heat Mass Trans.*, **25**, 935

Fuller E.N., Schettler P.D., Giddings J.C., 1966, A new method for predicting of binary gas phase diffusion coefficients, *Ind. Engng. Chem.*, **58**, 18

Glicksman L.R., Joos F.M., 1980, Heat and mass transfer in fixed beds at low Reynolds numbers, *J. Heat Trans.*, **102**, 737

Gunn D.J., de Souza J.F.C., 1974, Heat transfer and axial dispersion in packed beds, *Chem. Engng. Sci.*, **29**, 1363

Hermann E., 1991, *Katalysierte Stickoxidreduktion in der stationären und zirkulerenden Wirbelschicht*, thesis University of Karlsruhe.

Hlavácek V., Votruba J., 1974, Experimental study of multiple steady states in adiabatic catalytic systems, *Advances in Chemistry series, Chemical reaction Engineering II*, Evaston

Ho T.C., White B.S., 1991, Mitigation of backmixing via catalyst dilution, *Chem. Engng. Sci.*, 46, 1861

Hobson M., Thodos G., 1951, Mass transfer: laminar flow of gases through granular beds, *Chem. Eng. Prog.*, **47**, 370

Hsiung T.H., Thodos G., 1977a, Mass-transfer in gas-fluidized beds: measurement of actual driving forces, *Chem. Engng. Sci.*, **32**, 581

Hsiung T.H., Thodos G., 1977b, Mass-transfer factors from actual driving forces for the flow of gases through packed beds (0.1<Re<100), *Int. J. Heat Mass Trans.*, **20**, 331

Kumar H.B., Sublette K.L., Shah Y.T., 1993, Effect of high voidage on mass transfer coefficients in a fluidized bed, *Chem. Engng. Comm.*, **121**, 157

Kumar S., Upadhyay S.N., Mathur V.K., 1977, Low Reynolds number mass transfer in packed beds of cylindrical particles, *Ind. Engng. Chem. Proc. Des. Dev.*, **16**, 1

Kunii D., Levenspiel O., 1991, *Fluidization Engineering*, Butterworth-Heinemann, Boston

Kunii D., Suzuki M., 1967, Particle-to-fluid heat and mass transfer in packed beds of fine particles, *Int. J. Heat Mass Trans.*, **10**, 845

Martin H., 1978, low Péclet number particle-to-fluid heat and mass transfer in packed beds, *Chem. Engng. Sci.*, **33**, 913

Miyauchi T., Matsumoto K., Yoshida T., 1975, Liquid film coefficient of mass transfer in low Péclet number region for sphere packed beds, *J. Chem. Engng. Japan*, **8**, 228

Moulijn J.A., Van Swaaij W.P.M., 1976, The correlation of axial dispersion data for beds of small particles, *Chem. Engng. Sci.*, **31**, 845

Nelson P.A., Galloway T.R., 1975, Particle-to-fluid heat and mass transfer in dense systems of fine particles, *Chem. Engng. Sci.*, **30**, 1

Petersen E.E., 1965, *Chemical Reaction Analysis*, Prentice Hall, New Jersey, 194

Petrovic L.J., Thodos G., 1968, Mass transfer in the flow of gases through packed beds, *Ind. Engng. Chem. Fund.*, **7**, 274

Psyllos A., Papayannakos N., Philippopoulos C., CO oxidation in a Carberry reactor: manifestation of reaction

kinetics by controlled reaction/transport, *J. Chem. Engng. Japan*, **27**, 693
Ranz W.E., Marshall Jr. W.R., 1952a, Evaporation from drop: part I, *Chem. Eng. Prog.*, **48**, 141
Ranz W.E., Marshall Jr. W.R., 1952b, Evaporation from drop: part II, *Chem. Eng. Prog.*, **48**, 173
Resnick W., White R.R, 1949, Mass transfer in systems of gas and fluidized solids, *Chem. Eng. Prog.*, **45**, 377
Resnick W., Golt M., 1981, Particle-to-gas mass-transfer measurements and coefficients in fixed beds at low Reynolds numbers, *Int. J. Heat Mass Trans.*, **24**, 387
Rietema K., 1991, *The dynamics of fine powders*, Elsevier Science, London
Schlünder, E.U., 1977, On the mechanism of mass transfer in heterogeneous systems - in particular in fixed beds, fluidized beds and on bubble trays, *Chem. Engng. Sci.*, **32**, 845
Selke W.A., Bard Y., Pasternak A.D., Aditya S.K., 1956, Mass transfer rates in ion exchange, *A.I.Ch.E.J.*, **2**, 468
Sofekun O.A., Rollins D.K., Doraiswamy L.K., 1994, A random particle model for catalyst dilution, *Chem. Engng. Sci.*, **49**, 2611
Tsotsas E., 1992, On mass transfer, dispersion, and macroscopical flow distribution in packed tubes, *Chem. Engng. Proces.*, 31, 181
Upadhyay S., Tripathi G., 1975, Liquid-phase mass transfer in fixed and fluidized beds of large particles, *J. Chem. Engng. Data*, **20**, 1
Van der Ham A.G.J., Prins W., Van Swaaij W.P.M., 1994, Regenerative, high temperature desulfurization of coal gas in a circulating fluidized bed, in *Circulating Fluidized Bed Technology IV*, Pennsylvania, Engineering Foundation, 657
Verver , A.B., 1984, *The catalytic oxidation of hydrogen sulphide to sulphur in a gas-solid trickleflow*, thesis University Twente
Vollert J., Wether J., 1994, Mass transfer and reaction behaviour of a circulating fluidized bed reactor, *Chem. Engng. Technol.*, **17**, 201
Voltz S.E., Morgan C.R., Liederman D., Jacob S.M., 1973, Kinetic study of carbon monoxide and propylene oxidation on platinum catalysts, *Ind. Engng. Chem. Prod. Res. Dev.*, **21**, 294
Wakao N., Tanisho S., 1974, Chromatographic measurements of particle-gas mass transfer coefficients at low Reynolds numbers in packed beds, *Chem. Engng. Sci.*, **29**, 1991
Wakao N., Tanaka K., Nagai H., 1976, Measurements of particle-to-gas mass transfer coefficients from chromotographic adsorption experiments, *Chem. Engng. Sci.*, **31**, 1109
Wen C.Y., Fan L.T., 1975, *Models for flow systems and chemical reactors*, Dekker, New York, 167
Williamson J.E., Bazaire K.E., Geankoplis C.J., 1963, Liquid-phase mass transfer at low Reynolds numbers, *Ind. Engng. Chem. Fund.*, **2**, 126
Wilson E.J., Geankoplis C.J., 1966, Liquid mass transfer at very low Reynolds numbers in packed beds, *Ind. Engng. Chem. Fund.*, **5**, 9
Yerushalmi J., Turner D.H., Squires A.M., 1976, The fast fluidized bed, *Ind. Engng. Process Des. Dev.*, **15**, 47
Yerushalmi J., Cankurt N.T., 1979, Further studies of the regimes of fluidization, *Powder Technol.*, **24**, 187
Yu Yao Y.-F., 1984, The oxidation of CO and Hydrocarbons over noble metal catalysts, *J. Catal.*, **87**, 152

CHAPTER 3

SOLIDS HOLD-UP AND PRESSURE GRADIENT IN A SMALL LABORATORY RISER

ABSTRACT

In the developed region of a small laboratory riser (internal diameter 13 mm) the flow properties of three different types of powders (Geldart's classification AC: silica d_p=111 μm, ρ_p=426 kg/m^3; A: γ-alumina d_p=65 μm, ρ_p=1375 kg/m^3; BA: glass beads d_p=65 μm, ρ_p=2749 kg/m^3) have been investigated at ambient conditions. One of the main objectives of this study is to investigate whether or not the pressure gradient along the column length can be used directly to calculate the solids hold-up in such a small scale unit.

The average solids hold-up is measured for various gas and solids fluxes by two different techniques. The first method is to trap the solids during stationary operation between a number of quick-closing valves. The other method involves the direct measurement of the solids velocity by a new contactless method based on the recording of the characteristic luminescence of phosphorous material (54 μm, 4000 kg/m^3), added in small amounts to the bed material. A one-dimensional model is used to interpret the results.

The newly developed, fluoroptic, method is an appropriate method to determine the solids velocity in such a small riser. It is potentially suitable for measurements at actual reactor conditions, and in the acceleration zone of the riser. Significant differences between solids hold-up values, derived from pressure drop measurements on the one hand and those from the quick-closing valves method on the other, were observed for glass beads and silica, but not for γ-alumina. For A-type particles the pressure drop technique might yield solids hold-up values within reasonable accuracy. However, for larger and denser particles, solids-wall friction must be taken into account. For lighter particles the gas-wall friction must be accounted for. For none of the particle types applied, it was possible to predict the solids hold-up and pressure drops simultaneously within reasonable accuracy with the one-dimensional model by adjusting the value for the solids-wall friction coefficient only. Literature correlations, relating the slip velocity in the riser to operating conditions and particle properties, are inaccurate. An improved correlation is proposed, which predicts the solids hold-up in our small scale riser with much better accuracy (±20%) than relations proposed in literature. Also solids hold-up data from literature are predicted much better (±40%) with our correlation.

Especially for A powders cluster formation is likely to be an important phenomenon in explaining the differences between measured and calculated solids velocities. From the fluoroptic method indirect evidence for clusters can be obtained: a small fraction of fluoroptic material, with a higher density than the bed material, is transported at the same velocity as the bed material.

1 INTRODUCTION

"Fast fluidization is a technique for bringing a high velocity gas into intimate contact with fine solids in what is essentially an entrained, dense suspension" (Yerushalmi *et al.*, 1976). In the riser section of such a fast fluidized bed the gas phase velocity exceeds the transport velocity of the solids. These solids are carried over the top of the column, separated from the gas stream by means of cyclones, and re-introduced at the bottom from a storage vessel or standpipe. When high specific transfer rates or short contact times are required (e.g. when dealing with fast reactions), this type of reactor is being considered as a good alternative for the conventional bubbling fluidized beds. Possible advantages are (Contractor

and Chaouki, 1991; Patience *et al.*, 1992):

- High solids throughput and short, controllable residence times for solids and gas;
- Essentially plug flow of gas;
- A small degree of solids back-mixing (Cankurt and Yerushalmi, 1978);
- Good/excellent contact between gas and solids (high heat and mass transfer rates);
- High heat transfer rates to wall or immersed surfaces, and almost thermal uniformity across the reactor length;
- Good operating flexibility; independently adjustable solids and gas fluxes;
- Ease of solids circulation, e.g. for the external regeneration or cooling of solids, and
- Handling of cohesive solids, which are difficult to fluidize in conventional fluidized beds.

Known commercial-scale riser processes are the Fluidized Catalytic Cracking (FCC), the Synthol reactor for Fischer-Tropsch synthesis (Contractor and Chaouki, 1991), calcination of aluminium trihydrate to high purity alumina (Reh, 1986), and combustion or gasification of various fuels such as coal and/or biomass. According to Werther (1994) nowadays about 250 FCC units are processing one quarter of the world's crude oil production, and some 400 CFB combustion units with a total thermal power of 23000 MW are in operation. Various new industrial processes are described by Reh (1995).

A large amount of data, describing the axial hold-up profile is published in literature. There is general consensus on the existence of an axial and radial solids hold-up profile. The axial hold-up profile in the riser is generally composed of a dense region at the bottom where acceleration of the particles takes place, a dilute zone in the middle of the reactor, and again a slightly denser region at the top due to exit effects. It is accepted that the averaged slip velocity of the solids particles, i.e. the difference between the interstitial gas velocity and the mean velocity of the solids particles, deviates from the terminal velocity of the individual particles. As a 'rule of thumb' the ratio between the slip velocity and the terminal velocity, is taken to be 2, although values up to 10 to 40 are reported. These high values are attributed to several causes: i) acceleration of the particles, ii) friction between solids and wall, iii) radial segregation of solid particles or/and iv) the formation of clusters of particles. Much work has been done in the past to explain the effect of acceleration of particles, and to derive friction coefficients between the particles and the wall. Recent studies are focused on the other causes: with the advent of powerful computers, research activities were directed towards a fundamental understanding of the hydrodynamic properties of fast fluidized beds. Complex two-dimensional hydrodynamic models, based on fundamental principles of mass and momentum balances have been developed (see e.g. Zhang *et al.,* 1991; Nieuwland, 1995; Kuipers and Van Swaaij, 1997). Results of such comprehensive models indeed indicate the occurrence of segregation in risers. However, they are not able to predict the formation of clusters of particles, which have been observed in experimental studies (f.i. Ishii *et al.,* 1989; Zou *et al.,* 1994). Although the topic of particle clusters is relatively new, some conceptual ideas have been put forward already by Yerushalmi *et al.* (1978).

Only a limited amount of studies in literature is devoted to reactor performance in relation to gas-to-particle mass or heat transfer, or gas-solids contacting (Masai *et al.*, 1985; Dry *et al.*, 1987, 1992a, 1992b; Sun and Grace, 1990; Van der Ham *et al.*, 1994; Ouyang and Potter, 1993b, 1994; Vollert and Werther, 1994). Such studies use have frequently been carried out while using small scale laboratory reactor units in which the solids hold-up is a key parameter. This parameter can not be easily accessed directly, and often pressure drop experiments are used to derive it. Friction between solids and wall or gas and wall are then usually neglected. However, this assumption is seldom verified by *direct* comparison between the pressure gradients and the solids hold-up. One of the main objectives of this work is to investigate whether the pressure gradient in a laboratory riser can indeed be used to derive the solids hold-up directly. In the following section relevant literature on pressure gradients and solids hold-up is discussed chronologically.

2 PREVIOUS WORK

In an early paper Hariu and Molstad (1949) trapped solids (Geldart's A and B-powders) in two small riser systems by means of two three-way plug valves, positioned at the in- and outlet of the riser. They measured the average solids hold-up and pressure drop and stated that the pressure drop can be regarded as the sum of acceleration of solids, the static head of gas and solids, and the solids-wall or gas-wall frictional contribution. Because the solids acceleration term can be neglected in the so-called 'developed' region of the bed, and since the gas hold-up as well as the gas -wall friction contributions to the pressure drop are generally small, two major contributions to the pressure drop remain: the solids hold-up and the solids-wall frictional contribution. For the relatively large sand particles a large part of the pressure gradient could be attributed to particle acceleration in the bottom section. Due to experimental failures when A-powder (cracking catalyst) was applied, the problem whether friction can be neglected could not be solved for these particles.
In 1962 Stemerding reported that for FCC-particles (A-powder) the observed pressure drop over a certain riser length was significantly higher than the one that could be calculated on basis of the solids hold-up only. To account for the difference, he calculated an additional pressure drop for solids-wall friction with a fitting value of the friction coefficient. The author did not measure the solids hold-up directly, but derived it while assuming that the slip velocity was identical to the terminal falling velocity of the single particle. Nowadays it is generally accepted that for A-powders slip velocities can be much higher than these terminal velocities, due to f.i. particle clustering or radial segregation. Although Stemerdings relation is widely applied and referred to, his friction coefficients are derived on basis of doubtful assumptions.
Konno and Saito (1969) measured friction coefficients for B-type particles by comparing pressure drop data with solids hold-up data. These data were derived from particle velocities, which were measured in a small column. Unfortunately the measuring technique was not described in detail. A solids-wall friction coefficient was defined in a way similar to Stemerding. Surprisingly, for these particles the slip velocity was observed to be almost equal to the terminal velocity of the single particle. According to the authors, the additional pressure drop should be attributed to solids-wall friction, but the effect of solids-wall friction on the slip velocity is insignificant.
Reddy and Pei (1969) also measured particle velocities (using a photographic technique). For their B-type particles, the slip velocity was only slightly higher than the terminal velocity of the individual particle. Again the additional pressure drop was attributed to solids wall friction, and a correlation for the friction coefficient was proposed.
Van Swaaij *et al.* (1970) demonstrated by direct measurements that in the developed region of a riser, and for a typical A-powder, the shear stress is in the main flow direction at low solids volume fractions ($\beta<0.05$), yielding higher pressure drops than would be expected on basis of solids hold-up only. This result is in line with the findings of other authors. However, at higher values for the solids hold-up, lower pressure drops were observed than can be derived from the solids hold-up only. Van Swaaij *et al*. explained this by a negative shear stress due to the downward flow of solids close to the wall. From their data it can be derived that there is a relatively small difference between the measured pressure drop and the one estimated from the solids hold-up only (±10%).
Using coarser particles (B and D-type) Capes and Nakamura (1973) determined the average particle hold-up by means of a series of quick-closing valves. Differences between slip - and terminal velocities were also analayzed on basis of solids-wall friction, and again a correlation for the particle friction coefficient was developed.
General correlations for the solids-wall friction coefficient in (both horizontal and vertical) solids transport lines have been presented by Yang (1974). His correlations were initially based on data given in the early paper of Hariu and Molstad (1949); in later work additional

data obtained by Konno and Saito (1969) and Capes and Nakamura (1973) were added to improve these original equations (Yang, 1977; 1978). Considering Yang's papers, it can be concluded that his relations are developed specifically for coarse particles (Geldart's type B and D), and not for A-powders.

A direct comparison between the experimentally observed solids hold-up in the developed region (quick-closing valves) and the solids hold-up derived from pressure drop measurements (neglecting friction and acceleration of particles) was made by Arena *et al.* (1986) for a BA powder. The differences between the two could be quite significant (20-70%); the solids hold-up values derived from the pressure gradient were always higher than those observed from direct weighting of the trapped material. In a later paper (1988) they compared the hydrodynamic behaviour of two circulating fluidized bed units with different internal diameters, for A-type (FCC) as well as for a BA-powders (glass beads). The experimental technique was similar as in the previous paper, and the authors now concluded that a comparison of the solids hold-up derived from pressure drop data and the one measured directly confirmed the validity of the pressure gradient technique. An interesting observation was that the ratio between the slip - and the terminal falling velocity increased at higher gas velocities, for the smaller particles and in the larger diameter unit. They were in the range of 3 to 22 for FCC particles and 1 to 11 for glass beads.

Relatively large B and D particles were applied in a small riser by Breault and Mathur (1989). The solids volume fraction could be measured by means of a sensor spool at a position of about 1 m from the inlet of the riser. The friction coefficient relation proposed by these authors yields much higher values than those predicted by the correlations of the authors quoted before. Larger particles could indeed give rise to higher values for the friction coefficient. It is however somewhat doubtful whether the solids velocities were actually measured outside the acceleration region (or the decelerating region at the top of the riser), as was suggested by the authors, because they were measured only at approximately 1 m above the solids inlet.

Pagliolico *et al.* (1992) compared the solids hold-ups calculated from the pressure gradient with the solids hold-ups from slide valve experiments for an A-powder. They found a good agreement at the lower solids concentrations (< 1.6 vol.%) and high gas velocities. At higher solids hold-ups a significant difference was observed, which was attributed to acceleration. The authors demonstrated that for their riser system for these conditions the solids-wall friction could be neglected.

In a study by Plasynski *et al.* (1994) the effects of the operating pressure (1 to 42 bar) on friction were investigated for A, B and D type powders. The solids velocities were measured with magnetic coil probes. For the coarser particles it appeared that the slip velocity was almost equal to the terminal falling velocity of the individual particle. Besides, the solids-wall friction coefficient was reasonably well predicted by Yang (1978). For the B-particles however, there was a strong difference between the slip velocity and the terminal falling velocity, and the authors proposed an empirical correlation for the particle velocity. From particle friction factor calculations, they concluded that, for these particles and at high operating pressures, the frictional pressure drop due to solids and gas, could not be calculated as separate, independent parameters.

The operating conditions, the properties of the particles applied, and the correlations obtained for the friction coefficient from these studies are summarized in table I. From the literature cited above, it can be derived that:

i) For all type of particles, the slip velocity is larger than, or equal to the terminal velocity of the individual particle, depending on the type of material used. For coarser particles the difference between slip velocity and terminal velocity becomes smaller (see Konno and Saito, 1969; Arena *et al.*, 1986, Plasynski *et al.*, 1994).

ii) The difference between the actual measured pressure drop and the one based on solids hold-up only, should be attributed to solids-wall friction in case of B or D-type powders.

This additional pressure drop can be quite significant. For A-powders, however, it is much less important (see e.g. Breault and Mathur, 1989; Pagliolico *et al.*, 1992).

iii) The difference between slip and terminal velocity is likely to be caused by friction between solids and wall for B-type particles, whereas for A-powders it should be attributed to another cause, such as the formation of particle clusters or the radial segregation of solids.

2.1 This study

The objective of this work is to investigate whether the pressure gradient in a small laboratory riser can be used to calculate the solids hold-up directly, but also to verify the above mentioned conclusions. The solids hold-up is determined by means of two direct techniques: i) quick-closing valves and ii) an optical, non-intrusive technique that is based on the addition to the bed material of phosphoric material and measurement of its velocity. Using this last-mentioned technique, developed by Wagenaar *et al.* (1995), the probes used do not interfere with the flow inside the riser column, which is in contrast to many other methods (e.g. Hartge *et al.*, 1986, 1988). The fluoroptic technique is especially attractive because it can be used for both the acceleration and the developed zone. Besides, it is also potentially suitable for measurements at actual reactor conditions.

3 THE ONE-DIMENSIONAL MODEL OF A CFB RISER SECTION

The key parameter in a fast fluidized bed reactor is the solids hold-up β. It can not be easily assessed directly, and often the pressure drop is used to derive it. This solids hold-up is directly related to the average particle velocity by means of the solids mass balance. For gas-particle flow in a vertical tube, there are two ideal cases: i) the solids and the gas move upward with the same velocity (no-slip condition), and ii) the difference between gas and solids velocity (slip velocity) is equal to the terminal falling velocity of the individual particle. However, it has been widely accepted that the slip velocity between solids and gas can exceed the terminal velocity of a single particle considerably. This can be explained by (1) the acceleration of the solid particles (2) the friction between the solids and the wall (3) radial segregation of solids, and (4) formation of clusters of particles.

ad (1): At the inlet of the riser, the solid particles are accelerated by the gas. Near the bottom the solids hold-up is higher than in the so-called developed region of the fast fluidized bed, because of a lower average particle velocity (for instance Hariu and Molstad, 1949).

ad (2): Due to friction between solid particles and the wall the particles are decelerated; as a consequence the average particle velocity is decreased and the solids hold-up is higher than in case this friction is absent (a.o. Stemerding, 1962; Capes and Nakamura, 1973; Yang, 1974, 1978).

ad (3): Lateral particle segregation yields a dilute core region and a dense annulus structure. This local heterogeneity causes lower average particle velocities, and consequently high solids hold-ups (a.o. Rhodes *et al.*, 1988; Hartge *et al.* 1986, 1988; Bader *et al.*, 1988; Nieuwland, 1995).

ad (4): The particles are not carried individually by the gas, but enclosed in a dense strand of solids (cluster). The effective drag of the gas on the cluster is less than on the individual particles, by which the slip velocities increases (Yerushalmi *et al.*, 1976; Grace and Tuot, 1979; Horio *et al.*, 1989; Zou *et al.*, 1994).

Table I. Correlations to estimate the solids-wall friction coefficient in the riser of a CFB.

authors	D_t(m)	d_p (μm)	ρ_p (kg m^{-3})	type of material	u_g (m s^{-1})	G_s (kgm^{-2}s^{-1})	remarks	$f_p=4f_s$
Stemerding (1962)[a]	0.051	65		FCC catalyst	3..15	300..600	pressure drop	0.012
Reddy and Pei (1969)[a]	0.10	100..270		glass	7.9..14.2	0..10	photographs	$0.184u_p^{-1}$
Konno and Saito (1969)	0.0265 0.0468	120..1050, 120..530, 3250, 1440	2500, 8900, 1350, 1440	glass, copper, hairy vetch, millet	2..20	10..100	pressure drop, pitot tube	$0.114\sqrt{gD_t}\,u_p^{-1}$
Capes and Nakamura (1973)	0.0762	470..1080, 256..2340, 1780, 3400	2470..2900 7510..7700 1085 911	glass, steel, rape seed, polyethylene	3..30	0..150	valves	$0.206u_p^{-1}$
Yang (1978)	0.00678 -0.0762	110..3400	910..7850	various materials	2..30	0..270	data from various authors	$a\cdot(1-\varepsilon)/\varepsilon^3(u_t(1-\varepsilon)/(u_g^*-u_p))^c$ $u_g/u_t<1.5\Rightarrow\begin{cases}a=0.0410\\c=-1.020\end{cases}$ $u_g/u_t>1.5\Rightarrow\begin{cases}a=0.0126\\c=-0.979\end{cases}$
Kato *et al.*(1986)	0.04, 0.066, 0.096	43, 50, 120..385	840, 1500, 900, 1300	FCC catalyst, alumina	0.7..10	0.5..40	pressure drop, moving tube	$0.152\left(\frac{u_p}{\sqrt{gD_t}}\right)^{-0.77}$
Matsumoto *et al.* (1986)	0.02	520..2930, 210, 470	2500 8700	glass copper	5..20	30..100	pressure drop optical method	$0.04\left(\frac{u_g}{u}\right)^2\left(\frac{u_t}{\sqrt{gD_t}}\right)$
Breault and Mathur (1989)	0.038	300, 452, 296	2575, 2337, 2244	sand, limestone, gypsum	3.9..7.6	40..100	pressure drop	$48.8(1-\varepsilon)/\varepsilon^3u_p^{-1}$

[a] From Capes and Nakamura (1973)

Table IIa. Basic equations of the one-dimensional model (equations 1 to 4)

	steady state equation	developed region
solids		
continuity (equation 1a/b)	$\frac{\partial}{\partial z}\left(\rho_p u_p (1-\varepsilon)\right) = 0$	$u_p = \frac{G_s}{\rho_p (1-\varepsilon)}$
momentum (equation 2a/b)	$-\rho_p (1-\varepsilon) u_p \frac{\partial u_p}{\partial z} + C_d (1-\varepsilon)\varepsilon \frac{6}{4d_p}\frac{1}{2}\rho_g \left(u_g^* - u_p\right)\left\|u_g^* - u_p\right\| - 4f_s \frac{(1-\varepsilon)\rho_p u_p \left\|u_p\right\|}{2D_t} - \rho_p (1-\varepsilon) g = 0$	$-\rho_s (1-\varepsilon) u_p \frac{\partial u_p}{\partial x} + C_d (1-\varepsilon)\varepsilon \frac{6}{4d_p}\frac{1}{2}\rho_g (u_g^* - u_p)\left\|u_g^* - u_p\right\| - 4f_s \frac{(1-\varepsilon)\rho_s u_p \left\|u_p\right\|}{2D_t} - \rho_s (1-\varepsilon) g_x = 0$
		$u_p = u_g^* - \sqrt{\frac{\rho_p d_p}{\rho_g C_{ds}} \frac{4}{3} \varepsilon^{2.65} \left(g + \frac{4f_s u_p^2}{2D_t g}\right)}$
gas		
continuity (equation 3a/b)	$\frac{\partial}{\partial z}\left(\rho_g u_g^* \varepsilon\right) = 0$	$u_g^* = \frac{u_g}{\varepsilon}$
momentum (equation 4a/b)	$-\rho_p (1-\varepsilon) u_p \frac{\partial u_p}{\partial z} - \rho_g \varepsilon u_g^* \frac{\partial u_g^*}{\partial z} - 4f_g \frac{\varepsilon \rho_g \left\|u_g^*\right\| u_g^*}{2D_t} - 4f_s \frac{(1-\varepsilon)\rho_p \left\|u_p\right\| u_p}{2D_t} - \rho_p (1-\varepsilon) g - \rho_g \varepsilon g - \frac{\partial P}{\partial z} = 0$	$-\frac{\partial P}{\partial z} = 4f_g \frac{\varepsilon \rho_g \left\|u_g^*\right\| u_g^*}{2D_t} + 4f_s \frac{(1-\varepsilon)\rho_p \left\|u_p\right\| u_p}{2D_t} + \rho_p (1-\varepsilon) g + \rho_g \varepsilon g$

Table IIb. Constitutive equations for the one-dimensional model (equations 5 to 7)

	equation	author
drag coefficient (equation 5)	$C_{ds}=\begin{cases}\frac{24}{Re_p}(1+3.6\,Re_p^{0.687}) & Re_p<1000\\ 0.44 & Re_p>1000\end{cases}$	Schiller and Naumann (1935)
drag correction factor (equation 6)	$C_d = C_{ds}\cdot\varepsilon^{-2.65}$	Richardson and Zaki (1954)
gas-wall friction (equation 7a/b)	$f_g=\begin{cases}0.16\,Re_g^{-1} & Re_g<2000\\ 0.079\,Re_g^{-0.25} & 2000<Re_g<10^5\end{cases}$	Bird *et al.* (1960)

During the last decades several models have been proposed to describe the hydrodynamics of circulating fluidized beds. Early models (a.o. Stemerding, 1962; Yang, 1974) were developed to estimate the effect of acceleration, and to predict the solids concentration, solids velocities and pressure drops. The friction coefficient was a key parameter in explaining the differences between observed and calculated pressure gradients. With the advent of modern computers, more comprehensive modelling of CFB's became possible and the effect of segregation could be predicted. Some of these models are from the core-annulus type (e.g. Nakamura and Capes, 1973); others assume that gas and solids phases can be considered as continuous media (a.o. Tsuo and Gidaspow, 1990; Nieuwland 1995). Nowadays most of the theoretical studies are focused on predicting the presence of clusters of particles in dilute suspensions (e.g. Tsuo and Gidaspow, 1990). However, due to the assumption of continuous media these models are unable to describe cluster formation on a scale much smaller than the spatial resolution of the numerical mesh (O'Brien and Syamlal, 1994). Only very recently, Hoomans *et al.* (1998) applying a mixed Langrangian / Eulerian calculation schemes were able to demonstrate the existence of clusters in CFD models. Before these type of calculations can be used for development and design, their is still a long way to go.

A complete description of the complex hydrodynamics of the flow structure in a riser is beyond the scope of this study. Here it is assumed that the solids- and gas velocity are uniform across the bed diameter.
Based on this assumption a one-dimensional model is adopted (see e.g. Yang, 1974).

Upon deriving the appropriate equations the following assumptions have been made:
- Steady state situation;
- Gas and solids are continuous phases;
- Radial velocity and porosity gradients are absent;
- Gas behaves ideally;
- Spherical particles are considered, of uniform size and density;
- In- and outlet effects can be neglected, and
- Friction between solid phase and gas phase can be described by means of a Fanning type of equation.

The steady-state conservation equations for mass and momentum balances are presented in table IIa (e.g. Yang , 1974). Equations (1a) to (4a) contain four independent variables, i.e., interstitial velocities of gas and solids u_g^* and u_p, the void fraction ε, and the total pressure drop $-(\partial P/\partial z)$. They require solids fluxes, gas velocities, particle properties and correlations for drag force, gas-wall and solids-wall friction coefficients as input parameters, and can be solved numerically by means of a Runge-Kutta procedure.

For the drag coefficient of the single particle the correlation of Schiller and Naumann (1935) is frequently used, although several other relations are proposed in literature (see review by Flemmer and Banks 1986, and Haider and Levenspiel, 1989). It is generally adopted that the drag coefficient should be corrected for the presence of other particles by multiplying equation 5 with the Richardson-Zaki equation (equation 6, Richardson and Zaki, 1954). The gas-wall friction coefficient is described by the Hagen-Poiseuille equation in the laminar regime (Re<2100, equation 7a), and the Blasius formula up to Re $=10^5$ (equation 7b). The constitutive equations applied in this work are given in table IIb. For the friction factor f_p the possible empirical correlations are already given in table I.

As mentioned before, the experimental work in this study is limited to the 'developed' region of the fast fluidized bed, that is outside the acceleration region; the experimental conditions are chosen such that the acceleration terms in equations (1a) to (4a) can be neglected. The resulting equations for the developed region are equations 1b to 4b in table IIa.

4 EXPERIMENTAL PART

The experiments are carried out in a small CFB system, given in figure 1. It is made of transparent glass to facilitate the observation of the flow behaviour in the apparatus, and consists of the riser section (1), two cyclones, a solids flow measuring device (2), a collecting vessel/standpipe (3), and a riser inlet section (4). The riser section is made of a 13 mm I.D., 2 m long glass tube, provided with four squeezing valves at different axial positions. Solids, fed to the reactor through a standpipe and an inlet section, are transported in the riser by air (at ambient conditions) introduced at the bottom of the riser.

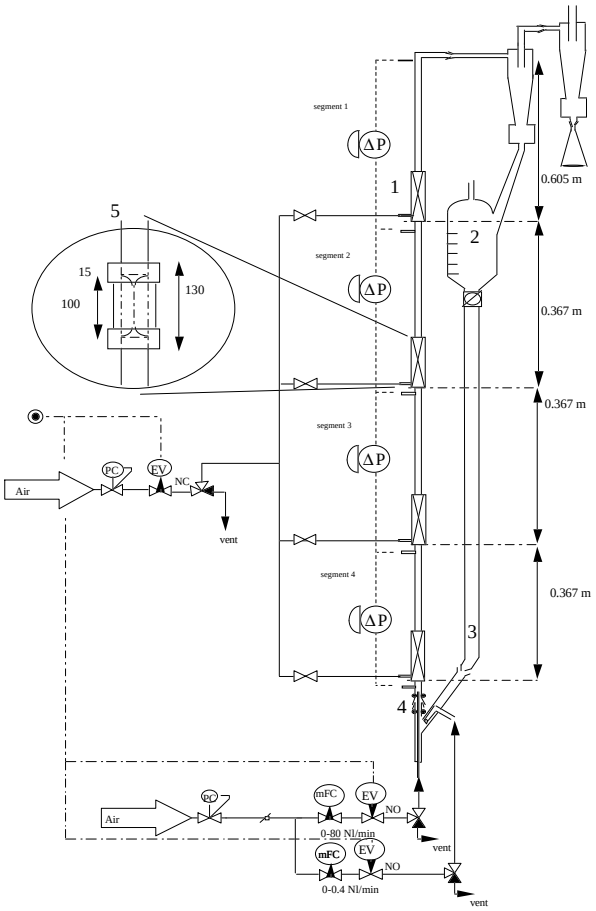

Figure 1. Flowsheet of the CFB system

1. Riser section (I.D. 13 mm)
2. Solids flow measuring device
3. Collecting vessel
4. Riser inlet section
5. Detail squeezing valve

Table III. Particle properties

type of particle	d_p	ρ_p
silica (Degussa)	111	426
γ-alumina (Engelhard)	65	1375
glass	65	2749
fluoroptic material	54	4000

The solids flux is controlled by means of an

additional gas inlet device at the bottom of the standpipe, and the solids flow is determined by a solids flow measurement device (2), which is positioned between the riser and the standpipe. This solids flow meter is a small container, in which the formation rate of a packed bed can be determined visually after closing a slide-valve at the bottom. Accumulation of solids is measured over a time period short enough to ensure that build-up or depletion of solids in different parts of the system does not affect the overall flow behaviour. The riser is equipped with five pressure points as indicated, and pressure gradients are measured with a U-tube water-manometer, viz. as the difference with the atmospheric pressure. Two mass flow controllers are used to adjust the gas flow.

The solids hold-up in the riser of our small circulating fluidized bed system can be measured with two different techniques. The first method involves the direct measurement of the solids velocity by a new non-intrusive method based on the recording of the characteristic luminescence of phosphorous material, which is added in small amounts to the bed material (Wagenaar *et al.*, 1995). This method will be discussed in more detail in the next section. The other method is to trap the solids during stationary operation between a number of quick-closing squeezing valves in various parts of the riser tube. A detailed drawing of such a squeezing valve is given in figure 1; it consists of a 130 mm long holder in which a 100 mm long rubber element is constructed. When air is fed to the squeezing valve (3 bar), the valve is closed almost instantaneously, due to the flexibility of the isopropylene squeezing. The time needed to close the valve completely after the onset of pressurization was observed to be in the order of 0.01 s. The solids hold-up in the riser of our CFB is determined at steady state operation (when no changes in pressure profile along the riser length and in gas and solids flow are observed anymore) by closing the valves: two magnetic valves are used to interrupt the gas and solids feed flows simultaneously with the closing of the squeezing valves. The amount of the solids in each section of the riser is collected and weighted.
The powders used in this study for the hold-up experiments are glass beads, γ-alumina (Engelhard Al-3912P) and silica powder (Degussa, Sipernat 22); relevant particle properties are listed in table III.

5 MEASUREMENT OF THE SOLIDS VELOCITY WITH THE FLUOROPTIC METHOD

5.1 Experimental set-up

Average solids velocities in risers of CFB set-ups can be calculated from the results of solids hold-up measurement by, for example, quick-closing valves. It can also be measured directly by using optical and capacitance probes (Hartge *et al.*, 1986; Ishii *et al.* 1989) or a laser-doppler technique (Yang *et al.*, 1990). In the optical or capacitance technique the probes must be inserted into the riser tube. This is a serious disadvantage, because disturbance of the flow can give rise to errors in the calculation of the average solids velocity. Besides, it has been shown that the optical probes must be calibrated extensively (Nieuwland, 1995).

The laser-doppler technique, a non-intrusive method, can only be used in very diluted systems ($\beta<0.01$) or small units. An extensive overview and comparison of different techniques to determine solids concentration and velocity in gas-solids two-phase flows has been given by Nieuwland (1995).

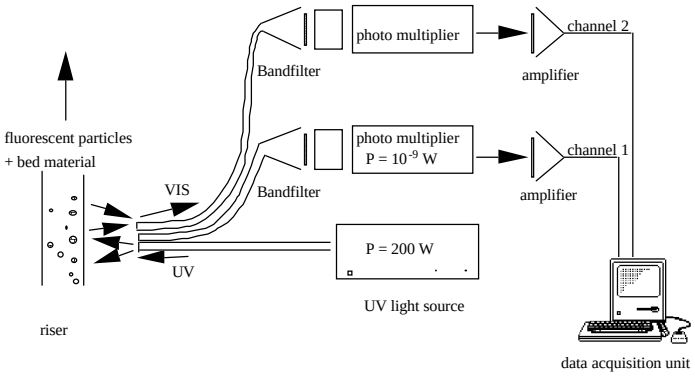

Figure 2. Scheme of the fluoroptic measurement set-up

In this study a different method for the direct measurement of solids velocities is adopted, more or less similar to the optical method applied by Matsumoto *et al.* (1986) for relatively large glass and copper particles. It also resembles the experimental techniques applied by Kuramoto *et al.* (1986) and Morooka *et al.* (1989), who treated microspherical particles with fluorescent dyes to follow the bulk motion of the particulate phase. Our fluoroptic measurement method, originally developed by Wagenaar *et al.* (1995) for non-contact measurement of particle temperatures, is based on the characteristic luminescence of phosphors. These are materials capable of emitting radiation when subjected to ultraviolet radiation. The luminescent centre is an ion of one of the rare-earth metals (for more details see f.i. Blasse and Bril, 1970). The emitted light from the fluoroptic material, travelling through a spot, can be collected with separate glass fiber probes. In this study the probes used can be positioned outside the tube; there is no interference with the flow through the riser. Similar to the laser-doppler technique, it is expected that the fluoroptic measurement technique can be used for diluted systems only. The fluoroptic technique is potentially suitable for measurements at actual reactor conditions, because well-suited quartz fibers can be applied at higher temperatures. Besides, it is attractive because it can be used for both the acceleration and the developed zone. The solids velocity is determined by mixing the bed material (850 gram glass beads, 500 gram γ-alumina or 200 gram silica) with a small amount of fluoroptic material (approximately 500 mg). This fluoroptic material is made by mixing the phosphor PNN/R-/R-A Y_2O_2S:Eu (Philips) into a melt of lead-mono-silicate $PbO(SiO_2)_{1.03,}$ on a 10 wt.% basis. After solidification of the mixture it is crushed and sieved: the properties are listed in table III. Figure 2 shows the principles of the measuring technique schematically. Phosphorous material is subjected to radiation coming from a 200 W UV-source through a quartz fiber cable. The light emitted by the fluoroptic material, which passes through the measuring spot, is collected by two external glass fiber probes, positioned at a known distance from each other. The bed material emits blue light, and the fluoroptic material only red. This (λ> 600 nm) is then separated, transformed into an electric signal and amplified by fotomultipliers. These signals are further processed by a data-acquisition unit. Calculation of the velocity of the fluoroptic material requires a cross-correlation method, yielding the cross correlation density, by which the lag time between the two signals, g and h, can be calculated:

$$\mathrm{Corr}(g,h,\tau) = \int_{-\infty}^{\infty} g(\tau+s)\cdot h(s)ds \qquad (8)$$

Obviously cross-correlation of two functions is useful only, if the signals are similar. In each individual experiment the solids velocity was calculated based on a sampling time of 1 sec (31 kHz), which allows the average solids velocity to be averaged over approximately 300 measurements.

5.2 Calibration

Prior to the determination of the solids velocity in the riser, a calibration set-up was used. A disc rotor on which a small amount of fluoroptic material had been deposited, was rotated at a known angular velocity. Angular velocities derived from the fluoroptic method are compared with the ones measured with a stroboscope. In figure 3a typical output signals recorded by the probes are presented; the belonging cross correlation density is given in figure 3b. The distinct maximum indeed indicates a good similarity between the two signals of channel 1 and 2.

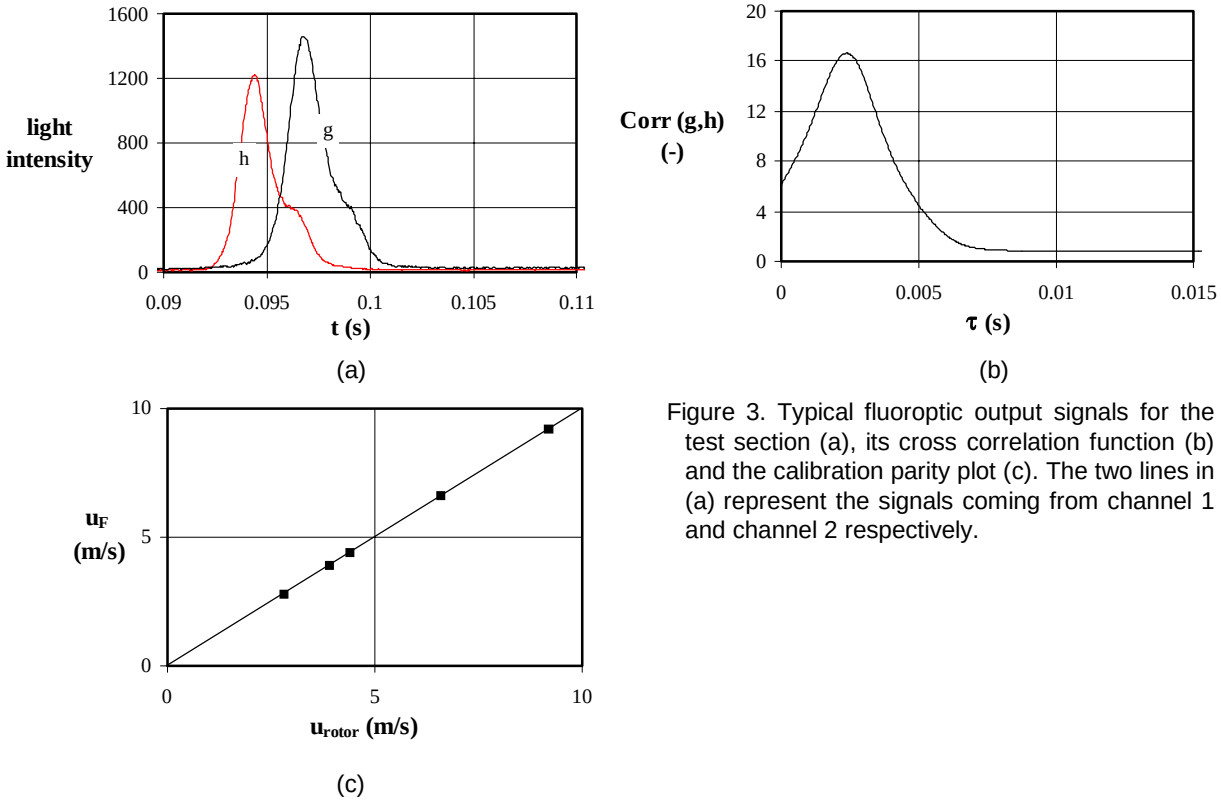

Figure 3. Typical fluoroptic output signals for the test section (a), its cross correlation function (b) and the calibration parity plot (c). The two lines in (a) represent the signals coming from channel 1 and channel 2 respectively.

In figure 3c the results of this calibration method are shown: there is very good agreement between the velocities derived from the fluoroptic method and the ones measured by the stroboscope.

5.3 Measurement of the solids velocity in the riser

The signals coming from the fluoroptic material in the riser differ significantly from the output signal obtained in the calibration. This is shown in figure 4a. The peaks indicate clusters of particles passing through the UV beam: individual fluoroptic particles are detected by the probes, which is confirmed by additional video-measurements. Because the probes are placed outside the fast fluidized bed, they do not interfere with the flow pattern.

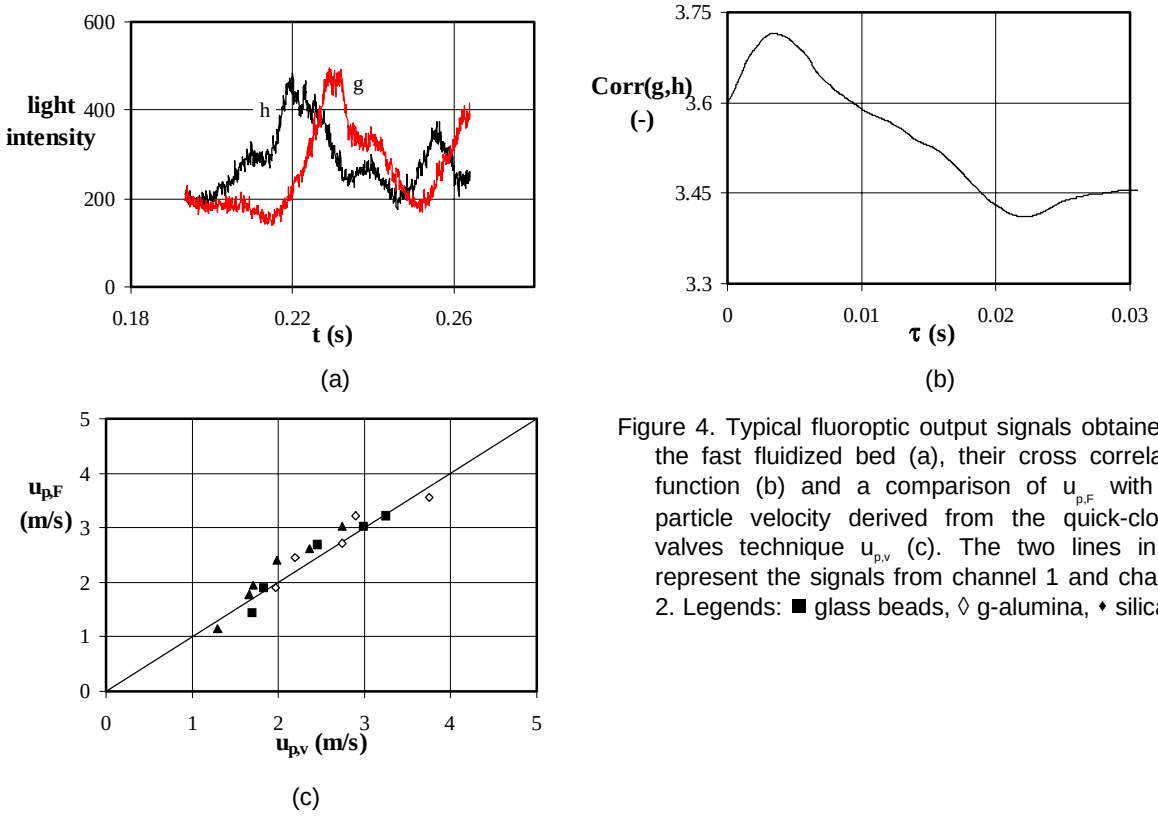

Figure 4. Typical fluoroptic output signals obtained in the fast fluidized bed (a), their cross correlation function (b) and a comparison of $u_{p,F}$ with the particle velocity derived from the quick-closing valves technique $u_{p,v}$ (c). The two lines in (a) represent the signals from channel 1 and channel 2. Legends: ■ glass beads, ◊ g-alumina, ♦ silica.

Therefore the two signals from the probes are quite similar. This is confirmed by figure 4b, in which the cross correlation density function of these signals is given. Values for the solids hold-up, obtained by means of the fluoroptic method, are compared with those calculated by means of the squeezing valves: in figure 4b the parity plot of both methods is given for all types of particles applied. Measurement of the average solids hold-up by means of the fluoroptic method appears to be possible within reasonable accuracy (±10%), despite the differences in particle properties.

6 RESULTS AND VALIDATION

6.1 Pressure gradient in an empty tube

To determine the pressure gradient contribution of the gas-wall friction term in the first term in the right-hand side of equation (4), this gradient was measured at various air flow rates. The two lines in figure 5 represent the calculated pressure gradient per meter riser length using the gas-wall friction coefficient derived for the laminar regime (equation 7a), and the one valid for the turbulent regime (Blasius, equation 7b). By comparing both lines with the experimental data points in figure 5 this last equation is shown to be the best description of the gas-wall friction coefficient over the entire gas range applied. Differences in experimental results for the four different tube segments are perhaps related to small variations in the ratio of glass-wall over valve-wall surface.

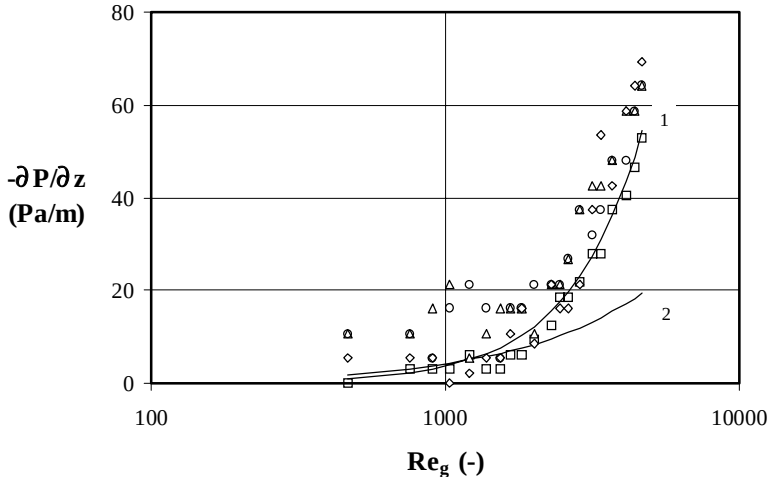

Figure 5. Pressure gradient $-\partial P/\partial z$ over the four segments of the empty riser versus the Reynolds number $Re_g=\rho_g u_g D_t/\eta$. The two lines represent values calculated values from the Blasius relation (1) and the laminar flow relation (2) for the friction coefficient f_g. Legends: □=top segment no. 1, Δ=segment 2, o=segment 3 and ◊=bottom segment no. 4.

6.2 Pressure gradient versus solids flux

In figure 6 the pressure gradient versus the solids flux is shown for glass beads (a), γ-alumina (b) and silica (c). The various symbols refer to the four different segments of the riser and two different gas velocities.

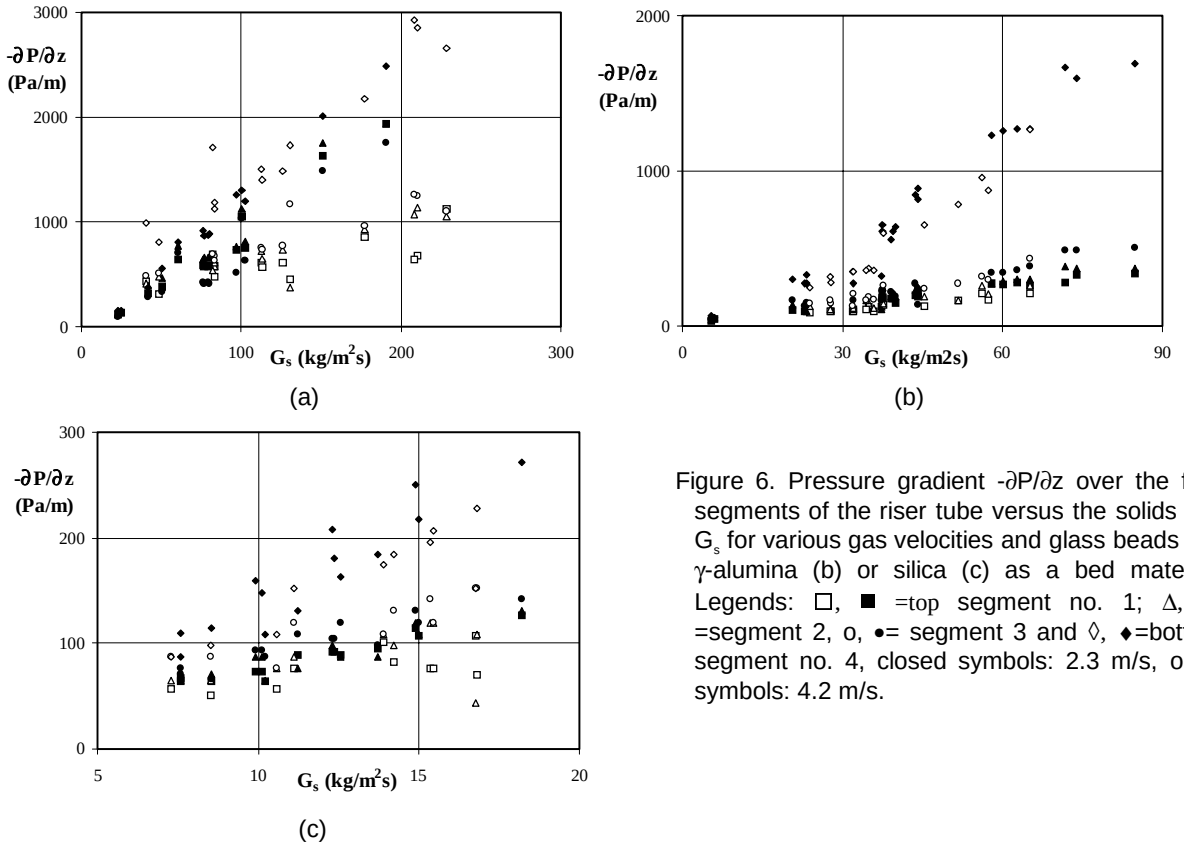

Figure 6. Pressure gradient $-\partial P/\partial z$ over the four segments of the riser tube versus the solids flux G_s for various gas velocities and glass beads (a), γ-alumina (b) or silica (c) as a bed material. Legends: □, ■ =top segment no. 1; Δ, ▲ =segment 2, o, ●= segment 3 and ◊, ♦=bottom segment no. 4, closed symbols: 2.3 m/s, open symbols: 4.2 m/s.

The relative empty tube contribution (see figure 5) to the total pressure drop depends of coarse on the density of the bed material, and is less than 5% for the glass beads, and less than 10% when γ-alumina is applied. However, it can contribute up to 20% of the total pressure drop for the lighter silica powder. As a consequence, the influence of the pressure drop due to gas-wall friction is quite significant for the silica material.
For each particle type the pressure gradient across the bottom section of the riser (segment 4: diamonds in figure 6) is higher than the one over the higher located segments, which is most likely due to the acceleration term in equation (4a) in table IIa. For glass beads this effect is less clear at a gas velocity of 2.3 m/s (closed symbols), but for γ-alumina and silica the acceleration effect is observed for both gas velocities applied. The ratio between the pressure drop of segment 4 over the one of segment 1 depends on the type of particles. Apparently the length of the acceleration zone is not the same for all three particle types. This phenomenon can be predicted qualitatively by the one-dimensional model. The length of the acceleration zone (for instance defined as the height in the riser column, where the solids velocity equals 99% of the end velocity) is in the order of 10 to 15 cm for glass beads, but only 1 to 2 cm for silica-powders used. Considering the length of the bottom segment no. 4, which is 36.7 cm, the effect of acceleration of particles must be negligible in segments 1 to 3 (the three top sections in figure 1). This is supported by the results in figure 6. The average solids hold-up values reported later in this chapter are derived from these three riser sections. From figure 6 another phenomenon is clear: increasing the gas velocity for the glass beads results in lower pressure drops. Following the definition of Karri and Knowlton (1991) this means that these experiments are carried out in the fast fluidization regime. For the other particle types the gas velocity has no marked effect on the observed pressure drop, and likely these data are obtained in the first part of the pneumatic transport regime.

6.3 Pressure gradient and solids hold-up

In this study one of the main points of interests is whether the pressure gradient over a riser length can be used to derive the solids hold-up directly. The solids hold-up measured by using the valves β_V and the hold-up calculated from the pressure gradient over the riser length (corrected for the empty-tube pressure drop) $\beta_{\Delta P}$, are presented in the parity plots of figures 7 for glass beads (a), γ-alumina (b) and silica (c), respectively. For glass beads (ρ_p=2749 kg/m^3) β_V is clearly smaller than $\beta_{\Delta P}$. The difference is likely to be due to particle-wall friction, as the influence of gas-wall friction can be neglected (< 5%). For γ-alumina, a reasonable agreement between the two measurement techniques is obtained.
For silica, just like for the glass particles, the quick-closing valve technique generally yields lower values for the solids hold-up than expected on basis of the pressure drop.

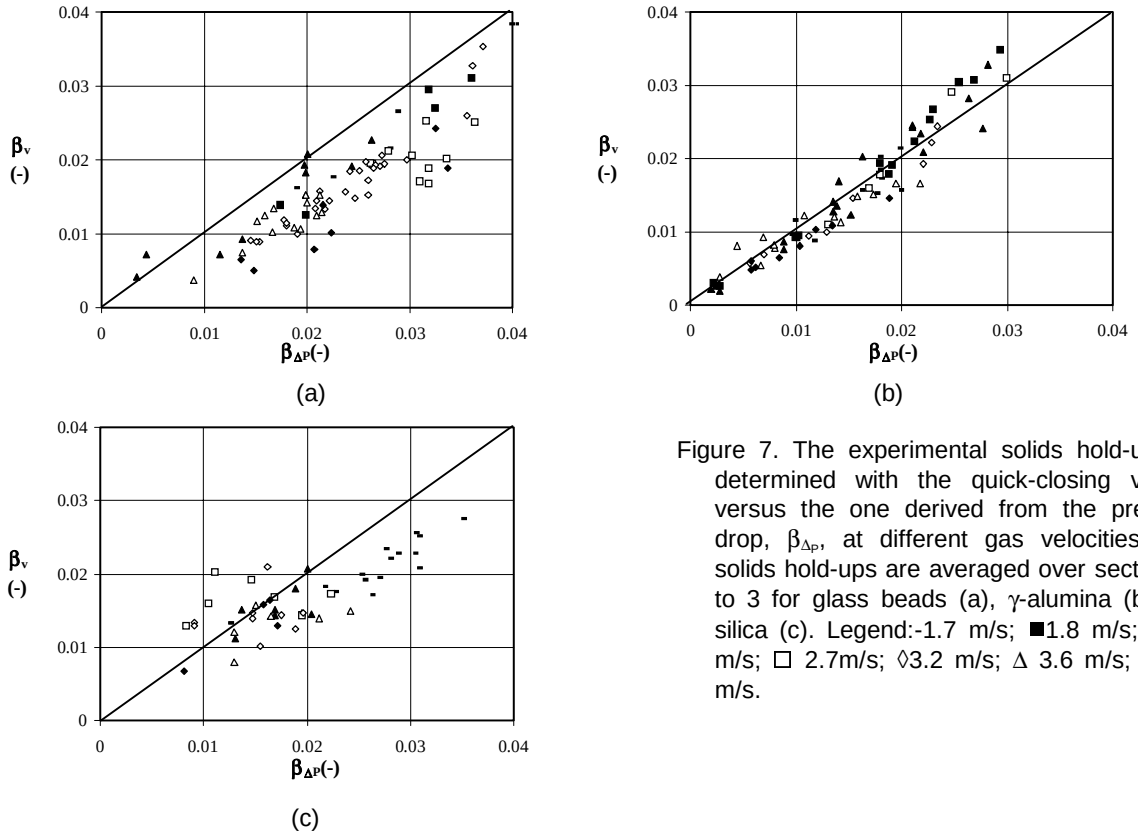

Figure 7. The experimental solids hold-up, β_v, determined with the quick-closing valves, versus the one derived from the pressure drop, $\beta_{\Delta P}$, at different gas velocities. The solids hold-ups are averaged over sections 1 to 3 for glass beads (a), γ-alumina (b) and silica (c). Legend:-1.7 m/s; ■1.8 m/s; ▲2.3 m/s; □ 2.7m/s; ◊3.2 m/s; Δ 3.6 m/s; ♦ 4.3 m/s.

In this case however, the effect of solids-wall and/or gas-wall friction on the total pressure is relatively large because of the low solids density (ρ_p=426 kg/m^3). This fact also explains the relatively large scatter in data for these low-density particles. Neglecting the solid-wall friction seems to be allowed for alumina only, and not for glass beads. For silica gas-wall friction must be accounted for, which is supported by the observed contribution of the gas-wall frictional term to the total pressure drop (up to 20%).

Apparently, for certain conditions solids-wall friction coefficient is an important parameter, and quite some work has been done in previous studies to determine this friction coefficient. value can be calculated on basis of equation 4b in table IIa. This relation can be rewritten, and ε and u_p (based on own results from the quick-closing valves or fluoroptic measurements) can be introduced:

$$f_p = \frac{\left(-\frac{\partial P}{\partial x} - (1-\varepsilon)(\rho_p - \rho_g)g - 4f_g \rho_g u_g^2 / (2\varepsilon D_t) \right)}{G_s u_p / (2D_t)} \qquad (9)$$

Figure 8 shows a comparison of calculated f_p values (open squares) with those obtained by some of the literature correlations listed in table I. For glass beads the values for the friction coefficients are in reasonable agreement with those predicted by the correlation of Yang (1978) and Konno and Saito (1969). On the other hand, for γ-alumina and silica it appears that those correlations more or less overestimate the wall-solids friction coefficient values found in this work. The difference between literature correlations and our experimental results might be attributed to the different bed diameters applied in earlier work and the coarse and dense powders, which were usually applied to establish these correlations.

However, the available 'simple' literature correlations for the solid-wall friction coefficient are incapable to predict the differences between the results for our particles, as the effect of particle type is not well reflected by such correlations.

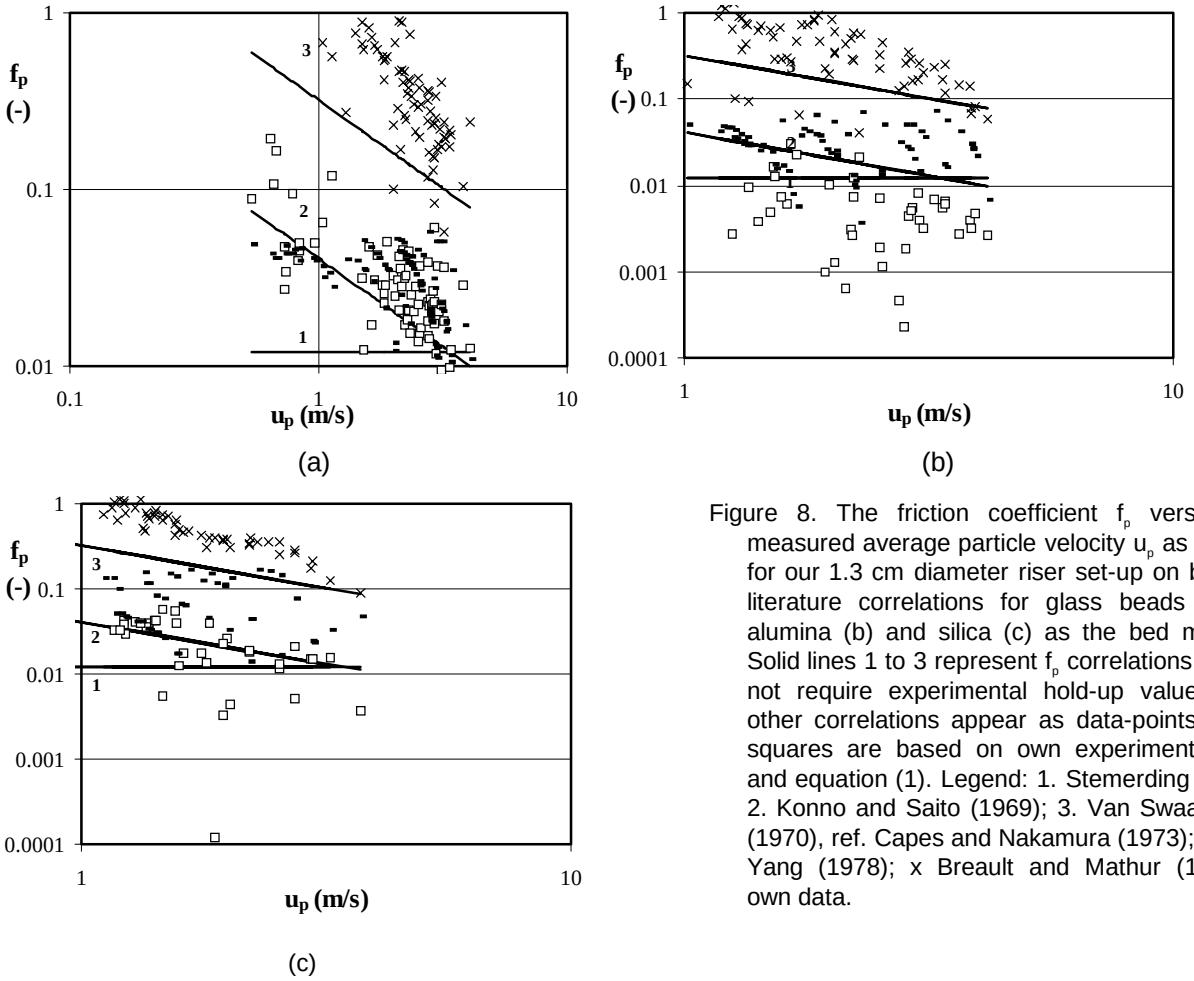

Figure 8. The friction coefficient f_p versus the measured average particle velocity u_p as derived for our 1.3 cm diameter riser set-up on basis of literature correlations for glass beads (a), γ-alumina (b) and silica (c) as the bed material. Solid lines 1 to 3 represent f_p correlations that do not require experimental hold-up values. The other correlations appear as data-points. Open squares are based on own experimental data and equation (1). Legend: 1. Stemerding (1962); 2. Konno and Saito (1969); 3. Van Swaaij *et al.* (1970), ref. Capes and Nakamura (1973); Data: - Yang (1978); x Breault and Mathur (1989); □ own data.

Own pressure drop and solids hold-up data are now compared with those obtained by the one-dimensional model. Since Yang's equation (table I) is the best one in comparison with own data (see figure 8), this equation was selected for the solids-wall friction coefficient in the model. A strong disagreement between the model predictions and experimental values of the solids hold-up and the pressure drop is now observed.

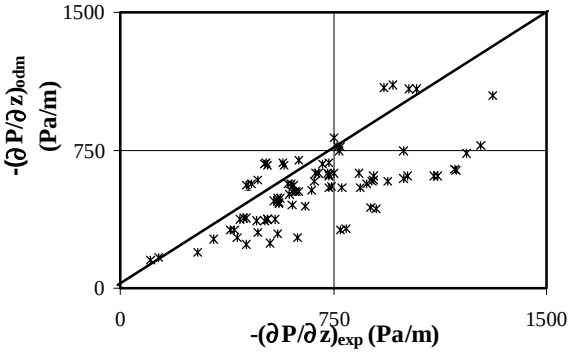

(a)

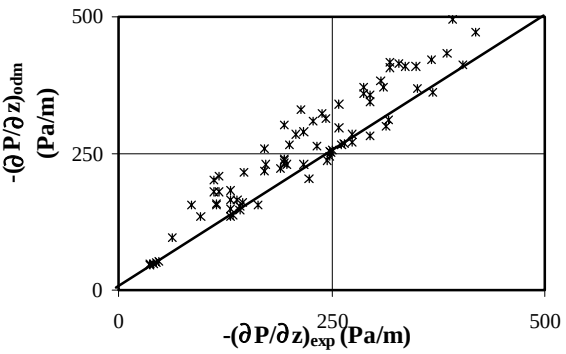

(b)

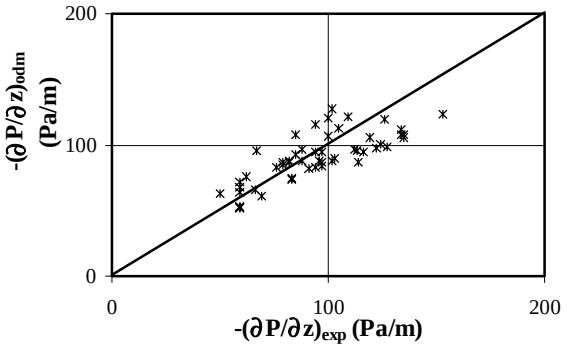

(c)

Figure 9. The pressure gradient $-(\partial P/\partial z)_{odm}$ calculated by the one-dimensional model versus the experimental pressure gradient $-(\partial P/\partial z)_{exp}$ for glass beads (a), γ-alumina (b) and silica (c) as the bed material. The Yang relation is used to calculate the solids-wall friction coefficient f_p in the one-dimensional model.

In figure 9 and 10 the pressure drop and solids hold-up, calculated by the one-dimensional model, is plotted versus the experimentally observed values obtained for all particles applied. Both, the pressure gradients and the solids hold-up, are not well predicted by the one-dimensional model.

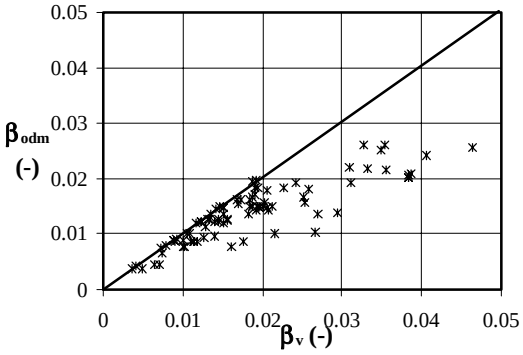

(a)

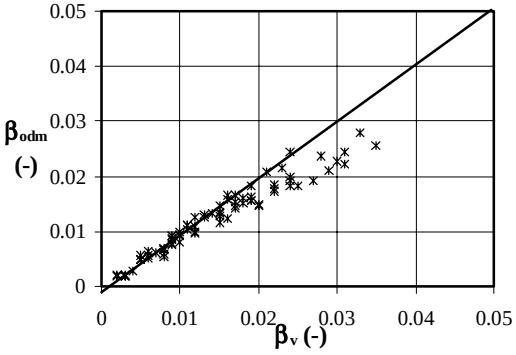

(b)

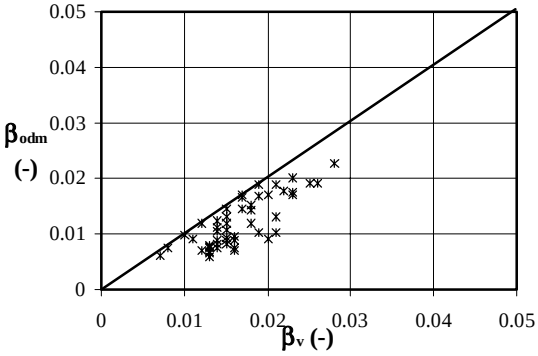

(c)

Figure 10. The solids hold-up, calculated by the one dimensional model β_{odm} versus the experimentally observed solids hold-up (quick-closing valves) β_v for glass beads (a), γ-alumina (b) and silica (c) as the bed material. The Yang relation is used to calculate the solids-wall friction coefficient f_p in the one-dimensional model.

This conclusion is valid, also when the other relations for the friction coefficient are applied. Even when the value for the friction coefficient is derived directly from the pressure drop (equation 9), measured for the particles of this study, the solids hold-up is not well predicted by this model. Obviously it is impossible to predict the solids hold-up *and* pressure drops simultaneously within reasonable accuracy by adjusting the value for the friction coefficient only. This anomaly seems to originate from other phenomena than friction: formation of clusters of particles is proposed here as a likely explanation.

6.4 Solids hold-up versus gas velocity and solids flux

In figure 11 the measured values for the solids hold-up, derived from the fluoroptic method and from the valve technique for the segments 1 to 3, are presented as a function of solids flux and gas velocity.

The solids hold-up increases with solids flux and decreases with gas velocity as expected from the one-dimensional model. The ratio of solids mass flux over solids hold-up, G_s/β, remains approximately constant, indicating that the particle velocity $u_p=G_s/(\beta\rho_p)$ is, as a first approximation, independent of the solids flux, which is in agreement with earlier published results. Figure 13 shows the particle velocity as a function of the applied gas velocity. Each data point in this figure represents the average value for all solids mass fluxes applied. By plotting averaged values an excessive scatter in data, that is caused by addition of experimental errors, is avoided.

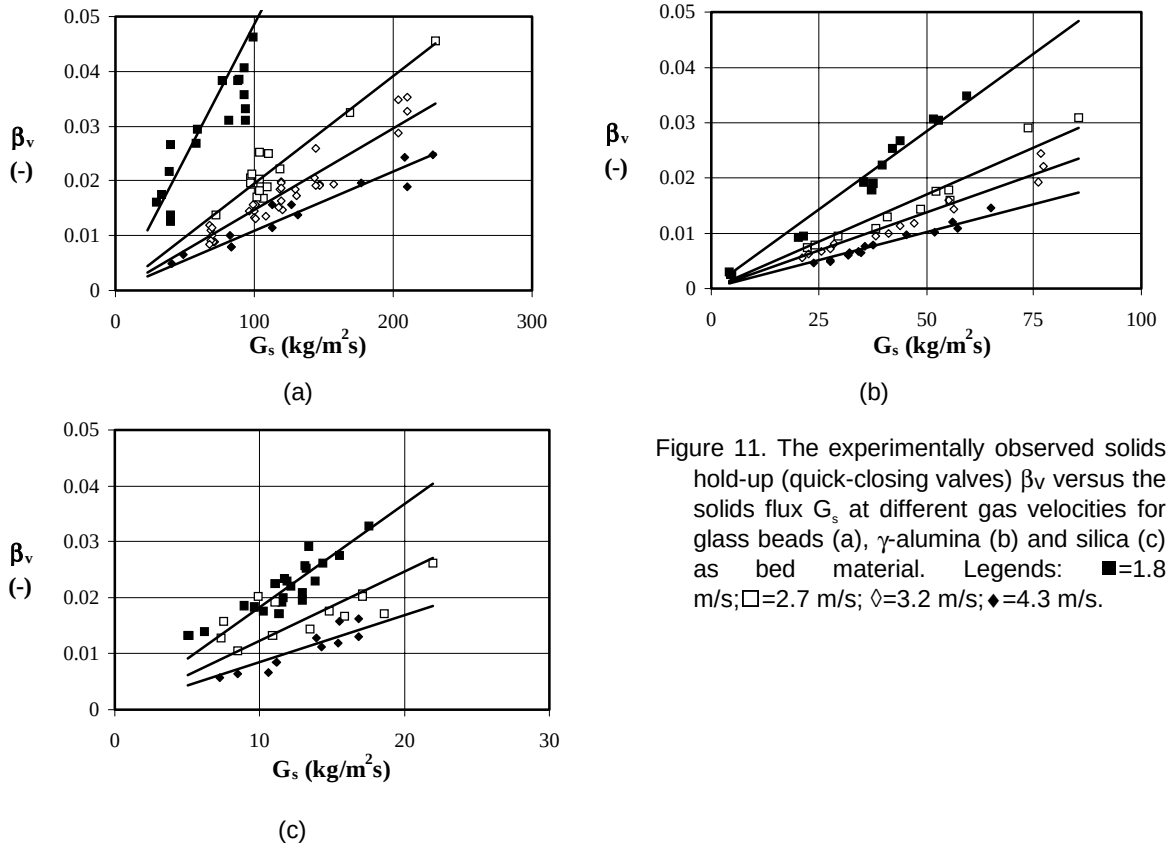

Figure 11. The experimentally observed solids hold-up (quick-closing valves) β_V versus the solids flux G_s at different gas velocities for glass beads (a), γ-alumina (b) and silica (c) as bed material. Legends: ■=1.8 m/s;□=2.7 m/s; ◊=3.2 m/s;♦=4.3 m/s.

The two ideal cases, i) no slip between gas and particles and ii) a slip velocity equal to the terminal velocity, are represented by the solid and dashed line respectively. Data points obtained from the fluoroptic method are plotted as diamonds, while the data obtained by

quick-closing valves technique are shown as squares. From figure 4c it was already concluded that, despite differences in density and particle size of the bed material and the fluoroptic particles, the difference between the two measuring techniques is small, which is reconfirmed by figure 12. Obviously the solids are transported as clusters, in which the fluoroptic tracer material is effectively enclosured. Figure 12 shows that the averaged particle velocity is approximately a linear function of the gas velocity. The slip velocity (u_g-u_p) is significantly higher than the terminal velocity of the individual particle; its ratio over u_t is maximal 5 for the glass beads, 7 for alumina and 20 for silica. This increasing ratio for smaller and less denser particles is in accordance with observations made by Arena *et al.* (1988), who reported values in the order of 1 to 11 for B-particles, and ranging from 3 to 22 for the type-A particles.

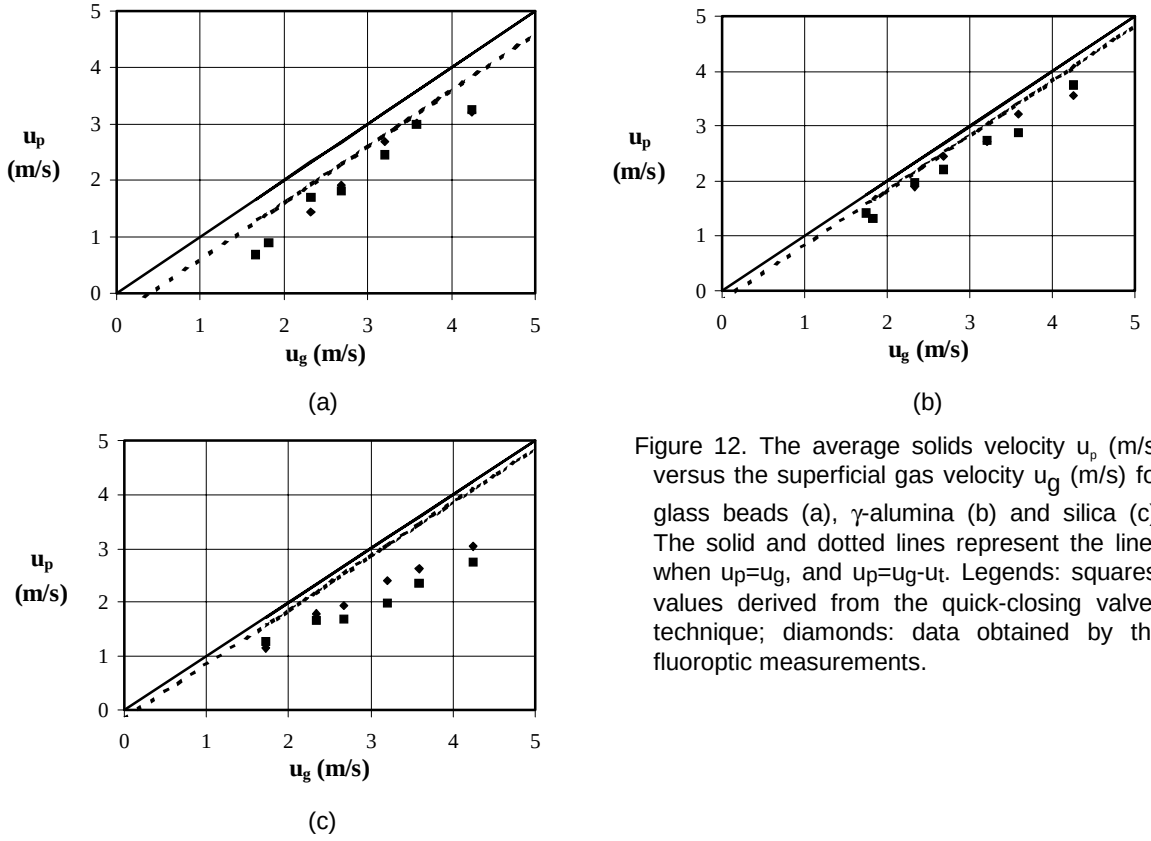

Figure 12. The average solids velocity u_p (m/s) versus the superficial gas velocity u_g (m/s) for glass beads (a), γ-alumina (b) and silica (c). The solid and dotted lines represent the lines when $u_P=u_G$, and $u_P=u_G-u_t$. Legends: squares: values derived from the quick-closing valves technique; diamonds: data obtained by the fluoroptic measurements.

7 ESTIMATION OF SOLIDS HOLD-UP IN THE CFB RISER SECTION

Clearly, for the particles applied in this study the one-dimensional model can not be applied to predict both pressure drop *and* solids hold-up simultaneously. Moreover, solids hold-up data from literature can not be predicted within reasonable accuracy by this model (unfortunately pressure drop data are only scarcely available). This is illustrated by figure 13a, in which solids hold-up data from own experiments and literature are plotted versus the solids hold-up value calculated by the one-dimensional model. The literature data are obtained from the review by Ouyang and Potter (1993a) and from other researchers (Yang *et al.*, 1990; Pagliolico *et al.*, 1992; van Swaaij *et al.*, 1970; Bodelin *et al.* 1994; Plasynski *et al.*, 1994; Hariu and Molstad, 1949; Lewis and Gilliland, 1949), altogether yielding approximately 500 data points, most of them obtained at ambient conditions. In table V the corresponding range of experimental parameters is given.

Table IV. Correlations for the prediction of the particle velocity in a riser: $E=\sqrt{(1/(N-1)\Sigma(\beta_{exp}-\beta_{cal})^2/\beta_{exp}^2)}$, $AAD=1/N\cdot\Sigma|\beta_{exp}-\beta_{cal}|$ and $AD=1/N\cdot\Sigma(\beta_{exp}-\beta_{cal})$

reference	particle velocity (m/s)	E	AAD	AD
terminal velocity analysis	$u_p = u_g - u_t$	0.37	0.0077	0.0075
Hinkle (1953)[a]	$u_p = u_g(1-0.0637 d_p^{0.3}\rho_p^{0.5})$	0.38	0.0082	0.0079
One-dimensional model (Yang, 1978)	$u_p = u_g - u_t\sqrt{\left(1+\frac{4 f_s u_p^2}{2 g D_t}\right)\varepsilon^{4.7}}$	0.43	0.0081	0.0074
Matsumoto (1986)	$u_p = u_g - 0.71 u_t\sqrt{(1+0.0065\frac{u_g^{2.5}}{u_t^{1.25}})}$	0.38	0.0082	0.0081
Kato *et al.* (1986)	$\frac{\varepsilon}{(1-\varepsilon)} = 230\left(\frac{u_g-u_t}{u_t}\right)^{1.5}\frac{u_t^{1.8}}{G_s D_t^{0.4}}$ $u_p = \frac{G_s}{\rho_s}\left(\frac{\varepsilon}{(1-\varepsilon)}+1\right)$	0.73	0.0099	-0.0027
Zaltash (1987)[a]	$u_p = \sqrt{(g d_p)}\left(\left(\frac{u_g}{\sqrt{(g d_p)}}\right)-\left(\frac{u_t}{\sqrt{(g d_p)}}\right)^{0.87}\right)(1-0.5\sin\theta)^{0.0765}\left(\frac{D_t}{d_p}\right)^{0.031}\left(\frac{\rho_p}{\rho_g}\right)^{-0.0321}$	0.99	0.013	-0.0088
Kato *et al.* (1989)	$Re_p = \frac{d_p\rho_g u_t}{\eta_g}\quad Z_i = 360\left(\frac{G_s}{\rho_p u_t}\right)^{1.2}\left(\frac{u_g-u_t}{u_t}\right)^{-1.45} Re_p^{-0.29}$ $\frac{\varepsilon}{(1-\varepsilon)} = 0.048\frac{\exp(z-Z_i)}{\exp(z-Z_i)+1}\left(\frac{u_g-u_t}{u_t}\right)^{1.35}\left(\frac{G_s}{\rho_p u_t}\right)^{-1.28} Re_p^{0.23} D_t^{-1.28}$ $u_p = \frac{G_s}{\rho_p}\left(\frac{\varepsilon}{(1-\varepsilon)}+1\right)$	0.56	0.0093	0.0048
IGT (1990)[a]	$u_p = u_g(1-0.68 d_p^{0.92} D_t^{-0.54}\rho_p^{0.5}\rho_g^{-0.2})$	0.43	0.0074	0.0093
Patience *et al.* (1992)	$u_p = \left(1+5.6\left(\frac{u_g}{\sqrt{g D_t}}\right)^{-1}+0.47\left(\frac{u_t}{\sqrt{g D_t}}\right)^{0.41}\right)\cdot\frac{\varepsilon}{u_g}$	0.68	0.010	-0.0053

[a] From Plasynski *et al.* (1994)

Table V. Range of operating variables used in deriving equation 13

variable	lower limit	upper limit
D_t (m)	0.007	0.254
d_p (μm)	49	500
ρp (kg/m^3)	794	3000
u_g (m/s)	1.5	12
G_s (kg/m^{2}s)	10	300

Figure 13a shows that, especially at higher solids hold-ups, the difference between the experimental hold-ups and those derived from the one-dimensional model strongly increases. The same conclusion holds for the ideal case that the slip velocity is equal to the terminal falling velocity of the individual particle (figure 13b). Perhaps other correlations may be better. However, opposed to gas-liquid systems, only few relations to predict the solids hold-up (or slip - or particle velocity) are proposed in literature. In table IV, a number of these relations, rewritten in particle velocities, are presented.
For comparison three indicators are used to evaluate the accuracy (Plasynski *et al.*, 1994); the square of the deviation E:

$$E = \sqrt{\frac{1}{(N-1)} \sum \frac{\left(\beta_{cal} - \beta_{exp}\right)^2}{\beta_{exp}^2}} \tag{10}$$

the average absolute deviation, AAD:

$$AAD = \frac{1}{N} \sum \left|\beta_{cal} - \beta_{exp}\right| \tag{11}$$

and the average deviation, AD, a measure of the overall tendency of prediction

$$AD = \frac{1}{N} \sum (\beta_{exp} - \beta_{cal}) \tag{12}$$

where β_{cal} is he solids hold-up derived from a literature correlation, and β_{exp} the experimentally obtained solids hold-up. From the values for these three parameters in table IV it follows that if the slip velocity is taken equal to the terminal velocity, the solids hold-up is calculated within better accuracy than each of the other correlations listed. None of these correlations can thus predict (our) set of solids hold-up data within reasonable accuracy, and even the tendency, especially at higher solids hold-ups than 1 vol.%, is questionable. This can also be concluded from the parity plots for the one-dimensional model and the one for the terminal velocity analysis (see figure 13).

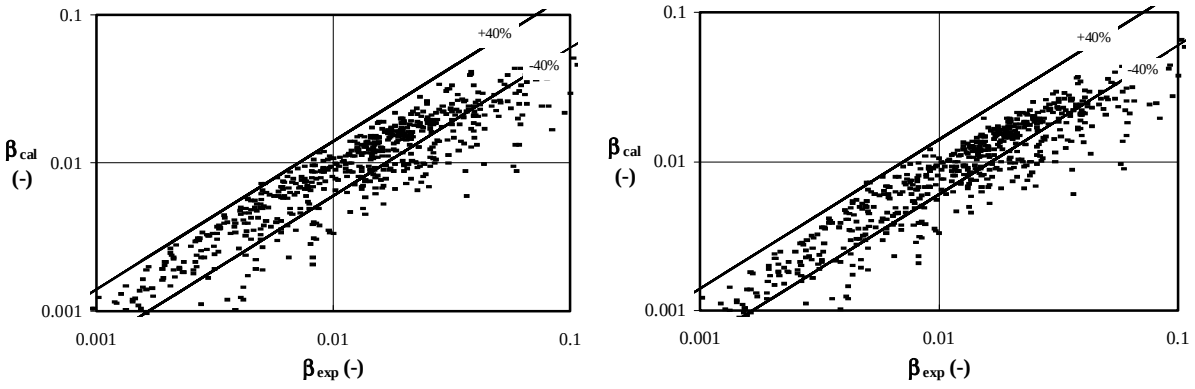

Figure 13. Parity plots for the experimental values of the solids hold-up and the calculated hold-ups derived from the one-dimensional model (a) and for the terminal velocity analysis (b). The solid lines represent ± 40% error lines.

Therefore an improved correlation is developed, and its derivation is based on the trends observed in literature regarding the slip velocity. From a least square analysis of the deviation of all data points (from literature and own experiments), the following relation is obtained:

$$u_s = u_t + 7.695 \cdot 10^{-4} \left(\frac{u_g}{\sqrt{g d_p}} \right) \left(\frac{D_t}{d_p} \right)^{1/3} \qquad (13)$$

It predicts our own experimental solids hold-up data within ± 20%, which is significantly better than the accuracy of other correlations in table IV (see figure 14a; E=0.2684, AAD=0.00395 and AD=0.00183). As shown in figure 14b the total set of the solids hold-up data is predicted within ± 40%.

From equation 13 it can be seen that

- The slip velocity is a function of the gas velocity, the reactor diameter and the particle diameter. As a first estimate, it is independent of the solids flux and density and (as the developed region of the riser is considered) of the riser length.
- For lower gas velocities, smaller reactor diameters, and coarser particles, the slip velocity approaches the terminal velocity of the individual particle; this is in agreement with the observations of Arena *et al.* (1986). It is likely that at these conditions clusters and/or radial segregation become less important.

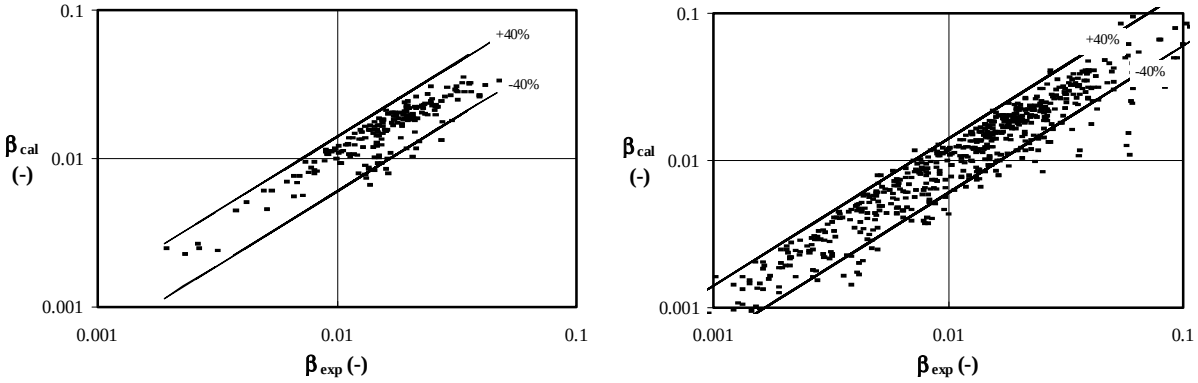

Figure 14. Parity plots for the experimental values of the solids hold-up and the calculated hold-ups derived from equation 13, for our data (a) and the set of data points from literature (b). The solid lines represent ± 40% error lines.

8 CONCLUSIONS

This study was focused on determination of the solids hold-up in the 'developed' region in the riser of a CFB by pressure drop measurements and by direct methods such as quick-closing valves and a non-intrusive method, the fluoroptic method. The following conclusions can be listed:

1. The fluoroptic method is an appropriate method to determine the solids velocity, at least in a small scale riser of a CFB. The fluoroptic measurement in laboratory set-ups is potentially suitable for measurements at actual reactor conditions, and in the acceleration zone of the riser.
2. Significant differences between solids hold-up values, derived from pressure drop measurements on the one hand, and those from the quick-closing valves method on

the other, were observed for glass beads and silica, but not for γ-alumina. For A-type particles the pressure drop technique may yield solids hold-up values within reasonable accuracy. However, for larger and denser particles, solids-wall friction must be taken into account. For lighter particles the gas-wall friction must be accounted for.

3. For none of the particle types applied, it was possible to predict the solids hold-up *and* pressure drops simultaneously within reasonable accuracy with the one-dimensional model by adjusting the value for the friction coefficient only.
4. For all powders considered, at a given gas velocity the solids hold-up is approximately proportional to the solids flux: the particle velocity is roughly independent on solids flux.
5. Literature correlations, relating the slip velocity in the riser to operating conditions and particle properties, are inaccurate. A new correlation is proposed for the slip velocity: it predicts solids hold-up in our small scale riser with much better accuracy (±20%) than relations proposed in literature. Also solids hold-up data from literature are predicted much better (±40%) with our correlation.
6. Especially for A powders cluster formation is likely to be an important phenomenon in explaining the differences between the measured solids velocities, and those calculated from the one-dimensional model. From the fluoroptic method indirect evidence for clusters can be obtained: a small fraction of fluoroptic material, with a higher density than the bed material, is transported at the same velocity as the bed material.

ACKNOWLEDGEMENT

We acknowledge the financial support of the Dutch Ministry of Economic Affairs through the Netherlands Energy Research Foundation ECN. We also acknowledge A. Pourkamal, A. Vunderink and R. Buitenhuis for their assistance in the experimental work.

NOTATION

AAD	average absolute deviation	-
AD	average deviation	-
C_d	drag coefficient	-
d_p	particle diameter	m
D_t	tube diameter	m
E	square of deviation	-
f_p	solids-wall friction coefficient $=4f_s$	-
f_g	gas-wall friction coefficient	-
g	first signal function of the fluoroptic probe	
g	gravitational constant	$m^2\ s^{-1}$
G_s	solids flux	$kg\ m^{-2}\ s^{-1}$
g	gravitational force per unit mass	$m\ s^{-2}$
h	second signal function of the fluoroptic probe	
N	number of data-points	-
P	pressure	$kg\ m^{-1}\ s^{-2}$
Re_g	gas Reynolds number $\rho_g D_t u_g/\eta$	-
Re_p	particle Reynolds number $\varepsilon\rho_g d_p(u_g/\varepsilon-u_p)/\eta$	-
u_{g_*}	superficial gas velocity	$m\ s^{-1}$
u_g	interstitial gas velocity	$m\ s^{-1}$
u_p	particle velocity	$m\ s^{-1}$
u_t	terminal velocity individual particle	$m\ s^{-1}$
z	axial riser co-ordinate	m

Greek symbols

β	solids hold-up	-
ε	porosity	-
μ	gas viscosity	kg m^{-1} s^{-1}
ρ_g	density gas	kg m^{-3}
ρ_p	density solids	kg m^{-3}

subscripts

cal	calculated from correlations
ΔP	derived from pressure drop measurements
exp	obtained from experimental work
f	derived from fluoroptic measurements
odm	derived from the one-dimensional model
v	derived from quick-closing valves

REFERENCES

Arena U., Cammarota A., Pistone L., 1986, High velocity fluidization behavior of solids in a laboratory scale circulating bed, in *Circulating Fluidized Bed Technology*, Pergamom Press, Toronto, 119

Arena U., Cammarota A., Massimilla L., Pirozzi D., 1988, The hydrodynamic behavior of two circulating fluidized bed units of different sizes, in *Circulating Fluidized Bed Technology II*, Pergamom Press, Oxford, 223

Bader R., Findlay J., Knowlton T.M., 1988, Gas/solids flow patterns in a 30.5-cm-diameter circulating fluidized bed, in *Circulating Fluidized Bed Technology II*, Pergamom Press, Oxford, 123

Bird R.B., Stewart W.E., Lightfoot E.N., 1960, *Transport Phenomena*, John Wiley & Sons, New York.

Blasse G., Bril A., 1970, Characteristic luminescence II: the efficiency of phosphors excited in the activator, *Philips Tech. Rev.*, **31**, 10

Bodelin P., Molodtsof Y., Delebarre A., 1994, Flow structure investigations in a CFB, *Circulating Fluidized Bed Technology IV,* Pennsylvania, Engineering Foundation, 118

Breault R.W., Mathur V., 1989, High-velocity fluidized bed hydrodynamic modelling. 1. Fundamental studies of pressure drop., *Ind. Engng. Chem. Res.*, **28**, 684

O'Brien T.J., Syamal M.,1994, Particle cluster effects in the numerical simulation of a circulating fluidized bed, in *Circulating Fluidized Bed Technology IV*, Pennsylvania, Engineering Foundation, 345

Cankurt N.T., Yerushalmi J., 1978, Gas backmixing in high velocity fluidized beds, in *Fluidization II*, Cambridge University Press, 387

Capes C.E., Nakamura K., 1973, Vertical pneumatic conveying: an experimental study with particles in the intermediate and turbulent flow regimes, *Can. J. Chem. Engng.*, **51**, 31

Contractor R.M., Chaouki J., 1991, Circulating fluidized bed as a catalytic reactor, in *Circulating Fluidized Bed Technology III*, Pergamom Press, Oxford, 39

Dry R.J., Christensen I.N., White C.C., 1987, Gas-solids contact efficiency in a high-velocity fluidised bed, *Powder Technol.*, **52**, 243

Dry R.J., White C.C., 1992a, Gas-solids contact in a circulating fluidised bed: the effect of particle size, *Powder Technol.*, **70**, 277

Dry R.J., White C.C., Clos R.C., 1992b, The effect of gas inlet geometry on gas-solid contact efficiency in a circulating fluidised bed, in *Fluidization VII*, Engineering Foundation, 211

Flemmer R.L.C., Banks C.L., 1986, On the drag coefficient of a sphere, *Powder Technol.*, **48**, 217

Grace J.R., Tuot J., 1979, A theory for cluster formation in vertically conveyed suspensions of intermediate density, *Trans. Inst. Chem.*, **57**, 49

Geldart D., 1973, Types of gas fluidization, *Powder Technol.*, **7**, 285

Haider A., Levenspiel O., 1989, Drag coefficient and terminal velocity of spherical and non-spherical particles, *Powder Technol.*, **58**, 63

Hariu O.H., Molstad M.C., 1949, Pressure drop in vertical tubes in transport of solids by gases, *Ind. Engng. Chem.*, **41**, 1148

Hartge E.-U., Li Y., Werther J., 1986, Analysis of the local structure of the two phase flow in a fast fluidized bed, in *Circulating Fluidized Bed Technology*, Pergamom Press, New York, 153

Hartge E.U., Rensner D., Werther J., 1988, Solids concentration and velocity patterns in circulating fluidized beds, in *Circulating Fluidized Bed Technology II*, Pergamom Press, Oxford, 165

Hoomans B., Kuipers J.A.M., Van Swaaij W.P.M., 1997, *personal communications*

Horio M., Ishii H., Kobukai Y., Yamanishi N., 1989, A scaling law for circulating fluidized beds, *J. Chem. Engng.*

Japan, **22**, 587
Horio M., Kuroki H., 1994, Three-dimensional flow visualization of dilutely dispersed solids in bubbling and circulating fluidized beds, *Chem. Engng. Sci.*, **49**, 2413
Ishii H., Nakajima T., Horio M., 1989, The clustering annular flow model of circulating fluidized beds, *J. Chem. Engng. Japan*, **22**, 484
Karri S.B.R., Knowlton T.M., 1991, A practical definition of the fast fluidization regime, in *Circulating Fluidized Bed Technology III*, Pergamom Press, Oxford, 67
Kato K., Ozawa Y., Endo H., Hiroyasu M., Hanzawa T., 1986, Particles hold-up and axial pressure drop in vertical pneumatic transport reactor (riser), in *Fluidization V*, Engineering Foundation, 265
Kato K., Shibasaki H., Tamura K., Arita S., Wang C., Takarada T., 1989, Particle hold-up in a fast fluidized bed, *J. Chem. Engng. Japan*, **22**, 130
Kiel J.H.A., 1990, *Removal of sulphur oxides and nitrogen oxides from flue gas in a gas-solid trickle flow reactor,* thesis Enschede
Konno H., Saito S., 1969, Pneumatic conveying of solids through straight pipes, *J. Chem. Engng. Japan*, **2**, 211
Kuramoto M., Kunii D., Furusawa T., 1986, Flow of dense fluidized particles through an opening in a circulation system, *Powder Technol.*, **47**, 141
Kuipers J.A.M., Van Swaaij W.P.M., 1997, Application of computational fluid dynamics to chemical reaction engineering, Rev. Chem. Engng., 13(3)
Lewis W.K., Gilliland E.R., Bauer W.C., 1949, Characteristics of fluidized particles, *Ind. Engng. Chem.*, **41**, 1104
Masai M., Tanaka S., Tomomasa Y., Nishiyama S., Tsuruya S., 1985, Reactant-catalyst contact in riser-tube reactor, *Chem. Engng. Commun.*, **34**,153
Matsumoto S., Harakawa H., Suzuki M., Ohtani S., 1986, Solid particle velocity in vertical gaseous suspension flows, *Int. J. Multiphase Flow*, **21**, 445
Morooka S., Kusakabe K., Ohnishi N., Gujima F., Matsuyama H., 1989, Measurement of local fines movement in a fluidized bed of coarse particles by a fluorescent tracer technique, *Powder Technol.*, **58**, 271
Nieuwland J.J., 1995, *Hydrodynamic modelling of gas-solid two-phase flows*, thesis Enschede
Ouyang S., Potter O.E., 1993a, Consistency of circulating fluidized bed experimental data, *Ind. Engng. Chem. Res.*, **32**, 1041
Ouyang S., Lin J., Potter O.E., 1993b, Ozone decomposition in a 0.254 m I.D. diameter circulating fluidized bed reactor, *Powder Technol.*, **74**, 73
Ouyang S., Potter O.E., 1994, Modelling chemical reaction in a 0.254 m I.D. circulating fluidized bed, in *Circulating Fluidized Bed Technology IV*, Pennsylvania, Engineering Foundation, 422
Pagliolico S., Triprigan M., Rovero G., Gianetto A., 1992, Pseudo-homogeneous approach to CFB reactor design, *Chem. Engng. Sci.*, **47**, 2269
Patience G.S., Chaouki J., Berutti F., Wong R., 1992, Scaling considerations for circulating fluidized bed risers, *Powder Technol.*, **72**, 31
Plasynski S.I., Klinzing G.E., Mathur M., 1994, High-pressure vertical pneumatic transport investigation, *Powder Technol.*, **79**, 95
Reddy K.V.S., Pei D.C.T., 1969, Particle dynamics in solids-gas flow in a vertical pipe, *Ind. & Engng Commun. Fund.*, **8**, 490
Reh L., 1986, The circulating fluid bed reactor- its main features and applications, *Chem. Engng. Proces.*, **20**, 117
Reh L., 1995, New and efficient high-temperature processes with circulating fluid bed reactors, *Chem. Engng. Technol.*, **18**, 75
Rhodes M.J., Lausmann P., Villain F., Geldart D., 1988, Measurement of radial and axial solids flux variations in the riser of a circulating fluidized bed, in *Circulating Fluidized Bed Technology II*, Pergamom Press, Oxford, 155
Richardson J.F., Zaki W.N., 1954, Sedimentation and Fluidisation: Part I, *Trans. Instn Chem. Engng.*, 32, 35
Schiller L., Naumann A., 1935, Uber die grundlegenden Berechnungen bei der Schwerkraftaufbereitung, *Z. Ver. Dtsch. Ing.*, **77**, 318
Smith C.E., Liu P.P., 1992, Coefficients of restitution, *J. Applied Mech.*, **59**, 963
Stemerding S., 1962, The pneumatic transport of cracking catalyst in vertical risers, *Chem. Engng. Sci.*, **17**, 599
Sun G., Grace J.R., 1990, The effect of particle size distribution on the performance of a catalytic fluidized bed reactor, *Chem. Engng. Sci.*, **45**, 2187
Tsuo Y.P., Gidaspow D., 1990, Computation of flow patterns in circulating fluidized beds, *A.I.Ch.E.J.*, **36**, 885
Van der Ham A.G.J., Prins W., Van Swaaij W.P.M., 1994, Regenerative, high temperature desulfurization of coal gas in a circulating fluidized bed, in *Circulating Fluidized Bed Technology IV*, Pennsylvania, Engineering Foundation, 657
Van Swaaij W.P.M., Buurman C., van Breugel J.W., 1970, Shear stresses on the wall of a dense gas-solids riser, *Chem. Engng. Sci.*, **25**, 1818
Vollert J., Wether J., 1994, Mass transfer and reaction behaviour of a circulating fluidized bed reactor, *Chem. Engng. Technol.*, **17**, 201

Wagenaar B.M., Meijer R., Kuipers J.A.M., van Swaaij W.P.M., 1995, Novel method for non-contact measurement of particle temperatures, *A.I.Ch.E.J.*, **41**, 773

Werther J., 1994, Fluid mechanics of large-scale CFB units, in *Circulating Fluidized Bed Technology IV,* Pennsylvania, Engineering Foundation, 1

Yang W.-C., 1973, Estimating the solid particle velocity in vertical pneumatic conveying lines, *Ind. Engng. Chem. Fundam.*, **12**, 349

Yang W.-C., 1974, Correlations for solid friction factors in vertical and horizontal pneumatic conveyings, *A.I.Ch.E.J.*, 605

Yang W.-C., 1977, A unified theory on dilute phase pneumatic transport, *J. Powder Bulk Solids Technol.*, **1**, 89

Yang W.-C., 1978, A correlation for solid friction factor in vertical pneumatic conveying lines, *A.I.Ch.E.J.*, **24**, 548

Yang Y.-L., Jin Y., Yu Z.-Q., 1990, Local slip behaviors in the circulating fluidized bed,*A.I.Ch.E.J. Symp. Ser.*, **296**, 81

Yerushalmi J., Turner D.H., Squires A.M., 1976, The fast fluidized bed, *Ind. Engng. Process Des. Dev.*, **15**, 47

Yerushalmi J., Cankurt N.T., Geldart D., Liss B., 1978, Flow regimes in vertical gas-solid contact systems, *A. I. Ch. E. Symp. Ser.*, **176**, 1

Zhang W., Tung Y., Johnsson F., 1991, Radial voidage profiles in fast fluidized beds of different diameters, *Chem. Engng. Sci.*, **46**, 3045

Zou B, Li H., Yashen X., Xinhua M., 1994, Cluster structure in a circulating fluidized bed, *Powder Technol.*, **78**, 173

CHAPTER 4

MASS TRANSFER AND INFLUENCE OF THE LOCAL CATALYST ACTIVITY ON THE CONVERSION IN A RISER REACTOR

ABSTRACT

In the riser of a small circulating fluidized bed reactor (ID 0.015 m), the contacting between the gas and the solids is studied by investigating its hydrodynamics (at room temperature and between 675 and 775 K), as well as by analyzing the effects of the local catalyst activity on the conversion rate. This was carried out for a reaction, for which the conversion is demonstrated to be controlled by mass transfer resistances for the oxidation of carbon monoxide over a Pt/γ-alumina catalyst. In the present experiments, the catalyst activity is varied by mixing the highly active particles with similar but inert γ-alumina (in ratios in between 150 to 2500 m^3_{inert}/m^3_{cat}).

Experimental results show that, at a given gas velocity, the solids hold-up is linearly dependent on the solids flux, while the slip velocity remains approximately constant. The values for the slip velocity are much higher than the terminal velocity of the individual particles.
It is demonstrated that at T=775 K the conversion rate is completely controlled by the mass transfer resistances on the scale of the individual particles. The observed Sherwood numbers obtained for the mass transfer controlled reaction plotted versus the particle Reynolds number show the same trend as those reported in the literature for packed and fluidized beds. As a first approximation, a negative square root dependency of the Sherwood number on the solid hold-up is observed. Increasing the gas velocity yields an improved gas-solids contacting.
The local catalyst activity, in our work varied by dilution with inert solids, appears to be an important parameter. At a high local activity, the conversion rate *per unit volume of catalyst* decreases significantly due to local depletion of reactant. The same conclusions can be derived from results published by Ouyang and co-workers, although different conditions and another reaction system were used.

1 INTRODUCTION

In the riser of a circulating fluidized bed system, small solid particles are contacted with a gas phase, which flows at velocities much higher than the terminal falling velocity of the individual particle. The particles are carried over the top of the riser, separated from the gas stream by means of cyclones, and re-introduced at the bottom of the column, for example via a storage vessel. When high throughputs and short (gas and solids) contact times are required, this reactor is considered to be a very good alternative to the more conventional fluidized bed types (see e.g. Contractor and Chaouki, 1991; Patience *et al.*, 1992). Several industrial processes are carried out in a riser reactor, like for instance the Fluidized Catalytic Cracking (FCC), the Fischer-Tropsch synthesis, the calcination of aluminium trihydrate to high purity alumina (Reh, 1986, 1995), and the combustion or gasification of coal and biomass. Commercial and potential processes that employ riser systems are reviewed by Berruti *et al.* (1995).

One of the important advantages claimed for risers is its excellent gas-solids contacting,

which implies that gas-to-particle momentum transfer rates as well as the mass or heat transfer rates are high. In the last decades, research in riser systems have been focused mainly on its hydrodynamics (see e.g. the early paper by Hariu and Molstad in 1949 or the more recent review by Ouyang and Potter, 1993a). Usual research topics are the axial and radial solids distribution, the solids hold-up and the pressure drop. From these studies it became clear that, when small particles are applied, the gas-to-solids momentum transfer rates are significantly lower than one might expect. The claim that mass or heat transfer rates (and consequently the conversion) in risers are high may then not be justified anymore, because large slip velocities suggest that the momentum is transferred from the gas to particle agglomerates (clusters, or strands) instead of to the individual particle. Unfortunately, few studies in the literature deal with mass or heat transfer (or with reaction) as the main subject (amongst others Sun and Grace, 1990, 1992; Van der Ham *et al.*, 1991, 1994 and Ouyang and co-workers 1993b, 1994, 1995).

In this chapter, additional data for mass transfer in the riser will be presented. These data have been collected from measurements for a reaction, for which at the applied conditions the conversion is demonstrated to be controlled by mass transfer resistances (viz. the oxidation of carbon monoxide over a platinum catalyst). Next, the effect of the local catalyst activity will be discussed, which is accomplished by diluting the active catalyst with inert but similar particles. The results will then be compared with earlier published data of Ouyang and co-workers (1995), who varied the local catalyst activity by changing the operating temperature for the ozone decomposition reaction. But first, preceding the discussion of the present authors' experimental work in section 3, a review of existing ideas and observations regarding gas-solids contacting will be presented in section 2. This review consists of three parts. The first part is concerned with hydrodynamics in a riser. Then, the literature is discussed in which the gas-solids contacting has been investigated by measuring heat transfer rates, mass transfer rates, or the apparent kinetics of an appropriate reaction system. Finally, the most important literature observations will be summarized.

2 HYDRODYNAMICS AND REACTION IN THE RISER OF A CFB SYSTEM

2.1 Hydrodynamics in Riser systems

For small particles (< 100 μm) in a riser, high gas-to-solids momentum transfer rates should be reflected by small differences between the velocity of the interstitial gas and that of the solid particles (the so-called slip velocity). In the ideal case of individual gas-solids contacting, the ratio of the slip velocity over the terminal velocity should be 1 or slightly higher if "hindered settling" applies, and is expected to be higher when the gas-to-solids momentum transfer rates are lower. The latter is exactly what is observed in risers when small particles are applied. The observed ratio of slip velocity over the terminal velocity range up to 10 or even 20. In the literature, three causes are identified for these larger values, viz. i) friction between solids and wall, ii) radial segregation of solid particles, and iii) formation of particle clusters. In the last decades, it was generally accepted that the radial solids profile and the friction between solids and wall are the main causes for the observed high values of the slip velocity. In several studies, it was shown that the solids flow in a riser is not uniform, neither axially nor radially (e.g. Zhang *et al.* 1991; Nieuwland, 1995). In recent years however, also powders cluster formation was considered to be an important phenomenon in explaining such large differences, especially for the small and light (viz. Geldart's A and C type; f.i. Yerushalmi *et al.*, 1978; Ishii *et al.,* 1989; Zou *et al.*, 1994). Indirect evidence of cluster formation in riser was given in chapter 3 by applying a new technique for the measurement of the particle velocity in the riser, which is called the fluoroptic method. A small fraction of (denser) fluoroptic material, added to the bed material, was transported at the same velocity as the bed material, although its particle properties

were clearly different. These authors showed further that the presence of particle clusters instead of individual particle behaviour in risers has a serious implication for the interpretation of the observed pressure drops over the riser, for example when using a simple one-dimensional model. For all type of particles applied (ranging from a Geldart AC particle to an AB-type), an accurate prediction of both, the pressure drop as well as the solids hold-up at the same time, is impossible, if it is assumed that such small particles are individually transported in a riser system.
In the same chapter, it was shown that for a large number of experimental results derived by several research groups, the average particle velocities in the developed region of the riser is independent on the solids flux. Results at a wide variation of experimental conditions indicated that the ratio of the slip velocity over the terminal velocity increases for smaller particles, higher gas velocities, and larger riser diameters (Arena *et al.*, 1988).

2.2 Reaction and mass or heat transfer in riser systems

If ideal gas-solids contacting in risers would occur, like in homogeneous very dilute flow, heat and mass transfer coefficients should be close to or higher than the values which are derived for a single spherical particle in a flowing medium (Ranz and Marshall, 1952):

$$\mathrm{Nu} = 2.0 + 0.6\,\mathrm{Re}^{1/2}\,\mathrm{Pr}^{1/3} \quad \text{or} \quad \mathrm{Sh} = 2.0 + 0.6\,\mathrm{Re}^{1/2}\,\mathrm{Sc}^{1/3} \qquad (1)$$

where Re represents the particle Reynolds number based on the slip velocity between the solids and the interstitial gas. If chemical reactions are considered, it should be possible to predict experimental conversions using relatively simple reactor models, including reaction kinetics.
Unfortunately, these expectations have not been validated thoroughly; only a limited number of studies has been dedicated to mass and heat transfer and chemical reactions in risers. They will be discussed hereafter, while distinguishing in heat transfer and mass transfer studies, and investigations in which reaction was the primary subject. All publications referred to are included in table I, which summarizes the conditions and results.

2.2.1 Heat transfer rates

Determination of heat transfer numbers (Nusselt number, $Nu=h_g d_p/\lambda$) was the subject of only few studies. In some of these studies particles were injected in a riser system, and contacted with hotter or colder gas (Bandrowski and Kaczmarzyk, 1978; Kato *et al.*, 1983; Watanabe *et al.*, 1991). Heat transfer numbers were then derived from the temperature rise or fall of the gas, by applying the appropriate heat and mass balances. Generally, they appeared to decrease at higher solids hold-ups and lower Reynolds numbers, especially in the region of small Reynolds numbers (viz. when smaller particle diameters were applied). Only for high Reynolds numbers (in practice large particles), and low solids hold-ups, the observed Nusselt numbers approach the values that can be derived from equation 1, but generally the values were lower.

In a series of papers, Dry *et al.* (1987, 1992, 1995) reported a different technique to measure the gas-solids contacting in riser systems. They injected a pulse of heated gas in the bottom section of a steady state operating riser, using a rapid-response thermocouple as a detector at the top. The loss in pulse area detected before and after adding particles to the riser was considered as a measure for the gas-solids contacting. In their derivation, equation 1 was used for the evaluation of the heat transfer coefficient, and an effective surface area was calculated from the gas-phase energy balance. Calculation of the so-called surface efficiency (viz. the ratio between the derived participating surface area and the available surface based on spherical particles) yielded very low values (i.e. 10^{-4}-10^{-3}). Similar to the authors referred to above, a higher value (viz. a better contacting) was observed at higher

gas velocities and for lower solids fluxes.
Explanations for the low values of the Nusselt numbers presented in literature are the overlap in the particle boundary layer (Watanabe *et al.*, 1991, which results in an overestimation of the driving force for heat transfer), or particle shielding by formation of clusters or streams of particles in the riser (Dry *et al.*, 1987, 1992, 1995).

2.2.2 Mass transfer rates

Several investigations in literature were dedicated to the measurement of gas-solids contacting while applying ad- or desorption systems (Kwauk *et al.*, 1986; Van der Ham *et al.*, 1991; Vollert and Werther, 1994) for the measurement of mass transfer rates.

Similar to the above mentioned heat transfer studies, in most of the mass transfer studies an increase in the mass transfer number was observed at lower solids hold-ups and higher superficial gas velocities. These observations remained valid even when turbulent fluidization was considered (Kumar *et al.*, 1993). In figure 13, to be discussed in detail later, measured and re-evaluated Sherwood and Nusselt numbers from the various publications are presented. The Sherwood number calculated from the appropriate mass balances by all these authors, fit in (or are even located below) the band of literature data for packed and fluidized beds, presented in the diagram of Sherwood/Nusselt versus Reynolds by Kunii and Suzuki (1967). This trend is shown in figure 13 by the shaded area, and is situated considerably (one or two decades) below the Ranz-Marshall equation for the relevant Reynolds regime. This obviously suggests poor gas-solids contacting in riser systems. Van der Ham *et al.* (1991, 1994) re-evaluated some literature studies, and showed that heat transfer numbers derived from the data obtained by Dry and White (1987) were decades lower than their own data and those derived from other literature sources. Despite this quantitative discrepancy (most probably due to an incorrect definition of the driving force) the qualitative trend in the observations of Dry and White is in agreement with those of other researchers.

2.2.3 Reaction rates

In studies, in which a reaction was involved, the overall conversion has usually been compared with the one calculated from a reactor model taking into account the intrinsic reaction kinetics, reactor geometry, and operating conditions (Masai *et al.*, 1985; Jiang *et al.*, 1991; Sun and Grace, 1990, 1991, 1992, 1994; Pagliolico *et al.*, 1992; Ouyang *et al.*, 1993, 1994, 1995; Marmo *et al.*, 1995). If gas-solids contacting is ideal, it should be possible to use a simple reactor model (f.i. a plug flow model) to predict the actual conversion. However, in most of the experiments published in the literature, lower conversions were observed than expected on basis of such a model.

Table I. Experimental work on gas-solids contacting in risers.

Authors	method	I.D. (m)	L (m)	material	ρ_p (kg/m^3)	d_p (μm)	Re	remarks
Bandrowski and Kaczmarzyk (1978)	Heat transfer	0.06	3.8	ceramic spheres	2469	700..2560	180..1800	$Nu = 0.00114\,\beta^{-0.5984}\,\mathrm{Re}^{0.8159}$
Kato *et al.* (1983)	Heat transfer	0.105 0.077 0.052	0.60 0.40 0.40	activated alumina	900	32..83	5..150	packings, countercurrent operation $Nu = 0.00238\left(\frac{1-\beta}{\beta}\right)^{0.97}\mathrm{Re}^{n}$ $n = 2.48\left(\frac{1-\beta}{\beta}\right)^{-0.28}$
Masai *et al.* (1985)	dehydratation of 2-propanol	0.028	1	silica-alumina	1000[a]	70[a]		low solids fluxes low gas velocities
Kwauk *et al.* (1986)	adsorption	0.024	1.5	active carbon		570	38	
Dry *et al.* (1987, 1992a, 1992b,1995)	heat pulse	0.09 0.102 0.60	7.2 3.86 7.5	FCC fine sand coarse sand	1370 2650 265	71 140 275	7..100	
Jiang *et al.* (1991)	ozone decomposition	0.102	6.32	impregnated FCC	1500	89		baffles
Watanabe *et al.* (1991)	heat transfer	0.021	1.8	glass beads activated alumina	2500 650	194..648	20..200	
Sun and Grace (1992)	ozone decomposition	0.1	2.6	FCC	1580	60		wide, narrow and bimodal particle size distribution
Pagliolico *et al.* (1992)	ozone decomposition	0.05	4.5	FCC	2970	82		low solids fluxes
van der Ham *et al.* (1991)	naphtalene adsorption	0.04		FCC	880	70	7..20	packings $Sh = 0.021\,\beta^{-0.55} \quad \mathrm{Re} = 5.38$ $Sh = 0.058\,\beta^{-0.50} \quad \mathrm{Re} = 10.38$
van der Ham *et al.* (1993)	H_2S absorption	0.015	1.2	FCC	1400	100	1..4	mass transfer/reaction in series
Vollert and Werther (1994)	NO adsorption	0.025	2.35	Hopkalit		169	8..15	
Marmo *et al.* (1995)	ozone decomposition	0.05	5					
Ouyang *et al.* (1993b, 1994, 1995a/b)	ozone decomposition	0.254	10.5	FCC	1380	79		

[a]estimated

For example, by systematically varying gas velocities, solids fluxes and apparent reaction kinetics, Ouyang and co-workers and Marmo *et al.*, demonstrated (independently from each other) that the conversion in a riser was lower than the one derived from various models, including the plug flow model and a combination of an ideally stirred tank reactor (CISTR) and a core-annulus model. The agreement between experimental and theoretical results improved with decreasing solids hold-up and increasing gas velocity. On the other hand, the experimental conversions presented by Pagliolico *et al.* (1992) for low reaction rates could be predicted within reasonable accuracy with a simple plug flow model.
Only the experiments of Masai *et al.* (1985) yielded much higher (instead of lower) conversions in the riser regime than predicted by theoretical models. However, it seems that these authors underestimated the actual solids hold-up: the relatively low gas velocities applied indicate that the measurements were carried out in the turbulent regime (see the transition criteria derived by Bi *et al.*, 1995; Bi and Fan, 1992).

2.2.4 Additional parameters

Some authors report on the effects of other factors than the solids hold-up and gas velocity, such as the particle diameter, reactor diameter and particle size distribution or the effect of the introduction of obstacles in the riser .
Dry *et al.* (1992, 1995) showed that the surface efficiency in his experiments decreased for smaller particles, suggesting that coarser particles are less likely to participate in cluster or stream formation. This is in agreement with the observations reported in the hydrodynamic results reported in chapter 3 of this thesis. Dry and co-workers also investigated the effects of the configuration of the inlet section and the dimension of the riser column. Unfortunately, no values for the particle surface efficiencies were given, and contact efficiencies can not be evaluated for these particular experiments.
The influence of the particle size distribution has been examined by Sun and Grace (1990, 1991, 1992) by measuring the conversion of the ozone decomposition reaction for three particle size distributions of FCC catalyst (wide, narrow and bimodal, all with nearly the same mean diameter and particle density). The results were again compared with theoretical models. For the narrow-size particle distribution, the observed conversion was always significantly lower than expected on basis of the ideally-stirred-tank-reactor. The latter result is in agreement with observations by Ouyang and co-workers and Marmo *et al.* Surprisingly, for this type of bed material Sun and Grace observed no significant differences in conversion behaviour for various fluidization regimes (bubbling, turbulent and fast) if equivalent reaction conditions (viz. at equal values of the non-dimensional reaction numbers $N_r=k_p\beta\tau$) were applied. For the wide-size distribution the conversion in the riser regime appeared to be higher than predicted by a suitable ideally-stirred-tank-reactor model. A better description for this particular case was obtained by applying a single-phase axial dispersion model. Apparently, for this particle size distribution the riser performance was improved. Sun and Grace attributed this to an increased solids concentration in the voids for the wider size distribution.
By several authors, the formation of particle clusters in the riser is considered as the major cause for the loss in the contacting between gas and solids. It was therefore suggested that the introduction of baffles in the riser, or increasing the gas velocity, should disturb the cluster structure and improves the radial gas and solids mixing. In some experimental studies it was indeed observed that such obstructions in risers resulted in higher conversions at similar operating conditions, viz. at equivalent solids hold-ups (Jiang *et al.*, 1991; Van der Ham *et al.*, 1991).

2.3 Summary of the literature findings

From this review, it should be concluded that the general idea that the gas-solids contacting

in a riser is excellent does not follow from the results of the reported experimental work. The contacting efficiency depends on the solids hold-up, gas velocity, particle size and size distribution and so on. Gas-solid contacting becomes worse at conditions of low Reynolds numbers (low gas velocities or small particles) and high solids hold-ups (viz. higher solids fluxes).

Apparently, in riser systems, both, the momentum and the mass/heat transfer rates, are much lower than expected for individual particle contacting. In the literature, this decreased gas-solids contacting at higher solids hold-ups and lower gas velocities is often attributed to the formation of cluster-like structures in the riser (Jiang *et al.*, 1991; Marmo *et al.*, 1995; Van der Ham *et al.*, 1991, 1994; Vollert and Werther, 1994). This explanation seems reasonable, because the existence of such clusters drastically may affect the hydrodynamic conditions, thereby decreasing the apparent mass or heat transfer coefficients. With respect to hydrodynamics, the gas exerts its drag force upon the particle clusters and not on the individual particle. In conversion processes two additional transfer resistances are then important, apart from the (possible) mass transfer resistance over the gas film around each particle. One is related to the mass transfer of reactant from the main gas bulk to the cluster surface, and the other to the effective diffusion inside such a cluster (mass transport in the clusters due to convection is then neglected). These resistances are schematically indicated in figure 1 for the extreme cases of (a) a conversion controlled by the reaction kinetics and (b) a conversion controlled by gas-to-particle mass transfer.

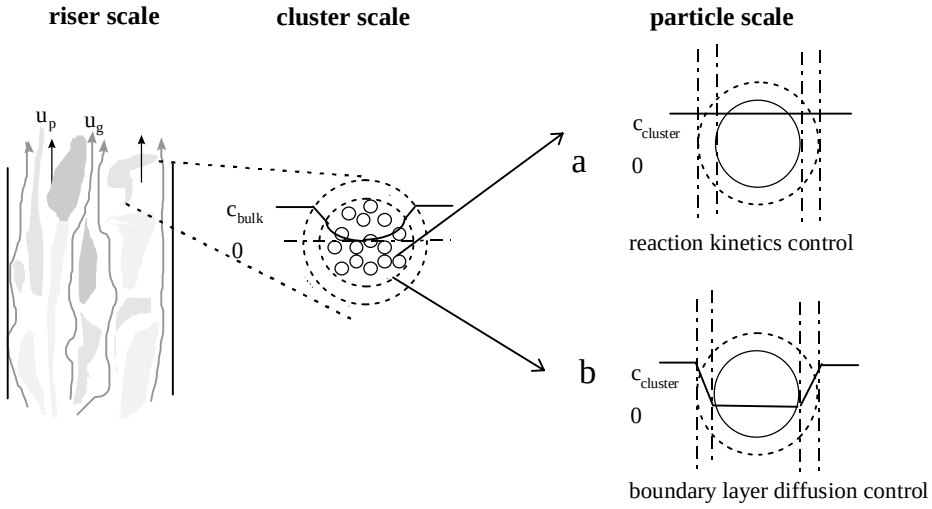

Figure 1. Possible local concentration profiles due to cluster formation
a) particle reaction controlled by the intrinsic reaction kinetics, and
b) particle reaction controlled by boundary layer diffusion.

The (observed) clustering and/or segregation of the solids in a riser thus causes a considerable gas by-passing for the individual particles by this shielding effect. Mass (and heat) transfer numbers measured in risers systems should then be much lower than those expected if the particles are contacted individually.

2.4 This work

Measuring conversion rates while varying the local reactivity of the catalyst, f.i. by decreasing the temperature (in case of conversion rates controlled by the intrinsic chemical

reaction rate), or by diluting with inactive particles, seems to be an attractive method to examine the gas-solids contacting in a riser. In the case of dilution of an extremely reactive catalyst, the reaction rate may be dominated by diffusion limitation inside the particle cluster or, at very high dilutions, in the gas film around the particles. At low dilution ratios however, the mass transfer rate to the cluster surface is rate controlling (the cluster effectivity is practically zero). In the present experiments, such a highly reactive system has been used, viz. the oxidation of carbon monoxide over a platinum catalyst at conditions where the local reaction rate is controlled by the gas-to-particle mass transfer resistance (see also chapter 2). The aim of using this reaction is twofold. Firstly, additional data for mass transfer in a small scale laboratory riser can be derived from the conversion experiments. Secondly, dilution of the active catalyst by inert material provides insight in the particle clustering phenomenon. In the present work, the results obtained are compared with conversion experiments performed by Ouyang and co-workers (1995) for the case of the kinetically controlled ozone decomposition reaction.

3 OXIDATION OF CARBON MONOXIDE

From chapter 1, a suitable model reaction is available for the study of contacting between solids and gas in the riser of a circulating fluidized bed. This reaction, the oxidation of CO over a platinum based catalyst offered advantages over other model reactions for various reasons suggested in chapter 1. The most important one is the that, when going from a kinetically controlled reaction at low temperatures to mass transfer controlled reaction at the higher temperatures, a shift in the apparent order in CO will be observed, viz. from a negative value to plus one (chapter 1 of this thesis). Furthermore, upon arriving in the mass transfer controlled regime, the apparent activation energy should be decreased to a value in line with the temperature dependency of diffusional transport. In chapter 2 it has been shown that mass transfer controlled conditions can be obtained in a packed bed (with particle clusters) at relatively mild operating conditions (< 800 K), even for very small particles (d_p=65 μm). Obviously, the CO oxidation over a platinum catalyst is a very suitable model reaction, because it allows for verification in several distinct ways whether the mass transfer rate or the reaction kinetics dominates the conversion process. A combination of observations enables the classification of the operation regimes with high confidence.

4 EXPERIMENTAL CONDITIONS

For the measurement of mass transfer rates in risers a platinum-based catalyst has been used. The 0.5 wt.% platinum/γ-alumina catalyst was taken from the same batch of active material as has been prepared in chapter 1. An impregnation method is applied using an aqueous solution of hydrogenhexachloroplatinate, H_2PtCl_6, and γ-alumina (Engelhard Al-3912P) was chosen as a carrier material, because of its mechanical stability in fluidized bed reactors (see chapter 1). To avoid any differences in particle properties, pure γ-alumina was used as the inert bed material. The only remaining (slight) difference was the one in average particle diameter, being 54 μm for the active particles and 65 μm for the inert ones. In table II some other properties of the bed material used are listed.

Table II. Main properties of the bed material at ambient conditions.

Property	γ-alumina
d_p (μm)	65
ρ_p (kg/m^3)	1375
u_t (m/s)	0.16
Ar (-)	13.8
Geldart's type	A

4.1 Riser facility

The oxidation of carbon monoxide is performed in the lab-scale riser facility shown schematically in figure 2. The dimensions of the lab-scale facility are the same as in the experimental work of Van der Ham *et al.* (1994). It consists of i) a gas mixing section to provide the required gas mixture for the oxidation reaction, ii) a circulating fluidized bed set-up surrounded by an electric oven, and iii) an analysis section. The circulating fluidized bed set-up is entirely made of quartz and consists of a riser section (ID 0.015 m, L. 1.17 m), two cyclones, a solids flow measuring device, a standpipe for storage of particles, and a L-valve for solids control. During the experiments, the concentrations of CO and CO_2 were monitored continuously by two Maihak analyzers.

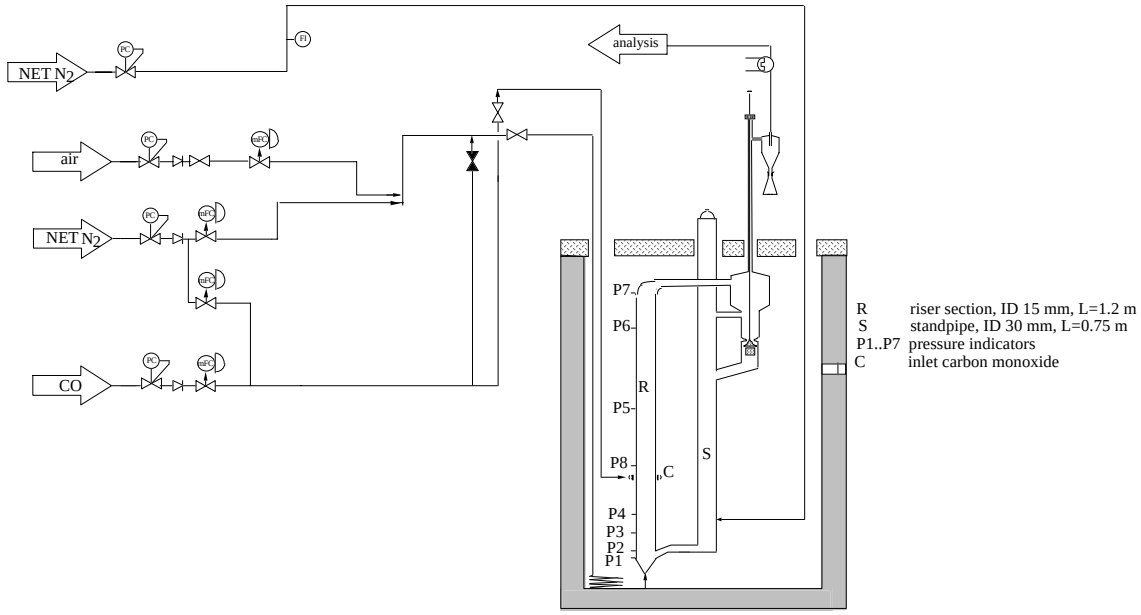

Figure 2. Schematic representation (non-scale) and flowsheet of the lab-scale circulating fluidized bed.

A series of thermocouples and pressure taps are positioned along the riser wall to measure and control the reactor temperature and pressure drops. The solids hold-up is determined with sufficient accuracy by measuring the axial pressure profile, thereby neglecting solids-wall friction, which is a reasonable assumption for the γ-alumina material applied in this work (chapter 3 of this thesis). The solids flux is measured by closing the outlet of the solids, down-flow of the cyclone, and measuring the time to collect a calibrated volume of particles (see figure 2). The gas flow through the bed is controlled by several Brooks mass flow controllers, allowing the gas velocities to be varied from 2.5 to 4.5 m/s, the oxygen content from 5 to 12 vol.%, and the carbon monoxide content in the range of 0.4 to 1.2 vol.% (balance N_2). The CO was introduced at a position 0.45 m above the gas inlet through 5 injection points (ID 0.5 mm), equally distributed over the riser periphery. From pressure drop experiments it has been established that in this part of the riser a developed region was present for all operating conditions applied. The conversion experiments were performed at temperatures varying from 620 to 775 K, with an active material diluted in ratios ranging from 150 to 2500 (volume of inert material over the volume of catalyst).

Fresh active material has been used whenever a new series of experiments with another dilution ratio was started. The experiments were carried out from high to low dilution ratios

ensuring that very small amounts of active material, inevitably remaining in the reactor, do not affect the subsequent conversion experiments. The γ-alumina was shown to be inactive for the specified reaction in the range of operating temperatures. Experiments with a bed material prepared by dilution of a less diluted bed material, used already before, with inactive alumina, yielded similar results as those for which a fresh mixture of active/inert material has been prepared. The results of all measurements appeared to be well reproducible, and no deactivation of the catalyst was noticed.

5 RESULTS

5.1 Hydrodynamics

First, the solids hold-up in the riser set-up has been determined at two temperatures (295 and 775 K respectively) and at various operating conditions by recording the pressure profile across the riser length. In an earlier paper it was shown already that, even in such a small-scale riser unit, the solids hold-up derived from pressure drop measurements (equation 2) is correct (see chapter 3). In figure 3, the measured solids hold-up is presented as a function of the solids flux for two superficial gas velocities.

$$-\frac{\partial P}{\partial z} = 4f_g \frac{(1-\beta)\rho_g u_g^* \left|u_g^*\right|}{2D_t} + \rho_p \beta g \approx \rho_p \beta g \qquad (2)$$

while the slip velocity can be found from:

$$u_s = \frac{u_g}{(1-\beta)} - \frac{G_s}{\rho_p \beta} \qquad (3)$$

The solids hold-up increases with the solids flux G_s and decreases with the gas velocity u_g, as might be expected from the simple one-dimensional model (Yang, 1977). At a given gas velocity, the ratio of solids flux over solids hold-up G_s/β, remains approximately constant, indicating that the particle velocity $G_s/(\rho_p\beta)$ is, as a first approach, independent of the solids flux. The slip velocity (equation 3) is therefore constant, which is in agreement with the results presented earlier in chapter 3 of this thesis.

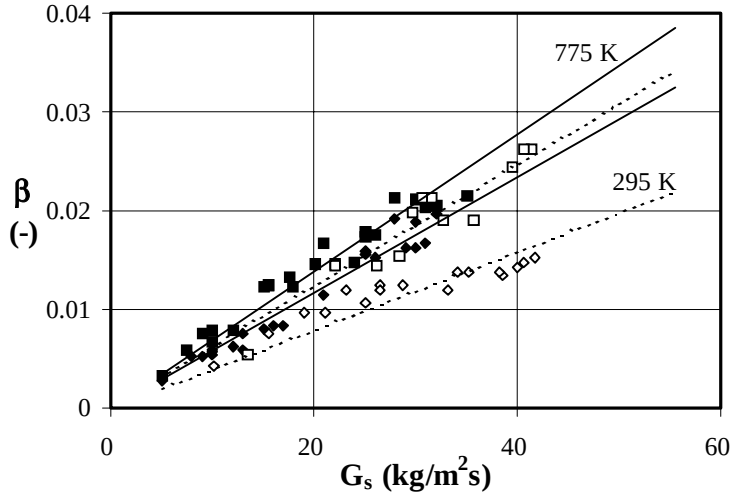

Figure 3. The solids hold-up, β, derived from the axial pressure profile (equation 2) versus the solids flux, G_s, at two different temperatures 295 and 775 K. Legends: ■ u_g=2.5 m/s, T=775 K; ◆ 3.5 m/s, and 775 K; □ 2.5 m/s, 295 K; ◊ 3.5 m/s, and 295 K. Trends are given as solid lines.

Clearly the solids hold-up is higher at elevated temperatures, which is in agreement with

results obtained by Vollert and Werther (1994). Apparently, the effect of an increasing gas viscosity is dominant over the effect of the corresponding decrease in gas density. This is also illustrated by the decrease (with almost a factor 10) in the Archimedes number (Ar=13.7 at 300 K, and Ar=1.7 at 775 K). At higher temperatures, lower terminal falling velocities are derived (u_t=0.175 m/s and u_t=0.09 m/s at 295 and 775 K respectively). However, experimental results also indicate that the ratio of the slip velocity over the terminal velocity increases for higher temperatures. These ratios are 10 and 25 for T=295 K and 775 K respectively (u_g=3.5 m/s in both cases). The slip velocities observed in the present paper are much lower than those obtained at ambient conditions in the chapter 3. Probably, this is due to the effect of the exit of the riser (the riser column lengths was 2 m in the earlier work, and 1.17 m for the riser used in the present work).

5.2 Mass transfer

5.2.1 Determination of the mass transfer controlled conditions

As stated earlier, the kinetics of the oxidation of CO over a Pt/γ-alumina can thus be described by means of a Langmuir-Hinshelwood reaction scheme (see chapter 2 of this thesis). Whether mass transfer or the kinetics is the controlling step, can easily be verified by both, i) determining the observed order in the carbon monoxide and oxygen concentrations and ii) calculation of the apparent activation energy.

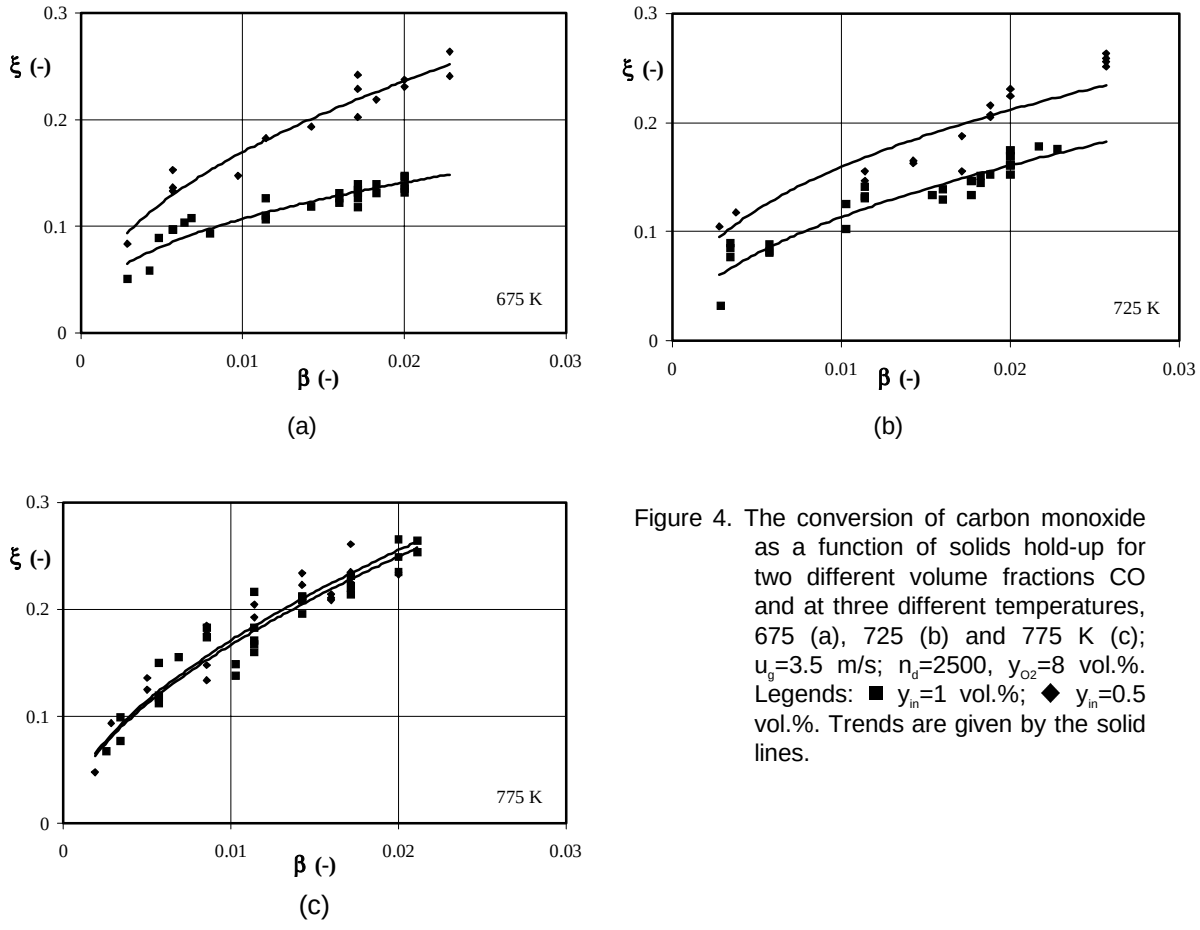

Figure 4. The conversion of carbon monoxide as a function of solids hold-up for two different volume fractions CO and at three different temperatures, 675 (a), 725 (b) and 775 K (c); u_g=3.5 m/s; n_d=2500, y_{O2}=8 vol.%. Legends: ■ y_{in}=1 vol.%; ◆ y_{in}=0.5 vol.%. Trends are given by the solid lines.

The first experiments in the present work have been carried out at a superficial gas velocity of 3.5 m/s and a dilution ratio n_d=2500. As a first remark, in these experiments multiple steady state solutions and oscillations have not been observed. In figure 4 the conversion, ξ, is plotted as a function of the solids hold-up, β, for two volume fractions CO (y_{in}=0.5 and 1 vol.%) and at three different temperatures (675, 725 and 775 K).
As expected the conversion increases with the average solids concentration β. Besides, at the lower temperatures, the conversion depends on the volume fraction CO: lower values yield higher relative conversions indicating an apparent reaction order in carbon monoxide below 1. Obviously, the reaction kinetics are still important at the lower temperatures. At the higher temperatures the effect of the inlet volume fraction of CO, y_{in}, vanishes. For 773 K a first order reaction in CO is observed, as the relative conversion becomes independent on the CO concentration. This indicates mass transfer controlled conditions. The conversion curve for y_{in}=0.5 vol.% remains approximately unchanged in the three diagrams, while the one for y_{in}=1 vol.% is affected notably by the temperature increase. This is in agreement with LH kinetics.

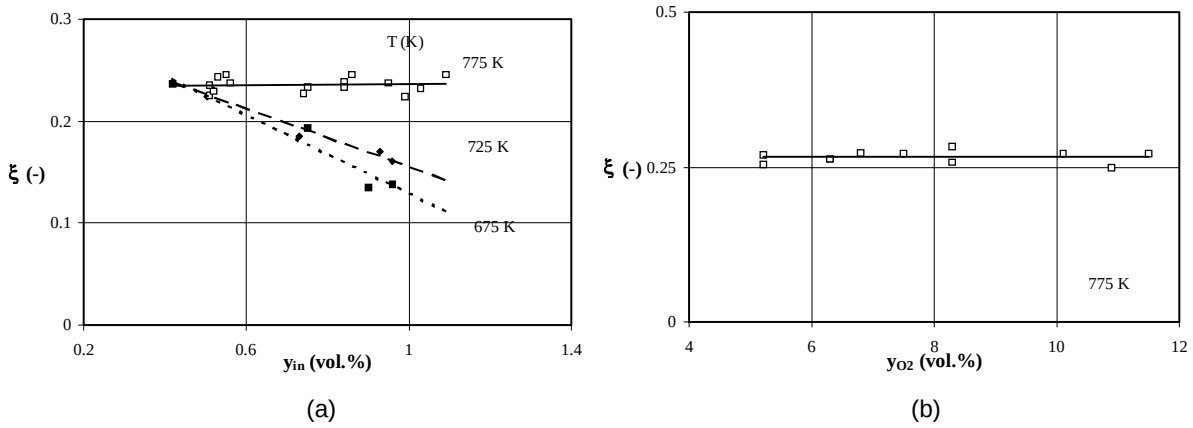

Figure 5. (a) The conversion of carbon monoxide as a function of the CO inlet volume fraction, y_{in}, for three different temperatures and (b) the conversion as a function of the volume fraction O_2, y_{O2}, at 775 K. Operating conditions: u_g=3.5 m/s; n_d=2500; β=0.02; y_{in}=0.8 vol.%, y_{O2}=8 vol.%. Legends: ■ 675 K, ◆ 725 K and □ 775 K.

The effects of reactant concentrations on the conversion are further elucidated in figure 5. Figure 5a shows the conversion as a function of y_{in} for 3 operating temperatures. At 675 and 725 K, lower conversions are observed at increasing values of y_{in}. This is in accordance with an apparent reaction order in carbon monoxide lower than 1. However, at 775 K the conversion becomes independent of y_{in}, suggesting that the reaction rate is mass transfer controlled at this temperature.

In figure 5b the conversion of CO is plotted as a function of the inlet volume fraction O_2, y_{O2}: clearly the oxygen inlet concentration does not affect the conversion. A zero order in oxygen is indeed plausible, because oxygen is available in large excess and the conversion rate at 775 K is determined by the mass transfer of CO only.

For mass transfer controlled conditions (and consequently first order reaction in the reactant), the apparent reaction rate constant per unit volume of catalyst, k_{ov}, can be derived easily from the conversion if plug flow behaviour of the gas is assumed over the measuring section of the riser with length ΔL:

$$k_{ov} = -\frac{u_g (n_d + 1)}{\beta \Delta L} \ln\left(\frac{c_{out}}{c_{in}}\right) \qquad (4)$$

in which n_d represents the dilution ratio in m_{inert}^3/m_{cat}^3.

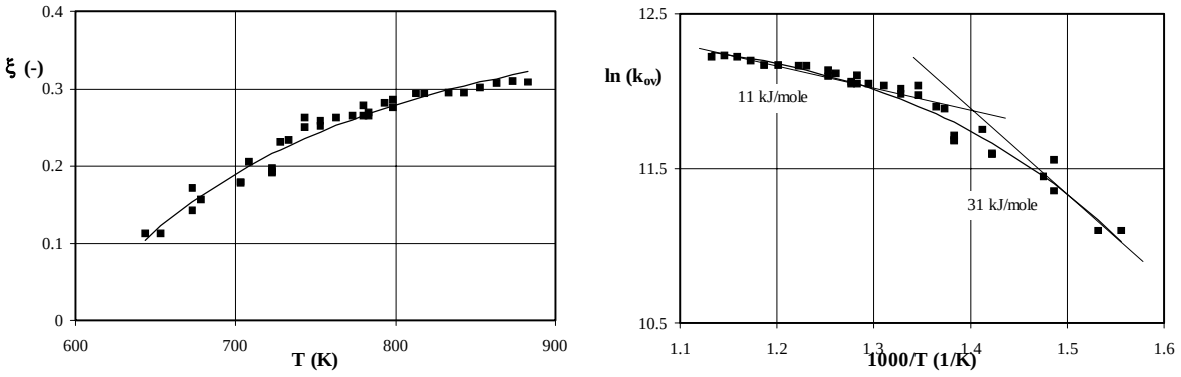

(a) (b)

Figure 6. (a) The conversion of carbon monoxide as a function of operating temperature and (b) the apparent kinetic rate constant calculated from equation 4 versus the reciprocal operating temperature; u_g=3.5 m/s; β=0.02; n_d=2500. Trends are indicated as solid lines.

Figure 6a shows the carbon monoxide conversion plotted against the operating temperature. At low temperatures it increases almost linearly with temperature. At higher temperatures however the slope of the curve decreases by the gradually increasing influence of mass transfer. Plotting the logarithm of k_{ov}, derived from equation 4, versus the reciprocal temperature (see figure 6b) the apparent activation energy for the reaction can be determined from the slope of the curve obtained. At temperatures below 735 K an apparent activation energy of 31 kJ/mole is estimated. At higher operating temperatures (> 750 K), this value reduces to approximately 11 kJ/mole. In comparison, for complete kinetically controlled conditions apparent activation energies of about 95 kJ/mole were derived (chapter 1).

Altogether, figures 4 to 6 support an important conclusion. Because the reaction is first order in the carbon monoxide concentration, the order in the oxygen concentration is zero, and the apparent activation energy is equal to the one that can be derived for gas-phase diffusion (≅ 11 kJ/mole according to Fuller *et al.*, 1966), mass transfer is identified as the reaction rate controlling step at temperatures > 750 K.
In chapter 1 it was shown, that by interpretation with a suitable particle model of independently measured conversion rates of the CO oxidation reaction, three regimes can then be distinguished, and those are shown in figure 7.

In this figure, the experimentally observed apparent reaction orders in CO, m, are compared with the model lines calculated for the case that the external mass transfer resistance is equal to the one inside the particle ($Bi_p=k_g d_p/2D_p=1$). The closed squares represent results of previous kinetic measurements in a fixed bed reactor (chapter 1), while the results in this work are included as closed triangles. The latter data points concerning the mass transfer experiments in the riser, indeed show that the reaction order is positive in the high temperature interval reaching unity at 775 K. At somewhat lower temperatures, the overall order decreases monotonously.

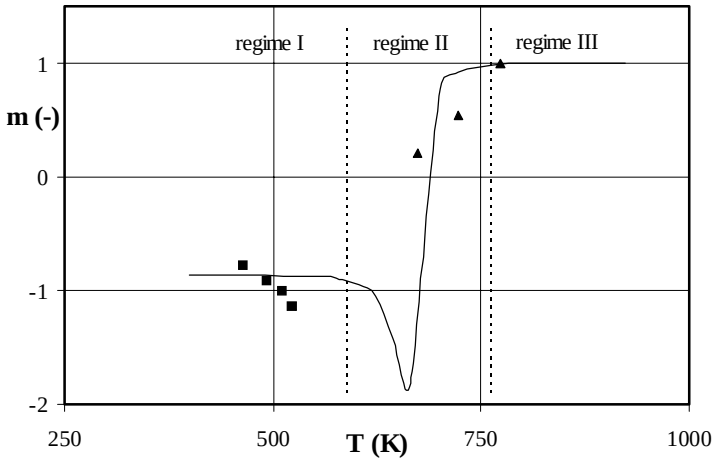

Figure 7. Reaction order of carbon monoxide as a function of the temperature. Comparison of simulated results for Bi_p=1 with some experimental data points of this work. Legends: ■ packed bed measurements (0.0078 m. I.D.): $(c_{O2})_{in}$ = 1.1-2.0 mole/m^3 and u_g = 0.4-0.6 m/s; ▲ this work: n_d = 2500, $(c_{O2})_{in}$ = 1.1-1.4 mole/m^3, β = 2 vol.% and u_g = 3.5 m/s.

5.2.2 Effect of solids hold-up and gas velocity

For mass transfer controlled conditions (T≥750 K), the order in CO is completely unity, and the overall Sherwood number Sh^0 can be derived from the apparent reaction rate constant, $k_{ov}=k_g a$, with $a=6/d_p$ as the specific surface area of the (spherically assumed) particle:

$$Sh^0 = \frac{k_{ov} d_p^2}{6D} \qquad (5)$$

D represents the bulk diffusion coefficient, which has been calculated by the correlation proposed by Fuller *et al.* (1962). In figure 8, Sh^0 is plotted as a function of the solids hold-up for three superficial gas velocities: 2.5, 3.5 and 4.5 m/s.

Although the data reported in figure 8 show much scatter (mainly due to fluctuations in the applied operating conditions, and to a lesser extent to inaccuracies of the measuring technique), several trends can be identified. At low solids concentrations the effective Sh^0 approaches a value in fair agreement with the one derived from equation 1 (Ranz and Marshall, 1952), which is plotted as a closed symbol on the y-axis. This clearly demonstrates that at T=775 K the conversion rate is completely controlled by the mass transfer resistances on the scale of the individual particles.
For higher solid hold-ups, the Sherwood numbers decrease significantly, approaching a more or less constant value, which is a factor 4 to 10 lower than the one predicted by equation 1. This decrease can not be attributed exclusively to axial dispersion of the gas at the higher conversion degrees. If an ideally stirred tank reactor is assumed instead of plug flow behaviour of the gas, at these relatively low conversions (less than 35%, see figure 6) the apparent Sherwood numbers will increase with at most 25%. Therefore, the decrease in Sh^0 with a factor 4 to 10 can only be caused by some segregation phenomena, such as cluster formation.

For all solids hold-ups, higher effective Sherwood numbers are observed at increased superficial gas velocities. Both, the effect of solids hold-up and gas velocity, are in good agreement with earlier published results (see f.i. Van der Ham, 1991, 1994; Ouyang *et al.*, 1995). The results obtained by Van der Ham *et al.* (1991) at a gas velocity of 2.2 m/s are

also indicated in figure 8: their Sherwood numbers are obtained in a regularly packed circulating fluidized bed reactor for the adsorption of naphtalene vapour on 70 μm FCC-particles at ambient conditions. Although the 'active' particles were not diluted with inert material, reasonable agreement with our results for a gas velocity of 2.5 m/s is obtained. Apparently, similar to the introduction of baffles or packings in the riser, dilution of active material suppresses the influence of cluster formation.

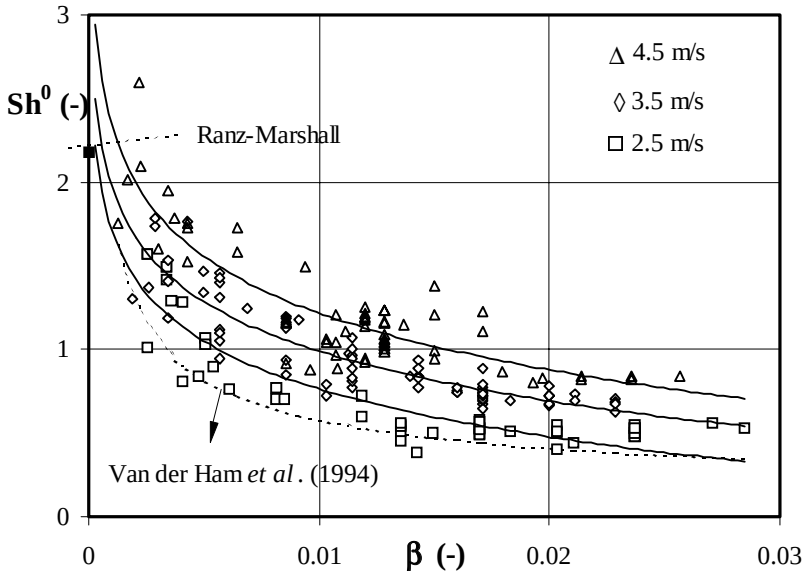

Figure 8. The apparent Sherwood number Sh^0 (equations 5 and 6) as a function of the solids hold-up and for three superficial gas velocities 2.5, 3.5 and 4.5 m/s. Operating conditions: T=775 K; n_d=2500. The dashed line represents the results by Van der Ham *et al.* (1991) for the adsorption of naphtalene vapour on FCC-particles in a regularly packed circulating fluidized bed at u_g=2.24 m/s and are used as an indication. The other solid lines merely indicate the trend in our results. Legends: □ u_g=2.5 m/s; ◊ u_g=3.5 m/s; Δ u_g=4.5 m/s. The closed symbol on top of the y-axis represent the Sh value calculated from equation 1.

5.2.3 Effect of dilution

Up to this point the effect of different parameters on the gas-solids contacting were considered for a dilution ratio n_d=2500 only; higher dilution ratio yielded too low conversions to be evaluated with sufficient accuracy. Despite this high value for the dilution an important effect of the solids hold-up on the observed Sherwood number could be noticed. Apparently, there is still a considerable effect of particle shielding. As the dilution ratio is decreased, and the kinetic rate constant per unit volume of reactor increased, this shielding effect is expected increase, because then the external gas-to-cluster surface mass transfer resistance is becoming more and more important, see figure 1.

In figure 9 the effective Sherwood number is plotted as a function of β for 3 different dilution ratios, n_d=150, 500 and 2500, for a gas velocity of 3.5 m/s.
Sherwood decreases significantly again with the solids hold-ups, and approaches an asymptotic value at approximately β>0.03. The Sherwood number is indeed strongly affected by the dilution ratio: for a dilution ratio of 150, Sh^0 is more than a decade lower than the value predicted by equation 1, which is presented as the closed symbol on the y-axis. In the calculation of Sh in this Ranz-Marshall equation, the Re number is based on the terminal falling velocity of the individual particle.

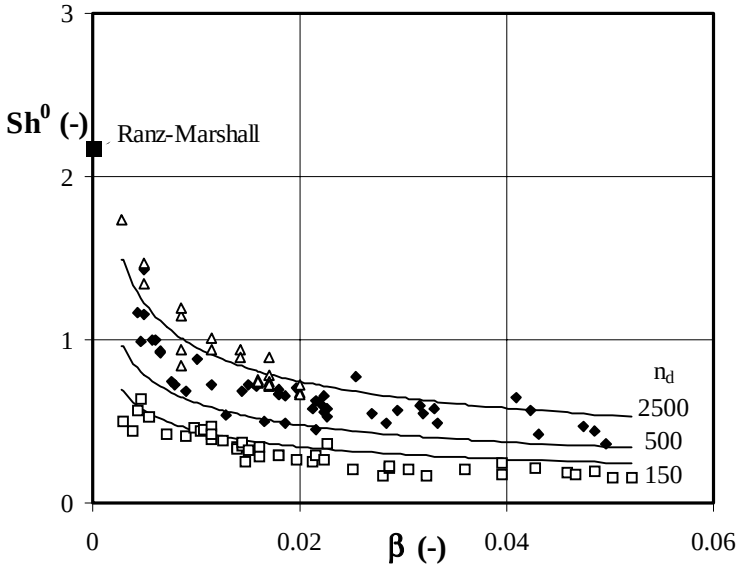

Figure 9. The effective Sherwood number Sh^0 as a function of the solids hold-up β for different dilution ratios n_d; u_g=3.5 m/s; T=775 K. Legends: Δ n_d=2500; ◆ n_d=500; □ n_d=150. The solid lines only illustrate trends. The closed symbol on top of the y-axis represents the value derived from equation 1.

These conclusions are further elucidated in figure 10, where the same results are plotted as Sherwood versus the dilution ratio n_d for three solids hold-up values.

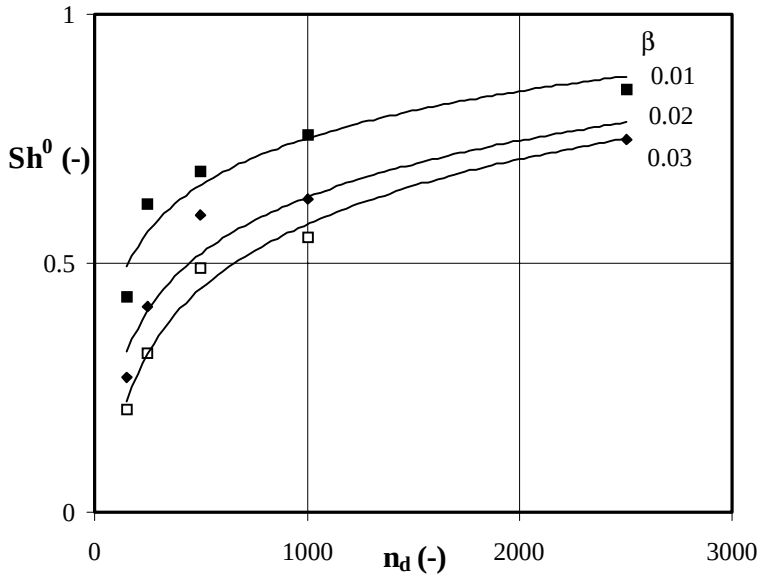

Figure 10. The overall Sherwood number Sh^0 as a function of the dilution ratio n_d for different solids hold-ups, β; u_g=3.5 m/s; T=775 K. Legends: ■ β=0.01; ◆ β=0.02; □ β=0.03. Trends are indicated as solid lines.

The figure shows the increase in Sh^0 as a function of the dilution ratio. At high n_d values (>1000), Sh^0 becomes less dependent on the dilution ratio, but even at values approaching n_d=∞, the Sherwood number level is still below the Ranz-Marshall prediction. Following the particle cluster concept, the active particles are now only affected by diffusional resistances inside the cluster. On the other hand, for lower dilution ratios, Sh^0 decreases significantly and becomes a strong function of n_d. Increasing the amount of active catalyst over inert material leads to a different effect of shielding, viz. the local depletion of reactant in the cluster caused by adjacent active particles. In that case, the active particle experiences a

much lower average reactant concentration. Consequently, the Sherwood number, which is derived on basis of the amount of active catalyst, is consequently decreasing. It will be shown later in this paper, that the available literature data indeed show that Sherwood values at n_d=0 are decades lower than those derived from the Ranz-Marshall equation (see figure 13).
The above mentioned phenomena can be explained from a particle cluster concept, see figure 1. In the present work, it is therefore concluded that cluster formation is the most important cause for the anomalies found in the literature. Hereafter, some additional evidence in favour of cluster formation will be presented.

5.2.4 Effect of the non-dimensional reaction number

While assuming that in the ideal case the conversion rate is controlled by the mass transfer resistance in the film around the active particles, and first order kinetics, the value for the theoretical maximum conversion rate constant $k_p\eta_p$ (with k_p as the theoretical maximum value for the intrinsic reaction rate constant, and η_p as the effectiveness factor of the single particle, based on the bulk concentration) can be taken as ShD/d_p, with Sh again being derived from the Ranz-Marshall equation. In this way, the non-dimensional reaction number for the riser system considered here can be defined as $N_r=k_p\eta_p\beta\tau/(1+n_d)$, and is varied by changing G_s (or β) and n_d. The $k_p\eta_p$ value obtained from the Ranz-Marshall equation is now an “intrinsic reaction rate constant” for mass transfer controlled conditions. The idea to relate the contact efficiency to the ‘ideal’ Ranz-Marshall value is supported by the results presented in figure 8, which indicate that this ideal value is approached indeed when β goes to zero. Values of the contacting efficiency η can be derived by dividing the measured conversion rate constant (obtained on basis of assumed plug flow behaviour) by the one derived from the Ranz-Marshall value, leading to $\eta=(k_{ov})_{PF}/(k_p\eta_p)$ (see figure 11).

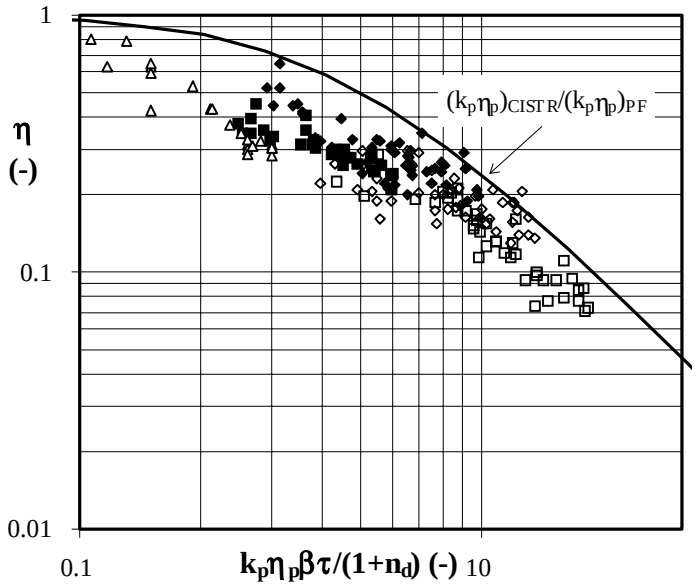

Figure 11. The contact efficiency, $\eta=(k_{ov})_{PF}/(k_p\eta_p)$, as a function of the non-dimensional reaction number at a gas velocity of 3.5 m/s, for all solids hold-ups. Legends: □ n_d=150;◊ n_d=250;◆ n_d=500;■ n_d=1000;Δ n_d=2500. The solid line represents the apparent loss in contact-efficiency for the extreme case of ideal contacting in an ideally-stirred-tank model $\eta=(k_p\eta_p)_{CISTR}/(k_p\eta_p)$, instead of the suggested plug model behaviour, that is represented by the line η=1.

At high reaction numbers the contacting appears to decrease significantly, due to the earlier discussed effects of the solids hold-up and the dilution ratio. The solid line in figure 11

represents the contacting efficiency obtained when an ideally-stirred-tank (and ideal contacting) instead of a plug-flow-reactor model is used upon the interpretation of experimental results: $\eta=(k_p\eta_p)_{CISTR}/(k_p\eta_p)$. The apparent loss in contacting may then be due to a wrong interpretation of the conversion data. The comparison with data points illustrates that the observed loss in contacting is even higher than for the extreme case of ideal gas phase mixing, which shows that the decrease in Sh^0 not be explained by axial dispersion only. In the introduction of this thesis it was shown that such a curve does not provide additional information about the rate controlling step. Besides, it can easily be calculated that for conversion levels below approximately 25% (which is the case for the high dilution ratio of n_d=2500, $k_p\beta\tau<0.3$), the differences between a plug-flow model and a stirred-tank interpretation are negligible anyway.
Apart from any reaction kinetic and external mass transfer resistances at the surface of the individual particles, it is evident that other resistances, presumably being located between the bulk of the gas and the surface of a particle cluster or inside the cluster, must be present in the riser flow. The influence of these additional resistances becomes more dominant at higher values for the non-dimensional reaction number.

6 DISCUSSION AND COMPARISON WITH PREVIOUS WORK

6.1 Literature concerning reactive systems

In studies where chemical reactions have been considered, the overall conversion was usually compared with the one calculated from a reactor model taking into account the intrinsic reaction kinetics, reactor geometry, and operating conditions. Ouyang *et al.* (1995) also defined the contacting efficiency as the ratio between the kinetic rate constant observed by ozon decomposition experiments in a riser and the one they derived from packed bed experiments, $\eta=k_{ov}/(k_p\eta_p)$ with $\eta_p=1$ (the theoretical maximum conversion rate constant is controlled by the intrinsic kinetics). The authors applied similar particles as used in the present work. Because they applied conditions for which the conversion rate on the particle scale was controlled by the rate of the chemical reaction, the non-dimensional reaction number $k_p\beta\tau$ could be varied by changing the operating temperature. In figure 12a, their data for the contacting efficiency are plotted as a function of the solids hold-up. Different symbols represent the various kinetic rate constants (or operating temperatures). It shows an negative root dependency on the solids hold-up, which is in line with our own data in figure 9 and with the earlier presented literature results. However, another distinct trend is notable: at low values for the solids hold-up, high contact efficiencies are observed, but in this region they decrease considerably with increasing reaction rate number.

Comparing figures 12a with figure 9, it is interesting to note that the data of Ouyang *et al.* show the same trend as those obtained in our work, despite the differences in applied technique and reactor diameter (0.015 m versus 0.254 m). Same trends have been reported earlier by Dry *et al.* (1987) and Van der Ham *et al.* (1994) for quite different experimental systems.

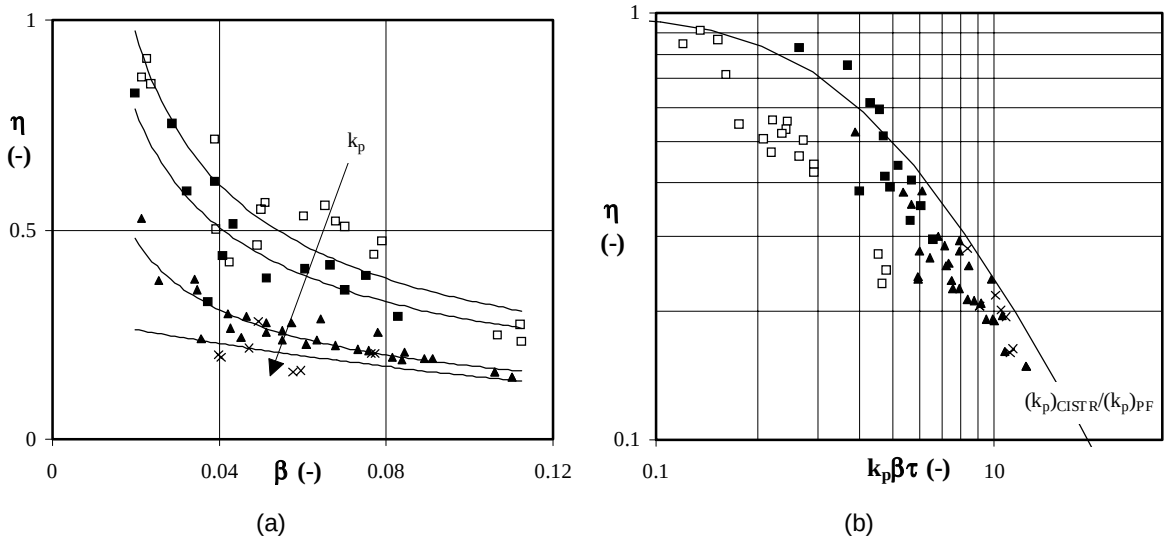

Figure 12. (a) The contact efficiency, η, for Ouyang's data (1995) as a function of solids hold-up and (b) the contact-efficiency versus the non-dimensional reaction number $k_p\beta\tau$. Legends: □ k_p=2-5 s^{-1}; ■ k_p=14-32 s^{-1}; ▲k_p=39-64 s^{-1}; x k_p=68-94 s^{-1}: indicated as solid lines in (a) are the trends in the effect of the solids hold-up; in (b) the solid line represents the apparent loss in contact-efficiency for the extreme case of ideal contacting in an ideally-stirred-tank model $\eta=(k_p\eta_p)_{CISTR}/(k_p\eta_p)$, instead of the suggested plug model behaviour, that is represented by the line η=1.

The influence of β on the contact efficiency for the data of the present work is significantly lower than for Ouyang's data. This can be explained by the fact that the values of the volumetric reaction rate for our data, $k_p\beta/(1+n_d)$, are considerably lower than the $k_p\beta$-values of Ouyang. This effect is already notable in figure 12a. At the low k_p-values in Ouyang's data, relatively high efficiencies are still observed beyond β=0.06, while for the high k_p-values the efficiency decrease is already quite significant at β<0.04. The influence of $k_r=k_p\beta$ on the efficiency derived from the data of Ouyang *et al.*, agrees very well with the dependency found in this study (order ≈ -0.25 to -0.3).
Although there is a large degree of agreement in results, an important difference can be observed in comparing our data with those of Ouyang *et al.* The effect of superficial gas velocity on the contact efficiency is notable in our mass transfer controlled experiments (see figure 8), but almost absent in Ouyang's data (see the original plot in their paper). This can be explained partly by the fact that intrinsic reaction kinetics (as in the case of Ouyang) should not be dependent on hydrodynamic conditions, whereas mass transfer numbers remain somewhat dependent on the Reynolds number. Another explanation might be that in our work the reactant was introduced in the developed region of the riser, whereas Ouyang's conversions are derived over the total riser length, including the acceleration zone. Perhaps, the structure of the acceleration region is less dependent on the superficial gas velocity.

It is now possible to compare the effect of the reaction number on the contact efficiency for our results (in which the conversion were controlled by mass transfer resistances) with its effect when the conversion is controlled by the intrinsic reaction kinetics, as in the case of Ouyang's data. Similar to figure 11, the contact efficiency derived from Ouyang's data can thus be plotted versus the non-dimensional reaction number. In figure 12b, the solid line indicates again the curve of the apparent contacting efficiency that can be derived if ideal mixing (and ideal contacting) is assumed for the gas phase instead of plug flow behaviour. This figure further shows again that at higher kinetic rate constants the contacting efficiency becomes worse. The kinetic rate constant should therefore be considered as an important parameter for the loss in contacting in a riser reactor. Similar to figure 11, the loss in contacting can be larger than the apparent contact-efficiency loss that can be expected as if

ideal contacting in a CISTR should have been considered instead of plug flow.
There is a single publication in which experimental conversions are well described by a simple plug flow model, viz. the paper by Pagliolico *et al.* (1992). However, the reaction conditions applied by these authors are differing from those of our work and of Ouyang *et al.* Whereas the experiments published by Pagliolico *et al.* (1992) are performed at low reaction numbers ($k_p\beta\tau\approx0.014$), the results obtained by Ouyang *et al.* (1995), see figure 12b, indicate that only for $k_p\beta\tau\gg0.1$ contact efficiencies in the riser decreases below one. This conclusion is supported by Marmo *et al.* (1995), who demonstrated that experimental data obtained at very low solids mass fluxes can still be described by a simple plug flow model. For these conditions, extra mass transfer phenomena do not play any role (viz. small or highly porous clusters). Unfortunately, Pagliolico and co-workers did not give any data for lower gas velocities, higher solids hold-ups, or at a higher reaction rate constant.

The apparent loss in contacting can not be attributed to any effect of axial mixing of the gas flow. In various papers it has been demonstrated that axial dispersion in risers of circulating fluidized beds set-ups can be neglected (amongst others Cankurt and Yerushalmi, 1978). Some authors already showed, that the presence of a core-annulus structure in the bed can neither explain the loss in contact efficiency (Ouyang *et al.*, Marmo *et al.*). As stated before, for Ouyang's data, the intra-particle and the single-particle external mass transfer resistances are certainly not the only cause for this collapse in contacting (the Thiele modulus for the single particle, ϕ_p, is smaller than 0.02, and therefore $\eta_p=1$; Westerterp *et al.*, 1987). Although the data in figure 11 and 12 show some scatter (also caused by experimental errors), it resembles the dependency of the effectiveness factor of a single particle versus a Thiele modulus. A modified cluster Thiele modulus, analogous to the single particle approach, could perhaps describe these data. However, for the prediction of the contact efficiency values for the cluster properties, such as cluster size and density, are required. They are expected to be influenced by the gas velocity and solids hold-up, and therefore not clearly defined. The determination of these parameters is subject of a further study.

6.2 Literature concerning direct mass and heat transfer measurements

In a previous section most of the literature concerned with gas-solids contacting has been discussed (see table I). The Sherwood data obtained in this work can now be compared with the earlier published results in the well-known plot of the Sherwood/Nusselt versus Reynolds number. It should be noticed that for the riser regime Re is based on the slip velocity between solids and gas. In figure 13 all relevant results are presented together with our own data for $n_d=250$ and $n_d=2500$. Despite the dilution of the active catalyst with inert material, the measured Sherwood numbers are still notably lower than those derived from the Ranz-Marshall equation, due to particle shielding. Only for high dilution ratios, high gas velocities and low solids volume concentrations the apparent mass transfer numbers approach the single-particle Ranz-Marshall expression. On the other hand, Sherwood numbers derived in this study are significantly higher than those of earlier publications, apparently due to the effect of dilution. In this respect, it is important to note that the apparent Sherwood numbers as observed here only reflects overall values, in which any other mass transfer resistance other than the gas-to-particle one is lumped.

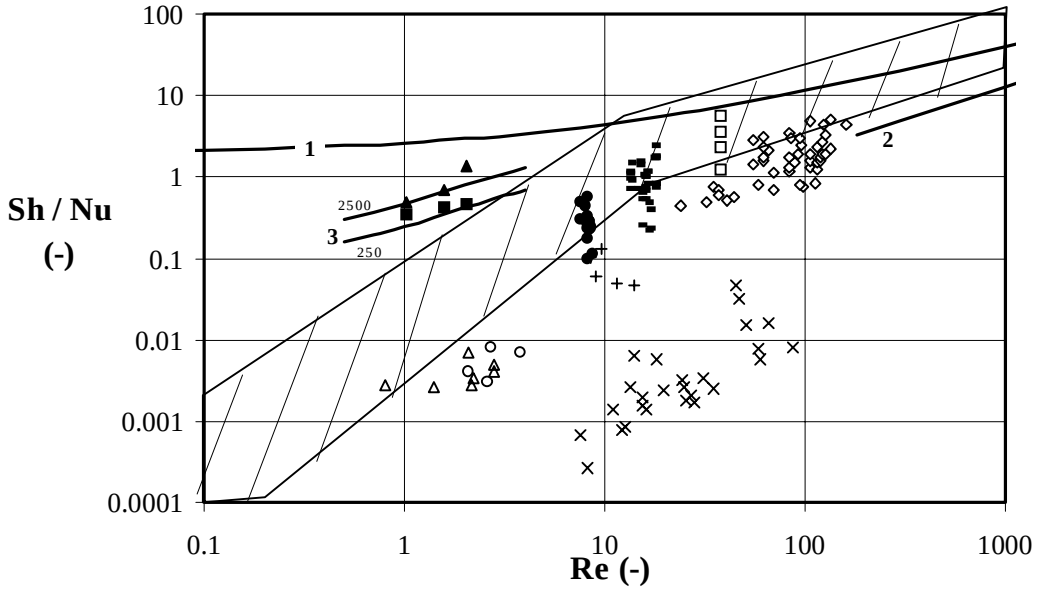

Figure 13. Sherwood and Nusselt numbers as a function of Reynolds number in circulating fluidized beds. Literature data for fluidized beds and packed beds are indicated (Kunii and Suzuki, 1967). Legends: x Dry *et al.* (1987, 1992a); □ Kwauk *et al.* (1983); ◊ Watanabe *et al.* (1991); Δ Van der Ham (1994); ❍ Van der Ham *et al.* (1994); ● Van der Ham *et al.* (1991); + Vollert and Werther (1994); own data; this work, β=0.02: ■ n_d=250; ◆ n_d=2500; **1.** Ranz and Marshall (1952a/b); **2.** Bandrowski and Kacmarzyk (1978) β=0.02; **3.** present data for n_d=2500, n_d=250, and β=0.02.

In appendix III of this thesis, the results of hydrodynamic measurements and of conversion measurements for the oxidation of carbon monoxide over a Pt/γ-alumina catalyst (both obtained with a small scale riser set-up; ID 0.015 m, L=1.17 m), are interpreted by a combination of a terminal falling velocity approach and the cluster model described in appendix II, to derive values for the apparent cluster size and its density.
The derived effective cluster diameter d_{cl} range from about 30 to 70 times the particle diameter (for superficial gas velocities of 4.5 down to 2.5 m/s), and appeared to be almost independent on the average solids concentration β in the riser. The cluster density β_{cl} ($0.05<\beta_{cl}<0.5$) increases at increasing average solids concentration, and with the gas velocity.

7 CONCLUSIONS

In this paper, the contacting between the gas and the solids is studied by investigating its hydrodynamics, as well as by performing conversion experiments for the mass transfer controlled oxidation of carbon monoxide over a Pt/γ-alumina catalyst.

First, from hydrodynamic measurements it was observed that the solids hold-up is linearly dependent on the solids flux. The calculated slip velocities are much higher than the terminal falling velocity of the individual particle. This result gives a first indication that the momentum exchange rate in a riser is far from ideal, and cannot be compared to single particle behaviour or even less to hindered settling.

It is demonstrated that at T=775 K the conversion rate is completely controlled by the mass transfer resistances on the scale of the individual particles. We substantiated the reduced contacting efficiency by observing the conversion rates for the CO oxidation over a Pt/γ-alumina catalyst under these completely mass transfer controlled conditions. The mass transfer controlled conditions were verified by using a strongly diluted bed material (active

catalyst over inert material in a ratio of 1:2500). A low value for the apparent activation energy was indeed measured at temperature above 750 K. Moreover, it was also observed that the orders in the reactant concentrations (CO and O_2) had shifted as to be expected from negative values for a kinetic controlled reaction rate towards +1 for mass transfer controlled conditions. The order in oxygen (+1 according to the verified reaction kinetics) becomes 0, as the conversion was controlled by the transfer of CO only (excess oxygen was present). These shifts in observed reaction orders are unique features of the reaction system and form a sensitive indication of the mass transfer regime.
It was shown that already at a high dilution ratio of 2500 m^3_{inert}/m^3_{cat}, the apparent Sherwood number depends on the (average) solids concentration approximately according to a negative square root dependency. This dependency has been reported already by a number of other investigators. The observed Sherwood number was found to be much lower than expected on basis of ideal gas-solids contacting, and it can be concluded, that in contrast with common believe, the gas-solids contacting in a riser is far from ideal.
Moreover, it was shown by dilution of the active material with inert γ-alumina, that the contact efficiency (defined as the ratio of the measured conversion rate constant over the theoretical maximum for the conversion rate constant) depends on the average local catalyst activity as well. Such an effect has never been published before: but based upon re-interpretation of results from other investigators (Ouyang and co-workers, 1995), a similar conclusion could be drawn. At low local catalyst activity the apparent gas-solids contacting improves significantly. Increasing the superficial gas velocity also results in an increased contacting between solids and gas.
The reduced gas-solids contacting in riser reactors systems, and the influence of the local catalyst activity on the observed contacting efficiency can be explained by the shielding of particles, due to the formation of clusters or strands of particles. A modified cluster Thiele modulus, based on the cluster dimensions could be used to describe the discrepancies between measured and theoretical conversions in riser systems. The effective cluster diameter d_{cl}, estimated in appendix III of this thesis, varies from about 30 to 70 times the particle diameter (u_g=4.5 down to 2.5 m/s), and does not depend very much on the average solids concentration β in the riser. The cluster density β_{cl} ($0.05<\beta_{cl}<0.5$) increases at increasing average solids concentration, and with gas velocity.

ACKNOWLEDGEMENT

We acknowledge the financial support of the Dutch Ministry of Economic Affairs through the Netherlands Energy Research Foundation ECN. We also thank E.P. van Elk and A. Groen for their assistance in the experimental work. We are also obliged to Dr. Shan Ouyang for providing us their experimental data.

NOTATION

a	specific surface area particle	m^{-1}
a	thermal diffusivity $\lambda/\rho_g c_p$	$m^2\ s^{-1}$
Ar	Archimedes number $d_p^3\rho_g(\rho_s-\rho_g)g/\mu_g^2$	-
c_{in}	reactant concentration inlet	mole m^{-3}
c_{out}	reactant concentration outlet	mole m^{-3}
c_p	specific heat	W m^{-3} K^{-1}
D	bulk diffusion coefficient	$m^2 s^{-1}$
d_p	average particle diameter	m
D_t	internal diameter riser	m
f_g	gas-wall friction coefficient	-
G_s	solids flux	kg m^{-2} s^{-1}
g	gravitational force per unit mass	m s^{-2}

h_g	heat transfer coefficient	$W\ m^{-2}\ K^{-1}$
k_g	gas-to-particle mass transfer coefficient	$m\ s^{-1}$
k_{ov}	apparent reaction rate constant per unit volume of catalyst	s^{-1}
k_p	theoretical maximum for the intrinsic reaction rate constant based on catalyst volume	s^{-1}
k_r	reaction rate constant based on reactor volume $k_p\beta$ or $k_p\beta/(1+n_d)$	s^{-1}
ΔL	riser length over which reaction is considered	m
m	apparent reaction order in carbon monoxide	-
n_d	dilution ratio	-
Nu	Nusselt number $h_g d_p/a$	-
P	pressure drop	Pa
Pr	Prandtl number $\eta_g/(\rho_g a)$	-
Re	Reynolds number based on slip velocity $\rho_g u_s d_p/\eta_g$	-
Sc	Schmidt number $\eta_g/(\rho_g D)$	-
Sh	Sherwood number $k_g d_p/D$	-
Sh^0	overall Sherwood defined by equation 5	-
T	operating temperature	K
u_g^*	interstitial gas velocity	$m\ s^{-1}$
u_g	superficial gas velocity	$m\ s^{-1}$
u_s	slip velocity	$m\ s^{-1}$
u_t	terminal falling velocity of the individual particle	$m\ s^{-1}$
y_{in}	inlet fraction carbon monoxide	vol.%
y_{O2}	inlet fraction oxygen	vol.%
z	axial riser co-ordinate	m

β	solids hold-up	-
η	contacting efficiency	-
η_p	particle effectiveness factor	-
η_g	gas viscosity	Pa s
λ	heat conductivity	$W\ m^{-1}\ K^{-1}$
ρ_g	gas density	$kg\ m^{-3}$
ρ_p	particle density	$kg\ m^{-3}$
τ	contact time	s
ξ	conversion of carbon monoxide	-

REFERENCES

Arena U., Cammarota A., Massimilla L., Pirozzi D., 1988, The hydrodynamic behavior of two circulating fluidized bed units of different sizes, in *Circulating Fluidized Bed Technology II*, Pergamom Press, Oxford, 223

Bandrowski J., Kacmarzyk G., 1978, Gas-to-particle heat transfer in vertical pneumatic conveying of granular materials, *Chem. Engng. Sci.*, **33**, 1303

Berruti F., Chaouki J., Godfroy L., Pugsley T.S., Patience G.S., 1995, Hydrodynamics of circulating fluidized bed risers: a review, *Can. J. Chem. Engng.*, **73**, 579

Bi H, Fan L.S., 1992, Existence of turbulent regime in gas-solid fluidization, *A.I.Ch.E.J.*, **38**, 297

Bi H.T., Grace J.R., Lim K.S., 1995, Transition from bubbling to turbulent fluidization, *Ind. Engng. Chem. Res.*, **34**, 4003

Cankurt N.T., Yerushalmi J., 1978, Gas backmixing in high velocity fluidized beds, in *Fluidization II*, Cambridge University Press, 387

Contractor R.M., Chaouki J., 1991, Circulating fluidized bed as a catalytic reactor, in *Circulating Fluidized Bed Technology III*, Pergamom Press, Oxford, 39

Dry R.J., White R.B., Close R.C., Joyce T., 1995, The effect of CFB scale-up on gas-solid contact efficiency, in *Preprints of the international symposium of the engineering foundation: Fluidization VIII*, 25

Dry R.J., White C.C., Close R.C., 1992a, The effect of gas inlet geometry on gas-solid contact efficiency in a circulating fluidised bed, in *Proceedings of the 7th engineering foundation conference on fluidization*,

Engineering Foundation, 211
Dry R.J., White C.C., 1992b, Gas-solids contact in a circulating fluidised bed: the effect of particle size, *Powder Technol.*, **70**, 277
Dry R.J., Christensen I.N., White C.C., 1987, Gas-solids contact efficiency in a high-velocity fluidised bed, *Powder Technol.*, **52**, 243
Fuller E.N., Schettler P.D., Giddings J.C., 1966, A new method for predicting of binary gas phase diffusion coefficients, *Ind. Engng. Chem.*, **58**, 18
Geldart D., 1973, Types of gas fluidization, *Powder Technol.*, **7**, 285
Grace J.R., Sun G., 1991, Influence of particle size distribution on the performance of fluidized bed reactors, *Can. J. Chem. Engng.*, **69**, 1126
Hariu O.H., Molstad M.C., 1949, Pressure drop in vertical tubes in transport of solids by gases, *Ind. Engng. Chem.*, **41**, 1148
Hlavácek V., Votruba J., 1974, Experimental study of multiple steady states in adiabatic catalytic systems, *Advances in Chemistry series, Chemical reaction Engineering II*, Evaston
Ishii H., Nakajima T., Horio M., 1989, The clustering annular flow model of circulating fluidized beds, *J. Chem. Engng. Japan*, **22**, 484
Jiang P., Bi H., Jean R.-H., Fan L.-S., 1991, Baffle effects on performance of catalytic circulating fluidized bed reactor, *A.I.Ch.E.J.*, **37**, 1392
Kato K., Onozawa I., Noguchi Y., 1983, Gas-particle heat transfer in a dispersed bed, *J. Chem. Engng. Japan*, **16**, 178
Kumar H.B., Sublette K.L., Shah Y.T., 1993, Effect of high voidage on mass transfer in a fluidized bed, *Chem. Engng. Commun.*, **121**, 157
Kunii D., Suzuki M., 1967, Particle-to-fluid heat and mass transfer in packed beds of fine particles, *Int. J. Heat Mass Trans.*, **10**, 845
Kwauk M., Ningde W., Youchu L., Bingyu C., Zhiyuan S., 1986, Fast fluidization at ICM , in *Circulating Fluidized Bed Technology*, Pergamom Press, Toronto, 33
Marmo L., Manna L., Rovero G., 1995, Comparison among several predictive models for circulating fluidized bed reactors, in *Preprints of the international symposium of the engineering foundation: Fluidization VIII*, 475
Masai M., Tanaka S., Tomomasa Y., Nishiyama S., Tsuruya S., 1985, Reactant-catalyst contact in riser-tube reactor, *Chem. Engng. Commun.*, **34**, 153
Nieuwland J.J., 1995, *Hydrodynamic modelling of gas-solid two-phase flows*, thesis Enschede
Ouyang S., Li X.-G., Potter O.E., 1995a, Circulating fluidized bed as a catalytic reactor: experimental study, *A.I.Ch.E.J.*, **41**, 1534
Ouyang S., Li X.-G., Potter O.E., 1995b, Investigation of ozone decomposition in a circulating fluidized bed on the basis of a core-annulus model, in *Preprints of the international symposium of the engineering foundation: Fluidization VIII*, 457
Ouyang S., Potter O.E., 1993a, Consistency of circulating fluidized bed experimental data, *Ind. Engng. Chem. Res.*, **32**, 1041
Ouyang S., Lin J., Potter O.E., 1993b, Ozone decomposition in a 0.254 m I.D. diameter circulating fluidized bed reactor, *Powder Technol.*, **74**, 73
Ouyang S., Potter O.E., 1994, Modelling chemical reaction in a 0.254 m I.D. circulating fluidized bed, in *Circulating Fluidized Bed Technology IV*, Pennsylvania, Engineering Foundation, 422
Pagliolico S., Triprigan M., Rovero G., Gianetto A., 1992, Pseudo-homogeneous approach to CFB reactor design, *Chem. Engng. Sci.*, **47**, 2269
Patience G.S., Chaouki J., Berutti F., Wong R., 1992, Scaling considerations for circulating fluidized bed risers, *Powder Technol.*, **72**, 31
Psyllos A., Papayannakos N., Philippopoulos C., 1994, CO oxidation in a Carberry reactor: manifestation of reaction kinetics by controlled reaction/transport, *J. Chem. Engng. Japan*, **27**, 693
Ranz W.E., Marshall Jr. W.R., 1952a, Evaporation from drop: part I, *Chem. Eng. Prog.*, **48**, 141
Ranz W.E., Marshall Jr. W.R., 1952b, Evaporation from drop: part II, *Chem. Eng. Prog.*, **48**, 173
Reh L., 1995, New and efficient high-temperature processes with circulating fluid bed reactors, *Chem. Engng. Technol.*, **18**, 75
Reh L., 1986, The circulating fluid bed reactor- its main features and applications, *Chem. Engng. Proces.*, **20**, 117
Sun G., Grace J.R., 1994, Experimental determination of particle dispersion in voids in a fluidized bed, *Powder Technol.*, **80**, 29
Sun G., Grace J.R., 1992, Effect of particle size distribution in different fluidization regimes, *A.I.Ch.E.J.*, **38**, 716
Sun G., Grace J.R., 1990, The effect of particle size distribution on the performance of a catalytic fluidized bed reactor, *Chem. Engng. Sci.*, **45**, 2187
Van der Ham A.G.J. Prins W., van Swaaij W.P.M., 1991, Hydrodynamics and mass transfer in a regularly packed circulating fluidized bed, in *Circulating Fluidized Bed Technology III*, Pergamom Press, Oxford, 605
Van der Ham A.G.J., Prins W., van Swaaij W.P.M., 1994, Regenerative, high temperature desulfurization of coal

gas in a circulating fluidized bed, in *Circulating Fluidized Bed Technology IV*, Pennsylvania, Engineering Foundation, 657

Vollert J., Werther J., 1994, Mass transfer and reaction behaviour of a circulating fluidized bed reactor, *Chem. Engng. Technol.*, **17**, 201

Watanabe T., Chen Y., Hasatani M., Xie Y., Naruse I., 1991, Gas-solid heat transfer in riser, in *Circulating Fluidized Bed Technology III*, Pergamom Press, Oxford, 283

Westerterp K.R., van Swaaij W.P.M., Beenackers A.A.C.M., 1987, *Chemical reactor design and operation*, John Wiley & Sons, New York

Yerushalmi J., Cankurt N.T., Geldart D., Liss B., 1978, Flow regimes in vertical gas-solid contact systems, *A.I.Ch.E.Symp.Ser.*, **176**, 1

Yang W.-C., 1977, A unified theory on dilute phase pneumatic transport, *J. Powder Bulk Solids Technol.*, **1**, 89

Yu Yao Y.-F., 1984, The oxidation of CO and Hydrocarbons over noble metal catalysts, *J. Catal.*, **87**, 152

Zhang W., Tung Y., Johnsson F., 1991, Radial voidage profiles in risers of different diameters, *Chem. Engng. Sci.*, **46**, 3045

Zou B, Li H., Yashen X., Xinhua M., 1994, Cluster structure in a circulating fluidized bed, *Powder Technol.*, **78**, 173

CHAPTER 5

HYDRODYNAMICS OF TURBULENT FLUIDIZED BEDS

ABSTRACT

Transition velocities for the onset of the turbulent fluidization regime and the axial solids hold-up profiles are determined for five particles types (glass beads of 110 μm, silica particles of 130 μm, γ-alumina of 70 and 90 μm respectively and a desulfurization sorbent of 169 μm) in a small scale fluidized bed column (I.D. 0.05 m and 0.75 m high). The bed could be operated at gas velocities up to 1.4 m/s. For every particle type considered, the observed transition velocities to the turbulent fluidization regime (u_c) are in good agreement with correlations presented in the literature. A simple hydrodynamic model describes the axial profile with good accuracy. The parameters required in the model are consistent with those presented in the literature.

1 INTRODUCTION

Fluidized bed reactors are frequently applied in industry when dealing for fast exothermic gas solid reactions. Gradually, the interest of researchers in this field is shifting from the bubbling fluidized bed towards beds that can be operated at higher gas velocities. Small particles (d_p<100 μm) can be fluidized at velocities far beyond the terminal falling velocity of the individual particles. A behaviour totally different from the bubbling bed regime emerges. The surface of the bed becomes diffuse, and a turbulent motion of solids clusters and voids of gas of various sizes and shapes is observed. This high-velocity regime for fine powders is referred to as the turbulent fluid bed regime. For 100 μm particles, the gas velocity in that regime may range from u_g=0. 8 m/s up to 2 m/s. Relatively small amounts of solids are then entrained over the top of the column, and there is still a dense bed retained in the bottom part. The solids concentration is a function of the height in the column and of the applied superficial gas velocity. For steady state operation, the entrained particles have to be collected by cyclones, and returned to the bed.
Despite its use in commercial operations (f.i. the regenerators in modern cat-cracking units), the possible advantages over conventional bubbling bed reactors as summarized hereafter, are still not always recognized:

- a higher gas throughput,
- a shorter and more uniform gas and solid phase residence time,
- improved gas-to-particle mass and heat transfer rates, and
- additional conversion taking place in the freeboard of the bed, where mass transfer resistances are less dominant.

In the literature available for turbulent fluid beds, most attention has been focused on the discrimination and the determination of the transition point where the bubbling bed changes to a turbulent bed (a.o. Bi and Fan, 1992, Chehbouni *et al.*, 1994). Few papers are dealing with the further experimental investigation of the hydrodynamics of gas or solid phase in this fluidization regime, concerning the expansion of the bed (Avidan and Yerushalmi, 1982) or the axial and radial porosity profile (a.o. Werther and Wein, 1994; Kunii and Levenspiel, 1990).

1.1 This work

Due to high gas velocities that can be applied compared to bubbling beds, turbulent fluid beds show the additional advantage that its diameter is smaller, and that by-passing of reactant (due to bubbles) may be avoided. The first is especially attractive for high-pressure applications, while the latter advantage is important when very high conversion rates are required. In future work, the present authors aim at the use of the turbulent fluid bed for the high temperature (>625 K), high pressure (>20 bar) desulfurization of coal gas. Specific advantages put forward for the application of the turbulent bed for coal gas desulfurization purposes are discussed in chapter 7 of this thesis. Prior to the presentation of the desulfurization results, in this chapter the turbulent fluid bed regime is characterized, while the axial porosity profile is determined for various particles (amongst which the future desulfurization sorbent) and superficial velocities.
Before describing the experimental techniques used, a short review will be presented about the hydrodynamics in turbulent beds. This review first includes a discussion on the difficulties related to the discrimination of the various transition points. Then, the turbulent regime will be discussed in more details with respect to solids and gas behaviour.

2 LITERATURE SURVEY OF THE TURBULENT BED HYDRODYNAMICS

2.1 Transition velocities

The turbulent regime is demarcated by the bubbling bed on the one hand and the fast fluidization regime (superficial gas velocities larger than the transport velocity of the particles, u_{tr}) on the other. The transition from the bubbling to the turbulent regime is considered as a change in the mechanism of bubble formation and breakage. Going from bubbling to turbulent fluidization, the bed hydrodynamics change from a regime where bubble formation and bubble coalescence are predominant to a regime with breaking and gradual disappearance of the large bubbles. These large bubbles then collapse into smaller bubbles and interstitial gas (Cai *et al.*, 1990; Chehbouni *et al.*, 1994). Contrary to the bubbling regime, the gas in the turbulent regime may be a continuous phase, with the solids as a dispersed phase. According to Grace (1990) the bed then shows periods during which there are slug-like structures in the bed, followed by periods with clusters and dilute zones, which are typical for the (higher velocity) fast-fluidization regime.

Many studies in the literature focus on the characterization of the lower and upper boundary of the turbulent regime (a.o. Yerushalmi and Cankurt, 1979; Sun and Chen, 1989; Bi and Fan, 1992; Chehbouni *et al.*, 1994, 1995; Gonzales *et al.*, 1995). Whereas the bubbling action of the bed becomes more vigorous beyond the minimum fluidization point (accompanied by an increase in the pressure fluctuation due to the larger size and amount of bubbles), the homogeneity of the fluidized bed increases again beyond another characteristic gas velocity u_c. In this regime, bubbles no longer appear distinctly, and clusters of particles (or agglomerates/strands) are observed. The boundary between bubbling and turbulent fluidization is therefore likely to be recognized by a change in pressure fluctuation (Yerushalmi and Cankurt, 1979). Although some other detection techniques are in use to identify the regime transition, such as visual observation, reading capacitance traces and local and overall bed expansion techniques, the pressure fluctuation technique is definitely the most commonly used.
The pressure fluctuation, P_f, and its non-dimensional value, $P_{f,rel}$, can be calculated from:

$$P_f = \sqrt{\frac{\sum_{i=1}^{N}(\Delta P_i - \Delta P)}{(N-1)}} \quad \text{and} \quad P_{f,rel} = \frac{P_f}{\Delta P} \qquad (1)$$

where ΔP_i, and ΔP represent the instantaneous and time averaged pressured drop over N data points. Through a plot of the fluctuation of the pressure drop over the bed as a function of the superficial gas velocity, most researchers define two characteristic velocities: the point where the pressure fluctuations peak, the critical superficial velocity u_c, and the velocity where the fluctuations level off, u_k (see figure 1).

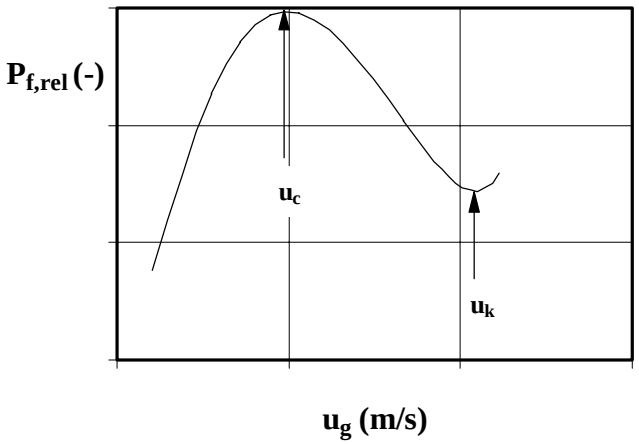

Figure 1. A representative plot of the pressure fluctuation (equation 1) versus the gas velocity. Indicated are the transition velocities u_c and u_k.

Extensive studies have been carried out to quantify the two transition points (see Chehbouni *et al.* 1995, for u_c and Bi and Fan 1992, for u_k). Some researchers consider the turbulent regime to start at u_c (Cai *et al.*, 1990), whereas other researchers consider u_c only to be the beginning of the transition to the turbulent regime, which then actually starts at the velocity u_k (Yerushalmi and Cankurt, 1979; Bi and Fan, 1992). Bi and Fan (1992) summarized the experimental findings in the literature for the values of u_k as a function of the Archimedes number Ar. They conclude that u_k exists only for Geldart's group A particles, and not for group B and D particles (perhaps due to the smaller effect of inter-particle forces). Brereton and Grace (1992) and Chehbouni *et al.* (1994) show that the measured u_k is a function of the distance between the pressure probes used. The observed value for u_c is only slightly affected by the measurement method (Bi and Grace, 1995). The value for u_c obtained from pressure fluctuations of the *differential* pressure between two individual probes tends to be higher than the one derived from the fluctuation of the pressure difference between the (bed) probe and ambient pressure. For the latter *absolute* pressure fluctuations, u_c is independent on the probe location, whereas its values varies slightly with the axial probe location for differential pressure fluctuations. The transient point occurs at a higher velocity near the bottom of the bed, suggesting that the transition takes place at the top region first and develops downward. Brereton and Grace, and Chehbouni *et al.* therefore state that the onset of turbulent fluidization is at u_c. Moreover, they concluded that u_k is an artefact without physical meaning due to the use of differential pressure transducers. This conclusion is supported by Bi and Grace (1995). It is nowadays agreed that the onset of turbulent fluidization is marked by u_c. An extensive overview of correlations for the prediction of the transition velocities is presented by Arnaldos and Casal (1996).

The following correlations appeared to be useful in the estimation of the transition velocities (Lee and Kim, 1990; Bi and Fan, 1992):

$$u_c:\ \mathrm{Re}_c = 0.70\,\mathrm{Ar}^{0.485}$$

$$u_k:\ \mathrm{Ar} \le 125;\ \mathrm{Re}_k = 0.601\,\mathrm{Ar}^{0.695} \quad \text{and} \quad \mathrm{Ar} \ge 125;\ \mathrm{Re}_k = 2.28\,\mathrm{Ar}^{0.419}$$

$$u_{tr}:\ \mathrm{Re}_k = 2.28\,\mathrm{Ar}^{0.419} \qquad (2)$$

2.2 Solids concentration in turbulent beds

During the past decade, the relevant literature on turbulent fluidization was focused on the measurement of transition velocities. Much less effort has been undertaken to determine and predict the axial solids profile over the bed, although this aspect of the turbulent bed is very important for its use as a chemical reactor. The determination of the solids hold-up in turbulent beds is complicated since its values are a strong function of bed height. Roughly, two separate regions in the bed (a dense phase at the bottom and a dilute phase on top) can be distinguished (see figure 2).

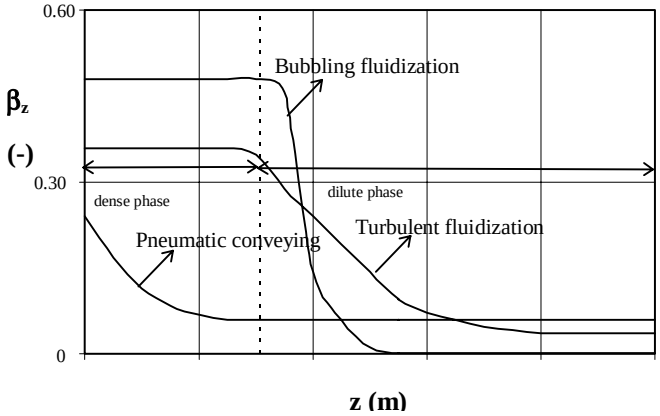

Figure 2. The solids concentration versus the bed height in various fluidization regimes.

This is different compared to reactors, operated in the bubbling or the pneumatic conveying regime, where the solids hold-up is approximately constant along the bed height. Compared to the fast fluidization regime ($u_g > u_{tr}$) the turbulent (dense) bed density does not depend on the solids re-circulating rate. The two regions of the turbulent bed (referred to as the dense and the dilute phase respectively) will be briefly discussed hereafter.

2.2.1 Dense phase solids concentration

Various authors have proposed empirical correlations to describe the dense phase solids concentration, β, in a turbulent bed. For FCC catalysts, for instance, King (1989) presented a simple rule of thumb equation that the bed expansion $(1-\beta)=(u_g+1)/(u_g+2)$.
At the higher gas velocities applied in small diameter turbulent beds, the structure of the remaining bubbles will be rather like slugs than bubbles. To estimate the dense bed expansion, Werther and Wein (1994) applied (semi-empirical) approaches for the slugging bed, originally developed by Matsen *et al* (1969) and Birkhoff and Carter (1957) to estimate the bed expansion in a turbulent bed:

$$\frac{H}{H_{mf}} = 1 + \frac{u_g - u_{mf}}{0.35\sqrt{2gD_t}} \text{ or } \frac{H}{H_{mf}} = 1 + \frac{u_g - u_{mf}}{0.35\sqrt{gD_t}} \text{ and } \beta = (1-\varepsilon_{mf})\frac{H_{mf}}{H} \qquad (3)$$

which are based on axisymmetrix and asymmetric slugs, respectively. However, for a wide range of particle diameters, various authors observed that for the turbulent flow regime the value of the bed expansion, derived by equation 3, is overestimated (Massimilla, 1973; Lee and Kim, 1990; Satija and Fan, 1985; Avidan and Yerushalmi, 1982). Noting that the turbulent regime is more homogeneous, Avidan and Yerushalmi (1982) represented the results of expansion measurements in the (empirical) Richardson-Zaki (1954) form:

$$\frac{u_g}{u_t} = (1-\beta)^n \qquad (4)$$

Here u_t represents the terminal falling velocity of the individual particle, and is thought to represent the size and density of the particle in the suspension; β is the solids hold-up averaged over the dense bed height. Values for n and u_t can be obtained from a logarithmic plot of the dense bed solids hold-up against the superficial gas velocity. Equation 5a has proven to be quite accurate in predicting bed expansion of particulate systems. However, for fine particles the value for u_t derived by equation 4 is observed to be many times larger than the actual terminal falling velocity of the individual particle. The reason is that fine particles in a turbulent bed tend to form particle clusters. Therefore Avidan and Yerushalmi slightly modified equation 4:

$$\frac{u_g}{u_t^*} = (1-\beta)^n \qquad (5)$$

In equation 5, it is assumed that u_t^* represent the terminal falling velocity of the particle cluster, and appeared to depend on the fluidization regime as well. This relation is nowadays quite well accepted in the literature (amongst numerous others Abed, 1984; Avidan *et al.,* 1985; Lee and Kim, 1990). It should be noted however, that the approach of equation 5 was already proposed in 1969 by Mogan *et al.*

A survey of power n values as derived in various studies on basis of equation 5 concerning the bubbling and the turbulent flow regime, is given in table I. Both, u_t^* and n, appeared to be constant over the gas velocity range when one fluidization regime is considered. This seems to imply a relatively constant ‘cluster size’ within the specific regime. The values are lower in the turbulent regime than in the bubbling bed regime. Values for n, for example, range from 3 to 6 for Geldart's A type particles in the turbulent regime, and are approximately twice that value for the bubbling or slugging regime.

Table I. A summary of index n and u_t^* in the bubbling and turbulent flow regime (equation 5).

Authors	type of material	D_t * L (m*m)	d_p (μm)	ρ_p (kg m^{-3})	turbulent u_t^* (m s^{-1})	n (-)	bubbling u_t^*(m s^{-1})	n (-)
Avidan and Yerushalmi (1982)[b]	FCC (used)	0.152 x 3.5	49	1070	3.4	5	22.6	9.2
	HFZ-20 (used)	0.343 x1.4	49	1450	6.3	4.4	38.7	8.3
	Dicalite 4200		33	1670	5.0	14	85.3	4.6
	FCC (fresh)		49	1070	2.8	6	12.2	10.2
	HFZ-20 (fresh)		49	1450	4.5	5.1	30.5	10
Massimilla (1973)	FCC	0.152 x 12	56	1000[a]	-	-	74.4	10.4
Carotenuto (1974)[c]	FCC	0.152	60	940[a]	2.6	5.6	9.8	8
Abed (1984)	FCC	0.152 x 8.3	55	850	3.2	4.2	9.8	6.2
Avidan *et al.* (1985)	CCZ-11	0.60 x 13	60[a]	1220	9.9	4.3	362	8.5
Sun and Chen (1989)	ammoxidation catalyst	0.80 x 7	64	1800	2.7	3.9	92.9	10.4
			54	1800	3.7	5.1	196.5	13.1
Lee and Kim (1990)	glass beads	0.10 x 3	362	2500	2.7	2.8	7.3	5.06
Canada and McLaughlin (1978)	glass beads	0.61 x0.61	650	2480	-	1.85	-	3.4
		0.61 x 0.61	2600	2900	-	3.3	-	3.7
		0.31 x 0.31	2600	2900	-	3.3	-	2.7

[a] From Lee and Kim (1990) [b] expanded top bed [c] from Avidan and Yerushalmi (1982)

2.2.2 Dilute phase solids concentration

Several investigators consider the solids in the bed to be homogeneously distributed over the reactor volume (f.i. Sun and Grace, 1992). However, in the turbulent regime a considerable amount of solids is present in the freeboard (referred to as the dilute phase in the present work) due to the entrainment of the particles. The local solids concentration β_z then becomes a function of the reactor height. In case of a chemical reaction, a significant part of the conversion can take place in the freeboard. Many correlations for the entrainment rate of particles (and implicitly the solids hold-up in the freeboard) have been proposed in the literature (see f.i. Kunii and Levenspiel, 1990), most of them being derived for small-scale bubbling beds. The following expression for the solids hold-up, β_z, in the freeboard of a bubbling bed:

$$\frac{\beta_z - \beta_{dilute}}{\beta_{dense} - \beta_{dilute}} = \exp(-a \cdot z) \qquad (6)$$

Equation 6 has been presented by Kunii and Levenspiel, and includes β_{dilute} as the maximum solids concentration that can be present in the dilute phase, and β_{dense} as the solids concentration at the upper surface of the dense bed. For fine particles $a \cdot u_g$ appears to be constant (Kunii and Levenspiel, 1990). For typical A-powders the values of this product range from 2 to 4 s^{-1}, whereas typical values of approximately 7 s^{-1} are reported for B-type particles (Kunii and Levenspiel, 1997).

2.2.3 Coupling of dense and dilute phase

For a more appropriate description of the turbulent bed, the results derived for the dense phase should be coupled with observations made for the dilute phase regime. In turbulent beds, a sigmoidal profile for the solids hold-up is generally observed. On contrary, in the pneumatic conveying regime the solids concentration shows an exponential decay at low solids fluxes, and a sigmoidal one at the higher (for $u_g > u_{tr}$ then also referred to as fast fluidization). Only a few attempts to describe the solid phase concentration over the entire reactor length for the turbulent fluid bed regime are known from the literature. Some are based on a one-dimensional model (derived for riser systems, see e.g. Yang, 1974; or the core-annulus model by Harris and Davidson, 1993). However, the result of this one-dimensional model (for which the equations are listed in chapter 3 of this thesis) is an exponential decay in the solids concentration over the bed length for the entire range of gas velocities. A more complex model seems therefore to be required to describe the sigmoidal profile in the turbulent regime. Nakamura and Capes (1973), and later Harris and Davidson (1993), for example, derived a core-annulus model. In their model (derived for the fast fluid bed), a mechanism for transfer of particles from the core to the annulus was introduced, together with a momentum balance for both the core and the annulus region. Although the predictions of the model compare favourably with experimental data for the fast fluid bed regime (that is at $u_g > u_{tr}$), its application is still restricted to a fast fluidized bed system; at the low solids fluxes typical for turbulent beds an exponential decay in the solids concentration is calculated. They state that, without introducing still more complex phenomena, like particle interaction, the sigmoidal profile can not be predicted.
Other models to be used also for turbulent beds, but again originally derived for fast fluid beds, are more empirical in nature. Kwauk *et al.* (1985) considered the bed to consist of clusters, dispersed in a dilute continuum of individual particles. The following empirical relation for the solids concentration β_z is derived, by which a sigmoidal shaped profile is obtained:

$$\frac{\beta_{dilute} - \beta_z}{\beta_z - \beta_{dense}} = \exp\left(-\frac{(z - z_i)}{z_0}\right) \qquad (7)$$

It includes four parameters: β_{dilute} represents the asymptotic value for the solids hold-up for a dilute-phase fluid bed (corresponding to the saturation carrying capacity of the gas), β_{dense} the asymptotic value for the solids hold-up for a dense-phase fluid bed, z_0 is the characteristic length over which the inflection takes place, and z_i the location of the so-called inflection point. Whereas the location of the inflection point can be calculated from the total solids inventory, the three remaining parameters must be obtained by fitting with experimental observations. Although the theoretical basis for this equation is missing (see f.i. Harris, 1992), equation 7 fits the experimental data reasonably well (Kwauk *et al.*, 1985; Hartge, 1985; Louge and Chang, 1990). However, 3 parameters, functions of operating variables and conditions, have to be known a priori. These parameters should be estimated from relations fitted to a wide range of experimental results.

Werther and Wein (1994) considered the solid phase in the turbulent bed as a combination of a bubbling bed model for the bottom of the reactor, and a fast fluidized bed model for the freeboard region (applying equation 7). After fitting the parameters required in these two models, the measured axial concentrations were in good agreement with those predicted by the model. From the experimental results obtained by Massimilla (1973) and Lee and Kim (1990), however, it is concluded that the use of a simple two-phase model to describe the solids hold-up in the dense phase of a turbulent bed remains questionable. For example, if the Werther and Wein approach was applied in a small fluid bed (D_r< 0.10 m), initial bubble diameters larger than the bed diameter can be calculated.

2.3 Gas flow behaviour

Another important parameter for fluid bed design is the flow behaviour of the gas phase. Gas phase modelling in turbulent beds appears to be difficult, mainly because of the lack in the understanding of the nature of the continuous and dispersed phase in the dense bed (Avidan, 1982; Mori *et al*., 1989; Grace, 1990). Plug flow behaviour in reactor modelling does not yield an adequate estimation of the experimentally observed conversions, probably because additional mass transfer resistances (analogous to bubble-to-emulsion transfer resistance) are still present. Plug-flow models including axial gas dispersion have been proposed by Avidan (1982) and applied by f.i. Mori *et al*. (1989), Grace (1990) and Foka *et al.* (1995). In few papers, conversion rates in turbulent beds were interpreted by two-phase models (Avidan, 1982; Pell and Jordan, 1988; Foka *et al*, 1995), originally derived for bubbling beds (see May, 1959; Van Deemter, 1967, 1980; Van Swaaij and co-workers, 1972, 1973, 1978).

2.4 A new proposal for the axial solids distribution

In the present approach the dense phase expansion is calculated on basis of the modified Richardson-Zaki equation (equation 5). For the freeboard, and similar to Werther and Wein, the equation of Kunii and Levenspiel (1990) is used to describe the exponential decay in the solids concentration (for $z>z_i$; equation 7):

$$z < z_i \; : \frac{u_g}{u_t^*} = (1 - \beta)^n \qquad (5)$$

$$z_i < z < L : \frac{\beta_z - \beta_{dilute}}{\beta_{dense} - \beta_{dilute}} = \exp\left(-a \cdot (z - z_i)\right) \qquad (8)$$

The transition point, z_i, and the closure between dense and dilute region can be calculated on basis of the mass balance:

$$M_{bed} = \int_0^{z_i} \left(1 - \left(\frac{u_g}{u_t^*}\right)^{1/n}\right) \rho_p A dz + \int_{z_i}^{L} (\beta_{dilute} + (\beta_{dense} - \beta_{dilute}) \exp\left(-a(z - z_i)\right) \rho_p A dz \qquad (9)$$

M_{bed} is always calculated from the measured overall pressure drop ΔP, because the amount of material in the reactor is influenced by the solids volume in the standpipe, and deviates from the initial amount of material added:

$$\Delta P = \frac{M_{bed} g}{O} \qquad (10)$$

The maximum concentration of solids that can be transported by the gas, β_{dilute}, can be calculated by the following empirical relation:

$$\beta_{dilute} = c \cdot \exp\left(b \cdot u_g\right) \qquad (11)$$

in which c is a proportionality constant and b an exponential decay constant.

Initially, five parameters must be known to calculate the dense phase solids hold-up and the axial hold-up profile: a, b, c, u_t^* and n. For all particles considered in this work it was observed that the influence of the saturated dilute phase concentration β_{dilute} (which is < 0.02 for typical type A-powders (Kunii and Levenspiel, 1990)) on the solids profile can be neglected, and in this study β_{dilute} is taken to be zero. Furthermore, the influence of the initial bed mass on the bed expansion is negligible (Avidan and Yerushalmi, 1982). The values for u_t^* and n can be derived by plotting the logarithmic value of β as a function of the gas velocity for the data points measured at a single initial bed mass (see equation 5). In the present model one single parameter, viz. the value for a, is then fitted to experimental results.

3 EXPERIMENTAL PART

3.1 Experimental set-up

The experimental (Pyrex glass) apparatus used is schematically given in figure 3, and consists of a 0.75 m long, 0.05 m ID column on top of which an expanded bed section (ID 0.1 m, 0.3 m long) is present. The fourfold (cross-sectional) area increase in the expanded top section reduces the superficial gas velocity, and allows most of the entrained particles to fall back into the bed. Air at ambient conditions was fed to a porous plate glass distributor by means of 3 Brooks mass flow controllers. The superficial gas velocities can be varied in the range from 0 to 1.5 m/s, based on the lower section cross-sectional area. Two cyclones with internal diameters of 0.063 m and 0.05 m respectively, were installed to separate the gas and the solids entrained over the top of the column. A dip-leg was used to return the entrained solids from the first cyclone back to the fluidized bed. For smooth operation of this dip-leg, a very small amount of air (about 0-10 ml/s) was introduced at its bottom.
Five type of powders are applied, as indicated in table II. One type of particles, referred to as sorbent, is to be used in the desulfurization reaction presented in chapter 7 of this thesis.

All the present experiments have been conducted at room conditions with air as the fluidizing gas.

Table II. Particle properties at ambient conditions.

material	d_p (μm)	ρ_p (kg m^{-3})	Ar	ε_{mf} (-)	u_{mf} (mm s^{-1})	u_t (m s^{-1})
γ-alumina	70	1375	16.8	0.550	1.8	0.20
γ-alumina	90	1375	36.9	0.527	2.1	0.28
silica	130	426	33.3	0.492	1.7	0.18
glass beads	110	2749	130.3	0.411	8.9	0.70
sorbent	169	1845	317.0	-	17.0	0.90

Two types of experiments have been carried out: i) the determination of the transition velocity from bubbling to turbulent fluidization, and ii) the measurements of the solids concentration as a function of the gas velocity and the height in the column.
For the determination of the transition velocities, in the wall of the bed 9 pressure taps were mounted at different vertical separation intervals. Differential pressures over the bed height were sampled by means differential pressure transducers, ranging from 0-2500 Pa and 0-1000 Pa.
The solids hold-up is calculated on basis of the pressure profile over the bed length, thereby neglecting friction between solids and wall, friction between gas and wall, and particle acceleration. In chapter 3 of this thesis, this approach was shown to be valid even at much higher gas velocities.

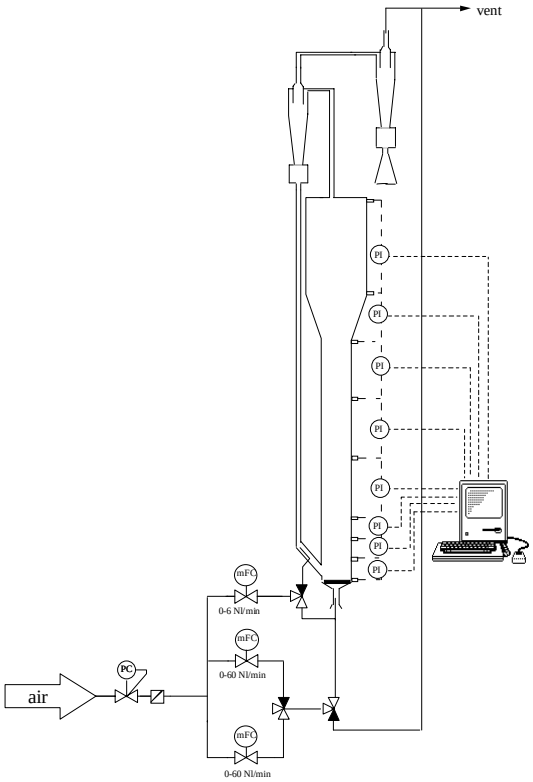

Figure 3. Flowsheet of the turbulent bed.

3.2 Transition velocities

Before determining the transition velocity to the turbulent fluidization regime for the various materials, their minimum fluidization velocity and the corresponding bed porosity have been determined. The results are listed in table II. For γ-alumina (90 μm) the transition velocities to the turbulent fluidization regime, u_c and u_k, are characterized through a plot of the pressure fluctuation P_f versus the superficial gas velocity. In the present experiments, the pressure fluctuations were measured over the total bed height. Figure 4 shows this fluctuation (figure 4a) and its normalized function, $P_{f,rel}$ (figure 4b), as a function of the gas velocity, and for various amounts of initial bed masses. Values for P_f and $P_{f,rel}$ increase sharply with the gas velocity, until they reach a maximum after which they decrease again. The characteristic gas velocity u_c can clearly be identified as the maximum in these curves, at approximately 0.58 m/s. The decrease of P_f for smaller initial bed masses (figure 4a) is caused by the lower apparent bed density over the measured probe interval; if the fluctuation is normalized (figure 4b) the effect of initial bed height diminishes.

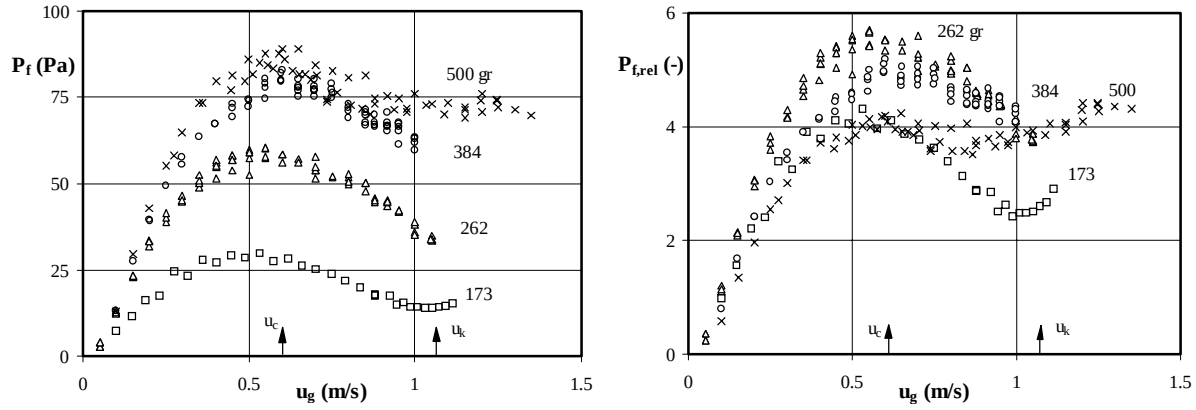

(a) (b)

Figure 4. (a) Dimensional and (b) normalized fluctuation for γ-alumina (90 μm). Legends: M_{bed} □ 173 gr; Δ 262 gr; o 384 gr; x 500 gr

For P_f as well as for $P_{f,rel}$ the effect of initial bed height on the value of u_c is negligible: a constant value of approximately 0.6 m/s is observed. On the other hand, with respect to the minimum in the curves (representing u_k), the effect of M_{bed} remains unclear. In contradiction with Bi and Grace (1995), the plots of P_f and $P_{f,rel}$ almost yield the same values for u_c. Similar plots for u_c could be obtained for γ-alumina (70 μm), silica and glass beads, and according to Lee and Kim (1990), these values should now be considered to represent the transition to the turbulent regime.

In the present work, the probe spacing for the measurement of the differential pressure fluctuations was taken over the total bed height, and following Bi and Grace (1995) this results in relatively high values for the transition velocities. The observed u_c-values should therefore be considered as the upper value for the transition velocity u_c.

The experimental values for u_k cannot clearly be evaluated from the experiments: the minimum in $P_{f,rel}$ is observed at a gas velocity of approximately 1.05 m/s. However, in the dimensional plot in figure 4a, the minimum value for P_f seems to depend on the initial bed height.

Table III. Transition velocities at ambient conditions

material	u_c (ms^{-1})	u_k (ms^{-1})
γ-alumina (70 μm)	0.60	0.88
γ-alumina (90 μm)	0.58	1.05
silica	0.40	-
glass beads	0.90	-
sorbent	1.20	-

This observation is in accordance with earlier published studies in which absolute pressures transducers were used (Chehbouni *et al.*, 1994; Bi and Grace, 1995). For the silica and glass beads, the minimum in the plot of the pressure fluctuation could not be detected: it was absent for the silica and could not be determined for the glass beads at all due to blocking of the cyclones at the exit of the bed. The results for all four particle types are listed in table III.

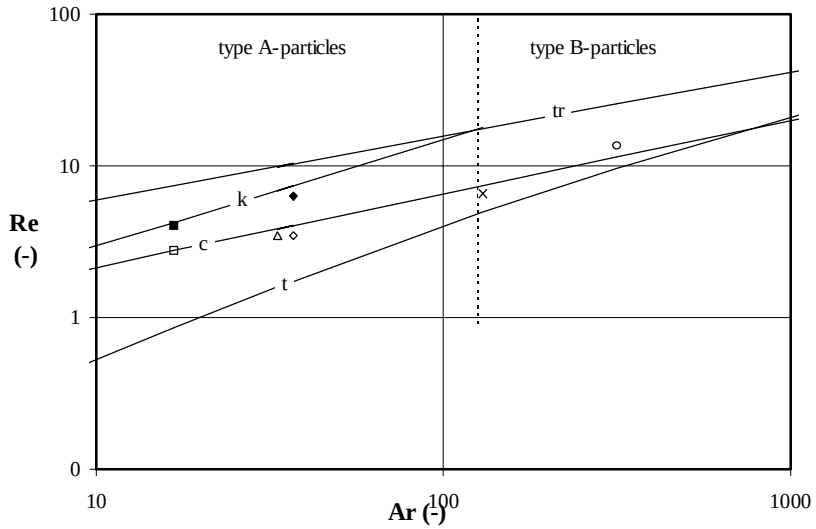

Figure 5. Comparison of measured and predicted values for the Reynolds number corresponding to the transition velocities u_t, u_c, u_k and u_{tr} as a function of the particle Archimedes number. Legends: squares = γ-alumina (70 μm); diamonds = γ-alumina (90 μm); triangles = silica; cross = glass beads; circles = sorbent material. The open symbols represent u_c and the closed one values for u_k. The solid lines represent equation 2 (Re_{tr} and Re_k from Bi and Fan (1992) and Re_c from Lee and Kim (1990)).

In figure 5 the Reynolds numbers belonging to the values of u_t (calculated), u_c and u_k (calculated by various authors as well as determined in the present experiments) are plotted as a function of the Archimedes number. All the Reynolds values increase with the Archimedes number. The solid lines represent the Reynolds number at the transition velocities predicted by the relations of Bi and Fan (1992; u_k and u_{tr}) and Lee and Kim (1990; u_c). Obviously, there is a very good agreement between the measured and the predicted values for the transition velocities.

3.3 Dense bed expansion

While studying the hydrodynamics of the turbulent bed, some authors consider it as a combination of a bubbling bed at the bottom of the reactor, and a fast fluidized bed for the freeboard. For the interpretation of the solids concentration in the dense bed region Werther and Wein (1994), for instance, used relations derived for the slugging bed. In the present paper it was suggested earlier that the dense bed expansion data can not be interpreted with such a simple slugging fluid bed approach (equation 3), as it overestimates the measured expansions. For comparison, in figure 6 our solids concentration data for γ-alumina (90 μm) presented as a function of the gas velocity are compared with values derived from equation 3 and with those from equation 5 (with the parameter u_t^* and n for each regime summarized in table IV).

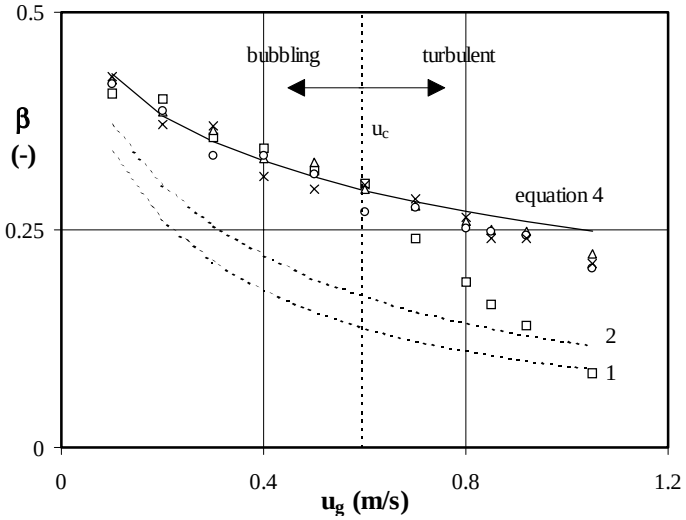

Figure 6. The average solids concentration in the dense bed as a function of gas velocity for the γ-alumina (90 μm). Legends: M_{bed} □ 173 gr; Δ 262 gr; o 384 gr; x 500 gr. The two dashed lines denoted 1 and 2 represent the average solids concentration that can be derived from the bed expansion relations of Matsen *et al.* (1969) and Birkhoff and Carter (1957) respectively. The other solid line represents equation 5; the parameter u_t^* and n for each regime are summarized in table IV.

The experimental solids concentration, averaged over the dense bed height, β, slowly decreases with the superficial gas velocity. Matsen *et al.* (1969) and Birkhoff and Carter (1957), the solid lines in figure 6 denoted by 1 and 2 respectively, predict a somewhat larger decline. Apparently, these expansion correlations overestimate the measured expansions, and this corresponds with the results presented by Massimilla (1973) and Lee and Kim (1990). In the same figure, the results for varying initial bed masses M_{bed} are displayed also. At the lowest value of M_{bed} and for the turbulent bed regime, the solids concentration decreases stronger than for all other initial bed masses, for which the data roughly coincide. Obviously, at the lowest value for M_{bed}, a clear dense phase does not exist anymore in the turbulent bed. With respect to the comparison with the predictions derived from equation 3, only at the low gas velocities the experimental bed expansion approaches the calculated value, which is not surprising as equation 3 is originally derived for slugging beds.
Figure 6 shows that the measured expansion data are predicted much better by equation 5.

Table IV. The index n and u_t^* and au_a, obtained in this study for the bubbling ($u_g < u_c$) and the turbulent flow regime to be used in equation 5 ($u_g > u_c$).

type of material	d_p (μm)	turbulent u_t^* (m/s)	n	bubbling u_t^* (m/s)	n	au_a (s^{-1})
γ-alumina	70	3.4	5.1	16.3	9.6	5.0
γ-alumina	90	3.8	5.2	11.8	8.5	5.2
silica	130	3.6	6.0	44.5	12.7	4.1
glass	110	26.6	6.10	10.4	5.2	20.1
sorbent	169	12.9	9.9	-	-	10.0

In table IV the empirical values of u_t^* and n (used in equation 5) are summarized for all bed particles applied. They are calculated for the bubbling ($u_g < u_c$) as well as for the turbulent fluidization regime ($u_g > u_c$). Because a clear dense phase is not noticed for M_{bed}=173 gr, the values for u_t^* and n are derived on basis of the measurements at the higher initial bed masses. Generally there is good agreement between our data (table IV) and those reported

in the literature (table I), for the bubbling as well as for the turbulent regime.

3.4 Axial solids hold-up profile: influence of gas velocity and initial bed mass

Because the contribution of the acceleration term to the total pressure drop can be neglected if compared to the solids hold-up contribution, the average solids hold-up can be calculated directly from the observed pressure drop. In figure 7a, axial solids hold-up profiles are plotted for γ-alumina (90 μm, M_{bed}=384 grams) and three gas velocities, and compared with the results derived from equations 5 to 11. Generally, a more or less sigmoidal solids profile is obtained with large solids hold-ups at the bottom of the column (the dense bed), and a very dilute phase at the top. As a consequence of increasing the gas velocity on the hold-up, the average dense bed concentration decreases, from 0.2 at a gas velocity of 1 m/s to 0.3 at 0.6 m/s. At the same time, the solids hold-up in the freeboard of the bed is increased slightly. Both effects can be explained by the enhanced entrainment of solid material.

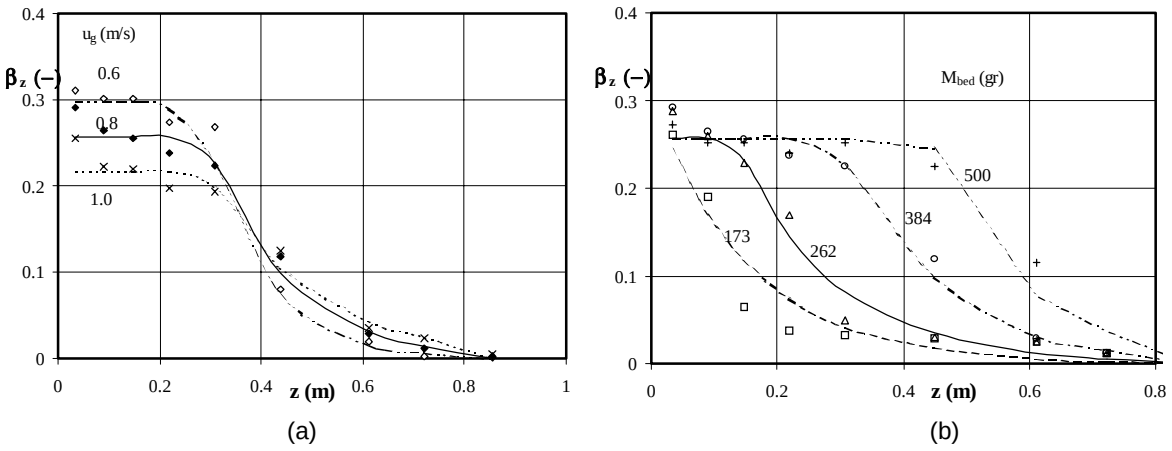

Figure 7. The local solids concentration versus the column bed height for γ-alumina (90 μm), with (a) a variation in the gas velocity (M_{bed} =384 gr) and (b) variation in initial bed mass (u_g=0.8 m/s). Legends: (a) ◊ u_g=0.6 m/s; ◆ 0.8 m/s ; x 1 m/s; (b) u_g=0.8 m/s and M_{bed} □ 173 gr; Δ 262 gr; o 384 gr; x 500 gr. The solid lines are calculated from equation 5 to 11.

Figure 7b shows the influence of initial bed mass, M_{bed}, on the axial solids hold-up for γ-alumina (90 μm) at a gas velocity of 0.8 m/s. At the higher values for M_{bed} the decrease in hold-up shifts towards higher axial positions in the column, as can be expected. An influence of M_{bed} on the dense bed solids hold-up can not be noticed; a constant value of approximately 0.25 is observed at u_g=0.8 m/s for the higher values of M_{bed}. For the lower value of M_{bed}, an exponential decay in the hold-up is obtained. Such a profile is typical for a riser in a circulating fluidized bed system, where the inflection point is absent. All the solid material is transported directly and a dense phase region is not present anymore.

Three parameters must be known to calculate the dense phase solids hold-up and the axial hold-up profile, viz a, u_t^* and n. The values for u_t^* and n can be obtained from equation 5, by plotting the logarithmic value of β as a function of the gas velocity for the data points collected (figure 6). A single unknown parameter then remains, which is the value for the decay constant a. For various particles Kunii and Levenspiel (1990) showed that $a \cdot u_g$ is constant. Its value can be now derived by applying a least-square fitting procedure using a downhill simplex method; the results are presented in table IV as well. For the particles considered in this study, the values for $(a \cdot u_g)$ are slightly higher than those proposed by Kunii and Levenspiel (1997), which are 2 to 4 s^{-1} for Geldart A solids, 5 s^{-1} for AB type of particles and 7 s^{-1} for B-particles. Only for the glass beads, much higher values are

calculated in the present work. This could be caused by the presence of the expanded top section in the present work. In this region, solids are forced to fall down as the gas velocity is decreased by a factor 4.
The experiments with glass beads are conducted in the bubbling (or even slugging) regime instead of the turbulent fluidization regime. This conclusion is supported by the observation that entrainment of glass particles (Geldart type B-powders) is negligible in the applied velocity regime.

For the materials considered, the axial solids hold-up can be fitted to a combination of equations 5 to 11. The solid lines in figure 7 show the calculated hold-up profiles for the different gas velocities (a) and for the various initial bed masses (b), using the values indicated in table IV, and applying equation 11 for the overall mass balance. The agreement between experimental and calculated results is very good.
If the data for the lowest value for M_{bed} are considered, a negative value for z_i is calculated: as was already indicated by the exponential decay in the measured solids hold-up as a function of axial position, and by the deviation in the observed bed expansion in comparison to the results at higher M_{bed}, the existence of a dense phase can be neglected for this case.

4 CONCLUSIONS

Compared to bubbling fluidization, turbulent fluidized beds show unique features which are caused mainly by the increased solids hold-up in the freeboard. In this study the primary interest is the determination of the axial solids hold-up profile in such a turbulent bed.
In a small column (L=0.75 m, I.D. 0.05 m), the transition velocities to the turbulent fluidization regime are determined for five types of particles. The observed transition velocities are in very good agreement with literature correlations.
For all particles, the axial solids hold-ups in this column have been measured as a function of the superficial gas velocity. A simple model based on the combination of the dense bed expansion (Avidan and Yerushalmi, 1982) and the entrainment model proposed by Kunii and Levenspiel (1990) has been developed. It appears to describe our results with good accuracy. The parameters required in this model have been obtained by a least square of the deviation between calculation and experiments. They are compared with results from the literature, and are consistent.

ACKNOWLEDGEMENT

We acknowledge the financial support of the Dutch Ministry of Economic Affairs through the Netherlands Energy Research Foundation ECN. We also acknowledge M.A. Tekstra, M.A. van Rooij, J.R. Ipema and N. Haye for their assistance in the experimental work.

NOTATION

a	decay constant	m^{-1}
Ar	Archimedes number $d_p^3 \rho_g(\rho_p-\rho_g)g/\mu_g^2$	-
b	constant in equation 11	m^{-1}
c	constant in equation 11	-
d_p	particle diameter	m
D_t	tube diameter	m
Fr_i	Froude number $u_i/\sqrt{(gD_t)}$	-
G_s	solids flux	kg $m^{-2}s^{-1}$
G_{s_0}	solids flux at the dense bed surface	kg m^{-2} s^{-1}
G_{s_*}	saturation carrying capacity	kg m^{-2} s^{-1}
g	gravitational constant	m s^{-2}

H	bed height	m
H_{mf}	bed height at minimum fluidization conditions	m
L	length	m
M_{bed}	initial amount of material in the bed	kg
n	power in Richardson-Zaki equation (equation 5)	-
N	number of data-points	-
O	cross-sectional area of the bed	m^2
ΔP	average pressure drop	kg m^{-1} s^{-2}
Re	Reynolds number $u_g d_p \rho_g / \mu_g$	-
t	time	s
u_c	maximum in pressure fluctuation	m s^{-1}
u_g	superficial gas velocity	m s^{-1}
u_{mf}	minimum fluidization velocity	m s^{-1}
u_k	minimum in pressure fluctuation	m s^{-1}
u_t	terminal velocity individual particle	m s^{-1}
u_{tr}	transport velocity of the particle	m s^{-1}
u_t^*	terminal velocity for cluster of particles (equation 5)	m s^{-1}
z	axial position in the column	m
z_0	characteristic length in the Li and Kwauk model	m
z_i	location of inflection point in the column	m
β	solids concentration averaged over the height	-
ε	porosity	-
ρ	density	kg m^{-3}

subscripts

c	corresponding with u_c
dilute	in the dilute phase
dense	in the dense phase
e	effective
f	fluctuation
g	gas phase
p	particles
i	instantaneous
k	corresponding with u_k
mf	at minimum fluidization conditions
tr	corresponding with u_{tr}
z	at a position z in the bed

REFERENCES

Abed R., 1984, The characterization of turbulent fluid-bed hydrodynamics, in *Fluidization IV*, 137

Arnaldos J., Casal J., 1996, Prediction of transition velocities and hydrodynamical regimes in fluidized beds, *Powder Technol.*, **86**, 285

Avidan A.A., Gould R.M., Kam A.Y., 1985, Operation of a circulating fluid bed cold flow model of the 100 B/D MTG demonstration plant, in *Circulating Fluidized Bed Technology*, Pergamom Press, New York, 287

Avidan A.A., Yerushalmi J., 1982, Bed expansion in high velocity fluidization, *Powder Technol.*, **32**, 223

Avidan A., 1982, Turbulent fluid bed reactors using fine catalysts, *CIESC-AIChE meeting, proceeding joint meeting of Chemical Engineering*, Beijing, sept 19-22, 411

Bi H.T., Grace J.R., 1995, Effect of measurement method on the velocities used to demarcate the onset of turbulent fluidization, *Chem. Engng. J.*, **57**, 261

Bi H.T., Grace J.R., Lim K.S., 1995, Transition from bubbling to turbulent fluidization, Ind. Engng. Chem. Res., **34**, 4003

Bi H, Fan L.S., 1992, Existence of turbulent regime in gas-solid fluidization, *A.I.Ch.E.J.*, **38**, 297

Birkhoff G., Carter D., 1957, *J.Rat. Mech. Anal.*, **6**, 769
Brereton C.M.H., Grace J.R., 1992, The transition to turbulent fluidization, *Trans. Inst. Chem. Engng.*, **70**, 246
Cai P., Jin Y., Yu Z.Q., Wang Z.W., 1990, Mechanism of flow regime transition from bubbling to turbulent fluidization, *A. I. Ch. E. J.*, **36**, 955
Cai P., Chen S.P., Jin Y., Yu Z.Q., Wang Z.W., 1989, Effect of operating temperature and pressure on the transition from bubbling to turbulent fluidization, *A.I.Ch.E. Symp.Ser.*, **270**, 37
Capes C.E., Nakamura K., 1973, Vertical pneumatic conveying: an experimental study with particles in the intermediate and turbulent flow regimes, *Can. J. Chem. Engng.*, **41**, 31
Carotenuto L., Crescitelli S., Donsi G., 1974, *Chim. Ind. (Suppl.)*, **12**, 185
Canada G.S., McLaughlin M.H., 1978, Large particle fluidization and heat transfer at high pressures, *A.I.Ch.E. Symp.Ser.*, **176**, 27
Chehbouni A., Chaouki J., Guy C., Klvana D., 1994, Characterization of the flow transition between bubbling and turbulent fluidization, *Ind. Engng. Chem. Res.*, **33**, 1889
Chehbouni A., Chaouki J., Guy C., Klvana D., 1995, Effets de differents parametres sur le vitesses de transition de la fluidisation en regime turbulent, *Can. J. Chem. Engng.*, **73**, 41
Foka M., Chaouki J., Guy C., Klvana D., 1995, Natural gas combustion in a catalytic turbulent fluidized bed, *Chem. Engng. Sci.*, **49**, 4269
Gonzales A., Chaouki J., Chehbouni A., Guy C., Klvana D., 1995, Effect of temperature on the onset of turbulent fluidization, in *Proceedings of the 8th engineering foundation conference on fluidization*, Engineering Foundation, 681
Grace J.R., 1990, High-velocity fluidized bed reactors, *Chem. Engng. Sci.*, **45**, 1953
Hartge E.U., Li Y., Werther J., 1985, Flow structures in fast fluidized beds, in *Fluidization V*, 345
Harris B.J., Davidson J.F, 1993, A core/annulus deposition model for circulating fluidized beds, in *Circulating Fluidized Bed Technology IV*, Pennsylvania, Engineering Foundation, 32
Horio M., 1986, High velocity operation of fluidized beds, *J. Inst. Powder Technol. Japan*, **23**, 80
King D.F., 1989, Estimation of dense bed voidagein fast and slow fluidized beds of FCC catalysts, in *Fluidization VI*, Engineering Foundation, Banff, 1
Kunii D., Levenspiel O., 1990, Entrainment of solids from fluidized beds I. Hold-up of solids in the freeboard. II. Operation of fast fluidized beds, *Powder Technol.*, **61**, 193
Kunii D., Levenspiel O., 1997, Circulating fluidized-bed reactors, *Chem. Engng. Sci.*, **15**, 2471
Kwauk M., Wang N., Li Y, Chen B., Shen Z., 1985, Fast fluidization at ICM, in *Circulating Fluidized Bed Technology*, Pergamom Press, Toronto, 33
Lee G.S., Kim S.D., 1990, Bed expansion characteristics and transition velocity in turbuelnt fluidized beds, *Powder Technol.*, **62**, 207
Louge M., Chang H., 1990, Pressure and voidage gradients in vertical gas-solid risers, *Powder Technol.*, **60**, 197
Massimila L., 1973, Behavior of catalytic beds of fine particles at high gas velocities, *A.I.Ch.E. Symp.Ser.*, **128**, 11
Matsen J.M., Hovmand S., Davidson J.F., 1969, Expansion of fluidized beds in slug flow, *Chem. Engng. Sci.*, **24**, 1743
May W.G., 1959, Fluidized-bed reactor studies, *Chem.Engng.Prog.*, **55**, 49
Mogan J.P., Taylor R.W., Booth F.L., 1969, A method of prediction of the porosities of high-pressure gaseous fluidization systems, *Can. J. Chem. Engng.*, **47**, 126
Mori S., Hashimoto O., Haruta T., Yamada I., 1989, Fundamentals of turbulent fluidized catalytic reactor, in *Fluidization VI*, 49
Nakamura K., Capes C.E., 1973, Vertical pneumatic conveying: a theoretical study of uniform and annular particle flow models, *Can. J. Chem. Engng.*, **51**, 39
Richardson J.F., Zaki W.N., 1954, Sedimentation and Fluidisation: Part I, *Trans. Instn Chem. Engng.*, 32, 35
Satija S., Fan L.S., 1985, Characteristics of slugging regime and transition to turbulent regime for fluidized beds of large coarse particles, *A.I.Ch.E.J.,* **31**, 1554
Sun G., Chen G., 1989, Transition to turbulent fluidization and its prediction, in *Fluidization VI*, Engineering Foundation, Banff, 33
Sun G., Grace J.R., 1992, Effect of particle size distribution in different fluidization regimes, *A.I.Ch.E.J.*, **38**, 716
Van Deemter J.J., 1980, Mixing patterns in large-scale fluidized beds, in *Fluidization*, edited by Grace J.R. and Matsen J.M., Plenum Press, New York, 69
Van Deemter J.J., 1967, The counter-current flow model of a gas-solids fluidized bed, in *Fluidization*, edited by Drinkenburg A.A.H., Netherlands University Press, Amsterdam, 334
Van Deemter J.J., 1961, Mixing and contacting in gas-solid fluidized beds, *Chem.Engng.Sci.*, **13**, 143
Van Swaaij, 1978, The design of gas-solids fluid bed and related reactors, *ACS Symp. Ser.*, **72**, 193
Van Swaaij W.P.M., Zuiderweg F.J., 1973, The design of gas-solids fluidized beds- prediction of chemical conversion, in *Fluidization and its applications*, edited by Angelino H., Couderc J.P., Gibert H. and Laguerie C., Cepadues editions, Toulouse, 454
Van Swaaij W.P.M., Zuiderweg F.J., 1972, Investigation of ozone decomposition in fluidized beds on the basis of

a two-phase model, in *Chemical reaction engineering*, Amsterdam, B 9-25
Werther J., Wein J., 1994, Expansion behavior of gas fluidized beds in the turbulent regime, *A.I.Ch.E. Symp. Ser.*, **310**, 31
Yang W.-C., 1974, Correlations for solid friction factors in vertical and horizontal pneumatic conveyings, *A.I.Ch.E.J.*, 605
Yerushalmi J., Cankurt N.T., 1979, Further studies of the regimes of fluidization, *Powder Technol.*, **24**, 187

CHAPTER 6

INTERPRETATION OF CONVERSION DATA FOR A FLUIDIZED BED OPERATED AT HIGH VELOCITIES

ABSTRACT

In a fluidized bed (ID 0.05 m), operated close to and in the turbulent fluid bed regime ($0.1<u_g<0.9$ m/s), the conversion rate of the mass transfer controlled oxidation of CO over a Pt/γ-alumina catalyst (65 μm) has been studied. The objectives were to derive mass transfer numbers, to investigate the gas-solids contacting efficiency and to evaluate four ways to interpret conversion data: i) in the well-known Sherwood versus Reynolds diagram to allow a comparison with published mass transfer data, ii) in a plot of the contact efficiency versus the reaction number for a comparison with results published for other chemical reaction systems, iii) on basis of the conventional two-phase model, and finally iv) by a cluster model, as used in previous chapters.

At high superficial gas velocities, the concept of particle clusters and voids is more realistic than the two-phase model considering discrete bubbles and a dense phase. Although the model may still be useful at the higher gas velocities, there is hardly any relation with the real flow pattern in the bed. Similar to earlier published results for the low velocity range, the two-phase model shows a decrease in the height of a mass transfer unit at the higher volumetric reaction rates, which could be explained in terms of chemical enhancement of the mass transfer.
The cluster model yields realistic values for the effective (spherical shaped) cluster size: calculated values for the effective cluster size decrease almost linearly from 700 to 200 times d_p for superficial gas velocities ranging from 0.1 to 0.9 m/s.

1 INTRODUCTION

Fluid bed reactors are applied in the chemical industry when dealing with fast exothermic, or regenerative heterogeneous reactions. The solid phase of a fluid bed is well mixed (isothermal reactor) and can be transported easily from one vessel to another (for example for catalyst regeneration). In chapter 5 of this thesis, the characteristics of the turbulent bed are discussed in more detail. When high through-put capacities and small reactor diameters are required (for example for high pressure processes), high-velocity fluidization is often considered to be a very good alternative for the more conventional (bubbling) fluidized bed. In the present chapter, the term high velocity fluid bed is used for the fluidization regime of fine particles ($d_p<100$ μm) at superficial gas velocities between $0.1<u_g<0.9$ m/s, that is starting at gas velocities much higher than the minimum bubbling velocity up to the transport velocity of the particles. Most of the fluid bed cat cracking regenerators, for example, have been operated in this regime, already for many decades.

The advantages claimed for high-velocity fluidized beds over the conventional bubbling fluidized beds are a better gas-solids contacting due to the absence of well defined bubbles (Van Deemter, 1980), the decrease in gas back-mixing (Cankurt and Yerushalmi, 1978), and the higher gas through-put.
The first claim concerning a better gas-solids contacting, has only been verified partially in the literature. In the last decades the research activities related to the turbulent regime were focused mainly on the determination of the transition from bubbling to turbulent fluidization

(amongst many others: Bi and Grace, 1995; Chehbouni *et al.*, 1994; see also chapter 5 of this thesis).

It seems reasonable to suppose that the gas-solids contacting can be improved significantly in high-velocity fluidization due to the absence of the bubble-to-emulsion mass transfer resistance. The gas-solids contacting determines to what degree the observed conversion rate deviates from the maximal possible conversion rate, which is derived by assuming all the particles to be ideally contacted by the reactant gas. For first order reactions, the contact efficiency η can be defined as:

$$\eta = \frac{k_{ov}}{k_p \eta_p} = \frac{\text{apparent conversion rate constant}}{\text{theoretical maximum conversion rate constant}} \qquad (1)$$

with k_{ov} and k_p representing the apparent conversion rate constant and the intrinsic reaction rate constant, respectively, both being based on the catalyst volume. Equation 1 is discussed in more detail in the introduction of this thesis. The value of η indicates effects of other conversion-rate controlling resistances than those inside or around the single particle. Values considerably lower than one are observed for various gas-solids reactors. For a bubbling fluid bed for instance, the conversion rate is known to be reduced by the bubble-to-dense phase mass transfer resistance. In a riser, the situation is different: the conversion rate can then be affected by the transfer of reactant from the gas bulk to particle agglomerates containing the reactive particles (see also chapter 4 of this thesis).

The turbulent fluid bed represents a difficult situation with aspects of both the bubbling bed and the fast fluid bed. In case of a very fast reaction, a reduction in contacting efficiency should be recognized from unexpected low values for the derived overall mass transfer numbers. Unfortunately, mass transfer data for turbulent beds are not readily available. In the present paper, experimentally determined mass transfer data for the turbulent fluid bed regime, and the effects of dilution with inert material, will be presented. These data have been collected from a series of experiments using the same reaction and procedure as presented in chapters 2 and 4 of this thesis. They will be interpreted in various ways to compare our findings with the few results of conversion experiments reported in the literature.
Preceding to the discussion of the experimental work, and the interpretation of the measurements in various ways, a review of existing ideas and observations regarding the high-velocity fluid bed performance will be presented in the subsequent section.

2 HIGH VELOCITY FLUIDIZED BED REACTOR PERFORMANCE

In chapter 5, the hydrodynamics of fluid beds operated at high gas velocities (but below the transport velocity), and specifically of the turbulent fluid bed, have been discussed in more detail. Going from low to high superficial gas velocities, the fluidization changes from a situation in which well defined bubbles are present (the bubbling bed), to one where the bubble structure is destroyed (the turbulent bed). In the latter, shapeless voids distributed over the bed volume appear and disappear with high frequency, resulting in an overall pseudo-homogeneous appearance. According to Sun and Grace (1990), the turbulent bed shows periods during which there are massive solid structures in the bed, containing rising gas packets, and periods in which the gas is present as the continuous phase with dispersed particles clusters.

The claim of a good gas-solids contacting in turbulent fluidized beds (suggested by, for example, Van Deemter, 1980) seems to be based on the absence of well-defined bubbles. This should facilitate the transfer of reactant from the bulk gas to the reactive particles. Nevertheless, pertinent data for mass transfer coefficients in turbulent beds (e.g. obtained

via absorption or desorption experiments) are not available. Besides, the number of papers in the literature dealing with a chemical reaction in a turbulent bed, is limited (amongst others Van Deemter, 1980; Avidan and Edwards, 1986; Krambeck *et al.*, 1987; Sun and Grace, 1990, 1992; Foka *et al.*, 1994). Furthermore, due to the lack of understanding of the physical nature of this fluid bed regime, any interpretation of conversion data is troublesome. In the papers known, conversion results have been interpreted by using the two-phase model proposed by May (1959), and Van Deemter (1961, 1967), or by a simpler axial dispersion model.
This latter model, for the turbulent bed regime used by Avidan and Edwards (1986) and Foka *et al.* (1994), is problematic because it can never predict conversions lower than those obtained for an ideally mixed reactor, while at the same time reactant by-passing (e.g. via the bubbles in the bubbling bed) is known to be the cause of such low conversions. A better approach would be to describe the conversion data in terms of the two-phase model.

3 THE TWO-PHASE MODEL

In the two-phase model, the limited gas-solids contacting is caused by the by-passing of reactant gas through bubbles (clearly visible in the bubbling bed). The main assumptions of the simplified two-phase model are: i) no solid particles in the bubble phase, ii) gas of the bubble phase passes in plug flow through the reactor, iii) dense-phase gas through-flow is negligible and iv) axial dispersion is caused by eddy-like diffusion in the dense phase.

The non-dimensional equations of the mass balance for stationary conditions and a first order reaction are:

$$\frac{\partial c_1}{\partial x} + N_\alpha (c_1 - c_2) = 0 \qquad \text{(bubble phase)} \qquad (2)$$

$$N_\alpha (c_2 - c_1) - \frac{1}{N_{ax}} \frac{\partial^2 c_2}{\partial x^2} + N_r c_2 = 0 \qquad \text{(dense phase)} \qquad (3)$$

with $N_\alpha=\alpha H/u_g$ being the number of mass transfer units, $N_{ax}=u_g H/(\varepsilon D_{ax})$ the number of diffusion units, $N_r=k_p \eta_p \beta H/((1+n_d)u_g)$ the number of reaction units, and n_d the dilution ratio; c_1 and c_2 are the concentration in the bubble, and dense phase respectively (Van Deemter, 1961, 1967; Van Swaaij and co-workers, 1972, 1973, 1978).
If the dense-phase mixing ($N_{ax}=\infty$) is neglected, integration of equations 2 and 3 leads to:

$$\frac{c_{out}}{c_{in}} = \exp\left(- \frac{N_\alpha N_r}{N_\alpha + N_r} \right) \qquad (4)$$

Accordingly, the conversion can be derived from the three non-dimensional groups N_α, N_{ax} and N_r (Van Swaaij, 1978). In the subsequent section, the role of these three non-dimensional numbers will be elucidated while paying special attention to the higher gas velocities.

Mass transfer. According to Van Deemter (1980), the mass transfer rate between the bubbles (or dilute phase) and the dense phase is the limiting factor in industrial scale turbulent fluid bed FCC regenerators. This author was the first one showing that these regenerators (mostly operated near or in the turbulent regime) usually yield very low contacting efficiencies (equation 1, $0.1<\eta<0.70$). Improved mass transfer sometimes occurs, presumable because of the applied higher gas velocities. Avidan and Edwards (1986) conducted the Mobil's methanol-to-gasoline reaction at turbulent conditions using type A-powder in a bench-scale unit (0.04 m ID), a pilot-plant (0.1 m ID), and in a 0.6 m ID

demonstration unit. Sun and Grace (1992) stated that bubble suppression, and consequently a higher overall mass transfer rate, could be obtained at the higher gas velocities and by increasing the fines level.

Reaction. The local conversion rate $k_p\eta_p\beta/(1+n_d)$ defined per unit reactor volume, can be varied by i) the local reaction rate constant k_p (e.g. through the operating temperature) ii) by changing n_d (diluting the active material with inerts) or iii) the variation of the solids concentration β. According to Van Deemter (1980) the contact efficiency seems to decrease at higher local conversion rates. Unfortunately, to our knowledge no other studies regarding the relation between the conversion and local reaction rate for high-velocity fluidization are published in the literature, apart from those to be discussed in the present paper.

Axial dispersion. The rate of axial dispersion of the reacting gas depends on the applied fluidization regime as well, and can influence the reactor performance. In the two-phase model, asymptotic limits are the case of and ideally-mixed-dense phase on the one hand, and a stagnant dense phase on the other. Unfortunately, only few axial mixing experiments have been reported in the turbulent fluidization regime (Van Deemter, 1980; Cankurt and Yerushalmi, 1978; Li and Weinstein, 1989; Foka *et al.*, 1996). According to these authors, the extent of gas back-mixing is high in the bubbling regime, but diminishes in the turbulent regime. The overall N_{ax} increases with increasing gas velocity. According to Van Deemter (1980), the axial mixing in the dense phase is important for industrial installations, but the mass transfer between dilute and dense phase remains the limiting factor. This conclusion seems to be supported by experiments showing that the conversion can be significantly lower than expected on basis of an ideally mixed tank reactor model (Sun and Grace, 1990, 1992).

Possible limitations of the simple two-phase model. Interpretation of conversion data in the two-phase model showed that for high local reaction rate constants k_r, the mass transfer apparently becomes better (Van Swaaij and co-workers (1972, 1975)). Possible explanations are i) the chemical enhancement of the bubble-to-dense phase mass transfer, ii) the axial mass transfer profile (presumably caused by the bubble growth), iii) additional reaction taking place within the bubbles and iv) additional reaction in the disengagement zone. Werther (1978) showed that the simple approach of the two-phase model with bubble-to-dense phase mass transfer and chemical reaction in series, is only valid up to a reaction rate (based on the dense phase volume) of $k_r \approx 1$ to 2 s^{-1}; at higher k_r-values chemical enhancement of mass transfer should be taken into account.
Another limitation of the two-phase model is perhaps related to the superficial gas velocity. For a turbulent fluid bed, the situation can be quite complicated if compared with the bubbling bed regime, due to the absence of a well defined bed structure.

4 THIS WORK

In previous chapters, some of the (probably inter-related) effects of mass transfer, reaction and dispersion for other reactors, viz. a packed bed and a riser (see chapters 2 and 4) were clarified. In these reactors, there is a reasonably well-defined (and almost homogeneous) structure of gas and solids. The actual performance of turbulent fluidized bed reactors, however, is still not well understood; interpretation of conversion data in the literature is usually based on the two-phase model (although there is no well-defined bubble and dense phase structure), or on the axial dispersion model (which is unable to predict conversions lower than an ideally mixed tank reactor).
In the present work, the objectives are to derive mass transfer numbers, to investigate the gas-solids contacting efficiency and to evaluate four ways to interpret the conversion data in high-velocity fluid beds. One of the four techniques is the cluster model, shown to be useful

in riser set-ups and in a packed bed.

The experimental procedure to obtain conversion data and mass transfer numbers is similar to the approach described earlier in this thesis (see chapters 1, 2 and 4). It uses the oxidation of carbon monoxide over a platinum on γ-alumina catalyst. A main feature is that the local conversion rate is varied by diluting the active catalyst with inert bed material. After presenting the conversion results, they are analyzed according to various methods, amongst which the two-phase model and the cluster model. In the latter model, the dominating rate controlling mechanism is supposed to be the mass transfer rate to and inside the particle cluster.

5 EXPERIMENTAL CONDITIONS

For the mass transfer controlled conversion measurements, the same platinum-based catalyst has been used as described earlier in chapter 1, while pure γ-alumina was used as the inert bed material. The only remaining (slight) difference was the one in average particle diameter, being 79 μm for the active particles and 65 μm for the inert ones. In table I some other properties of the bed material used are listed. The amount of catalyst in the reactor was calculated in each individual experiment by measuring the pressure drop: it ranged from approximately 150 to 200 gr, depending on the applied gas velocity.

Table I. Main properties of the powder used (at ambient conditions).

property	γ-alumina
d_p (μm)	65
ρ_p (kg/m^3)	1375
u_t (m/s)	0.16
u_c (m/s)	0.58
Ar	13.8
Geldart's type	A

5.1 Turbulent fluid bed facility

The oxidation of carbon monoxide has been carried out in the lab-scale turbulent fluidized bed facility shown schematically in figure 1.

The dimensions of the lab-scale facility are similar to those of the cold flow reactor, described previously (chapter 4). The set-up consists of i) a gas mixing section to provide the required gas mixture for the oxidation reaction, ii) a heated turbulent fluidized bed section, and iii) an analysis section for continuous CO and CO_2 monitoring by two Maihak analyzers. The turbulent fluidized bed (0.05 m ID, 0.75 m in height) is equipped with an expanded top bed (0.10 m ID, 0.30 m height), both made of quartz. The fourfold area increase in the expanded top section reduces the superficial gas velocity, which allows most of the entrained particle to fall back in the bed. Two cyclones, with internal diameters of 63 mm and 50 mm ID are applied to separate the entrained solids from the gas. The solids are returned to the fluidized bed by means of an external dip-leg. To ensure smooth operation of the dip-leg, a very small amount of nitrogen (approximately 2 ml/s) was introduced at its bottom. In all experiments, the conversion was measured at the exit of the reactor (including the bed and the disengagement zone).

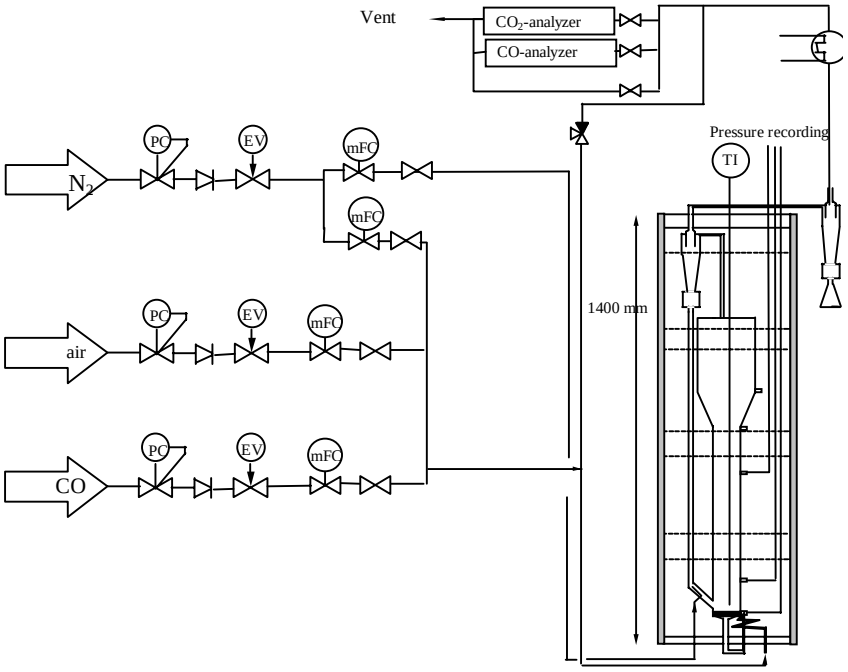

Figure 1. Schematic representation (non-scale) of the lab-scale turbulent fluidized bed.

Mass flow controllers have been applied to adjust the superficial gas velocity in the reactor, and the gas stream compositions. Gas velocities were in the range of 0.1 to 0.9 m/s could be applied. The oxygen concentrations in the gas could be varied from 8 to 12 vol.%, whereas carbon monoxide concentrations were in the range of 0.2 to 1 vol.% (balance N_2). The fluidized bed was operated at ambient pressures, and placed in an electrical column oven to enable operating temperatures up to 1200 K. A series of thermocouples was positioned along the riser wall to measure and control the reactor temperature. The oven was further equipped with a spy-glass for visual observation of the fluidization behaviour in the reactor. The axial pressure profile could be recorded at any time by a series of pressure taps along the fluid bed column.

5.2 CO oxidation measurements

In chapter 1 of this thesis, the oxidation of CO over a Pt/γ-alumina catalyst was shown to be a promising model reaction. For temperatures > 750 K, the conversion rates were controlled by mass transfer. It has been shown in chapter 1 that, for this model reaction, the shift from a negative order reaction to a first order reaction when going to the mass transfer controlled regime, is a valuable extra tool that can be used to verify whether mass transfer is actually dominant.

The temperature in the present oxidation experiments was varied from 575 to 775 K, while the active material was diluted in ratios varying from n_d=5058 to 30560 m_{inerts}^3/m_{cat}^3. The active particles for this work are taken from the same batch of catalyst material as prepared for chapter 1. Lower dilution ratios could not be applied because that would result in too high conversions (close to 1) and possible errors in the analysis of the reaction gas. The experiments were carried out from high to lower dilution ratios, ensuring that very small amounts of active material, inevitably remaining in the reactor, do not affect the subsequent conversion experiments. The results of all measurements appeared to be well reproducible. Prior to further experimental work, it was observed that the inert material, pure γ-alumina, was inactive in the oxidation of carbon monoxide within the range of operating temperatures; deactivation of catalyst does not occur. These observations are in agreement with the results earlier obtained for the packed bed and the riser set-up (chapters 2 and 4).

5.3 Back-mixing of gas

Before measuring the reactor performance and calculating the contact efficiencies of the reactor, a few back-mixing measurements have been conducted to investigate whether axial mixing can be important. The experimental set-up and measuring technique used for these back-mixing measurements has been applied in various other investigations (amongst others Bohle and van Swaaij, 1978; Cankurt and Yerushalmi, 1978; Avidan, 1982; Foka *et al.*, 1994): an easy detectable inert tracer gas is injected continuously at a pre-selected bed level, while sample gas is withdrawn from locations below (upstream of) the injection point.

The analysis of back-mixing experiments can be carried out by the two-phase model. From the solution of the mass balances over the reactor length (equations 2 and 3), conservative values for the axial dispersion number, N_{ax}, can be derived by solving the differential equations 2 and 3 with N_r=0. It has been assumed that the tracer concentration at the bottom of the bed is negligibly small (Van Deemter, 1961). At a location upstream of the injection point, the solution for the dense phase becomes:

$$\frac{c_{z-L}}{c_L} = \left(\gamma\frac{\lambda^2-1}{4\lambda} + \frac{\lambda+1}{2\lambda}\right)\exp\left(\frac{\lambda-1}{2}\frac{\alpha(z-L)}{u_g}\right) \text{ with } \lambda^2 = 1+\frac{4H_\alpha}{H_{ax}} \qquad (5)$$

The limits for H_α and H_{ax} with γ=0 (all reactant is injected in the bubble phase) can be found by plotting the logarithm of the concentration as a function of the vertical position z. Upstream, the logarithm of the left-hand side of equation 5 should fall on a straight line with a mixing slope of $S=(\lambda-1)/(2H_\alpha)$, while the intercept of this line with (z-L)=0 is equal to $\ln((\lambda+1)/(2\lambda))$. From the combination of both, the slope and the intercept, values for N_α and N_{ax} can be estimated.
Another approach to describe the present axial dispersion data, uses the pseudo-homogeneous model, and yields the number of back-mixing units $N_{bm}=u_gH/(\varepsilon D_{bm})$, which can be considered as a very conservative estimate of the number of axial dispersion units:

$$\frac{\partial c}{\partial t} = D_{bm}\frac{\partial^2 c}{\partial z^2} - \frac{u_g}{\varepsilon}\frac{\partial c}{\partial z} \quad \Rightarrow \quad \ln\left(\frac{c_{z-L}}{c_L}\right) = \left(\frac{u_g}{\varepsilon D_{bm}}(z-L)\right) \qquad (6)$$

Following Van Deemter, the mixing slope S derived from equation 6 can be translated in terms of the number of actual axial dispersion units N_{ax}, if H_α is known a priori:

$$S = \frac{\sqrt{\left(1+4N_{ax}/N_\alpha\right)}-1}{2H_\alpha} \qquad (7)$$

Approximate values for H_α as a function of the reactor diameter and bed height are presented by Van Swaaij (1985). From this paper, a value of approximately H_α=0.08 m can be derived for our 0.05 ID fluid bed (H=0.2 m).

In the mixing experiments, carbon monoxide in nitrogen was taken as the tracer gas: it was injected and withdrawn from the centre of a bed consisting of inert γ-alumina. These experiments were initially conducted at 375 K. However, because possible adsorption of tracer gas on the solids has a considerable influence on the effective back-mixing coefficient (see f.i. Bohle and van Swaaij, 1978), and the adsorption phenomena strongly depends on the temperature, some of the back-mixing experiments were conducted also at the higher temperature of 775 K, applied later in the CO oxidation experiments.

Before discussing the results of back-mixing and the CO conversion experiments, some

hydrodynamic results will be discussed first in the subsequent section.

6 RESULTS

6.1 Hydrodynamics

For the interpretation of the conversion data, values of the average solids concentration are required. The axial solids concentration profile has been determined in the small turbulent fluidized bed set-up at various operating conditions. As the contribution of the acceleration term to the total pressure drop can be neglected if compared with the solids hold-up contribution, the solids hold-up can be calculated directly from the observed pressure drop. Figure 2a shows the solids profile along the reactor height for two different superficial gas velocities at ambient conditions. The solid lines represent the results from a simple model, reported earlier in chapter 5. The model results ($a \cdot u_g$=5 s^{-1}, u_t^*=3.4 m/s and n=5.1), are in fair agreement with the experimental data. Only for the lowest pressure sample point at z=0.05 m a notable difference is observed (see also chapter 5).

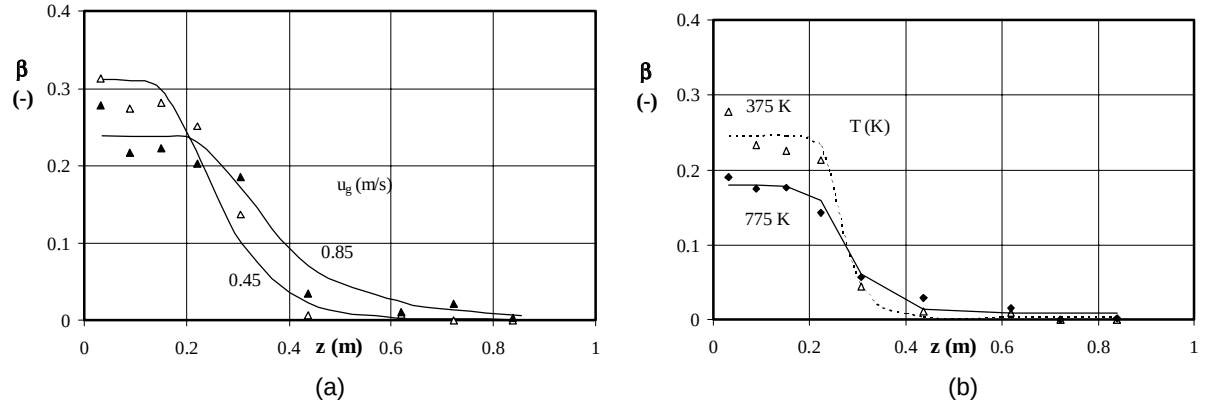

Figure 2. The axial solids hold-up profile for (a) various gas velocities at a temperature of 300 K and (b) various temperatures and a gas velocity of 0.6 m/s. Legends: (a) ♦ 0.45 m/s; Δ 0.85 m/s, (b) Δ 375 K; ♦ 775 K. The solid lines in (a) are the results from a model presented in chapter 5 ($a \cdot u_g$=5 s^{-1}, u_t^*=3.4 m/s and n=5.1), the ones in (b) only indicate trends.

In figure 2b the effect of an increasing temperature on the axial solids hold-up profile is plotted for a gas velocity u_g=0.6 m/s. At higher temperatures the hold-up in the dense region (at the bottom of the bed) is decreased in favour of the hold-up in the dilute region (the freeboard). It can be easily calculated that the terminal falling velocity of the individual particles decreases at the higher temperature. If the size and density of particle clusters is assumed to be independent on the temperature, the terminal falling velocity of the cluster will also decrease at higher temperatures. Consequently, more (clusters of) particles will be entrained by the fluidization gas, leading to an increased solids concentration in the freeboard.

6.2 Transition velocities

For a correct interpretation of the conversion experiments, the transition from the bubbling to the turbulent fluid bed regime should be known. At ambient conditions, the transition velocities to the turbulent fluidization regime, u_c and u_k, can be well derived from a plot of the pressure fluctuation P_f versus the gas velocities. In chapter 5, the fluctuation and its normalized function have been presented as a function of the gas velocity. Values for P_f and $P_{f,rel}$ appeared to increase sharply with the superficial gas velocity until a certain maximum beyond which they decrease again. For the γ-alumina at room temperature, the characteristic gas velocity u_c could be clearly identified at approximately 0.58 m/s. At higher

temperatures, the transition velocity u_c increases slightly, due to the effect of a higher gas viscosity and lower gas density (not shown in this paper). This change in gas properties causes a strong decrease in the Archimedes number, $Ar=d_p^3\rho_g(\rho_p-\rho_g)g/\mu_g^2$. At temperatures above 575 K the intensity of the pressure fluctuation decreases strongly, and in the present experiments the transition point could not clearly be distinguished anymore. The correlation of Cai *et al.* (1989), derived for 325<T<725 K, enables the estimation of the transition velocity towards the turbulent fluidization regime at higher operating temperatures:

$$\frac{u_c}{\sqrt{gd_p}} = \left(\frac{0.211}{D_r^{0.27}} + \frac{2.42\cdot 10^{-3}}{D_r^{1.27}}\right)\left(\frac{\mu_{g,20}}{\mu_g}\right)^{0.2}\left[\left(\frac{\rho_{g,20}}{\rho_g}\right)\frac{\left(\rho_s-\rho_g\right)}{\rho_g}\frac{D_r}{d_p}\right]^{0.27} \qquad (8)$$

Typical values are $u_c \approx 0.58$ m/s at room temperature, and $u_c \approx 0.75$ m/s at 775 K. In the present work, the CO conversion experiments (at T=775 K) are conducted at gas velocities ranging from 0.1 up to 0.9 m/s, that is partly in the bubbling fluid bed regime and partly in the turbulent regime.

6.3 Back-mixing experiments

In figure 3a, the mixing slope for a typical axial back-mixing experiment (obtained by equation 6) has been plotted. Figure 3b shows back-mixing data from various publications plotted versus the gas velocity: it includes the data points of this work. The present authors observed values for εD_{bm} around 0.03 and 0.04 m^2/s for a gas velocity of 0.4 and 0.7 m/s respectively, both at a reactor temperature of 375 K. As a first estimate, the number of back-mixing units N_{bm} in the dense bed (height $H \approx 0.2$ m) is about 2 to 3. As mentioned before, adsorption of CO on the γ-alumina is likely to occur at the lower temperatures, and some back-mixing measurements have also been carried out at a temperature of 775 K (the closed circles in figure 3b). For the higher temperature of 775 K, values of around 0.04 m^2/s are found, again yielding a value of N_{bm} = 2 to 3. Apparently, for this temperature interval, the back-mixing appears to be independent on the temperature.
In figure 3b a single data-point is indicated (x) for the back-mixing coefficient in the freeboard region of the fluid bed. Similar to Cankurt and Yerushalmi (1978) a lower value for the back-mixing has been obtained in the freeboard region, εD_{bm}=0.029 m^2/s, with a corresponding N_{bm}=12 (at a freeboard height of H=0.5 m).

Taking into account the mass transfer rate between bubbles and dense phase (H_α=0.08 m), for the dense bed (H=0.2 m), the number of actual axial dispersion units can now be estimated from equation 7 to be in the order of N_{ax}=5-10. On basis of this evaluation, it is assumed hereafter that axial dispersion of gas in the dense phase is negligible in the conversion experiments to be presented.

Values for the back-mixing coefficient εD_{bm} reported by other investigators, and derived by applying the homogeneous model of equation 6, are also indicated in figure 3b. In many cases, the back-mixing coefficient gradually increases with increasing gas velocity, up to a certain maximum value (at a velocity close to the transition towards the turbulent regime), beyond which it decreases again. The absolute values for the back-mixing coefficient, however, are widely differing. This is caused by differences in bed diameter, in particle properties and in the adsorption capacity of the solid material for the specific tracer gas. For example, Avidan (1982) showed that the back-mixing coefficient is proportional to the bed diameter, while it decreases with the fines content in the bed material.

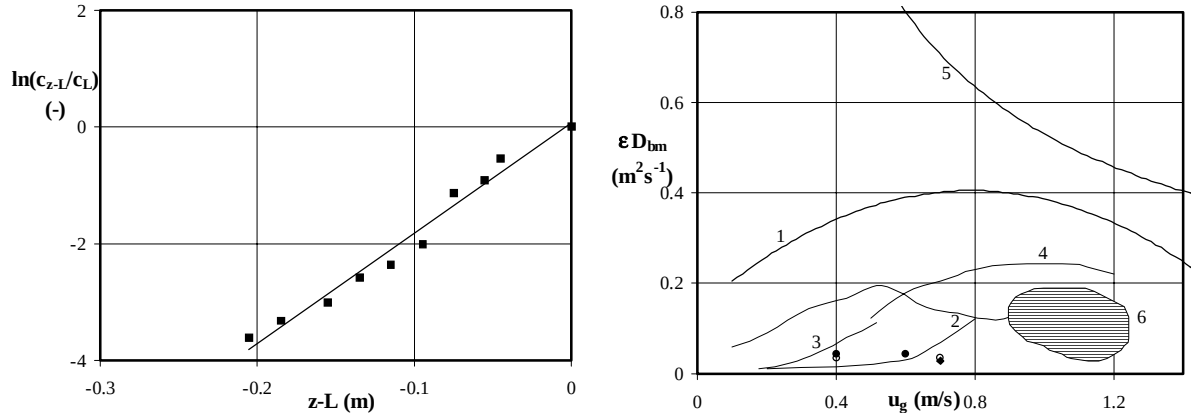

(a) (b)

Figure 3. (a) The logarithm of the non-dimensional concentration versus the axial position in the turbulent bed (equation 6) at u_g=0.7 m/s and T=375 K, and (b) the back-mixing coefficient εD_{bm} versus the gas velocity. Legends: **1** Cankurt and Yerushalmi (1978) D_r=0.152 m, **2** Guo *et al.* (1987) D_r=0.07 m, **3** Gilliland and Mason (1949, 1952) D_r=0.025-0.075 m, **4** Lee *et al.* (1988) D_r=0.1 m, **5** Li and Wu (1991) D_r=0.09 m, **6** data presented by Foka *et al.* (1994) D_r=0.1 m, **7** Foka *et al.* (1996) D_r=0.1 m, ❍ own data, dense phase T=375 K, ● own data, dense phase T=775 K, ♦ own data, dilute phase at T=375 K

Some of the curves in figure 3b are in close agreement with the own back-mixing data. The measured back-mixing coefficients at 775 K, for example, nicely fits in the trend indicated by Guo *et al.* (1987). Their back-mixing data were determined by applying almost identical conditions: they have been measured for similar particles (FCC particles, 44 μm), a comparable reactor diameter (0.07 m), and with inert H_2 as the tracer gas.

6.4 Determination of mass transfer controlled reaction rates

The reactor performance, and the effect of various parameters on the contact efficiency (equation 1), have been investigated by applying the oxidation reaction of CO with oxygen over a Pt/γ-alumina catalyst. In chapters 2 and 4, it was already demonstrated that this reaction could be used to determine gas-to-particle mass transfer coefficients in a small packed bed or a riser of a circulating fluid bed set-up.
Apart from the dilution ratio, other parameters influencing the conversion in a reactor are the gas velocity, the CO and O_2 inlet concentrations, and the reaction temperature. Contrary to the riser, the solids concentration can not be varied in a bubbling or turbulent fluid bed; it is determined exclusively by the gas velocity (see also figure 2b).

Figure 4 shows the carbon monoxide conversion $\xi=1-c_{out}/c_{in}$ plotted versus the gas velocity for various dilution ratios, n_d=5088 up to n_d=30560. As expected if plug flow behaviour of the gas is assumed, the conversion decreases exponentially with increasing gas velocity, due to the shorter contact time. At lower dilution ratios (viz. more active material) the conversion is increased.

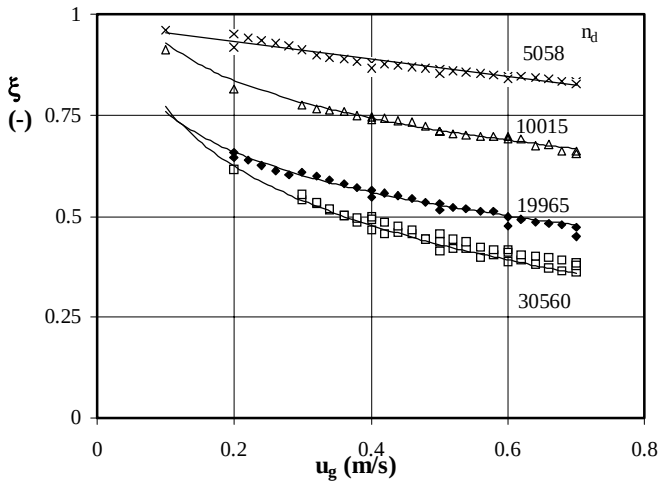

Figure 4. The carbon monoxide conversion ξ versus the gas velocity for various dilution ratios at a reactant inlet fraction of 0.5 vol.% CO and a oxygen inlet fraction of 10 vol.% , T=775 K. Legends: x n_d=5058, Δ n_d=10015, ♦ n_d=19965, and □ n_d=30560.

Whether the conversion is controlled by mass transfer or the reaction kinetics can easily be verified by i) determining the observed order in CO and O_2, and ii) calculation of the apparent activation energy.

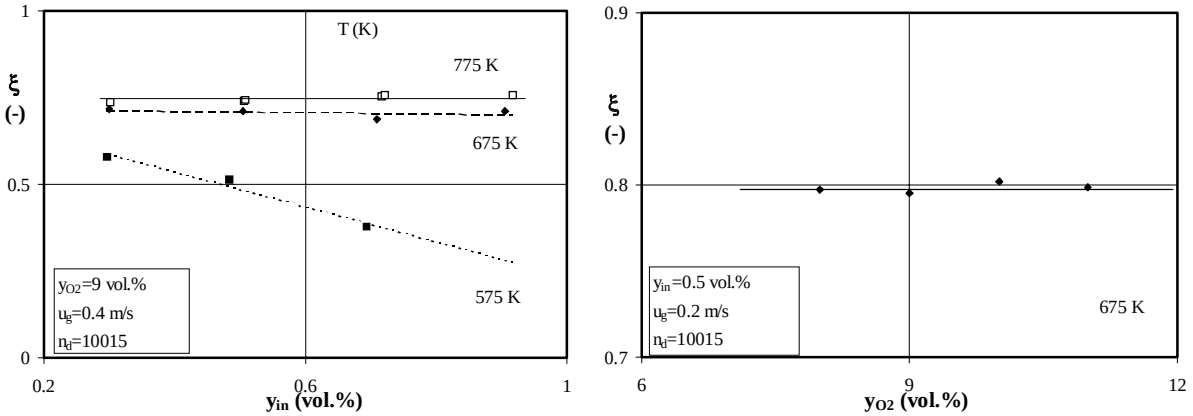

Figure 5. (a) The carbon monoxide conversion ξ versus the CO inlet fraction y_{in} for y_{O2}=9 vol.%, n_d=10015, u_g=0.4 m/s, and (b) the CO conversion versus the oxygen inlet fraction y_{O2}, for y_{in}=0.5 vol.%, n_d=10015, u_g=0.2 m/s, T=675 K. Legends: □ 775 K, ♦ 675 K, ■ 575 K.

Figure 5a represents the conversion ξ as a function of the CO inlet concentration, y_{in}, for 3 operating temperatures and for the relatively low gas velocities u_g<0.4 m/s. At a temperatures of 575 K, the conversion decreases clearly with increasing inlet fractions of CO, indicating an apparent reaction order in carbon monoxide smaller than 1. The apparent order increases at the higher temperatures. From 675 K, the conversion becomes independent of y_{in}, suggesting that the reaction rate is mass transfer controlled at this temperature level. In figure 5b the conversion of CO is plotted as a function of y_{O2}, the volume fraction O_2. Again, at the high temperature level, the oxygen inlet concentration does not affect the conversion anymore, and a zero order in oxygen is therefore plausible from 675 K. Both, the apparent order in CO and in O_2, are in accordance with the values that may be expected if mass transfer becomes the rate controlling step.
Starting from these first and zero-order kinetics in the CO-and O_2-concentration, respectively, the apparent reaction rate constant per unit volume of catalyst k_{ov} can be

derived easily from a pseudo-homogeneous approach, while assuming plug flow behaviour of the gas, and neglecting the axial dispersion of the gas:

$$\frac{\partial u_g Ac}{\partial x} = -k_{ov} c \frac{\beta A \Delta L}{(1+n_d)} \Rightarrow k_{ov} = -\frac{u_g (n_d+1)}{\beta \Delta L} \ln\left(\frac{c_{out}}{c_{in}}\right) \qquad (9)$$

In equation 9, n_d represents the dilution ratio, A the cross-sectional area of the reactor, and ΔL the length of the reactor section over which the conversion is determined.

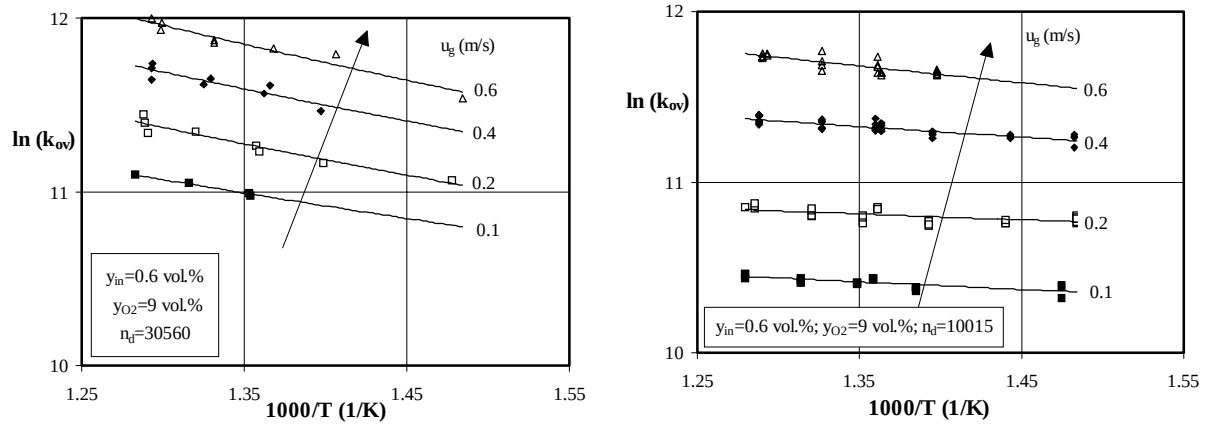

Figure 6. Dependency of the observed apparent rate constant on the operating temperature and the gas velocity for the temperature range between 675 and 775 K, a dilution ratio of (a) n_d=30560 and (b) n_d=10015 and a reactant inlet concentration y_{in}=0.6 vol.%.

In figure 6a the derived apparent reaction rate constant, k_{ov}, has been plotted versus the inverse operating temperature for various gas velocities. The data points in this plot have been obtained at a dilution ratio n_d=30560. At the higher temperatures and gas velocities a significant increase in k_{ov} is observed. From the slopes of the curves in figure 6a over the temperature range of 675 to 775 K, an apparent activation energy of E_a=12 to 16 kJ/mole can be derived. They appear to be almost independent on the gas velocity. In figure 6b a similar plot is presented, but now for a lower dilution ratio n_d=10015. The apparent activation energy ranges here from 8 kJ/mole at u_g=0.6 m/s to 4 kJ/mole for u_g=0.1 m/s. Two major observations result from the comparison of figure 6a and 6b. At the lowest dilution ratio, a stronger influence of the gas velocity on the apparent reaction rate constant is observed, and a decreased activation energy, both indicating a somewhat more pronounced effect of mass transfer limitation. Nevertheless, the low values for the activation energy suggest that for both dilution ratios, the mass transfer mainly controls the conversion rate. This is in line with the results presented in figure 5, where (for n_d=10015) a first order in CO was observed for the considered temperature range between 675 and 775 K.

In figure 7, the effect of the dilution on the apparent rate constant is further illustrated. It shows that k_{ov} increases with increasing temperature and dilution ratio.

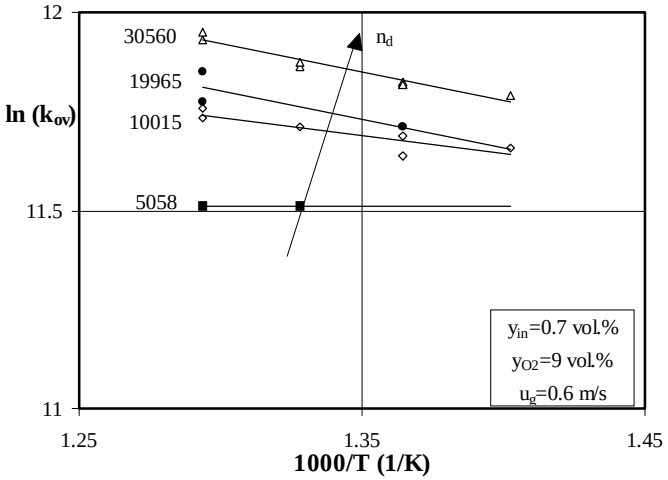

Figure 7. The observed apparent rate constant as a function of the inverse temperature for various dilution ratios. Temperature range: 715<T<775 K; inlet concentrations: y_{in}=0.7 vol.% and y_{O2}=9 vol.%; u_g=0.6 m/s.

From figures 5 to 7 the following conclusions can be summarized. First, at higher temperatures the reaction becomes first order in the carbon monoxide concentration, while the order in the oxygen concentration approaches zero. The apparent activation energy for n_d=10015 approximates 8 kJ/mole, whereas at n_d=30560 it approaches a value of E_a=10 kJ/mole. Both values are close to the figure derived for gas-phase diffusion ($\cong$ 11 kJ/mole according to Fuller *et al.*, 1962). It can be distinguished, however, from the plots of ln(k_{ov}) versus 1/T, that the lowest values of E_a are always found for the least diluted systems, or the highest local reaction rate. This may indicate a shift in the location of the predominant mass transfer resistance, viz, from the boundary layer around the cluster at low values of n_d, to the cluster interior at high values of n_d. Apart from any remaining effects of the chemical kinetics on the activation energy, the k_g-value over the boundary layer of the cluster depends on $D^{2/3}$ (with Sh calculated from the Ranz-Marshall equation(1952)), whereas its value becomes proportional to D for the cluster's interior (with Sh to be taken constant).

6.5 Effects of the gas velocity and the dilution ratio on apparent Sherwood numbers

For the reaction rates which are completely controlled by mass transfer, Sherwood numbers can be derived directly from the apparent kinetic rate constant, k_{ov}. Assuming spherical particles, the apparent Sherwood number Sh^o can be calculated from:

$$Sh^o = \frac{k_{ov} d_p^2}{6D} \qquad (10)$$

Here, D represents the molecular diffusion coefficient, which can be derived from the correlation proposed by Fuller *et al.* (1966). In figure 6 it was shown that the value for the reaction rate constant (and the corresponding apparent Sherwood number derived by equation 10), increases with increasing u_g, but decreases at the lower dilution ratios. This picture is further completed in figure 8. It shows the Sherwood number as a function of the gas velocity for all four dilution ratios applied. The apparent Sherwood number becomes higher for higher gas velocities and higher n_d.

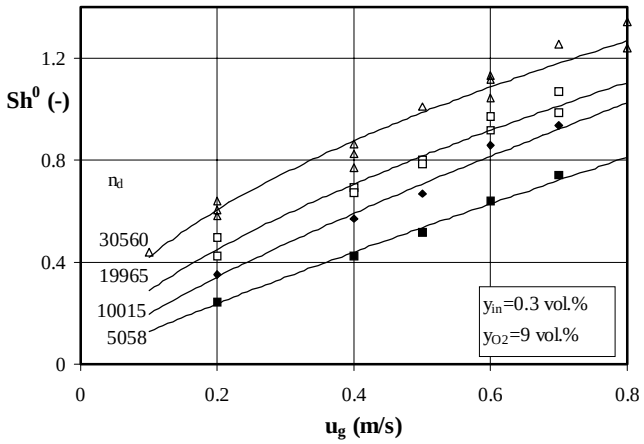

Figure 8. The dependence of the apparent Sherwood number, equation 10, on the gas velocity for various dilution ratios and an operating temperature of 775 K.

It is interesting to note that, despite the high dilution ratios applied, the apparent Sherwood numbers are still lower than expected on basis of ideal contacting. The decrease with a factor 2 to 10, depending on the applied gas velocity and dilution ratio, is comparable with the results obtained in the small riser applied in chapter 4. The increase in Sh^0 with gas velocity is due to the increase in the number of bubbles.

In the following section, the observed conversion data are interpreted and compared with results published in the literature in various ways. The most simple way is to present them in the well-known plot of the apparent Sherwood number versus the Reynolds number. In this way, our mass transfer numbers can be compared with mass transfer data published for other gas-solids reactors.
Secondly, the contact efficiency data (calculated by equation 1) can be plotted versus the reaction number $N_r=k_p\beta\tau/(1+n_d)$. In this way, the present conversion data can be compared with those obtained in other (not necessarily mass transfer controlled) reactive systems. Reactive systems in the high velocity regime published in the literature are concerned with ozone decomposition (Sun and Grace, 1992) or natural gas combustion (Foka *et al.*, 1996).
Then, our CO-oxidation data points are interpreted by the two-phase model, described by equations 2 and 3. This model is based on the presence of a well-defined bubble and dense phase, which, however, are likely to be absent in the turbulent fluid bed regime.
Therefore, and finally, the data are interpreted by the cluster model, presented in more detail in chapters 2 and 4, and appendix II of this thesis.

7 DISCUSSION AND COMPARISON WITH PREVIOUS WORK

7.1 Mass transfer numbers in turbulent fluid beds

Mass (and heat) transfer data in various reactors can be compared easily in the well-known plot of Sherwood (respectively Nusselt) number versus the particle Reynolds number, the latter being defined on basis of the slip velocity between the solids and gas.
In figure 9 the data published for packed and bubbling fluidized beds are represented by the shaded area (see f.i. Kunii and Suzuki, 1967). The mass transfer numbers calculated in the present work (equation 10) are presented in two curves (denoted by 4), one for a dilution ratio of n_d=5058, and the other for n_d=30560. These data are much higher than those for packed and bubbling fluidized beds, but somewhat lower than the Sherwood numbers for individual particle contacting (curve 1), represented by the Ranz-Marshall equation (1952). At higher Reynolds numbers (corresponding with higher gas velocities), and high dilution

ratios the observed mass transfer number approaches this ideal case, but still remains somewhat lower.

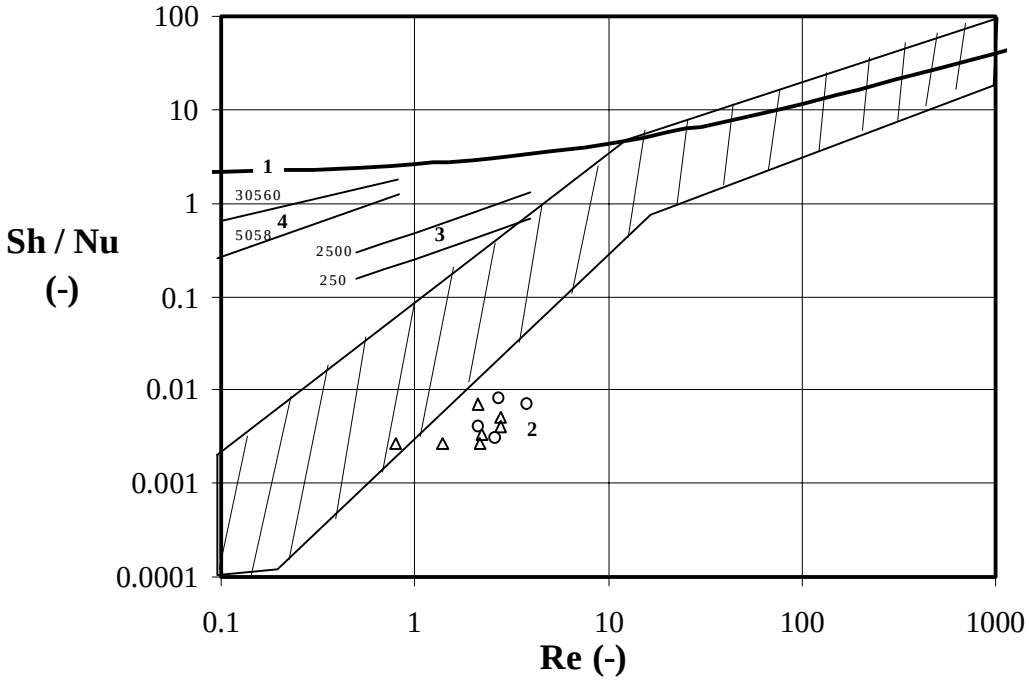

Figure 9. Sherwood and Nusselt numbers as a function of Reynolds number in fluidized beds. Literature data for fluidized beds and packed beds are indicated (Kunii and Suzuki, 1967). Legend: **1.** Ranz-Marshall (1952); **2.** Δ Van der Ham (1994), ❍ Van der Ham (1994); **3.** CO oxidation experiments in a riser (chapter 4); **4.** The present work: for n_d=5058 and n_d=30560.

Gas-to-particle mass (or heat) transfer data for the turbulent flow regime are not readily available in the literature. Therefore, our data are compared with mass transfer data in other reactor types. Concerning results obtained for the riser of a circulating fluid bed, both the data of Van der Ham (1994; undiluted material), and the own results reported earlier in chapter 4 (n_d=250 and 2500) are included in figure 9 (triangles, circles and curve 3 respectively). Despite the lower gas velocities applied in this work, and consequently lower Reynolds numbers, the apparent Sherwood numbers in the turbulent regime are significantly higher than those obtained in the riser of a circulating fluid bed set-up. This is almost certainly due to the higher degree of dilution applied in the present work. It is important to note that the apparent Sherwood numbers as observed here only reflect overall values, in which all possible mass transfer resistances are lumped. Obviously, the mass transfer data should be handled with great care.

7.2 Effect of reaction number on the contact efficiency

7.2.1 Interpretation of the present conversion data

The contact efficiency η is defined by equation 1 as the ratio of the measured conversion rate over the theoretical maximum value. In figure 5 to 7 it was shown that the conversion rate is controlled by mass transfer resistances. In the ideal case, the mass transfer resistance is located entirely in the particle boundary layer. The theoretical maximum can be calculated from the reaction rate that is observed when only the resistances on a particle level are important, that is when the particles are ideally contacted by the gas. For that extreme case, the value for the theoretical maximum conversion rate, corresponding with $k_p\eta_p=k_ga$, can be derived by using the Ranz-Marshall equation (1952). The contact-efficiency

is then calculated from the conversion data as the ratio between the observed Sherwood number (equation 10) and the one derived by Ranz and Marshall. One way of comparison is to present them in a plot of the contact efficiency, η, versus the reaction number N_r, defined by $N_r=k_p\beta H/(u_g(1+n_d))$ with k_p derived from the Ranz-Marshall equation; in this way our conversion results ($0.5<k_p\beta/(1+n_d)<3$ s^{-1}) can be compared easily with those published in the literature.

Figure 10 shows some of our data interpreted in this way. The plotted data have been evaluated for a temperature of 775 K and various gas velocities.

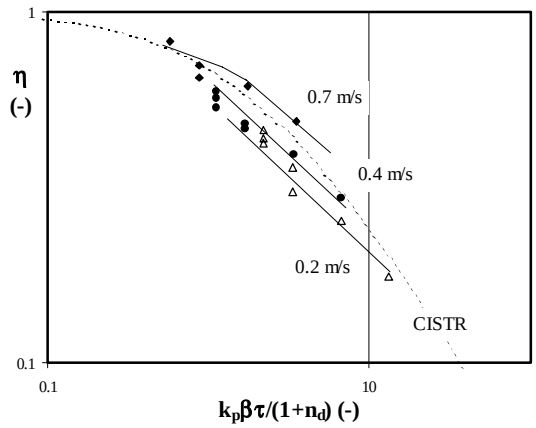

Figure 10. The contact efficiency, η, as a function of the reaction number for various gas velocities at a temperature of 775 K. The dashed line represents the contact-efficiency in the extreme case that an ideal stirred tank model is valid for the gas phase instead of the suggested plug flow behaviour, and only plotted for illustration. Legends: Δ u_g=0.2 m/s, ● u_g =0.4 m/s, and ♦ u_g =0.7 m/s. The solid lines indicate trends.

The contact efficiency decreases strongly with increasing reaction number. Contact efficiencies in the range of $0.2<\eta<0.8$ are now obtained, which is in agreement with contact efficiency data published by Van Deemter as well as by Sun and Grace (1990, 1992). These authors applied similar values for the reaction number. The dashed line indicates the curve of the contacting efficiency that can be calculated if the gas phase of the fluid bed is supposed to be ideally mixed and the gas-solids contacting to be ideal. As axial dispersion could be almost neglected in the conversion experiments, this curve should be considered as an indication only. Our data points are below the CISTR curve for the low gas velocities, and above for the higher gas velocity of 0.7 m/s. At the lowest gas velocities the contacting is even worse than for the extreme (and unrealistic) case of the ideal mixed tank model. Similar behaviour has been observed for bubbling fluidized beds. It is surprising (and not always recognized) that the contact efficiency remains poor over the total range of the gas velocity. Notwithstanding the commercial interest in and the use of turbulent fluidized beds, to our knowledge no studies regarding the relation between the conversion and mass transfer limitation for turbulent beds are published in the literature, apart from those to be discussed in the subsequent section and the one of Van Deemter (1980).

7.2.2 Interpretation of the conversion data of Sun and Grace and Foka *et al.*.

Sun and Grace (1990, 1992) measured ozone conversions in the turbulent fluidization regime using different particle size distributions (viz. bimodal, narrow and wide, all with nearly the same diameter, 60 μm, and particle density, 1580 kg/m^3). Foka *et al.* (1994, 1996) investigated the catalytic combustion of methane in a turbulent fluid bed reactor.
Similar to the CO oxidation results plotted in figure 10, the conversion data from these

investigators can be interpreted in terms of the contact efficiency and the reaction number (figure 11a and 11b, respectively). To calculate the maximum conversion rate constant k_p (η_p=1), the value for the intrinsic reaction rate constant was required in this case because the measurements were carried out in the kinetically controlled regime. They have been generously provided by the authors (Sun and Grace, 1997; Foka *et al.*, 1997).

The calculated contact efficiencies strongly decrease as a function of the reaction number. They are again equal to (figure 11b) or worse (figure 11a) than the curve of the CISTR model (and ideal contacting). Similar to our CO oxidation experiments, these observations can certainly not be explained by an axial dispersion model, as the curve for the CISTR represents the boundary condition. In figure 11a the different symbols represent data for various particle size distributions, bimodal (□), narrow (■), and wide (x). The bed of the wide particle size distribution shows an improved contacting compared with the other two, according to the authors due to an increased solids content inside the bubbles.
The data of Foka *et al.* are presented in figure 11b. They also analyzed their conversion data by a (pseudo-homogeneous) axial dispersion model, and suggested a good description, although this is not fully supported by their calculations (the solid line in figure 11b). Contrary to our data and to some of Sun and Grace, the results of Foka *et al.* indicate a somewhat better contacting than the CISTR-approach. This better contact efficiency may be due to the larger particle size applied (Geldart type A particles were used in the present work and in the work of Sun and Grace, and Geldart type B by Foka *et al.*), because larger particles are less likely to form clusters of particles (Dry and co-workers, 1992; but also indicated by the experiments reported in chapter 3).

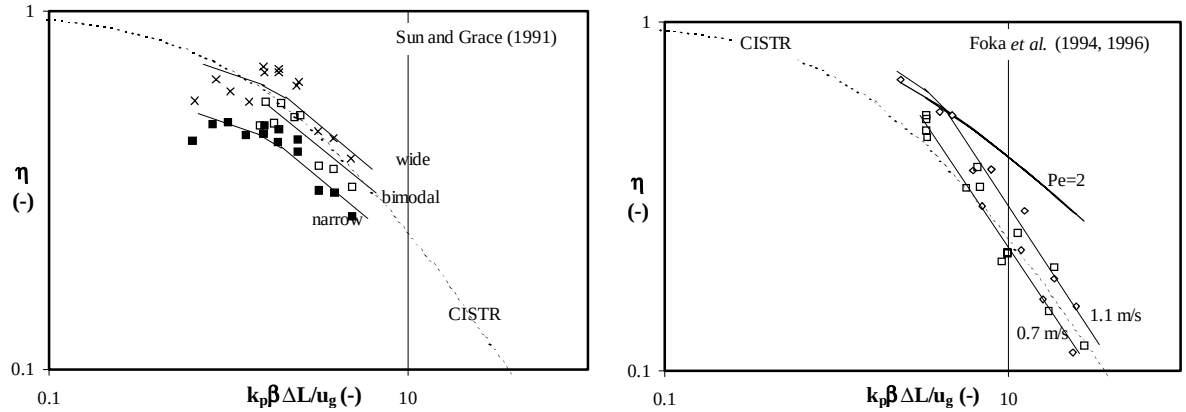

Figure 11. The contact efficiency, η, as a function of the reaction number for various gas velocities, recalculated from Sun and Grace (1991) and Foka *et al.* (1994, 1996). The dashed line represents the contact-efficiency for the extreme case of an ideally stirred tank model for the gas phase assuming ideal contacting. Legends: a) □=bimodal, ■=narrow, and x=wide size particle distribution, $0.7<u_g<1.2$ m/s; b) □ u_g =0.7 m/s, ◊ u_g =1.1 m/s. One of the solid curves in figure b represent the contact efficiency derived from plug flow with axial dispersion (Pe=2). All others in a and b indicate trends

As has been shown in the introduction of this thesis, from the curves in figure 11, one can not distinguish whether any diffusional resistances or mixing effects are the main reason for the contact-efficiency loss in the conversion experiments. Apart from any possible kinetic or the external mass transfer resistance at the surface of the individual particles, an additional conversion rate controlling resistance must be present, apparently becoming more dominant at higher reaction rate constants. This additional rate controlling step may be the 'bubble'-to-emulsion mass transfer rate (two-phase model) or the gas-to-cluster mass transfer resistance and the diffusional resistance inside the cluster (cluster model).

7.3 Interpretation of the conversion data with the two-phase model

For bubbling beds, it is generally accepted that the bubble-to-emulsion mass transfer resistance is often dominating (van Deemter, 1961; van Swaaij and co-workers 1972, 1973, 1978; Werther, 1980). Conversion rates can then be successfully interpreted in terms of the two-phase model, represented by equations 2 and 3. The use of the two-phase model for the high-velocity fluidization regime is disputable, as the bed seems to become more homogeneous. From our CO conversion results, values for the apparent number of mass transfer units N_α (and for the corresponding height of the mass transfer unit H_α) can be calculated while applying equation 4. This value of H_α is plotted versus the reaction rate constant based on the dense phase volume $k_r=k_p\beta/(1+n_d)$. Figure 12 shows the conversion results from the present work interpreted by the two-phase model as distinct data points.

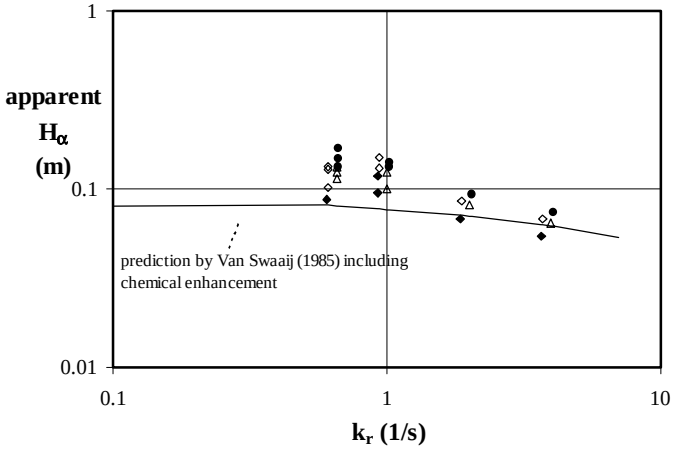

Figure 12. The apparent height of a transfer unit $H_\alpha=u_g/\alpha$ as observed for the CO-oxidation. Legends: Δ u_g=0.2 m/s, ● u_g =0.4 m/s, ◊ 0.6 m/s and ♦ u_g =0.7 m/s. Indicated as a solid line is the H_α (H=0.20 m) proposed by Van Swaaij (1985) including chemical enhancement (equation 11). Conditions in the two-phase model: ε_b=0.1, N_α=2.5, $D_{eff}=6\cdot10^{-5}$ m^2/s, u_g=0.2 m/s and H=0.2 m.

In this interpretation, it is assumed that the dense-phase mixing can be neglected ($N_{ax}=\infty$). The bed height (H=0.20 m) has been determined from the initial bed mass, and the observed average solids concentration of the dense region, recorded by the pressure drop.
From the data points in figure 12, it can be concluded that the value of H_α is not affected by the gas velocity, which is in line with the observation for bubbling beds. According to the two-phase model, the observed H_α should also be independent on the reaction rate constant k_r. Based on ozone conversion experiments in a 0.05 m diameter fluid bed of porous silica, Van Swaaij (1985) arrives at a value of H_α=0.08 m, after interpretation with his 'simple' two-phase model. This value gives a reasonable approximation for the N_α-value derived from the present CO oxidation experiments for the range of the low k_r-values. However, for higher k_r-values (k_r>1 s^{-1}), the resistance for mass transfer appears to decrease, and α (the apparent mass exchange coefficient between bubbles and dense phase) increases.
Explanations for this observation are presented earlier in this chapter: chemical enhancement is proposed as the most likely explanation and it can be accounted for by applying equation 11 (Werther, 1978):

$$\xi = 1-\frac{c_{out}}{c_{in}} = 1-\exp\left(-\frac{\left(\phi^{-1}-1\right)\mathrm{Ha}+\tanh(\mathrm{Ha})}{\left(\phi^{-1}-1\right)\mathrm{Ha}\cdot\tanh(\mathrm{Ha})+1}\mathrm{HaN}_\alpha\right) \qquad (11)$$

with $Ha = \frac{\sqrt{k_r D_{eff}}}{k_m}$, $k_m = \frac{3.44 \cdot 10^{-4}}{\chi}\sqrt{1+27.2(u-u_{mf})}$, χ=0.055 (porous particles)

and $N_r = \frac{k_r(1-\varepsilon_b)H}{u_g}$ with ε_b as the bubble gas hold-up

where k_r represent the reaction rate based on the dense phase, k_m the mass transfer coefficient and ϕ the ratio of the film volume over the dense phase volume.
Equation 11 allows us to recalculate the belonging conversion degree as a function of the reactivity, while accounting for the effect of chemical enhancement. It is now interesting to see what the relation between H_α and k_r would have been without accounting for chemical enhancement. The derived ozone conversions of Van Swaaij (1985) are then interpreted in the same way as the current CO conversions, viz. on basis of equation 4. This leads to the solid line in figure 12, which indeed shows the same trend as the data point series. At higher k_r-values, the apparent H_α decreases, implying a reduced resistance for bubble-to-dense phase mass transfer. The experimental data points follow the trends of Van Swaaij's prediction quite well.

If, on forehand, the value for H_α is assumed to be 0.08 m, a value for N_r can be derived from equation 11 on basis of the CO conversions observed in the present work. It is now interesting to compare the N_r-values derived from equation 11 with those predicted by the Ranz-Marshall equation (1952). The agreement illustrated in the parity plot of figure 13 confirms that the intrinsic CO-oxidation rate is largely determined by the external gas-to-particle mass transfer rate.

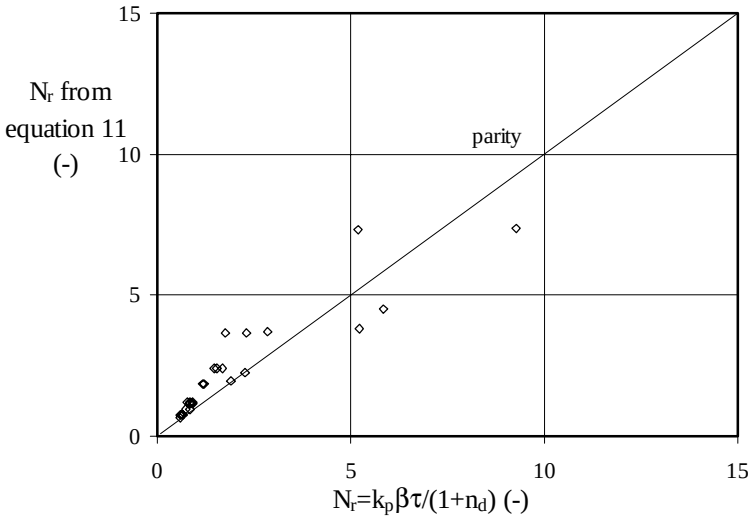

Figure 13. The reaction number N_r derived from equation 11 plotted versus N_r calculated from $N_r=k_p\beta\tau/(1+n_d)$ with $k_p=k_g a$ and k_g derived from the Ranz-Marshall equation. Conditions in the two-phase model: ε_b=0.1, N_α=2.5, D_{eff}=6·10^{-5} m^2/s, and H=0.2.

It was stated earlier in this chapter that the use of the two-phase model at high superficial gas velocities is questionable because distinct bubbles are absent. The bed structure shows then features of both the bubbling bed and the riser or fast fluid bed. In chapter 4 and appendix III of this thesis, the conversion data of a riser reactor could be related to the existence of particle clusters. In fact, interpretation in terms of chemical enhancement in the two-phase model, or in terms of particle clusters, are just two considerations of the same phenomenon. The bubble-to-dense phase mass transfer resistance can then be represented by the resistance located in the boundary layer around the cluster, and the

chemical enhancement by diffusion and reaction inside the cluster. To compare the current data with the conversion data in a riser (chapter 4), they will now be analyzed by applying the cluster model.

7.4 Interpretation of the conversion data in the cluster model

Just like in the extreme case of a riser regime, it is more likely that in the turbulent bed regime, specially at the higher gas velocities, the particulate phase is structured in clusters, which are frequently formed and disintegrated. The additional mass transfer resistances in this cluster concept are then located at both sides of the interface between bulk gas and cluster, that is by diffusion through the boundary layer around the cluster, and diffusion inside the particle cluster. This cluster is just a modelling concept to characterize the heterogeneity in the fluid bed: the flow structure is more complex and it might be difficult to find any well-defined hydrodynamic entities that resemble the model cluster.
The effective cluster size is then an important parameter in evaluating the contact-efficiency loss (see also chapter 2 and 4). In the model, it is assumed that the active material is homogeneously distributed over a spherical cluster volume, while all clusters have the same size and density. The clusters are further supposed to be distributed evenly over the reactor volume. As they are transient entities, it is further assumed that the life time of the particle cluster is large compared to the characteristic time for the intrinsic reaction and/or the diffusion rates. The relevant equations required for the determination of the apparent cluster size are given below:

$$k_{ov} = \left(\frac{1}{\eta_{cl}^{*}} + \frac{3\phi_{cl}^{2}}{Bi_{cl}} \right)\left(\frac{1}{\eta_{p}^{*}} + \frac{3\phi_{p}^{2}}{Bi_{p}} \right) k_{p} = \eta_{cl}\eta_{p}k_{p} \qquad (12a)$$

k_{ov} represents the experimentally observed reaction rate constant, derived by equation 9, and η_p and η_{cl} are defined by:

$$\frac{1}{\eta_{p}} = \frac{1}{\eta_{p}^{*}} + \frac{3\phi_{p}^{2}}{Bi_{p}} \qquad \frac{1}{\eta_{cl}} = \frac{1}{\eta_{cl}^{*}} + \frac{3\phi_{cl}^{2}}{Bi_{cl}} \qquad (12b)$$

in which:

$$\phi_{p} = \frac{d_{p}}{6}\sqrt{\frac{k_{p}}{D_{p}}}, \quad Bi_{p} = \frac{k_{g}d_{p}}{2D_{p}} \text{ and } \eta_{p}^{*} = \frac{1}{3\phi_{p}^{2}}\left(\frac{3\phi_{p} - \tanh(3\phi_{p})}{\tanh(3\phi_{p})} \right) \qquad (12c)$$

$$\phi_{cl} = \frac{d_{cl}}{6}\sqrt{\frac{k_{cl}}{D_{cl}}}, \quad Bi_{cl} = \frac{k_{g,cl}d_{cl}}{2D_{cl}} \text{ and } \eta_{cl}^{*} = \frac{1}{3\phi_{cl}^{2}}\left(\frac{3\phi_{cl} - \tanh(3\phi_{cl})}{\tanh(3\phi_{cl})} \right)$$

$$\text{and } k_{cl} = k_{p}\eta_{p}\frac{\beta_{cl}}{(1+n_{d})}$$

In table II, relations and constants used in the cluster model are summarized.

Table II. Relations and constants used in particle and cluster model. All parameters are calculated for the oxidation of carbon monoxide as the model reaction.

Parameter	expression
bulk diffusion coefficients Fuller *et al.* (1966)	$D = 3.16\cdot 10^{-8}\dfrac{T^{1.75}}{P\left(\nu_{CO}^{1/3}+\nu_{air}^{1/3}\right)^2}\left(\dfrac{1}{M_{CO}}+\dfrac{1}{M_{air}}\right)^{1/2}$
Knudsen diffusion coefficient	$D_{Knudsen} = 97\cdot r_{pore}\left(\dfrac{T}{M_{CO}}\right)^{1/2};\ r_{pore} = 2\cdot 10^{-8}\,m$
particle diffusion coefficient	$D_p = \dfrac{D_{Knudsen}\varepsilon_p}{\tau_p};\ \varepsilon_p = 0.54;\ \tau_p = \sqrt{2}$
cluster diffusion coefficient	$D_{cl} = \dfrac{D(1-\beta_{cl})}{\tau_{cl}};\ \tau_{cl} = \sqrt{2}$
particle mass transfer coefficient	$k_g = \dfrac{Sh_p D}{d_p};\ d_p = 65\mu m;\ Sh_p = 2$
cluster mass transfer coefficient	$k_{g,cl} = \dfrac{Sh_{cl} D}{d_{cl}};\ Sh_{cl} = 2 + 0.6\left(\dfrac{\rho_g d_{cl} u_g}{\eta_g}\right)^{1/2}\left(\dfrac{\eta_g}{\rho_g D}\right)^{1/3}$

On basis of the experimental data derived for n_d=5050 and n_d=10015, the cluster diameter, d_{cl}, has been calculated, assuming that the cluster solids concentration β_{cl}=0.6. The result is presented in figure 14.

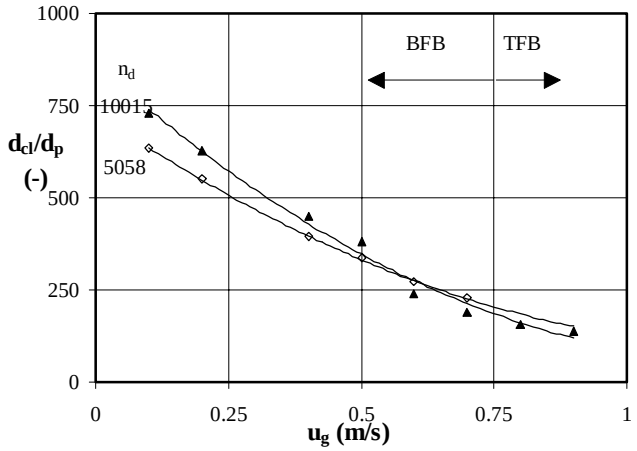

Figure 13. The ratio of the cluster-over-particle diameter d_{cl}/d_p for the fluid bed CO oxidation results as a function of the fluidization velocity u_g. Legends: ◊ n_d=5058; ▲ n_d=10015. The solids lines indicate the trends.

At the lower gas velocities, the effective cluster-over-particle diameter d_{cl}/d_p decreases almost linearly with the gas velocity, but it levels of at gas velocities u_g>0.7 m/s, that is close to turbulent fluid bed conditions. The effective cluster size varies from 750 to 150 times d_p for gas velocities ranging from 0.1 to 0.9 m/s. The decrease of the cluster size is exactly what is supposed by Van Deemter (1961): “as the gas velocity is increased, clusters are more easily disintegrated, have a shorter lifetime and become smaller”. Theoretically, the cluster diameter should be independent on the local conversion rate, and this is shown in figure 14. Although the curves for n_d=5058 and n_d=10015 slightly deviate at the lower gas velocities (possibly also influenced by experimental errors), at gas velocities larger than 0.4 m/s both

curves indeed coincide. The absolute values for the cluster size ranges from one to four centimetres, which is relatively large compared to a reactor diameter of D_r=0.05 m. However, it should be noted that the trends in this figure show *apparent* sizes, assuming spherical shaped clusters. Incorporating the non-sphericity will lead to smaller clusters. Besides, the non-sphericity most probably influences the gas-to-cluster mass transfer coefficient as well (see also appendix III of this thesis). In the latter appendix, much lower d_{cl}/d_p-values (<100) were evaluated from conversion experiments in a small riser ($2.5<u_g<4.5$ m/s). This indicates that gas-solids contacting in risers is better than in this lower gas velocity range.

7.5 Summary of the interpretation methods

The question arises what kind of interpretation is the most suitable one for such high-velocity fluid beds. Obviously, axial dispersion models can not explain the reduced conversion in turbulent beds. The influence of axial dispersion in this type of reactor appears to be unimportant compared to the effect of mass transfer resistances. In fact, axial dispersion models can not predict (experimentally observed) conversions lower than the extreme case of an ideally mixed tank reactor.
While interpreting our mass transfer data in terms of the effective Sherwood number (figure 9), one should realize that the calculated Sherwood numbers are merely overall values. In these Sherwood numbers, all additional resistances (like the bubble-to-dense phase, the gas-to-cluster mass transfer resistance and the diffusional resistance inside the cluster) are lumped. They do not represent the actual mass transfer rate on the scale of the individual particle.
Conversion results presented as the contact efficiency versus the reaction number (figures 10 to 11) offer the advantage of a possible comparison with other (and not necessarily mass transfer controlled) reaction systems. In the introduction of this thesis, it has been shown that from the efficiency curve one can not distinguish whether any diffusional resistances or reactant mixing effects are important to explain the conversion loss.
The interpretation by the two-phase model (figure 12 and 13) is useful for bubbling beds, and for high-velocity beds in first approach. However, at the higher gas velocities, the bubble model has not really a relation to the nature of the bed anymore, as clear bubbles are absent. The decrease in H_α at higher reaction rate numbers can be explained by chemical enhancement, which is already incorporated in the cluster model.
For the higher gas velocities, the presence of clusters corresponds more closely to the real structure of the turbulent bed as the bed then reflects the structure of a riser or fast fluid bed. Although both methods represent just two different approaches of the same phenomenon, chemical enhancement of mass transfer in the two-phase model is already incorporated in the cluster model. The calculated values for the effective cluster size are quite large, but not that unrealistic (figure 14). Considering the simplicity of the cluster model (for example, all clusters have the same density and size and are spherical shaped), this approach seems to be promising in describing such a high velocity fluid bed. Comparison with effective cluster sizes in risers indicated that gas-solids contacting is better in riser systems, but even then certainly not ideal.

8 CONCLUSIONS

In a fluidized bed (ID 0.05 m), operated at high velocities (but below the transport velocity; $0.1<u_g<1$ m/s), the largely mass transfer controlled oxidation experiments of CO over a Pt/γ-alumina were applied to investigate the gas-solids contacting. Similar to observations reported in previous chapters, the mass transfer controlled reaction rates could be verified by a low value for the apparent activation energy and the order in the reactant concentrations.

The conversion results are interpreted in four ways: i) as overall mass transfer coefficients in the well-known Sherwood versus Reynolds diagram to allow a comparison with published mass transfer data for other gas-solids reactors, ii) in a plot of the contact efficiency versus the reaction number to compare them with results published for other reactive systems, iii) on basis of the conventional two-phase model, and finally iv) in a cluster model. The following conclusions can be listed:

- The derived Sherwood numbers ($0.2<Sh<1.3$) are merely overall values, in which the bubble-to-dense phase or the gas-to-cluster mass transfer resistance are lumped. They do not represent the mass transfer rate on the scale of the individual particles, and depend on the dilution ratio.
- The contact-efficiency depends strongly on the local reaction rate. This conclusion could be derived also from the kinetically controlled conversion experiments of other investigators.
- Interpretation of the results by the two-phase model shows that the height of a mass transfer unit decreases significantly with increasing local reaction rate beyond $k_r>1\ s^{-1}$. Various authors explained this phenomenon by chemical enhancement in the boundary layer, or an increased solids concentration in the bubble. The latter is likely to occur at the relatively high fluidization velocities applied, say $u_g>u_c$. At these gas velocities, the use of the two-phase model for the interpretation of the present results can be useful, although there are no well-defined bubbles in the bed anymore.
- The cluster model shows that the effective cluster-over-particle diameter d_{cl}/d_p decreases almost linearly with the gas velocity. The values range from 750 to 200 times d_p for gas velocities from 0.1 up to 0.9 m/s. They are quite large, but not unrealistic. Considering the simplicity of the cluster model (for example, all clusters have the same density and size and are spherical shaped), it seems a useful approach to describe such a high velocity fluid bed.

Just like in the case of a riser regime, it is likely that at the higher gas velocities (that is in the turbulent bed $u_g>u_c$), the particulate phase is structured in clusters, which are frequently formed and disintegrated. The concept of particle clusters shows to be promising. The additional mass transfer resistances are then located at both sides of the interface between the bulk gas and the cluster, that is a diffusional resistance through the boundary layer around the cluster, and inside the particle cluster. For the time being, the calculated values for the effective cluster size are quite large, amongst other factors because the proposed simplified model yet lacks parameters like the non-sphericity of the cluster.

ACKNOWLEDGEMENT

We acknowledge the financial support of the Dutch Ministry of Economic Affairs through the Netherlands Energy Research Foundation ECN. We also thank R. de Wit and E. Middelink for their assistance in the experimental work. We are also obliged to Prof. J.R. Grace and Prof. J. Chaouki for providing us their experimental data.

NOTATION

A	the cross-sectional area of the reactor	m^2
a	decay constant	m^{-1}
a	specific surface particle	m^{-1}
Ar	Archimedes number $d_p^3\rho_g(\rho_p-\rho_g)g/\mu_g^2$	-
Bi_{cl}	Biot number cluster $k_{g,cl}d_{cl}/(2D_{cl})$	-
Bi_p	Biot number particle $k_g d_p/(2D_p)$	-
c	reactant concentration	mole m^{-3}
c_1	reactant concentration bubble phase, equations 2 and 3	mole m^{-3}

c_2	reactant concentration dense phase, equations 2 and 3	mole m^{-3}
c_{in}	reactant concentration inlet	mole m^{-3}
c_L	reactant concentration at position L	mole m^{-3}
c_{O2}	oxygen concentration	mole m^{-3}
c_{out}	reactant concentration outlet	mole m^{-3}
D	molecular diffusion coefficient	$m^2 s^{-1}$
D_{ax}	axial dispersion coefficient	$m^2 s^{-1}$
D_{bm}	back-mixing coefficient	$m^2 s^{-1}$
d_{cl}	effective cluster diameter	m
D_{cl}	effective diffusion coefficient inside the particle cluster	$m^2 s^{-1}$
D_{eff}	effective diffusion coefficient in the dense phase	$m^2 s^{-1}$
$D_{Knudsen}$	Knudsen diffusion coefficient	$m^2 s^{-1}$
ΔL	length of the reactor	m
d_p	average particle diameter	m
D_p	effective diffusion coefficient inside the particle	$m^2 s^{-1}$
D_r	reactor diameter	m
E_a	activation energy	J $mole^{-1}$
H	expanded bed height	m
H_α	height of a mass transfer unit u_g/α	-
Ha	Hatta number, equation 11	-
k_{cl}	reaction rate constant per unit volume of cluster	s^{-1}
k_g	mass transfer coefficient	m s^{-1}
$k_{g,cl}$	gas-to-cluster mass transfer coefficient	m s^{-1}
k_m	bubble-to-dense phase mass transfer coefficient	m s^{-1}
k_{ov}	measured reaction rate based on catalyst volume	s^{-1}
k_p	reaction rate constant based on catalyst volume	s^{-1}
k_r	reaction rate constant based on dense phase volume	s^{-1}
n	power in Richardson-Zaki equation (see chapter 5)	-
N_α	reaction number $\alpha H/u_g$	-
N_{ax}	axial dispersion number $u_g H/(\varepsilon D_{ax})$	-
N_{bm}	back-mixing number $u_g H/(\varepsilon D_{bm})$	-
n_d	dilution ratio	-
N_r	reaction number $k_p \beta H/((1+n_d)u_g)$	-
P	pressure	Pa
R	gas constant	J $mole^{-1}K^{-1}$
R(c)	reaction rate	mole m^{-3} s^{-1}
Re	Reynolds number $\rho_g u_g d_p/\eta_g$	-
r_{pore}	radius of catalyst pore	m
Sc	Schmidt number $\eta_g/(\rho_g D)$	-
Sh^0	experimentally observed Sherwood number	-
T	operating temperature	K
u_g	superficial gas velocity	m s^{-1}
u_c	transition velocity for the onset of turbulent fluidization	m s^{-1}
u_{mf}	minimum fluidization velocity	m s^{-1}
u_t	terminal falling velocity individual particle	m s^{-1}
u_t^*	terminal velocity for cluster of particles (chapter 5)	m s^{-1}
u_{tr}	transport velocity of the particles	m s^{-1}
x	non-dimensional axial coordinate z/H	-
y_{in}	inlet fraction carbon monoxide	vol.%
y_{O2}	inlet fraction oxygen	vol.%
z	axial position	m
α	mass exchange coefficient	s^{-1}

β	solids concentration	-
β_{cl}	solids concentration in a cluster	-
χ	constant in equation 11	-
ε	porosity = (1-β)	-
ε_p	particle porosity	-
ϕ	ratio of the film volume over the dense phase volume	-
ϕ_{cl}	Thiele modulus of a spherical cluster	-
ϕ_p	particle Thiele modulus	-
γ	fraction of gas injected in the bubble phase, equation 5	-
η	contact efficiency defined by equation 1	-
η_{cl}	cluster effectiveness factor on basis of bulk conditions	-
η_{cl}^*	cluster effectiveness factor	-
η_g	gas viscosity	Pa s
η_p	particle effectivity on basis of bulk conditions	-
η_p^*	particle effectiveness factor	-
ν_i	diffusional volume of component i	$m^3 mole^{-1}$
λ	defined by equation 6	-
ρ_g	gas density	kg m^{-3}
ρ_p	particle density	kg m^{-3}
τ	contact time	s
τ_{cl}	cluster phase tortuosity	-
τ_p	particle tortuosity	-
ξ	conversion	-

REFERENCES

Avidan A., 1982, Turbulent fluid bed reactors using fine catalysts, CIESC-AIChE meeting, proceeding joint meeting of Chemical Engineering, Beijing, sept 19-22, 411

Avidan A., Edwards M., 1986, Modeling and scale up of Mobil's fluid-bed MTG process, in *Fluidization V*, edited by Østergaard K. and SØrensen A., Engineering Foundation, New York, 457

Avidan A., Yerushalmi J., 1985, Solids mixing in an expanded top fluid bed, *A.I.Ch.E.J.*, **31**, 835

Bi H.T., Grace J.R., 1995, Effect of measurement method on the velocities used to demarcate the onset of turbulent fluidization, *Chem. Engng. J.*, **57**, 261

Bohle W., van Swaaij W.P.M., 1978, The influence of gas absorption on mass transfer and gas mixing in a fluidized bed, in *Fluidization II*, edited by Davidson J.F. and Keairns D.L., Cambridge University Press, Cambridge, 167

Cai P., Chen S.P., Jin Y., Yu Z.Q., Wang Z.W., 1989, Effect of operating temperature and pressure on the transition from bubbling to turbulent fluidization, *A.I.Ch.E. Symp.Ser.*, **270**, 37

Cankurt N.T., Yerushalmi J., 1978, Gas Back-mixing in high velocity fluidized beds, in *Fluidization II*, edited by Davidson J.F. and Keairns D.L., Cambridge University Press, Cambridge, 387

Chehbouni A., Chaouki J., Guy C., Klvana D., 1994, Characterization of the flow transition between bubbling and turbulent fluidization, *Ind. Engng. Chem. Res.*, **33**, 1889

De Vries R.J., Van Swaaij W.P.M., Mantovani C., Heijkoop A., 1972, Design criteria and performance of the commercial reactor for the Shell chlorine process, in *Chemical reaction engineering*, Amsterdam, B 9-59

Dry R.J., White C.C., 1992, Gas-solids contact in a circulating fluidised bed: the effect of particle size, *Powder Technol.*, **70**, 277

Foka M., Chaouki J., Guy C., Klvana D., 1994, Natural gas combustion in a catalytic turbulent fluidized bed, *Chem. Engng. Sci.*, **49**, 4269

Foka M., Chaouki J., Guy C., Klvana D., 1996, Gas phase hydrodynamics of a gas-solid turbulent fluidized bed reactor, *Chem. Engng. Sci.*, **51**, 713

Foka M., Chaouki J., Guy C., Klvana D., 1997, personal communications

Fuller E.N., Schettler P.D., Giddings J.C., 1966, A new method for predicting of binary gas phase diffusion coefficients, *Ind. Engng. Chem.*, **58**, 18

Gilliland E.R., Mason E.A., 1949, Gas and solid mixing in fluidized beds, *Ind.Engng.Chem.*, **41**, 1191

Gilliland E.R., Mason E.A., 1952, Gas mixing in beds of fluidized solids, *Engng.Process Dev.*, **44**, 218

Grace J.R., Sun G., 1990, Fines concentrations in voids in fluidized beds, *Powder Technol.*, **62**, 203

Grace J.R., Sun G., 1991, Influence of particle size distribution on the performance of fluidized bed reactors, *Can. J. Chem. Engng.*, **69**, 1126

Guo F., 1987, Gas flow and mixing behavior in fine-powder fluidized bed, *A.I.Ch.E.J.*, **33**, 1895

Krambeck F.J., Avidan A.A., Lee C.K., Lo M.N., 1987, Predicting fluid-bed reactor efficiency using adsorbing gas tracers, *A.I.Ch.E.J.*, **33**, 1727

Kumar H.B., Sublette K.L., Shah Y.T., 1993, Effect of high voidage on mass transfer in a fluidized bed, *Chem.Engng.Commun.*, **121**, 157

Kunii D., Suzuki M., 1967, Particle-to-fluid heat and mass transfer in packed beds of fine particles, *Int. J. Heat Mass Trans.*, **10**, 845

Lee G.S., Kim S.D., Park W.H., 1988, Gas mixing characteristics in turbulent fluidized beds, in *Proceedings of the Asian conference on fluidized bed & three phase reactors*, edited by Yoshida K. and Morooka S., 68

Lewis W.K., Gilliland E.R., Glass W., 1959, Solid-catalyzed reaction in a fluidized bed, *A.I.Ch.E.J.*, **5**, 419

Li J., Weinstein H., 1989, An experimental comparison of gas back-mixing in fluidized beds across the regime spectrum, *Chem.Engng.Sci.*, **44**, 1697

Li Y., Wu P., 1991, A study on axial gas mixing in fast fluidized bed, in *Circulating Fluidized Bed Technology III*, edited by Basu P, Horio M. and Hasatani M., Pergamom Press, Oxford, 581

May W.G., 1959, Fluidized-bed reactor studies, *Chem.Engng.Prog.*, **55**, 49

Mori S., Hashimoto O., Haruto T., Yamada I., Kuwa M., Saito Y., 1989, Fundamentals of turbulent fluidized catalytic reactor, in *Fluidization VI*, edited by Grace J.R., Shemilt L.W. and Bergougnou M.A., Engineering Foundation, New York, 49

Ranz W.E., Marshall Jr. W.R., 1952a, Evaporation from drop: part I, *Chem. Eng. Prog.*, **48**, 141

Ranz W.E., Marshall Jr. W.R., 1952b, Evaporation from drop: part II, *Chem. Eng. Prog.*, **48**, 173

Sun G., Grace J.R., 1990, The effect of particle size distribution on the performance of a catalytic fluidized bed reactor, *Chem. Engng. Sci.*, **45**, 2187

Sun G., Grace J.R., 1992, Effect of particle size distribution in different fluidization regimes, *A.I.Ch.E.J.*, **38**, 716

Sun G., Grace J.R., 1997, personal communications

Van Deemter J.J., 1961, Mixing and contacting in gas-solid fluidized beds, *Chem.Engng.Sci.*, **13**, 143

Van Deemter J.J., 1967, The counter-current flow model of a gas-solids fluidized bed, in *Fluidization*, edited by Drinkenburg A.A.H., Netherlands University Press, Amsterdam, 334

Van Deemter J.J., 1980, Mixing patterns in large-scale fluidized beds, in *Fluidization*, edited by Grace J.R. and Matsen J.M., Plenum Press, New York, 69

Van der Ham A.G.J., Prins W., Van Swaaij W.P.M., 1994, Regenerative, high temperature desulfurization of coal gas in a circulating fluidized bed, in *Circulating Fluidized Bed Technology IV*, Pennsylvania, Engineering Foundation, 657

Van Swaaij W.P.M., Zuiderweg F.J., 1972, Investigation of ozone decomposition in fluidized beds on the basis of a two-phase model, in *Chemical reaction engineering*, Amsterdam, B 9-25

Van Swaaij W.P.M., Zuiderweg F.J., 1973, The design of gas-solids fluidized beds- prediction of chemical conversion, in *Fluidization and its applications*, edited by Angelino H., Couderc J.P., Gibert H. and Laguerie C., Cepadues editions, Toulouse, 454

Van Swaaij, 1978, The design of gas-solids fluid bed and related reactors, *ACS Symp. Ser.*, **72**, 193

Van Swaaij W.P.M., 1985, Chemical reactors, *Fluidization*, chapter 18, Academic Press, London, 595

Werther J., 1980, Modeling and scale-up of industrial fluidized bed reactors, *Chem. Engng. Sci.*, **35**, 372

Westerterp K.R., van Swaaij W.P.M., Beenackers A.A.C.M., 1987, *Chemical reactor design and operation*, John Wiley & Sons, New York

CHAPTER 7

HIGH TEMPERATURE H_2S REMOVAL WITH AN IRON/MOLYBDENUM-OXIDE SORBENT IN A HIGH VELOCITY FLUIDIZED BED

ABSTRACT

Regenerative, high-temperature process coal gas desulfurization with an iron / molybdenum-oxide sorbent material has been investigated by experiments in a batch-wise operated high-velocity dense fluid bed at ambient pressures. During the desulfurization, as well as during the oxidation step, gas velocities up to 1.3 m/s were applied, which implies operation in the bubbling and the turbulent fluidized bed regime.
For the regeneration of the sorbent, (diluted) air was used. In the present work, the effect of the oxygen concentration on the sulfur removal efficiency in the subsequent sulfidation cycle was studied, as well as the formation of sulfates during this oxidation step.

The results are promising, showing that the capacity of the sorbent is independent on the oxygen concentration applied during the preceding oxidation step. An additional reduction between the desulfurization and the oxidation step hardly improves the desulfurization efficiency. It indicates that the formation of sulfates during the oxidation reaction can be neglected. The results further show that the sorbent's mechanical strength is high, while no loss in reactivity towards the H_2S-sorption is observed. The absorption capacity of the selected material appears to be more than 85% of the theoretical maximum. Sulfidation results show that up to a fractional sorbent conversion of X=0.25, the sulfidation reaction rates are so high that (external) mass transfer resistances are dominant. Notwithstanding the short contact-times applied, sulfur removal efficiencies with fresh sorbent material (X<0.25) were over 99 %. Nevertheless, the derived mass transfer coefficients are much lower than expected on basis of ideal gas-solids contacting, reflecting the presence of additional resistances other than the gas-to-particle one. This could be clearly demonstrated by re-interpreting the conversion data in a two-phase model with enhancement.

1 INTRODUCTION

Integrated gasification combined cycle (IGCC) power plants have been the subject of considerable research over the past decades throughout the whole world (a.o. Schrodt, 1980; Sugitani *et al.*, 1987; Kobayashi, 1990; Gangwal, 1991; Ayala *et al.*, 1995). In the second half of the eighties, it was decided in the Netherlands to investigate the option of power production according to the concept of integrated gasification combined cycle (IGCC) more intensely. In 1989, the SEP built a IGCC demonstration plant of 250 MW(el) at Buggenum (the Netherlands), which was completed in November 1993. Several runs on a mixture of coal gas and natural gas were realized in early 1994, and integration tests are still going on. A system study, initiated by the Netherlands Agency for Energy and the Environment (NOVEM, 1990) concluded that the application of a dry cleaning process at a high temperature level (> 623 K) will improve the overall efficiency of the IGCC plant significantly, compared to an installation with conventional wet gas cleaning. One of the major process steps involved in such a dry gas cleaning is the high temperature desulfurization, i.e. the removal of H_2S and COS from the hot coal gas. At these high temperatures liquid sorbents can not be applied as they will evaporate; solid sorbents should

be used instead. Obviously, a good match between sorbent and reactor is required. The choice of reactor configuration strongly depends on the characteristics of the preferred absorbent: a few reactor types have been investigated for desulfurization purposes (packed bed, moving bed, bubbling fluidized bed, and the riser of a fast fluidized bed set-up), mostly on laboratory- or demonstration-scale only. Recently, Venderbosch *et al.* (1997) presented a review on the effect of various parameters on desulfurization efficiency. In the present work three criteria, reactor choice, sorbent design and regeneration method are integrated. A promising reactor for coal gas desulfurization will be discussed in the subsequent section, and a favourable sorbent with respect to thermodynamics, mechanical strength and regenerability, will be proposed. Finally, experimental work with the proposed sorbent will be presented.

2 REACTOR SELECTION FOR DESULFURIZATION OF COAL GAS

Generally, it is more and more accepted that a *continuous* desulfurization operation is required for the desulfurization process (see e.g. Van der Ham, 1994). In such a continuous operation solids transport from absorber to regenerator is required, leading to fluid bed contactors as attractive reactors. Fluid bed technology is well known and widespread throughout the industry; it is applied especially when large heat effects are involved in the process. Upon selection of an optimal desulfurization reactor in combination with a favourable sorbent, one should be aware of all chemical, physical but also the hydrodynamical aspects possibly influencing the rate of the H_2S sorption. The following successive steps may be identified:

1. diffusion of H_2S from the bulk of the gas to the external particle surface,
2. diffusion of H_2S through the pores of the sorbent and through the product layer formed around the unreacted core of the sorbent material,
3. the intrinsic rate of the reaction between H_2S and the solid reactant,
4. back-diffusion of the product gas out of the solid particle
5. back-diffusion of products from the particle to the bulk of the gas.

The chemical reaction rate (step 3) and the internal diffusion processes (steps 2 and 4) depend on the composition and structure of the sorbent material (and consequently on the applied preparation method), while the gas-to-particle, external mass transfer resistances (steps 1 and 5) are mainly dictated by the properties of the gas and the particles, the reactor and particle geometry and the applied operation conditions.

A major drawback of bubbling fluid bed operation is the inevitable by-passing of (reactant) gas through rising bubbles. Although no pertinent conversion data are available for high-velocity fluid beds (the turbulent fluid bed or the riser of a circulating fluid bed), the general idea in the literature is that in this regime severe gas by-passing may be avoided. This is attractive only if attrition-resistant and very reactive sorbent particles can be applied (Krambeck *et al.*, 1987). An additional advantage of such a high-velocity fluid bed reactor is its smaller reactor diameter, which is important for high-pressure application.

Examples of these high-velocity fluid beds are the turbulent fluid bed and the riser of a circulating fluid bed set-up. In an earlier thesis, the desulfurization reaction was investigated in the riser of a small-scale circulating fluid bed set-up using an iron-oxide on carrier sorbent material (Van der Ham, 1994). Problems were, amongst others, sulfate formation during regeneration. In the present work, the absorption reaction of H_2S on the ECN's iron-oxide/molybdenum sorbent (operated at temperature in between 625 and 725 K) is conducted in a small-scale TFB set-up. This ECN sorbent is expected to show a better regeneration performance. In the following section this reactor type will be discussed in more details.

3 HIGH VELOCITY FLUIDIZED BED OPERATION

As stated before, in a bubbling fluidized bed, large bubbles can exist, which will result in an additional resistance to mass transfer and by-passing of reactant gas. The size of the bubbles can be reduced by applying Geldart's type A powders (Kunii and Levenspiel, 1991). Another method to reduce the bubble effects could be to increase the gas velocity. At velocities beyond the transition point of the turbulent fluid bed, the surface of the bed becomes diffuse, and a turbulent motion of solids clusters and gas voids of various sizes and shapes is observed. Due to this formation of clusters, these fine powders can be processed at much higher superficial gas velocities than one should expect on basis of their terminal falling velocity (for example, 100 μm diameter FCC particles with a terminal falling velocity of about 0.2 m/s can be relatively easily processed at gas velocities up to 1 m/s; the so-called fast fluid bed regime starts at approximately u_g=2 m/s). The above described regime is nowadays referred to as the turbulent fluidized bed regime, in which relatively small amounts of solids are entrained over the top of the column, while there is still a dense bed retained in the bottom part. For steady state operation, the entrained particles have to be collected by cyclones, and returned to the bed. The (local) solids hold-up is a function of the gas velocity only.
Despite its widespread application on a commercial scale (f.i. many of the regenerators in modern cat cracking units primarily operate in this regime), the advantages over conventional fluidized bed reactors are still not always recognized. The most significant ones may be the higher gas throughput and the shorter and more uniform gas phase residence time

These advantages could be of major importance, if desulfurization of coal gas at high pressures is considered. A higher gas throughput leads to smaller reactor diameters at the high pressures applied, and consequently to lower capital cost. Higher bulk-to-gas mass transfer rates implies higher sulfur removal efficiencies (one should consider that the conversion rates for the sulfidation of the fresh iron-supported sorbent probably will be controlled by mass transfer resistances).

In the last decades, the velocity at which the turbulent fluidization regime begins, has been a source of considerable discussion, see also chapter 5 of this thesis. Operating in the turbulent fluidization regime however, requires two additional conditions to be fulfilled for the reactor and catalyst design. Due to the increase in particle entrainment compared to bubbling fluid beds, the design of the cyclone section must be adopted to return these particles to the reactor bed and the applied catalyst particles should be attrition resistant.
During the last decades, screening of a suitable sorbent for application in a coal gas desulfurization process is subject of extensive research, as will be discussed in the next paragraph.

4 SORBENT CHOICE

Pioneering work on high-temperature desulfurization was mainly concerned with sorbent development and characterization (reactivity, capacity, deactivation) in small and simple, cyclic operated packed bed reactors. Extensive reviews of interesting sorbents are given by Westmoreland and Harrison (1976), Heesink (1994), and Van der Ham *et al.* (1994, 1997). Generally, desulfurization sorbents are divided into the group of expensive, synthetic sorbents having a long life-time, and the one of cheap, natural sorbents. In the preparation of synthetic sorbents, Westmoreland screened 28 metals (primary present as oxides) of which eleven candidates were selected based on their thermodynamic properties. In the temperature range of 625 to 725 K 8 metals remained (Co, Cu, Fe, Mn, Mo, V, W and Zn). At the beginning of the research activities for the desulfurization process and the sorbent development, relatively high operation temperatures (> 850 K) were preferred to maximize the increase in overall thermal efficiency of the IGCC process. For the iron-oxide sorbentia,

such a high temperature level was unfavourable due to their thermodynamic properties, because the desulfurization equilibrium is then shifted to the reactant side (Van der Wal, 1987; Jain *et al.*, 1991). The H_2S equilibrium concentration over iron oxide rises rapidly at temperatures above 800 K, at which the possible removal degree becomes too low. Therefore, other sorbents, especially those based on zinc, were considered as good candidates in the early 1980's. Extensive research led to the development of zinc ferrite, $ZnFe_2O_4$ (Jain *et al.*, 1991), zinc titanate, $ZnTiO_2$ (Mojtahedi and Abbasian, 1995), a combination of molybdenum oxide (MoO_3) and zinc titanate (Ayala and Jain, 1992), and Z-Sorb, zinc oxide in a porous matrix containing a nickel oxide promotor (f.i. Ayala *et al.*, 1995; Khara *et al.*, 1995). All these sorbents were examined for application at temperatures above 850 K. However, the preferred temperature range has been decreased lately from above 850 K to 600-800 K. This temperature range seems a reasonable compromise between cycle efficiency, capital costs and operation costs, which was already mentioned in the late 80's (Corman, 1986). Four research groups recently joint forces to develop advanced sorbents for desulfurization of coal gas in the temperature range of 625-825 K (Abbasian *et al.*, 1996). At this lower temperature level of 600-800 K, iron oxide is again an attractive sorbent; apart from its high reactivity, it has the following advantages:

- cheap,
- non-toxic,
- high H_2S removal efficiency, and
- easy regenerable, although iron sulfates can be formed.

In a continuous desulfurization process an important parameter is the mechanical strength of the sorbent. To overcome the risk of particle decrepitation after successive desulfurization cyles, supported or impregnated sorbents are developed in the last decade. In case of iron oxide, various investigators propose to replace the inexpensive unsupported materials like ore, and mixtures of iron oxide with coal ash, with artificial sorbents prepared by impregnation of iron compounds (Fe-nitrate, $Fe(OH)_2$ etc.) on a porous carrier material (silica, alumina or FCC particles) (for instance Van der Wal, 1987).
Furthermore, it is nowadays well recognized that also the sorbent regeneration (f.i. the oxidation) method can have a negative effect on the subsequent desulfurization process, for example due to the possible sintering of the sorbent, or the formation of metal sulfates. For the iron based sorbent there are three potential regeneration routes: 1) the recovery of elemental sulfur using SO_2 as the oxidizing agent (Schrodt and Best, 1978; Tseng *et al.*, 1981), 2) the production of H_2S by regeneration with steam or steam-air mixtures (Tamhankar *et al.*, 1985), or 3) the oxidation of the sorbent with (diluted) air, generally yielding SO_2 (Schrodt, 1980; Van der Wal, 1987; Van der Ham *et al.*, 1994). Despite the formation of metal (i.c. iron-) sulfates, so far the latter method seems to be the most feasible option.
In the following, research on unsupported and supported iron-oxide based sorbents, and relevant for the present work, will be discussed shortly. For a more detailed overview the reader is referred to another paper (Venderbosch *et al.*, 1997).

4.1 Unsupported sorbentia

For the desulfurization of coal gas, iron oxide is often mentioned as sorbent material. It was used in the so-called 'Dry Boxes' of the former gas factories to desulfurize town gas (Kohl and Riesenfeld, 1974). The sulfidation of H_2S yielded ferrous sulfide as the solid reaction product, f.i. according to:

$$Fe_2O_3 + 2\ H_2S + H_2 \quad \leftrightarrow \quad 2\ FeS + 3\ H_2O \qquad [1]$$

Iron oxide was already applied in a pilot-plant scale fluidized bed set-up for the removal of

hydrogen sulfide from coke oven gas at operating temperatures in between 600 and 675 K by the South Western Gas Board in the 1950's (Bureau and Olden, 1967). This pilot-plant proved the technical feasibility, and a full-scale commercial plant was installed afterwards to treat coal-derived gases at the Exeter Works of the South Western Gas Board. Unfortunately, decrepitation and attrition of the sorbent occurred during extensive cycling, and overall sorbent losses were considerably higher than had been expected. Furthermore, revenues from the produced sulfuric acid were also disappointing. Eventually, economic concerns largely caused the Exeter plant to shut down in 1965.

The decrepitation of the unsupported iron-oxide sorbents and sorbents based on mixtures of iron-oxide (with fly ash from a coal gasifier, or with porous silica) was also observed as a serious disadvantage by other investigators (e.g. Edwards, 1979). Tamhankar *et al.* (1981) indicated that after an initial fast reduction (by CO and H_2) of Fe_2O_3 to spongy iron, the much slower H_2S absorption reaction on the iron dominated the desulfurization reaction. This result was confirmed by Van der Wal (1987) who showed in lab-scale fixed bed experiments that, for unsupported iron oxide particles, the reaction rate is indeed low during the first sulfidation. However, immediately after the first oxidation the sulfidation capacity and the reaction rate is increased significantly due to the creation of additional surface area. This is the result of i) breakage of the particle structure and an increase in porosity, due to differences in the molar volume of the solid reactants and products (Fe_2O_3, Fe_3O_4, FeO, FeS, $FeSO_4$) involved in the various possible reactions, and ii) the redistribution of FeO (or Fe) in a finely dispersed form. For the unsupported iron oxide it was found that the physical strength was lost completely and the structure of the particle collapsed during subsequent sulfidation / regeneration cycles.

Despite this disadvantage, iron oxide was applied as the sorbent material for the desulfurization on pilot plant scale of coal gas derived from the fluidized bed gasifier (40 ton coal per day) in Yubari, Japan. Subsequently, Ishikawayama-Harima Heavy Industries (IHI) and the New Energy and Industrial Technology Development Organization (NEDO) developed a commercial scale desulfurization process (for a 200 ton coal per day gasifier) on the basis of this unsupported iron-ore. The desulfurization plant consists of a two-stage bubbling fluidized bed desulfurizer and a separate regenerator. As expected, attrition losses were relatively high, and this could not be improved by using a mixed Fe_2O_3/TiO_2 as sorbent material. Attrition losses then appeared to be more than five times higher than with the unsupported iron oxide (Nakayama *et al.*, 1996).

In the last decade, some research was directed towards finding attrition and decrepitation-resistant types of (unsupported) sorbents and less abrasive processes. For example, based on the successful operation of a 2 t-coal/d hot gas cleanup process unit, a 20 t-coal/d hot gas packed bed pilot plant was erected in 1993 at the location site of Nakoso, Japan (Suehiro and Fujishima, 1993; Nakayama *et al.*, 1996). To anticipate on the sorbent decrepitation, a fixed bed was applied, containing an iron-oxide/titanium-oxide sorbent in a honeycomb structure. The process was rather successful, as exit H_2S concentrations were close to the chemical equilibrium concentration. However, it did not have the advantages related to the continuous operation.

4.2 Supported sorbentia

A practical solution for the problems of low reactivity and risk of particle decrepitation was proposed by Van der Wal (1987). He prepared an iron oxide-on-silica sorbent by deposition-precipitation of iron hydroxide ($Fe(OH)_2$) in a suspension of the (micron-sized) silica powder to be used as the carrier material. The iron oxide was finely dispersed in the porous structure of the silica. Using this preparation method, a threefold improvement was reported:

no reduction of iron-oxide to elemental iron and hence prevention of soot formation, a high resistance against deactivation and a high surface area. The latter resulted in very high initial conversion rates, in close agreement with those to be expected when external mass transfer resistances are rate controlling. The latter observation was reported by investigators at the University of Twente, who increased the reactivity and the mechanical strength of the sorbent further by depositing the iron-oxide on a mechanically strong carrier material, viz. fluid cracking catalyst (Van der Ham *et al.*, 1994). The average diameter of the carrier material was chosen such that it could be directly applied in continuously operated (fluid bed related) reactors (d_p=100 μm). Initial work to measure its reactivity and capacity was carried out in a lab-scale packed bed reactor at atmospheric pressure with a simplified, artificial coal gas. Conversion rates of the fresh material were so high, that despite the small average particle diameter applied, gas-to-particle diffusion was still the rate-limiting step. Unfortunately, at temperatures higher than approximately 870 K, a considerable loss in reactivity was observed, and this was perhaps due to the sorbent sintering while oxidizing with O_2. The authors also observed a tendency of the sorbent material to form sulfates. A similar effect was also found when iron oxide on an alumina-silica based porous carrier was applied in a moving bed desulfurization process of coal gas (4 ton coal per day; Nakayama *et al.*, 1996; Ichikawa *et al.*, 1993). In the latter unit, the high oxygen partial pressures applied during the regeneration promoted the formation of sulfates, and these appeared to be stable up to 840 K. To avoid the release of SO_2 during the following desulfurization step, the sulfates had to be reduced to FeS by valuable coal gas, thereby reducing the sulfidation capacity.

Van Yperen (1994) showed that the addition of molybdenum-oxide to the iron-oxide on an amorphous aluminium phosphate carrier suppresses the formation of the iron sulfates. Furthermore, he showed that for the silica supported iron-oxide particles, the presence of water yielded a strong decrease in activity and capacity, due to the formation of iron-silicates during the sulfidation step. Eventually, his work resulted in a sorbent consisting of amorphous aluminium phosphate as the optimal support material with a mixture of molybdenum oxide and iron as the actual sorbent material. The combination of these three materials in different weight percentages (5.8-25 wt.% Fe_2O_3 and 0-11 wt.% MoO_3) proved to have the following advantages: i) molydenum sulfates are not formed, and the addition of molybdenum oxide suppressed the formation of iron sulfate, ii) the activity of the sorbent was less sensitive towards water present in the coal gas, iii) no iron-silicates were formed, and iv) the carrier material is thermally much more stable than silica. There was another small loss in capacity however, due to the formation of iron phosphates.

5 THIS WORK

The above developed strong and stable sorbent type, showing less sulfate formation even at the severe oxidation conditions, seems to be a good starting point for the development of a new desulfurization process. In the present work an iron/molybdenum sorbent, basically similar to the one prepared by van Yperen, is applied in a high velocity fluid bed. Its characteristics fulfil the requirements necessary during the desulfurization step as well as during oxidation of the sulfided material. Compared to riser systems, a relatively large residence time of the sorbent material is obtained.
The first interest of the present work is to investigate the effect of regeneration of the sulfided bed material with (diluted) air on the subsequent sulfidation cycle. In some experiments also reduction is carried out, prior to a new sulfidation step of the sorbent.
From the desulfurization experiments, contact-efficiency values can be calculated by estimating the intrinsic reaction kinetics from the two-phase model incorporating chemical enhancement. The results can then be compared with contact efficiency data presented earlier in this thesis. This work was conducted in close co-operation with the Energy

Research Foundation (ECN) in Petten, the Netherlands.

6 EXPERIMENTAL

The sulfidation/oxidation experiments are conducted in the lab-scale high velocity fluidized bed set-up schematically shown in figure 1. The set-up consists of i) a gas mixing section to provide the gas mixture required for the sulfidation, oxidation and reduction reactions, ii) a heated reactor section, and iii) an analysis section. Basically, the unit is similar to the one applied by Heesink during his desulfurization experiments with calcined limestone, and half-calcined dolomite (Heesink, 1994). In our experiments the reactor is replaced by another type of fluid bed. This so-called high velocity fluidized bed is made of quartz, has an internal diameter of 0.05 m, and is 0.75 m in height. It is further equipped with an expanded top section (0.10 m ID and 0.30 m in height). The fourfold area increase in the expended top section reduces the superficial gas velocity, and allows most of the entrained particle to fall back into the bed. Two cyclones, with internal diameters of 63 mm and 50 mm respectively, are applied to separate the entrained solids from the gas. The solids are returned to the fluidized bed by means of an external dip-leg. To ensure smooth operation, a very small amount of nitrogen (2 Nml/s) is introduced at the bottom of the dip-leg.

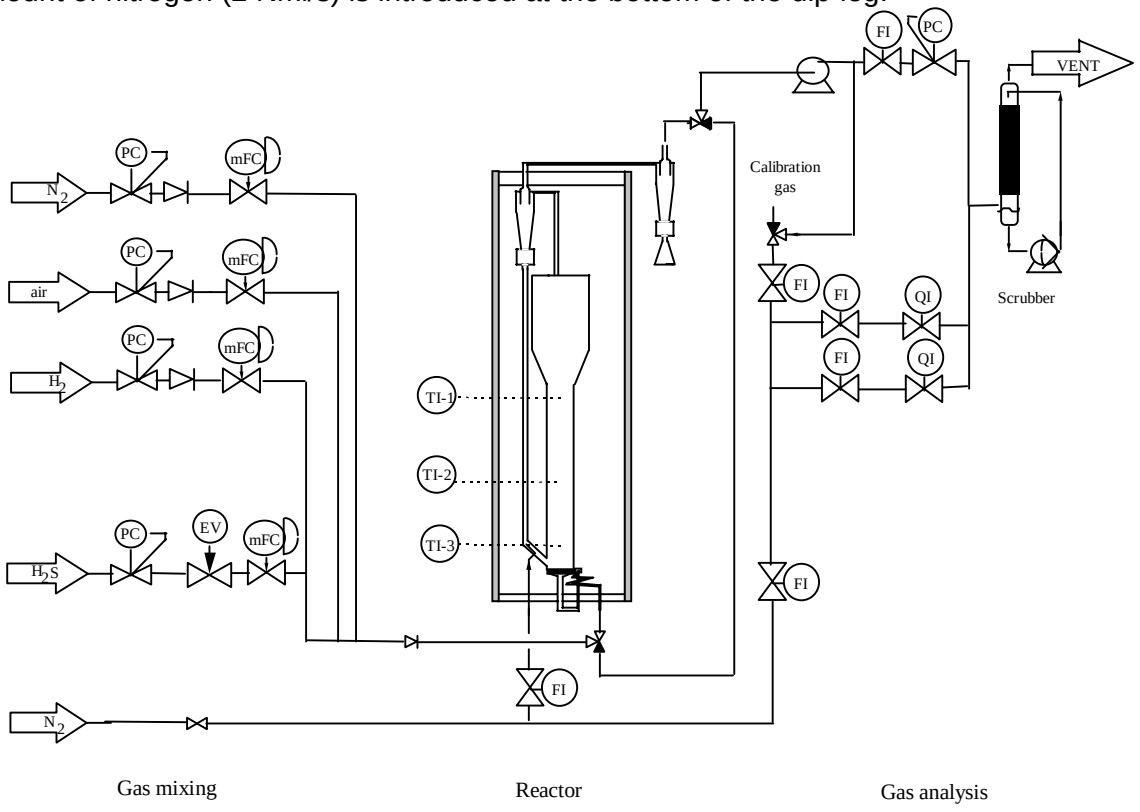

Figure 1. Schematic representation (non-scale) of the lab-scale turbulent fluidized bed.

Mass flow controllers have are applied to adjust the gas stream composition; a mixture of hydrogen, nitrogen and H_2S is used during the desulfurization process, a mixture of air and nitrogen during the oxidation, and a mixture of hydrogen and nitrogen for the reduction of the regenerated sorbent. The continuous sample flow, withdrawn from the reactor effluent stream by a small pump, is split into two parts, one being sent to a Maihak SO_2-analyser (maximum 2 vol.%, accuracy 5 % of full-scale), and the other to an on-line photo ionization detector for H_2S analysis (PID, type HNU 52-02, with a detection level from sub-ppm to 1500 ppmv). The latter is equipped with a 10.2 eV lamp, which supplies a specific amount of energy just enough to ionise H_2S or elemental sulfur, but not the other gaseous components

like H_2, H_2O and N_2. During the experiments, the exit concentrations (H_2S or SO_2) can exceed the maximum allowable concentration specification of the analyzers. Therefore the set-up is provided with an option to dilute the off-gas by nitrogen from a separate mass flow controller.
Before venting the reactor off-gas to the atmosphere, it is scrubbed with a sodium hydroxide solution to remove sulfuric compounds (H_2S during absorption and SO_2 during the regeneration).

The fluid bed reactor is operated at ambient pressures, and placed in an electrical column oven, enabling operating temperatures up to 1000 K. The oven is provided with a spy-glass for visual observation of the fluidization behaviour in the reactor. A series of thermocouples is positioned along the reactor wall to measure the reactor temperature profile. Furthermore, the fluidized bed is provided with several pressure taps for measuring the solids hold-up, thereby neglecting solids-wall friction and acceleration of the particles. During all the experimental work, pressure profiles along the reactor wall are recorded. An on-line computer is used for data acquisition.

Table I. Operating conditions during standard tests, and during initialization

	operating window	**standard conditions**	**tentative runs during the cycles 2 to 6**
sulfidation	u_g=0.1-1.3 m/s	u_g=0.8 m/s	u_g=0.15 m/s
	500-2925 ppm H_2S	2925 ppm H_2S	7500 ppmv H_2S
	3.3-10 vol.% H_2	10 vol.% H_2	10 vol.% H_2
	625-725 K	675 K	675 K
		balance N_2	balance N_2
oxidation	2-20 vol.% O_2	u_g=1 m/s	u_g=1 m/s
		20 vol.% O_2	2 vol.% O_2
		675 K	675 K
		balance N_2	balance N_2
reduction	yes/no	u_g=0.8 m/s	u_g=0.05 m/s
		10 vol.% H_2	10 vol.% H_2
		675 K	675 K
		balance N_2	balance N_2

In table I, the operating window and standard conditions applied during the sulfidation, the oxidation and the reduction, are summarized. At standard conditions, the experiments include successively: 1) batch-wise sulfidation of H_2S at 675 K with a gas mixture containing 2925 ppmv H_2S, 10 vol.% H_2, and balance N_2, 2) oxidation of the loaded sorbent with a gas mixture containing oxygen concentrations up to 20 vol.% (balance N_2), and 3) reduction with a gas mixture containing 10 vol.% H_2. The superficial gas velocities range from 0.1 to 1.3 m/s, and the temperature is varied from 625 to 725 K. The amount of sorbent in the reactor is approximately 300 grams, and is taken from a batch of sorbents supplied by the Energy Research Foundation (ECN) in Petten, the Netherlands. Properties of the sorbent are listed in table II. The average particle diameter and density are 169 μm and 1845 kg/m^3 respectively, which corresponds to the B-type of particles in the fluidization map of Geldart (1973). During all cycles of subsequent desulfurization, oxidation and reduction, a single batch of sorbent is used and no fresh material is added to the reactor.

Table II. Main properties of the applied sorbent at ambient conditions

Property	
d_p (μm)	169
ρ_p (kg/m^3)	1845
u_{mf} (m/s)	0.02
u_t (m/s)	0.91
BET area (m^2/g)	108
pore diameter (nm)	11.2
Fe_2O_3/MoO_3 (wt%/wt%)	9/9
Geldart's type	B

7 RESULTS

7.1 Effect of the oxygen concentration during oxidation on the successive sulfidation characteristics

In the present work, we are interested in the effects of oxidation conditions, and more specifically the oxygen content of the regeneration gas mixture, on the subsequent sulfidation reaction. In the initial desulfurization cycles, relatively moderate operating conditions are applied: a low gas velocity of 0.15 m/s during the desulfurization, and a low oxygen concentration (2 vol.%) in the oxidation step (see table I). Fortunately, the break-through experiments showed no sorbent-deactivation at all. Final breakthrough at for an inlet H_2S concentration of 2925 ppmv is approximated at 8 hours sulfidation time, whereas breakthrough at 100 ppmv H_2S occurs already after about 2 hours. Overall sulfur capacities of the sorbent particles vary from 6 to 7 wt.%. These values are in good agreement with the theoretical capacity of 6.6 wt.%, which can be derived by assuming that the sorbent consists of 9 wt.% Fe_2O_3 and 9 wt.% MoO_3, supposed that the sulfation product are $FeMo_2S_4$ and FeS. Both products are then produced according to:

$$Fe_2O_3 + 2\,H_2S + H_2 \leftrightarrow 2\,FeS + 3\,H_2O \quad [2a]$$
$$Fe_2O_3 + 4\,MoO_3 + 8\,H_2S \leftrightarrow 2\,FeMo_2S_4 + 15\,H_2O \quad [2b]$$

Starting from the 7th cycle onwards, higher gas velocities are applied. Before discussing this in more details, the results of cycle 8, as presented in figure 2 should be considered.

Table III. Additional reactions possible during sulfidation

$H_2S + O^* \leftrightarrow 1/x\,S_x + H_2O$	[3a]
$H_2S + 3\,O^* \leftrightarrow SO_2 + H_2O$	[3b]
$2\,H_2S + SO_2 \leftrightarrow 3/x\,S_x + 2\,H_2O$	[3c]
$SO_2 + 3\,H_2 \leftrightarrow 2\,H_2O + H_2S$	[3d]
$SO_2 + 2\,H \leftrightarrow 2\,H_2O + 1/x\,S_x$	[3e]
$H_2 + 1/x\,S_x \leftrightarrow H_2S$	[3f]

At the beginning of the sulfidation step, a SO_2 peak with a maximum concentration of about 5000 ppmv was observed, followed by a H_2S peak up to 100 ppmv. The SO_2-peak at the beginning of the desulfurization experiment has been observed by Van Yperen (1994) as well, but he did not report the one for H_2S. He attributed the SO_2-peak to the decomposition of sulfates formed during the oxidation step. Because H_2S is known to be a stronger reducing agent than H_2, it is likely that the SO_2 peak at the beginning of the sulfidation step in figure 2 is also caused by an (extended) reduction of the sulfates still present in the

sorbent material after the reduction step,. The H_2S peak in figure 2 may then arise from some (equilibrium) reactions, that can occur as well. Some of these reactions are summarized in table III. As a possibility, H_2S may react with oxygen absorbed at the surface of the sorbent, first yielding SO_2 but eventually also reacting towards elemental sulfur (equations 3a to 3c).

After the initial peaks of SO_2 and H_2S, the H_2S concentration stays below 20 ppmv during the first half hour. During this initial sulfidation stage, the H_2S removal is very high (> 99 %), even for the high gas velocity applied (0.8 m/s). After the first half hour, the H_2S concentration gradually increases upon completion of the sorbent loading (the set-up is operated batch-wise). This phenomenon is commonly observed in the literature on H_2S sorbents. After a certain time, the conversion rate becomes governed by effects of reaction kinetics, pore and/or solid state diffusion. In our experiments, a relatively sharp break-through curve is observed, eventually yielding H_2S reactor off-gas concentrations similar to the inlet concentration. The pulse at t=1.2 hr is a result of the dilution of the reactor outlet gas necessary to keep the H_2S concentration in the detector window.

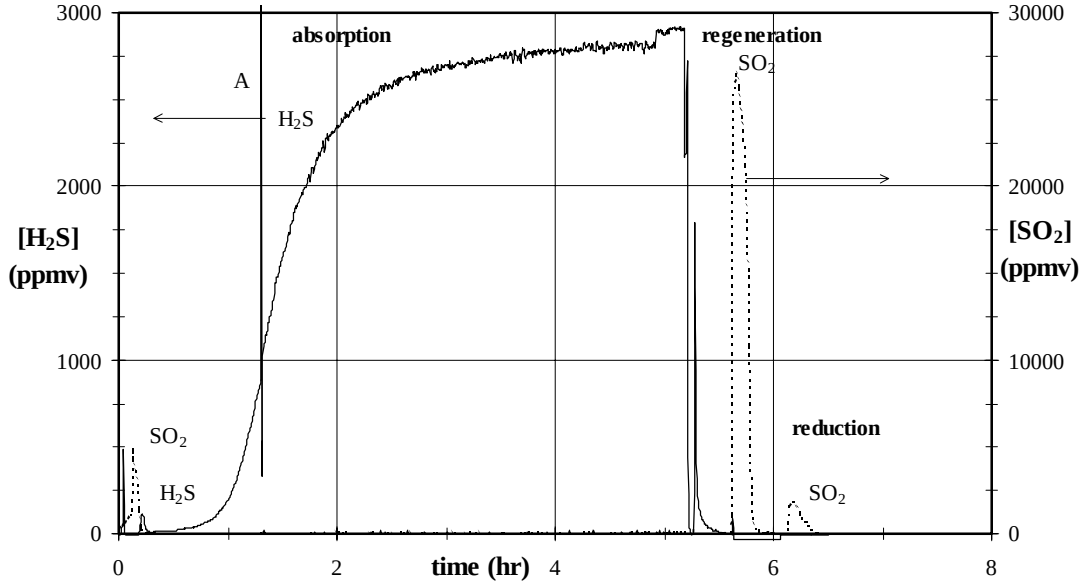

Figure 2. Representative break-through curves measured during batch-wise sulfidation, oxidation and reduction of the sorbent for the 8th cycle. Sulfidation: T=675 K, M_{bed}=300 g, u_g=0.8 m/s, 2925 ppm H_2S, 10 vol.% H_2. Oxidation: T_0=675 K, u_g=1.0 m/s, 5 vol.% O_2; Reduction: T=675 K, u_g=0.8 m/s, 10 vol.% H_2. The pulse at t=1.2 hr (point A) is a result of the dilution of the reactor outlet gas necessary to keep the H_2S concentration in the detector window.

The total sulfur capacity at complete break-through amounts 5.7 wt%, corresponding with approximately 85 % of the theoretically possible capacity. After complete sulfidation of the sorbent material, the reactor is purged with inert nitrogen, followed by oxidation of the sorbent. In the cycle described in figure 2, a mixture of nitrogen and air, containing 5 vol.% O_2, is fed to the reactor of which the initial temperature was 400°C. The SO_2-concentration sharply increases during the oxidation, and after about 15 minutes the SO_2-concentration strongly levels of. A maximum SO_2 outlet concentration during these 15 minutes of approximately 2.6 vol.% is observed, which is quite close to the stoechiometric concentration of 2.8 vol.% which should be achieved by oxidation of FeS and $FeMo_2S_4$ to Fe_2O_3 and MoO_3:

$$4\ FeS + 7\ O_2 \leftrightarrow 2\ Fe_2O_3 + 4\ SO_2 \quad [4a]$$

$$4\ FeMo_2S_4 + 31\ O_2 \leftrightarrow 8\ MoO_3 + 2\ Fe_2O_3 + 16\ SO_2 \quad [4b]$$

It seems likely that all of the oxygen fed to the reactor is converted during the oxidation step. The end of the oxidation is marked by a sharp decrease in the SO_2-concentration. At completion of the oxidation, the reactor is again purged with nitrogen, and a reduction of the sorbent is conducted using a gas mixture 10 vol.% H_2 in nitrogen. During this reduction step about 5 % of the sulfur absorbed on the sorbent after sulfidation, is recovered as additional SO_2, suggesting that sulfates are formed during the preceding oxidation step. The total sulfur balance of this cycle is about 100 %. Typical values for the sulfur balance are in the range of 90 to 100 %, although some experiments yield values down to 80 or up to 120 %. Complete sulfidation of the sorbent material in cycle 8 takes almost 5 hours, oxidation with 5 vol.% oxygen only 15 minutes, and reduction of the material another 15 minutes. The oxidation with higher O_2-concentrations will proceed faster and will take less than 15 minutes.

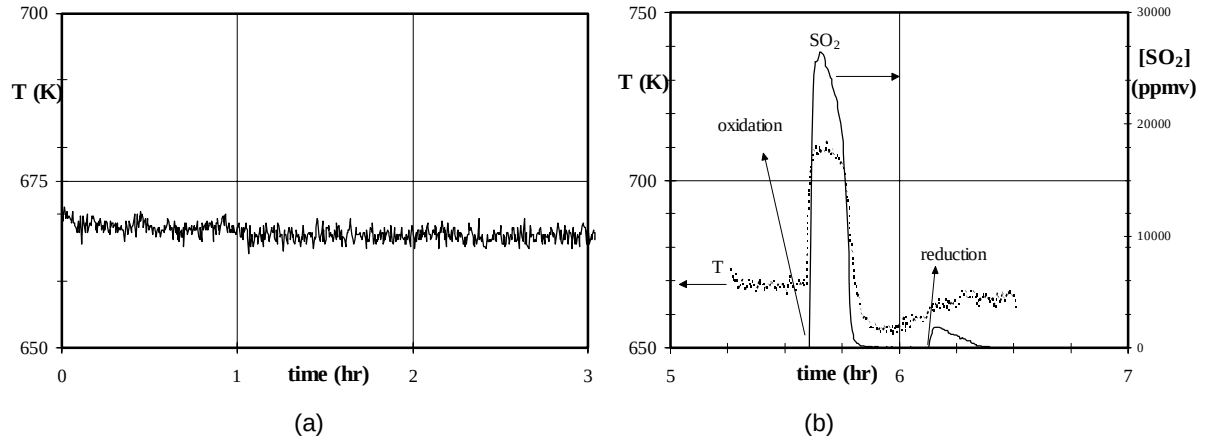

(a) (b)

Figure 3. A representative SO_2 and temperature profile during (a) sulfidation and (b) oxidation and reduction of the sorbent material. For the operating conditions; see figure 2.

During the sulfidation, the oxidation and the reduction of the sorbent material, the temperature was recorded at three levels in the reactor, one at a central position in the dense bed, one just above this dense bed level, and one in the freeboard (designated by TI-1 to TI-3). The temperature in the bed is plotted versus the sulfidation time for cycle 8 in figure 3a, and during the oxidation and reduction step in figure 3b. The temperature remains almost constant during the total desulfurization step, which is accordance with the low value for the reaction enthalpy for the sulfidation of iron oxide (ΔH_r=-27 kJ/mole H_2S) reported by Van der Ham (1994).

During the oxidation, the temperature increase of the reactor bed is considerable ((≈ 50 K). This is obviously due to the strong exothermic oxidation reaction (≈ 350 kJ/mole O_2). In all the experiments, it is observed that temperature differences between the various axial positions in the bed are small (and probably due to calibration errors). The SO_2 concentration is also plotted as a function of time in figure 3b. The strong correlation between the SO_2 formation and the temperature increase is evident, which indicates that the response of the analyzer on a step change at the entrance of the reactor is fast enough for accurate measurements.
As stated before, during the sorbent reduction with 10 vol.% H_2 in nitrogen, some SO_2 is produced, proofing that sulfates are formed during the preceding oxidation step.

The increase in the bed temperature during the oxidation of the sorbent is a function of the rate of oxidation, and therefore also of the inlet oxygen concentration. In the work of Van der Ham (1994) it was shown that severe sorbent deactivation (resulting in sulfidation reactivity and sulfur capacity loss) occurred if the sorbent was regenerated in a small bubbling fluid

bed reactor with a gas mixture containing 20 vol.% O_2, This was probably due to temperatures > 875 K in his reactor. In their work, the sorbent deactivation appeared to be reversible, as breakthrough curves regained its original shapes when in the subsequent cycles a lower oxygen concentration during the oxidation was used. In this work similar experiments were conducted, and the results obtained are shown in figure 4. Four H_2S break-through curves are plotted for sorbent material previously regenerated with a gas mixture containing respectively 5, 10, 15 and 20 vol.% O_2.

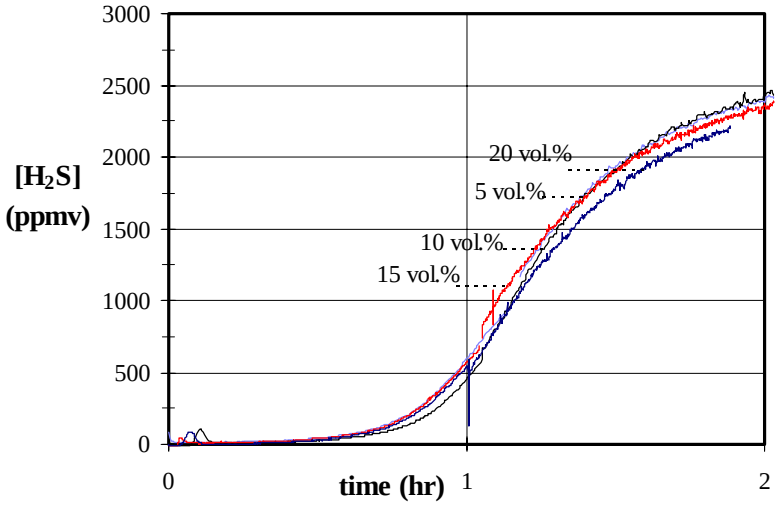

Figure 4. The breakthrough curve of H_2S at standard conditions, after a preceding oxidation step at 400°C with a gas mixture containing 5 up to 20 vol.% O_2 for the cycles 9, 13, 16 and 17.

All curves in figure 4 show a similar shape, and identical reactivities and sulfur capacities. Clearly, the sorbent applied in the present paper shows only a small loss in reactivity and capacity even after oxidation with undiluted air. Most probably, the sorbent maintained its original capacity and reactivity due to a limited temperature increase during the oxidation reaction. Van der Ham (1994) showed that to avoid deactivation of the iron-oxide sorbent, the maximum temperature in the reactor should not exceed about 875 K. In the present experiments, the maximum temperature was always less than 825 K. This is explicitly shown in figure 5a, where the maximum temperature rise of the reactor bed, ΔT_{max}, at a central position in the reactor is plotted as a function of the oxygen inlet concentration, y_{O2}.

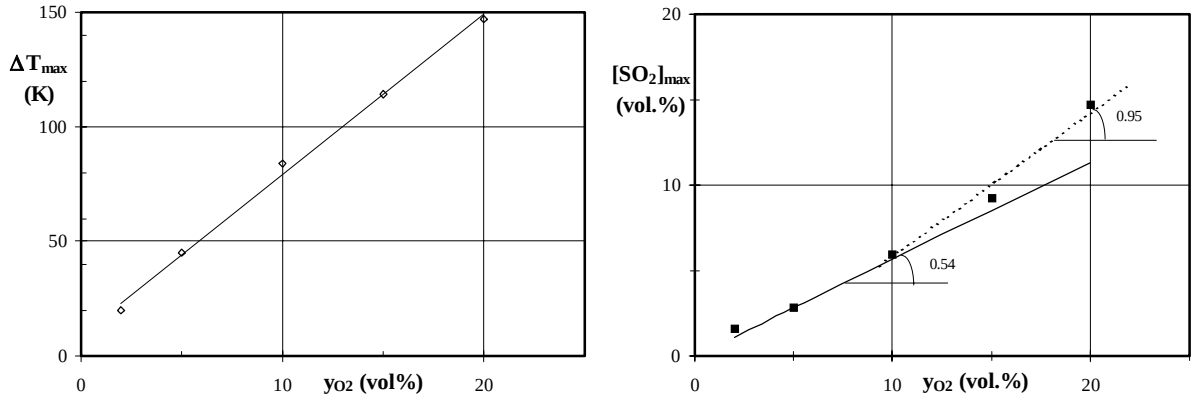

Figure 5. (a) Maximum temperature increase ΔT_{max} and (b) the maximum SO_2-concentration $[SO_2]_{max}$ during the subsequent oxidation steps versus the inlet concentration of oxygen y_{O2}. In (a) the solid line indicate the trends, in (b) the solid line represents the theoretical maximum SO_2 concentration according to

the reaction equations 4a and 4b.

An almost linear relationship between ΔT_{max} and y_{O2} is shown with a temperature increase of about 8 K/ vol.% O_2. This results in a maximum temperature increase of 160 K when undiluted air is applied. Compared to an adiabatic gas temperature rise of 108 K/ vol.% O_2, it can be calculated easily that, for the present reactor, a minor fraction of the heat (25 %) is used for heating the gas and the solid sorbent, but that most of the heat (75%) is transferred through the wall of the reactor to the oven.
As stated before, temperatures above 875 K can result in sintering of the sorbent material, eventually leading to a decreased sulfur capacity, sorbent strength and sorbent reactivity (Van der Ham *et al.*, 1994). In the present work, the maximum bed temperature did not exceed 825 K. This may be a reason that no loss of capacity and activity has been observed.
In figure 5b, the measured maximum SO_2 concentrations during the oxidation reaction with (diluted) air are presented, and compared with the theoretical SO_2-concentration assuming that the oxidation reaction occurs according to equations 4a and b, and that all of the oxygen in the inlet gas is used in the oxidation reaction (maximum ratio of SO_2 over $O_2 \cong$ 0.54 mole/mole). For oxygen inlet concentrations $\leq$ 10 vol.%, the agreement is good. However, at higher oxygen concentrations the measured SO_2 concentrations are significantly higher than the calculated ones. Almost certainly, this is caused by the occurrence of other oxidation reactions: for example the oxidation of the FeS towards Fe_3O_4 (ratio $\cong$ 0.60) or FeO (ratio $\cong$ 0.63) or the oxidation of the molybdenum sulfide towards MoO_2 instead of MoO_3. In the latter case, even more SO_2 will be produced per unit volume of oxygen (ratio $\cong$ 0.82).

When pure iron-oxide particles are applied as a sorbent material, sulfate formation during the oxidation of the sorbent can be a problem (Van der Wal, 1987), especially when the oxidation temperature is kept below 775 K. It causes capacity and/or reactivity loss of the sorbent in following desulfurization steps. Consequently, the formation of sulfates may have serious consequences for the design of a desulfurization process. Van Yperen (1994) showed for his sorbent a strong reduction in sulfate formation, due to the addition of molybdenum to his sorbent. In order to test whether also for our sorbent the formation of sulfates is important, experiments with and without a sorbent reduction step before the successive desulfurization step are compared. Reduction of the sorbent is conducted by passing H_2 over the sorbent at elevated temperatures (> 673 K), thereby reducing the sulfates towards SO_2.

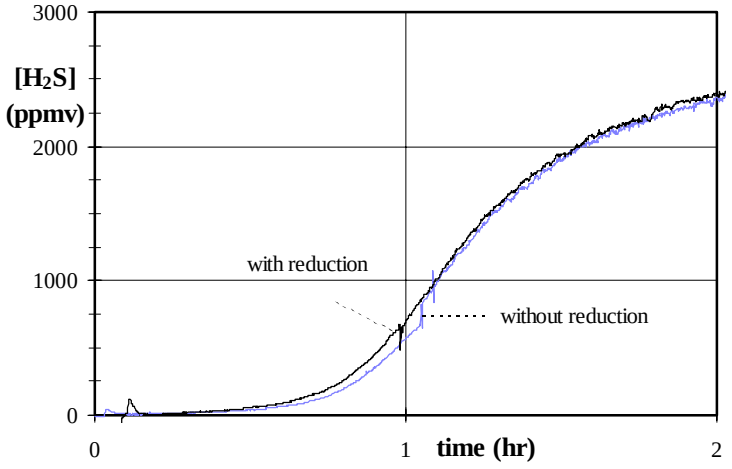

Figure 6. The breakthrough curve of H_2S at the standard conditions presented in table I after a sorbent reduction with 10 vol.% H_2 in nitrogen at 675 K, and one without a pre-reduction step for the cycles

16 and 20. Prior to these sulfidation steps, the sorbent was regenerated with undiluted air.

In figure 6 two H_2S-breakthrough curves obtained for our sorbent are plotted, one for which the sorbent was first reduced by 10 vol.% H_2 in N_2, and the other without such a pre-reduction step. Clearly, both curves are almost identical; generally, a small decrease in sulfur capacity was observed when the reduction step was omitted.

Fortunately, due to the limited sulfate formation during the oxidation step (approximately 5% of the total sulfur absorbed is released as SO_2 during the pre-reduction step, see figure 3), it does not have any serious consequences for the subsequent sulfidation. Perhaps, the applied oxidation temperature of 675 K seems to be high enough for this sorbent to avoid excessive sulfate formation on the sorbent.

Figure 7 shows the sulfur capacity at an arbitrary chosen break-through of 100 ppm H_2S, S_{100}, as a function of the cycle number, N_c. Several parameters of the sulfidation, the oxidation and the reduction were varied (see also table I). Figure 7 shows some indication about the strength of the sorbent. In the first 5 cycles (in which the gas velocity was approximately 0.15 m/s), a strong variation in sorbent capacity can be seen, which is perhaps due to effects of sorbent initialization and stabilization, but also because of the lower gas velocities applied in these preliminary investigations.
The next cycles (up to cycle 28) were conducted at a constant gas velocity of 0.8 m/s during sulfidation, while the oxygen concentration during the oxidation was varied, and, after cycle 15 the reduction step was omitted. Despite these variations in the process conditions, a very small loss of about 5 % in capacity at 100 ppm breakthrough (and thus in reactivity as well) was observed up to 40 cycles. The reproducibility of the cycles is good. An almost constant sulfur absorption capacity of about 2.3 wt.% (corresponding with 35 % of the theoretical maximum) at 100 ppmv H_2S-breakthrough was observed. This value was independent on the oxygen concentration applied during the preceding oxidation step.

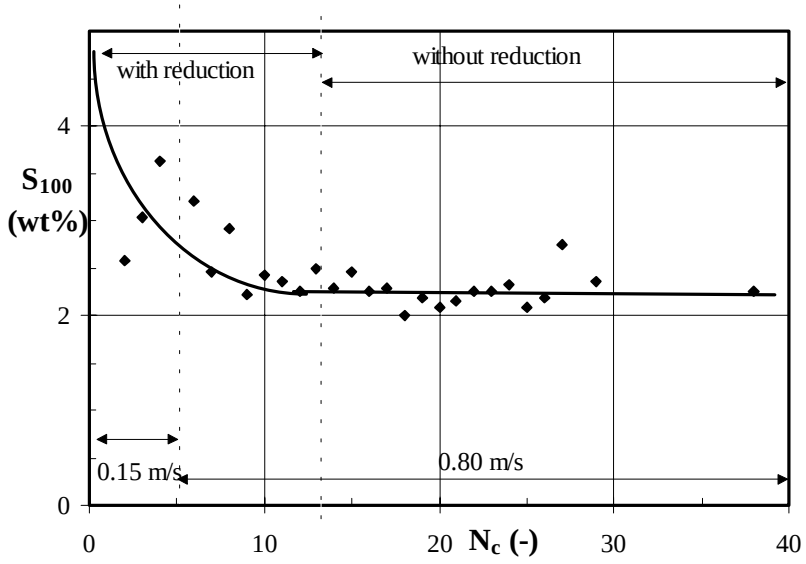

Figure 7. Sulfur capacity at break-through of 100 ppm, S_{100}, as a function of cycle number, N_c for all sulfidation experiments. The solid line indicates the trend in S_{100}.

Before, during and after the fluid bed test program, sorbent samples were taken from the reactor contents and analyzed. In table IV the results are summarized.
Table IV clearly shows that during all experiments the particle characteristics remained

almost the same.

Table IV. Characterization results of sorbent material before and after fluid bed tests

method/property	fresh	cycle 6-25	cycle 48	sulfided cycle 48
mean particle diameter (μm)	169	182	148	148
BET area (m^2/g)	108.8	n.d.	94.0	92.7
average pore diameter (nm)	11.2	n.d.	12.1	11.6

During the first 25 cycles, a small increase in particle diameter was observed, obviously due to entrainment of small particles. These were recovered in the second cyclone, and analysis revealed an average particle diameter of about 30 μm for the entrained particles. After 48 runs, the average particle diameter decreased slightly, perhaps due to the higher gas velocities and/or temperature during the desulfurization step in between the cycles 39 to 45. Fortunately, the total amount of particles entrained from the reactor bed could be neglected (at the end of the extensive experimental program less than 5 wt.% of the initial amount of sorbent had been blown out of the reactor).
After all 48 cycles only a small decrease in BET surface area is observed, indicating that the structure of the individual particles remains almost unchanged. The sulfided sorbent shows values similar to those measured for the fresh material, indicating that the pores of the sorbent are not blocked due to sulfide formation.

7.2 Interpretation of sulfidation experiments

In the present work, the gas velocity was varied during the sulfidation step to investigate the reactor performance. In some of the experiments, the superficial gas velocities in the bed exceeded the terminal falling velocity of the individual particle (0.91 m/s, see table II), and in a few experiments it was higher than the transition velocity marking the onset of the turbulent fluidization regime, which is approximately 1.1 m/s at 675 K. Unfortunately, at these high velocities, the H_2S inlet concentrations were lower than 2925 ppmv due to the limitations of the H_2S mass flow controller. The effect of the gas velocity (with similar H_2S inlet concentrations) on the H_2S-breakthrough is plotted in figure 8a. It shows the H_2S outlet concentration versus the sulfidation time for gas velocities up to 0.8 m/s. At higher gas-velocities break-through of H_2S occurs at lower sulfidation times. Clearly, this is due to two major reasons: firstly because of the higher amount of H_2S fed to the reactor at the higher gas velocities (proportional to u_g), and secondly because of the lower contact-times between the gas and the solids (which is proportional to $1/u_g$).
For analysis and mutual comparison of results, obtained at different experimental operating conditions, concentration and time data were transformed into non-dimensional quantities presented in figure 8b. The average non-dimensional fractional sorbent conversion, X, is plotted as a function of the non-dimensional time Ψ ($=t/t^+$), with t^+ defined as the time required for the 100 % conversion of the sorbent material in case the reaction is infinitely fast during the entire experiment:

$$\psi = \frac{t}{t^+} \quad \text{with}$$

$$t^+ = 10^4 \cdot \frac{M_{bed} S}{u_g A \rho_{H_2S} [H_2S]} \cdot \frac{m_{H_2S}}{m_S} = \frac{\text{kg of S that can be absorbed on sorbent}}{\text{kg of S applied per second}} \qquad (1)$$

with $[H_2S]$ in ppmv, S the maximum theoretical sulfur capacity in wt.% (≈ 6.6 wt.%), ρ_{H_2S} as

the density (kg/m^3) of the hydrogen sulfide, and M_{bed} the amount of sorbent material (kg) present in the reactor.

The average fractional sorbent conversion, X, is defined as:

$$X = \frac{\int (1-Y)\cdot u_g A \rho_{H_2S}[H_2S]\cdot dt}{10^4 \cdot S \cdot M_{bed}} \frac{m_S}{m_{H_2S}} \qquad (2)$$

in which Y represents the non-dimensional gas phase concentration, c_{out}/c_{in}, and m_S, and m_{H2S}, the molecular weight of sulfur and H_2S respectively.

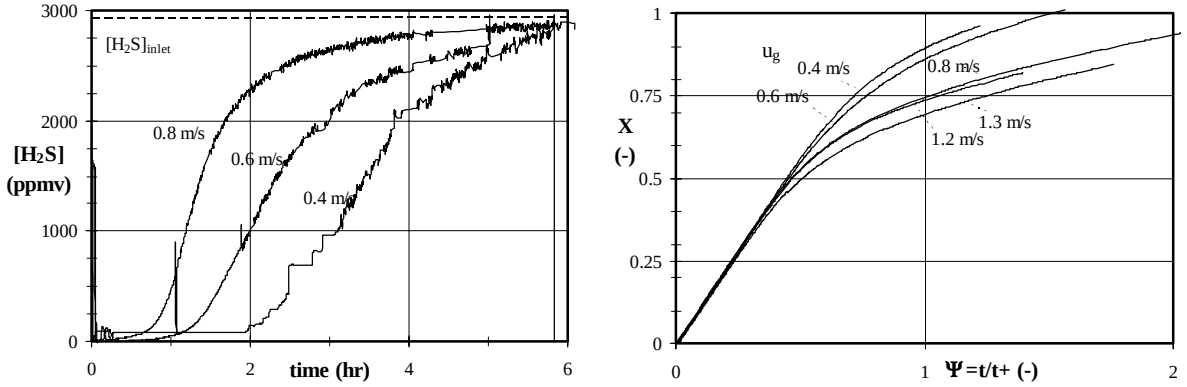

Figure 8. (a) The H_2S-breakthrough curve at standard conditions, while varying the gas velocity from 0.4 to 0.8 m/s and (b) the average fractional sorbent conversion, X, versus the non-dimensional time Ψ.

In the initial stage of desulfurization (Ψ<0.5), the fractional sorbent conversion is independent on the gas velocity. Despite the lower contact-times at the higher velocities the sorbent conversion profiles coincide. Almost all of the H_2S fed to the reactor is then consumed by the sorbent; still, very small H_2S concentrations (depending on the gas velocity ranging from 10-40 ppm) could be accurately detected at the reactor outlet.

It will be shown later in this paper that at the start stage of the desulfurization process the reaction rates are so high that the mass transfer resistance dominates the conversion rate. Increasing the gas velocity then leads to a higher mass transfer rate (for example due to more smaller bubbles). The effect of a decreasing contact time could then be compensated for by a higher mass transfer rate, i.e. a better gas-solids contacting. In the final stage of the desulfurization process (Ψ>0.5), the solids conversion rate becomes controlled by the intrinsic reaction kinetics, since the effect of shorter contact times is then directly reflected by lower H_2S removal rates, and lower values of the sorbent conversion rate dX/dΨ.

Because high sulfur removal efficiencies are required in industrial applications, we are especially interested in the early stage of the desulfurization step (viz. at low solid conversions) in the present work. From dispersion experiments (similar to those presented in chapter 6 of this thesis), it could be concluded that for the present fluid bed system the back-mixing in the dense phase can be neglected. Assuming first order reaction kinetics over the entire X-range (this is certainly the case for the sulfidation of Fe_2O_3 at the low X-values, when the sulfidation rates are controlled by external mass transfer resistance), the overall conversion rate constant k_{ov} on basis of the sorbent volume can be calculated from the gas phase conversion, while assuming plug flow of gas:

$$\frac{\partial u_g Ac}{\partial \xi} = -k_{ov} c \frac{M_{bed}}{\rho_B} \qquad \Rightarrow \qquad k_{ov} = -\frac{u_g A \rho_B}{M_{bed}} \ln(Y) \tag{3}$$

with Y as the non-dimensional H_2S-concentration ($=c_{out}/c_{in}$). The overall conversion rate is a function of fractional conversion of the sorbent material X (defined by equation 2), and consequently of the operating time. In figure 9 the calculated value for the overall conversion rate constant k_{ov} (equation 3) is plotted versus the fractional sorbent conversion X (equation 2) for gas velocities ranging from 0.4 m/s up to 1.3 m/s.

For each gas velocity, the k_{ov} becomes almost independent of X at the low X-values, whereas a strong decrease is observed at the higher values, viz. X > 0.1 at u_g = 1.3 m/s and X > 0.2 at u_g = 0.4 m/s. Furthermore, at low values for X, the conversion rate constant increases with the gas velocity, while at higher X-values the overall rate constant is almost independent of u_g. Based on these results, it seems that in the lower X-regime, conversion rates are controlled by the overall external mass transfer resistance, and that the mass transfer coefficient increases at higher gas velocities. For the lowest X-values the ratio of k_{ov}/u_g is almost constant. Upon interpretation in the two-phase model, to be discussed later in this paper, this indicates that the height of a mass transfer unit in this reactor is constant.

As expected, at higher X-values, conversion rates are controlled by the intra-particle phenomena like the intrinsic reaction and or diffusion (this conclusion is in line with the findings of Van der Ham *et al.* (1994) that, at low X-values for a fresh or regenerated iron-oxide based sorbent particle, the conversion rate in a small scale riser set-up is controlled by mass transfer resistance).

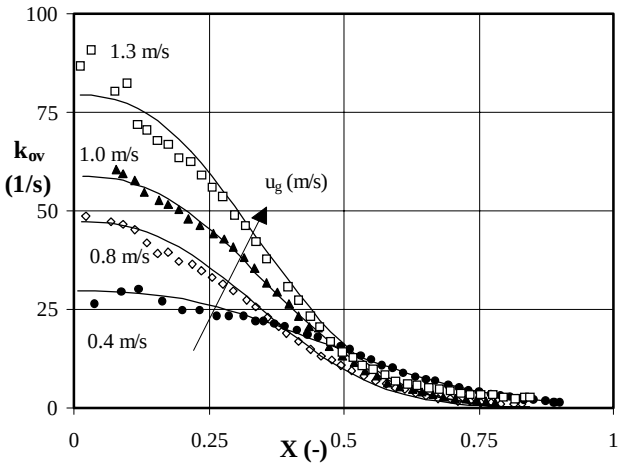

Figure 9. The overall conversion rate constant k_{ov} defined on sorbent volume basis versus the fractional sorbent conversion X at 675 K for different gas velocities. Legends: • u_g=0.4 m/s, ◊ u_g=0.8 m/s, ▲ u_g=1.0 m/s, • u_g=1.3 m/s. The solid lines show only trends.

This conclusion is additionally confirmed by plotting k_{ov} in an Arrhenius type of plot, where the conversion rate constant is presented as a function of the reciprocal temperature. A number of sulfidation experiments have therefore been carried out at various temperatures, viz. 575 K, 625 K and 675 K. First, in figure 10 the k_{ov} is plotted as a function of X for the 3 temperatures indicated at superficial gas velocity of u_g=0.8 m/s.

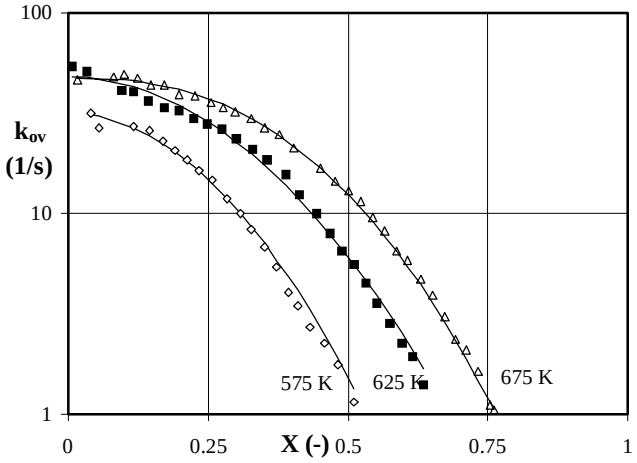

Figure 10. The overall conversion rate constant k_{ov} defined on sorbent volume basis versus the fractional sorbent conversion X of the sulfidation reaction at different operating temperatures and u_g=0.8 m/s. Legends: Δ T=675 K, ■ T=625 K and ◊ T=575 K.

At low X values, the overall conversion rate constant does not depend very much on the temperature, suggesting a low value for the intrinsic activation energy E_{act}. At higher X-values, however, the reaction rate is strongly influenced by the operating temperature yielding higher values for the activation energy.

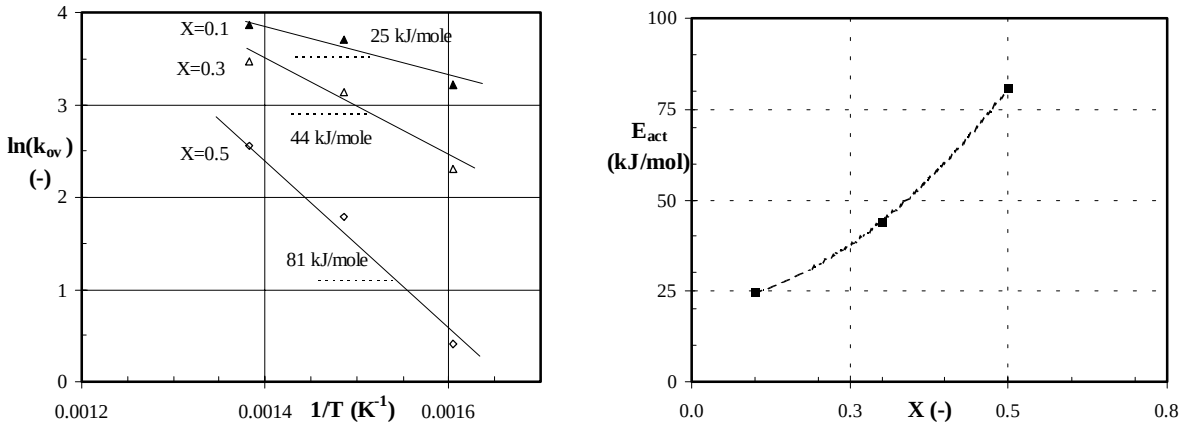

(a) (b)

Figure 11. a) The conversion rate constant versus the reciprocal temperature for various sorbent conversions X and u_g=0.8 m/s, and (b) the apparent activation energy versus the conversion X over a temperature range 575<T<675 K and u_g=0.8 m/s. Legends (a): ▲ X=0.1, Δ X=0.3 and ◊ X=0.5 .

These results are further clarified in figure 11. At X=0.1, the overall conversion rate constant is only slightly dependent on the operating temperature. From figure 11, an activation energy lower than 25 kJ/mole for X=0.1 can be estimated. This still suggests some influence of the intrinsic reaction kinetics, however it should be noted that its value is strongly influenced by the result obtained at the lowest temperature of T=575 K. If only the results for the two temperatures of T=625 and T=675 K are considered, a much lower value of E_{act}=5 kJ/mole can be derived. The activation energy increases with X, and at a higher sorbent conversion of X>0.5, activation energies of more than 80 kJ/mole are estimated. The experimental results indicate that initially the conversion rate is largely mass transfer controlled, especially at the higher temperatures T≥675 K, where it is completely mass transfer limited. Presumably, this is due to the bubble-to-emulsion phase mass transfer resistance (possibly with enhancement) in the fluid bed. Experiments with diluted sorbent material are in

agreement with this observation. In a separate experiment, a break-through curve was measured for bed material with 90 wt.% of the particles replaced by inert material (this situation resembles the performance of a continuous desulfurization process). At low X-values, the conversion rate constant per unit volume of active material was approximately a decade higher than the one obtained for the undiluted experiments. Apparently, even in the case that the bed is diluted with inert material, the conversion rate is controlled by a similar additional mass transfer resistance as the one that is rate controlling in the undiluted bed.
The situation of the diluted bed reflects the situation of the reactor to be operated on a commercial scale, and in which only a fraction of the bed content is active. Within this respect, it should be remarked that during the oxidation of the sorbent in the diluted bed with air, a significantly smaller temperature increase of the bed (approximately 30 K) was observed compared to the situation that all particles were active. At these actual operating conditions, the actual bed reactivity will be different from the reactivity that would be observed if all particles had a conversion extent equal to the average conversion extent of the bed. For various types of conversion behaviours, Heesink (1994) derived mathematical functions to account for this phenomenon.

Values for the apparent overall mass transfer coefficient can now be derived from the (estimated) abscissa of the plot in figure 9, and expressed in terms of a Sherwood number, assuming spherical particles with a specific surface area $a=6/d_p$:

$$Sh = \frac{k_{ov} d_p^2}{6D} \qquad (4)$$

Figure 12 shows the results as a Sherwood/Nusselt versus Reynolds diagram. It includes the results of both types of experiments, for the diluted as well as for the undiluted bed. The literature data for packed and for fluidized beds are presented by the shaded area, whereas individual results from various authors in the high velocity fluidized bed regime (amongst others those of Van der Ham *et al.* 1994 for a small riser system) are displayed as symbols or as lines.

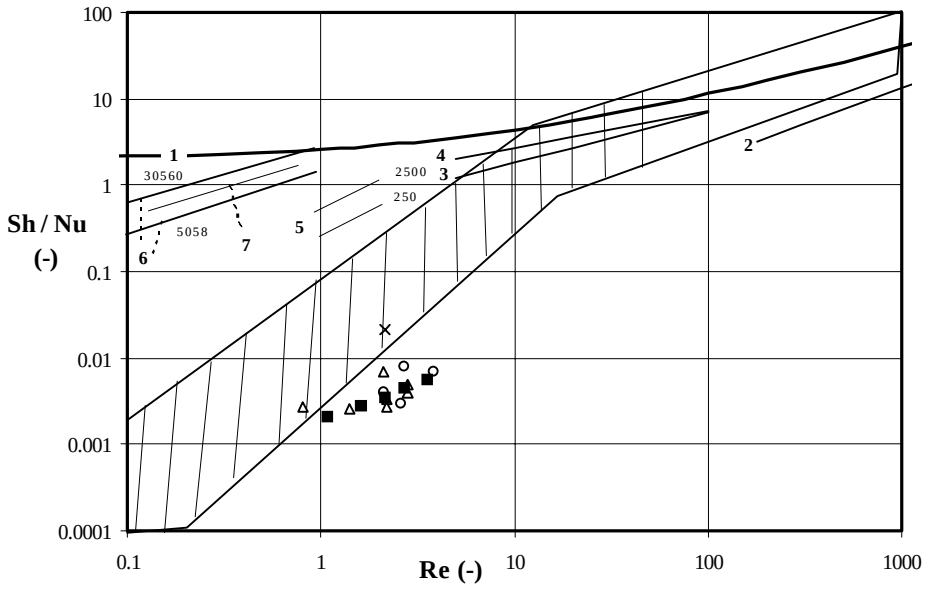

Figure 12. Sherwood and Nusselt numbers as a function of Reynolds number in packed and fluidized beds. Legends: ■ this work (100% active particles); X this work (10% active particles); Δ Van der Ham (1994);❍ Van der Ham *et al.* (1994); **1.** Ranz and Marshall (1952a/b); **2.** Bandrowski and Kacmarzyk (1978) β=0.02; **3.** Kumar *et al.* (1993) β=0.02; **4.** Kato *et al.* (1983) β=0.02; **5.** CO oxidation in a riser (chapter 4) n_d=2500 and n_d=250: **6**. CO oxidation in the high velocity fluid bed in chapter 6 n_d=30560 and n_d=5058; **7**. CO oxidation in a small packed bed (chapter 2) n_d=160.

The mass transfer number, and therefore Sh, increases with Reynolds number. The data derived in the present work show the same trend as those obtained by Van der Ham *et al.* (1994). They are much lower than expected for the case of ideal gas-solids contacting, represented by the Ranz-Marshall (1952) equation. This is in agreement with the literature data derived earlier for other gas solids reactors. The lines denoted **5** and **6** represent the conversion data for the oxidation of CO over a Pt-catalyst in a riser set-up (chapter 4), and the high velocity fluid bed (chapter 6) respectively. In these experiments, the active material was diluted in a ratio n_d with inert material. Apparently, dilution of active material yields higher mass transfer numbers, defined on basis of the active particles. This is also confirmed by the dilution experiment in the present work. The single data-point for this diluted bed (x) is almost a decade higher than those for the undiluted bed. In general, gas-solids contacting, also for these larger particles, and for the high velocity regime, is (much) worse than expected on basis of individual gas-solids contacting.
As stated already in chapter 6, it is important to note that the apparent Sherwood numbers derived from these conversion experiments only reflect mathematical values, in which (amongst others) the bubble-to-dense phase or gas-to-cluster mass transfer resistance are lumped. They should be handled with great care, the more so because in industrial reactors dilution of the active catalyst is seldom applied.

7.3 Interpretation with the two-phase model

The low value for the activation energy indicates that the conversion rates are dominated by mass transfer resistances for sorbent conversion values X<0.25, and by the intrinsic reaction kinetics for X>0.5. By re-evaluating the conversion data, and correct them for any mass transfer resistances (that should be known a priori), values for the intrinsic reaction rates can be estimated. The simple two-phase model (characterized by an average height of a transfer unit H_α and the corresponding number of mass transfer units N_α) can be used to re-evaluate the conversion data (Van Swaaij and Zuiderweg, 1972). In chapter 6, it was shown that the apparent mass transfer height decreases for k_r>1s^{-1}. Werther (1980) showed that the simple approach of the simple two-phase model and chemical reaction in series is only valid up to a reaction rate (based on the dense phase volume) of $k_r \approx 1$ to 2 s^{-1}. For the higher k_r-values, the chemical enhancement of mass transfer was given as an explanation for the improved mass transfer. The conversion can then be calculated from:

$$\xi = 1 - \frac{c_{out}}{c_{in}} = 1 - \exp\left(- \frac{\left(\phi^{-1} - 1\right)\mathrm{Ha} + \tanh(\mathrm{Ha})}{\left(\phi^{-1} - 1\right)\mathrm{Ha} \cdot \tanh(\mathrm{Ha}) + 1} \mathrm{HaN}_\alpha \right) \qquad (5a)$$

where

$$\mathrm{Ha} = \frac{\sqrt{k_r D_{eff}}}{k_m} \qquad (5b)$$

is the Hatta number, ϕ the ratio of film volume over the total dense phase volume, and D_{eff} the effective diffusion coefficient in the dense phase. For the bubble-to-dense phase mass transfer coefficient k_m the following relation was proposed (Werther, 1980):

$$k_m = \frac{3.44 \cdot 10^{-4}}{\chi}\sqrt{1+27.2(u-u_{mf})} \quad \text{with} \quad \chi=0.055 \text{ (porous particles)} \qquad (5c)$$

For the special case of Ha<<1, equation 5a reduces to the relation proposed by Van Swaaij (1978):

$$\xi = 1-\frac{c_{out}}{c_{in}} = 1-\exp\left(-\frac{N_\alpha N_r}{N_\alpha + N_r}\right) \qquad (6)$$

For the present H_2S conversion data, the k_{ov}-values are in the order of 25 to 80 s^{-1} for 0<X<0.25, and equation 6 is not valid in that X-range. Equation 5a should be used to re-evaluate the intrinsic reaction rate at the lower X-values. Then, the value for N_α should be known a priori. For the reactor with ID=0.05 and a bed height of 0.16 m, a value of H_α=0.1 m can be estimated (Van Swaaij, 1985). If constant value of N_α=1.6 is assumed, the value for k_r as a function of the sorbent conversion can be derived from equation 5a ($D_{eff}=6\cdot10^{-5}$ m^2/s). In figure 13, the results are presented for 0.8<u_g<1.3 m/s.

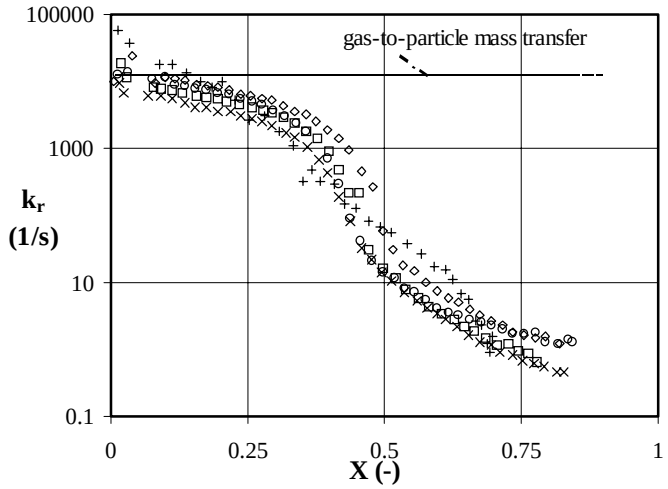

Figure 13. The value for the reaction rate constant (per unit volume of dense phase) k_r derived from equation 6a as a function of the fractional sorbent conversion for the H_2S-conversion data; N_α=0.2, T=675 K, ϕ=0.01. Legends: x u_g=0.8 m/s; □ u_g=1.0 m/s; ◊ u_g=1.2 m/s; ° u_g=1.3 m/s; + 10% active particles and 0.8 m/s. The solid line indicates the apparent k_r-values derived from gas-to-particle mass transfer limitation with Sh=2.

As expected, the derived value for k_r depends on the fractional conversion over the whole X-range of the fractional sorbent conversion. Its value decreases almost 5 decades over 0<X<1. Contrary to the data in figure 9, it is almost independent on the gas velocity, which is to be expected for the intrinsic reaction kinetics. The highest calculated k_r-values are in the order of 10^4 s^{-1}, close to the values that can be derived for gas-to-particle mass transfer rates ($k_r\beta=k_g a\beta=1.2\cdot10^4$ s^{-1}, with $\beta\approx0.5$ as the dense phase solids concentration, and indicated as a solid line in figure 13). This indicates that for the low sorbent conversion values, the conversion rate is dominated by the gas-to-particle mass transfer.

In figure 13, the re-evaluated data for the diluted bed of 10% active particles, corrected for the dilution ratio n_d=10, are also presented. The derived values are in close agreement with those derived for the undiluted bed, again to be expected if intrinsic reaction kinetics are considered.

From the k_r-values plotted in figure 13, the contact efficiency η can be derived following:

$$\eta = \frac{k_{ov}(\text{figure } 9)}{k_r \text{ (figure } 13)} \qquad (7)$$

In figure 14, the values for η are plotted as a solid line versus the reaction number N_r. Similar to the diagrams presented in the chapter 4 and 6 for the riser regime and the high velocity fluid bed, the contact-efficiency decreases significantly with reaction rate. Values of $0.01<\eta<1$ are recovered for $0.1<N_r<10^2$

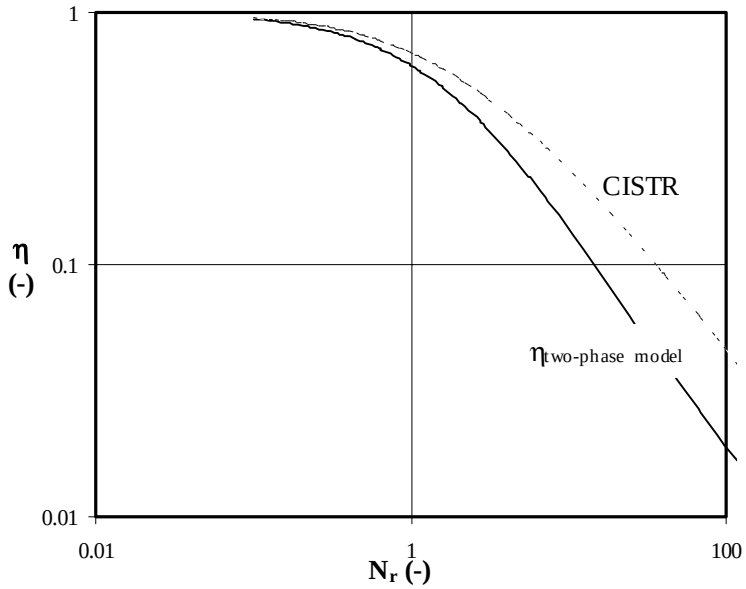

Figure 14. The contact-efficiency, $\eta=k_{ov}/k_r$, as a function of the non-dimensional reaction number N_r for the desulfurization data of the present work. The dashed line plotted represents the apparent loss in η for the extreme case of ideal contacting in an ideally stirred tank model instead of the suggested plug flow behaviour ($\eta=1$), and the solid line for the two-phase model.

The dashed line in figure 14 represents the apparent loss in η for the extreme case of ideal contacting in an ideally stirred tank model instead of the suggested plug flow behaviour ($\eta=1$). The re-interpreted η-values of the present work (solid line; two-phase model) are much lower than the CISTR (with ideal contacting) approach, and this is consistent with the conversion data presented in chapter 6 of this thesis.

7.4 Interpretation of the conversion data in the cluster model

It is likely that in this high velocity fluid bed regime, the particulate phase is structured in clusters, which are frequently formed and disintegrated. Similar to the approach described in chapter 6 for the CO conversion data, the cluster concept can be used to evaluate the H_2S desulfurization data for the effective cluster size. In fact, and stated earlier in chapter 6, the interpretation in terms of chemical enhancement in the two-phase model or in terms of clusters, are just two aspect of the same phenomenon.
The clusters are supposed to be distributed evenly over the reactor volume, and the relevant assumptions of the model are presented in chapter 6, together with the relevant equations and relations.
The cluster diameter, d_{cl}, has been calculated, assuming that the cluster solids concentration $\beta_{cl}=0.6$, and the result are presented in figure 14.

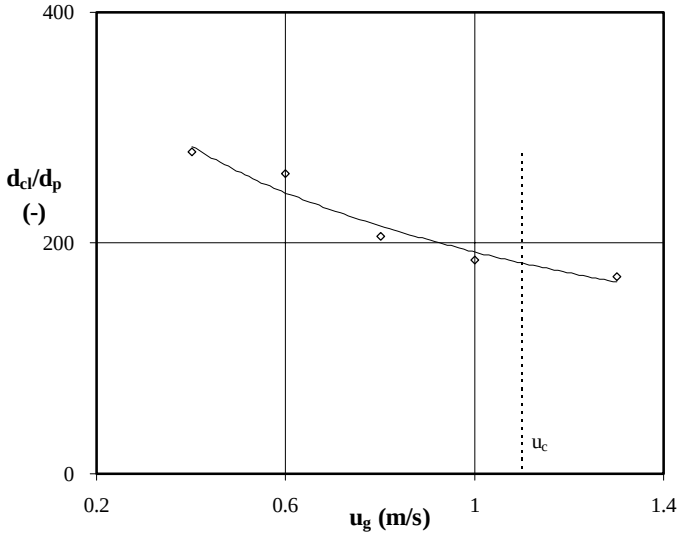

Figure 15. The ratio of the cluster-over-particle diameter d_{cl}/d_p for the fluid bed H_2S desulfurization results as a function of the fluidization velocity u_g. The solids line indicates the trend.

Figure 15 shows similarity with the results presented in chapter 6. The effective cluster-over-particle diameter d_{cl}/d_p decreases with the gas velocity, and it slightly levels of at gas velocities close to turbulent fluid bed conditions (u_g>1.0 m/s). The size varies from 300 to 150 times d_p over the gas velocity range from 0.1 to 1.3 m/s. Similar to the results in chapter 6, the absolute values for the cluster size ranges from one to four centimetres, which is relatively large compared to the reactor diameter D_r=0.05 m. However, it should be noted that the trends in this figure show *apparent* sizes, assuming spherical shaped clusters. Incorporating the non-sphericity will lead to smaller cluster diameters. Besides, the non-sphericity most probably influences the gas-to-cluster mass transfer coefficient as well (see also appendix III of this thesis).

8 CONCLUSIONS

In this paper a regenerative, high-temperature process for coal gas desulfurization using a small particle diameter iron/molybdenum-oxide sorbent material (169 μm) is investigated. During the desulfurization as well as the oxidation step, gas velocities up to 1.3 m/s (which is close to the turbulent fluid bed regime) were applied in a batch-wise operated fluid bed at ambient pressures, which is equipped with an expanded top section to avoid excessive particle entrainment. The effect of (diluted) air during the oxidation on the subsequent sulfidation step is investigated, while in some experiments also a reduction step prior to the next sulfidation step of the sorbent is conducted. An almost constant sulfur absorption capacity of about 50% of the theoretical maximum at 100 ppmv H_2S-breakthrough was observed, independent on the oxygen concentration applied during the preceding oxidation step. During oxidation of the sorbent material with (diluted) air, a temperature increase of about 8 K/ vol.% O_2 was observed (ΔT_{ad}=108 K/ vol.% O_2). Pre-reduction of the sorbent after oxidation yields only a small increase in sulfur capacity, which means that the formation of sulfates during the oxidation reaction is negligible. Despite the severe operating conditions, no noticeable loss of sorbent material due to attrition or erosion was observed.

The sulfidation results are excellent, showing more than 99% sulfur removal, even at the highest gas velocities and moderate temperatures levels applied (675 K). Up to a fractional sorbent conversion X of 0.25, the sorption rates are so high that (external) mass transfer resistances still dominate the conversion rate. The gas-solids contacting (also for the high velocity regime) is much worse than expected on basis of individual gas-solid particle

contacting. This can be expected for a system which essentially remains a bubbling bed with the short-cutting due to bubbles.

These conclusions have been demonstrated by using a two-phase model with chemical enhancement. Re-evaluating the overall reaction rate constant for the presence of bubble-to-emulsion gas phase resistances indicate that, for the low X-values, the intrinsic reaction rates are controlled by the gas-to-particle mass transfer rates.

Similar to the model results presented in chapter 6, the calculated values for the effective cluster size are quite large, but not that unrealistic. Considering the simplicity of the cluster model (for example, all clusters have the same density and size and are spherical shaped), this approach seems the be promising in describing a high velocity fluid bed, because the presence of clusters corresponds more closely to the real structure of the turbulent bed.

ACKNOWLEDGEMENT

We acknowledge the financial support of the Dutch Ministry of Economic Affairs through the Netherlands Energy Research Foundation ECN. We also thank E. Middelink for his assistance in the experimental work. We are obliged to dr. ir. A.G.J. van der Ham for taking part in the discussions.

NOTATION

A	cross-sectional area of the reactor	m^2
b	stoechiometric coefficient of component B	-
C_A	molar concentration of reactant A in bulk fluid	mole m^{-3}
D	molecular diffusivity	$m^2\ s^{-1}$
d_p	average particle diameter	m
D_{eff}	effective diffusion coefficient in the dense phase	$m^2 s^{-1}$
E_{act}	activation energy	kJ $mole^{-1}$
Ha	Hatta number, equation 5	-
k	intrinsic reaction rate constant in the grain	m s^{-1}
k_g	mass transfer coefficient	m s^{-1}
k_m	mass exchange coefficient	m s^{-1}
k_{ov}	overall conversion rate, defined by equation 4	s^{-1}
k_r	reaction rate constant based on dense phase volume	s^{-1}
m_{H2S}	molecular weight of H_2S	kg $mole^{-1}$
m_S	molecular weight of sulfur	kg $mole^{-1}$
M_{bed}	amount of sorbent present in the bed	kg
N_c	cycle number	-
n_d	dilution ratio	-
Nu	Nusselt number	-
S	theoretical maximum sulfur capacity of the sorbent	6.6 wt.%
S_{100}	sulfur capacity at 100 ppmv breakthrough	wt.%
Sh	Sherwood number of the particle $k_g d_p/D$	-
t	time coordinate	s
T	temperature	K
t^+	stoechiometric time, see equation 1	s
u_g	superficial gas velocity	m s^{-1}
u_{mf}	minimum fluidization velocity	m s^{-1}
X	averaged fractional conversion of the sorbent	-
Y	non-dimensional gas phase concentration in the bulk C_A/C_{A0}	-
y_{O2}	volume fraction of gas during the oxidation step	vol.%
z	axial co-ordinate	m

$[H_2S]$	volume fraction of H_2S	ppmv
$[SO_2]$	volume fraction of SO_2	ppmv

Greek Symbols

β	solids concentration	-
χ	constant in equation 5	-
ΔT_{max}	maximum temperature rise during the oxidation step	K
ΔT_{ad}	adiabatic temperature rise	K
ϕ_{H2S}	molar H_2S flow rate	mole s^{-1}
ρ_B	density of the sorbent	kg m^{-3}
ρ_{H2S}	density of H_2S	kg m^{-3}
ξ	non-dimensional axial co-ordinate z/L_B	-
Ψ	non-dimensional time t/t^+	-

subscripts

g	grain
p	particle
max	maximum

REFERENCES

Abbasian J., Slimane R.B., Wangerow J.R., Ayala R.E., Venkataramani S., Flytzani-Stephanopoulos M., Cicero D.C., 1996, *Third Int. Symp. and exh. on Gas cleaning at high temperatures*, Karlsruhe, 18-20 Sept., 607

Arnaldos J., Casal J., 1996, Prediction of transition velocities and hydrodynamical regimes in fluidized beds, *Powder Technol.*, **86**, 285

Ayale R.E., Feitelberg A.S., Furman A.H., 1995, Development of a high-temperature moving bed coal gas desulfurization system, in: *Proceeding of the 12th annual international Pittsburgh coal conference* (edited by Chiang S.H.), University of Pittsburgh, 1053

Bi H.T., Grace J.R., 1995, Effect of measurement method on the velocities used to demarcate the onset of turbulent fluidization, *Chem. Engng. J.*, **57**, 261

Bi H.T., Grace J.R., Lim K.S., 1995, Transition from bubbling to turbulent fluidization, *Ind. Engng. Chem. Res.*, **34**, 4003

Bisschoff K.B., 1969, General solution of equations representing effects of catalyst deactivation in fixed-bed reactors, Ind. Engng. Chem. Fund., **8**, 665

Bureau A.C., Olden M.J.F., 1967, The operation of the Frodingham desulfurising plant at Exeter, *Chem. Engng.*, March, 55

Chehbouni A., Chaouki J., Guy C., Klvana D., 1994, Characterization of the flow transition between bubbling and turbulent fluidization, *Ind. Engng. Chem. Res.*, **33**, 1889

Chehbouni A., Chaouki J., Guy C., Klvana D., 1995, Effets de differents parametres sur le vitesses de transition de la fluidisation en regime turbulent, *Can. J. Chem. Engng.*, **73**, 41

Corman J.C., 1986, *System analysis of simplified IGCC plants*, U.S. Department of Energy Topical Report DOE/ET/14928-2233

Edwards M.S., 1979, H2*S-removal processes for low-BTU coal gas*, Department of Energy/Fossil contract no. W-7405-eng-26

Gangwal, S.K., 1991, Hot-gas desulfurisation sorbent development for IGCC systems, in: ICHEME Symp.Series, 123, 159

Geldart D., 1973, Types of gas fluidization, *Powder Technol.*, 7, 285

Heesink, 1994, *High temperature coal gas desulphurization: applying calcareous sorbents and fluidized bed contactors*, PhD thesis University of Twente

Ichikawa K., Kuwamata N., Kamei K., 1993, Development of a simultaneous sulfur and dust removal process for IGCC power generation system, in: *Proceedings of the 3rd Int. Symp. On gas Cleaning at high temperatures*, 419

Jain S.C., Gupta R., Gangwal S.K., 1991, Development of zinc ferrite sorbents for desulphurization of hot coal gas in a fluid-bed reactor, A.I.Ch.E. Summer Meeting, Pittsburgh, Pennsylvania, USA

Khara G.P., Delzer G.A., Kubicek D.H., Greenwood G.J., 1995, Hot gas desulfurization with Philips Z-Sorb sorbent in moving and fluidized bed reactors, *Environmental Progress*, 14, 146

Kimura H., 1994, *Test results of hot gas clean-up facility (desulfurization unit) for 200 t/d entrained flow coal gasification pilot plant*, intern report Ishikawajima-Harima Heavy Industries CO., Ltd.

Kobayashi S., 1990, *Test results of Yubari Hot gas desulfurization pilot plant*, Coal Conversion Technology Department Ishikawajima-Harima Heavy Industries Co. Ltd

Kohl A.L., Riesenfeld F.C., 1974, *Gas Purification*, 2th ed., Gulf Publishing Co., Houston, 343

Krambeck F.J., Avidan A.A., Lee C.K., Lo M.N., 1987, Predicting fluid-bed reactor efficiency using adsorbing gas tracers, *A.I.Ch.E.J.*, **33**, 1727

Kunii D., Levenspiel O., 1991, *Fluidization Engineering*, Butterworth-Heinemann, Boston

Kunii D., Suzuki M., 1967, Particle-to-fluid heat and mass transfer in packed beds of fine particles, *Int. J. Heat Mass Trans.*, **10**, 845

Lee G.S., Kim S.D., 1990, Bed expansion characteristics and transition velocity in turbulent fluidized beds, *Powder Technol.*, **62**, 207

Mazet N., Spinner B., 1992a, Modeling of gas-solid reactions. 1. Nonporous solids, *Int. Chem. Engng.*, **32**, 271

Mazet N., Spinner B., 1992b, Modeling of gas-solid reactions. 2. Porous solids, *Int. Chem. Engng.*, **32**, 395

Mojtahedi W., Abbasian J., 1995, H_2S removal from coal gas at elevated temperature and pressure in fluidized beds with zinc titanate sorbents: 1. cyclic tests, *Energy and Fuels*, 9, 429

Nakayama T., Araki S., Takahata E., Takahashi A., 1996, Development of hot gas cleanup technology for IGCC-technical trends of 3 types hot gas cleanup process., J. Japanese Inst. of Energy, 75, 351

NOVEM, 1990, *Systeemstudie hoge temperatuur gas reiniging bij KV-STEG-systemen*, Ref.nr. 90-310, Dossiernr. 8725-21421/500

Ranz W.E., Marshall Jr. W.R., 1952a, Evaporation from drop: part I, Chem. Eng. Prog., **48**, 141

Ranz W.E., Marshall Jr. W.R., 1952b, Evaporation from drop: part II, Chem. Eng. Prog., **48**, 173

Schrodt J.T. Hilton G.B., Rogge C.A., 1975, High-temperature desulfurization of low-CV fuel gas, *Fuel*, **54**, 272

Schrodt J.T., 1980, *Hot desulfurization I: use of gasifier ash in fixed bed process*, US DOE Report DOE/ET/10463-Ti, Washington DC.

Schrodt J.T., Best H.E., 1978, Sulfur recovery from fuel gas desulfurization sorbents, *A. I. Ch. E. Symp. Ser.*, **74**(175), 184

Schrodt J.T., Mohan C.P., 1981, Fuel gas desulfurization in fluidized-beds of gasifier waste ashes, *A. I. Ch. E.. Symp. Ser.*, **77**(211), 1

Suehiro M., Fujishima H., 1993, Fixed bed type hot gas cleanup technology for integrated coal gasification combined cycle power generation, in: *Fifth Japan/USA technical meeting on surface coal gasification*, October 13, Tokyo, Japan

Sugitani T., Kakai J., Yamamoto H., Kawai I., Kobayashi S., Ishii T., Hozumi S., 1987, Fundamental studies and present status of IHI hot gas desulfurization process, in: *International Conference on Coal Science* (edited by J.A. Moulijn *et al.*), 915

Szekely J., Evans J.W., Sohn H.Y., 1976, Gas-solid reactions, Academic Press, New York

Tamhankar S.S., Garimella S., Wen C.Y., 1985, Kinetic studies on the reactions involved in the hot gas desulfurization using a regenerable iron oxide sorbent-III. Reactions of the sulfided sorbent with steam and steam-air mixtures, *Chem. Engng. Sci.*, **40**, 1019

Tamhankar S.S., Hasatani M., Wen C.Y., 1981, Kinetic studies on the reactions involved in the hot gas desulfurization using a regenerable iron oxide sorbent-I, *Chem. Engng. Sci.*, **36**, 1181

Tseng S.C., Tamhankar S.S., Wen C.Y., 1981, Kinetic studies on the reactions involved in the hot gas desulfurization using a regenerable iron oxide sorbent-II, *Chem. Engng. Sci.*, **36**, 1287

Van der Ham A.G.J., Heesink A.B.M., Prins W., van Swaaij W.P.M., 1996, Proposal for a regenerative high-temperature process for coal gas clean-up with calcined limestone, *Ind. Engng. Chem. Res.*, 35, 1487

Van der Ham A.G.J., Venderbosch R.H., Prins W., van Swaaij W.P.M., 1996, Desulfurization processes of fuel gas and stagewise desulfurization, in: *Desulfurization of Hot Coal Gas with Regenerable Metal Oxide Sorbents: New Developments (NATO-ASI series)*, 7-19 July, in press

Van der Ham, 1994, *Regenerative high temperature desulfurization of coal gas in a circulating fluidized bed*, PhD thesis University of Twente

Van der Ham, A.G.J., Prins W., van Swaaij W.P.M., 1994, Regenerative, high temperature desulfurization of coal gas in a lab-scale circulating fluidized bed set-up, in: *Circulating Fluidized Bed Technology IV*, Pergamon Press, Canada

Van Swaaij W.P.M., Zuiderweg F.J., 1972, Investigation of ozone decomposition in fluidized beds on the basis of a two-phase model, in *Chemical reaction engineering*, Amsterdam, B 9-25

Van der Wal W.J.J., 1987, *Desulfurization of process gas by means of iron-oxide-on-silica sorbents*, PhD thesis University of Utrecht, the Netherlands

Van Yperen R., 1994, *On the high-temperature desulfurization of coal gas*, thesis University of Utrecht.

Venderbosch R.H., Van der Ham A.G.J., Prins W., 1997, Removal of H_2S from coal gas: effects of various parameters on the desulfurization efficiency, in: *Desulfurization of Hot Coal Gas with Regenerable Metal Oxide Sorbents: New Developments (NATO-ASI series)*, 7-19 July, in press

Werther J., 1980, Modeling and scale-up of industrial fluidized bed reactors, *Chem. Engng. Sci.*, **35**, 372

Westmoreland, P.R., Harrison D.P., 1976, Evaluation of candidate solids for high-temperature desulfurization of low BTU gases, *Env. Sci.Techn.*, **10**(7), 659

APPENDIX I

VERIFICATION OF MASS TRANSFER CONTROLLED CONVERSION RATES

ABSTRACT

In chapter 2 of this thesis it has been demonstrated that at T≥750 K the CO oxidation rates in a small packed bed are almost completely controlled by the external mass transfer rate. It was shown that the apparent reaction rate constant increases and the reaction order decreases with dilution, and this was explained by assuming that the packed bed is built up from particle clusters. In this appendix, model calculations are used to present further evidence for this assumption. To this end, the expression for the intrinsic reaction rate, presented in chapter 1 is used to evaluate the conversion rate controlling mechanism for a single particle, as well as for a cluster of particles.

INTRODUCTION

The conversion data in chapter 1, controlled by the intrinsic reaction kinetics, could be described by the rate expression:

$$R(c) = \frac{4.267 \cdot 10^{11} \exp\left(-\frac{75.41 \cdot 10^3}{RT}\right) \cdot c \cdot c_{O_2}}{\left(1 + 43.06 \exp\left(\frac{3.127 \cdot 10^3}{RT}\right) \cdot c\right)^2} \qquad (1)$$

with c and c_{O2} represent the carbon monoxide and oxygen concentration, respectively. Equation 1 can be extrapolated to higher temperatures to examine whether mass transfer resistances can be considered as the rate controlling step. For conversion of a gaseous reactant inside a porous (spherical) catalyst volume, the steady state differential mass balance is given in chapter 1:

$$\frac{\partial}{\partial r}\left(r^2 D_i \frac{\partial c}{\partial r}\right) - r^2 R(c) = 0 \qquad (2a)$$

with the boundary conditions:

$$r = 0\,;\ \frac{\partial c}{\partial r} = 0 \ \text{ and } \ r = R_i\ ;\ D_i \frac{\partial c}{\partial r} = k_g (c_\infty - c_i) \qquad (2b)$$

where the subscript i denotes the scale of the catalyst volume, either on particle scale i=p or the scale of a particle cluster i=cl.

PARTICLE SIMULATION

A numerical technique (a finite-difference technique with a Newton-Raphson method), similar to the one used in chapter 1, is applied to solve equation 1 for the LH-kinetics with respect to the carbon monoxide concentration, and excess of oxygen inside the particles. Although the reaction rate has been measured at much lower temperatures of up to T=475 K, extrapolation towards T=750 K is required in view of the operating conditions in chapter 2.

For the effective intra-particle diffusion coefficient a constant value of $D_p=10^{-5}$ m^2s^{-1} has been taken. Assuming that the particles are present as stagnant entities in the particle cluster, and that the highest value for the external mass transfer coefficient can be derived by assuming that $Sh_p=2$ (see chapter 2), a value for $Bi_p=2.4$ can be calculated.

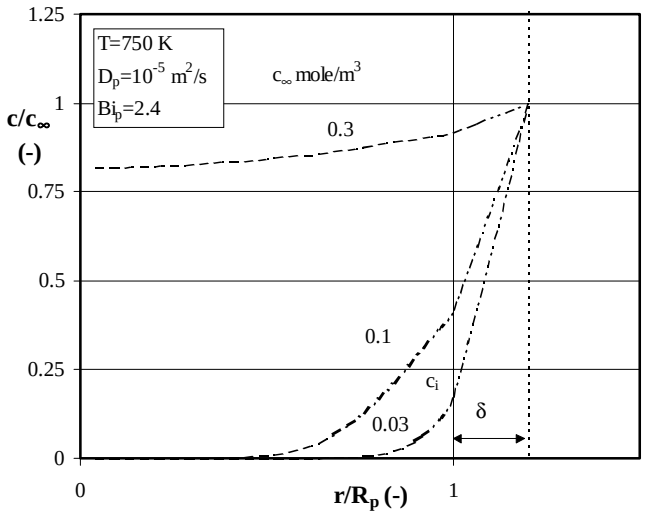

Figure 1. The carbon monoxide concentration inside the particle (d_p=52 μm) for a temperature of 750 K, and three reactant local concentrations outside the particles, ranging from c_∞=0.03 mole m^{-3} to c_∞=0.3 mole m^{-3}. The symbol δ represents the film thickness around the particle.

The equations are solved for particles with an average particle diameter of d_p=52 μm (details are presented in chapter 1). Typical results are presented in figures 1 and 2. In figure 1, the concentration profile inside the particle is plotted for a temperature of 750 K, and three local concentrations outside the particles, in the range from c_∞=0.03 mole m^{-3} up to c_∞=0.3 mole m^{-3}. Outside the particles, the concentration ratio c/c_∞=1, and over the boundary film, δ, a linear concentration profile has been assumed. For the presented concentration interval two extremes are plotted. For the lowest concentration outside the particle (and Bi_p=2.4), the concentration gradient is almost completely located in the boundary layer around the particle, and the reactant concentration strongly decreases with the position inside the particle. The conversion rate is almost completely controlled by the external mass transfer resistance. For the highest concentration outside the particle, the reactant concentration at the particle surface approximates the bulk concentration, and the concentration gradient inside the particle is less steep. In the latter case, the intrinsic reaction kinetics and internal diffusion of reactant are the rate controlling steps.
These effects can be summarized by plotting the ratio of the concentration at the surface over the bulk concentration c_i/c_∞ versus the concentration outside the particles (figure 2).

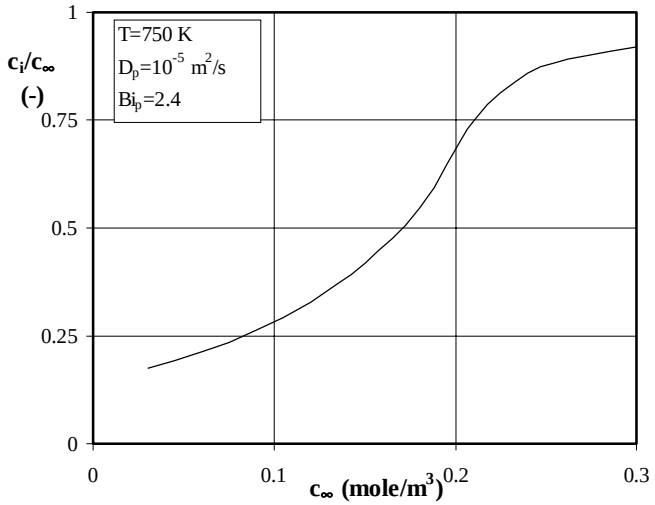

Figure 2. The ratio of the CO concentration at the surface of the particle c_i over the concentration around the particle c_∞ versus c_∞ for T=750 K, $D_p=10^{-5}$ m^2/s and Bi_p=2.4.

In chapter 1, it was already explained that the effect of the concentration on the curve in figure 2 is caused by the Langmuir-Hinshelwood type of reaction rate expression. Although figure 1 should be handled with great care (because equation 1 is extrapolated outside the range of operating conditions for which is was derived), it indicates that our conversion experiments for c_∞<0.10 mole/m^3 (0.6 vol.%) are obtained at (almost) mass transfer controlled conditions. This is also illustrated in figure 3. The calculated reaction rate R(c) is plotted as a function of the reactant bulk concentration. Similar to figure 4 of chapter 1, the particle reaction rate first increases with c_∞, and then passes a maximum (higher than the intrinsic reaction rate expression), after which it becomes completely controlled by the intrinsic reaction kinetics. For the lowest c_∞-value, the particle reaction rate is close to the one derived for complete mass transfer limitation ($R(c)=k_g c_\infty$ (with k_g derived from Bi_p and D_p) plotted as a straight line in figure 3.

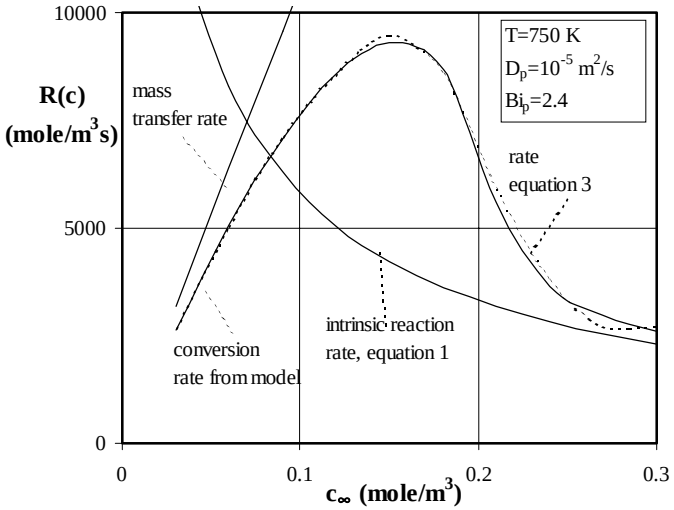

Figure 3. Numerically calculated reaction rate as a function of the concentration around the particle, for the LH kinetics of equation 1, a temperature T=750 K, and Bi_p=2.4. Indicated as solid lines are the curves for mass transfer controlled conditions (Sh_p=2), for the intrinsic reaction rate, equation 1, and the fitted reaction rate expression indicated by equation 3.

Figure 6a in chapter 2 shows that for n_d=80 and T=750 K, the apparent order in the reactant

is one over the carbon monoxide inlet concentration range $0.05<c_{in}<0.15$ mole/m^3 ($0.3<y_{in}<0.9$ vol.%). This corresponds to complete mass transfer limitation. However, the deviation from mass transfer limitation, shown in figure 2 to be about 20 % for c_{in}=0.03 mole m^{-3}, is substantially and much larger than experimentally observed. Apparently, equation 1 underestimates the intrinsic reaction rate for the higher temperatures.

In chapter 2 it was demonstrated that the order in carbon monoxide, evaluated for $0.05<c_{in}<0.15$ mole/m^3, decreases with increasing dilution ratio (figure 6a). In the packed bed experiments, it is also demonstrated that at T==750 K the apparent rate constant k_{ov} is increasing with the dilution ratio n_d. The increase in k_{ov} is particularly notable for the low CO inlet concentration c_{in}=0.05 mole/m^3, that is at the completely mass transfer controlled reaction rates, with a corresponding first order in the reactant (figure 7 of chapter 2). Both effect can not be explained on the scale of the individual particles.

CLUSTER SIMULATION

It is now interesting to investigate whether the presence of clusters can predict the shift in reaction order, and the increase in the reaction rate for the higher dilution ratios. In the analysis hereafter, it is assumed that the active particles are homogeneously distributed over the cluster volume. Equation 1, rewritten for the size of a cluster, is solved while assuming $D_{cl}=10^{-5}$ m^2/s. In these calculations, it is supposed that the local reaction rate on the scale of particles, which (according to figure 1 to 3) depends on the local concentration, can be derived from the curve fitted from the numerically derived conversion rate shown in figure 3:

$$R(c) = \left(8.29\cdot 10^{-4} - 2.25\cdot 10^{-4}\cdot c + 0.30\cdot c^2 - 2.05\cdot c^3 + 6.83\cdot c^4 - 8.54\cdot c^5\right)^{-1} \qquad (3)$$

First, and similar to figure 1, the concentration profile, but now for the particle cluster, is derived for a temperature of 750 K and for the lowest dilution ratio applied (n_d=80). The results are presented in figure 4.

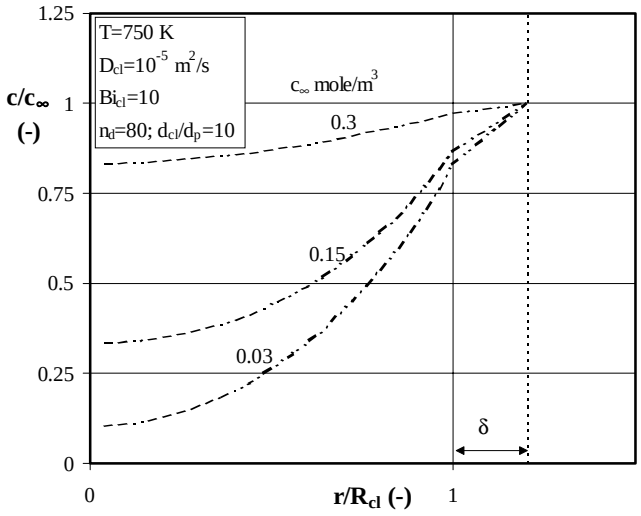

Figure 4. The carbon monoxide concentration inside the cluster (d_{cl}/d_p=10) for a temperature of 750 K, Bi_{cl}=10, n_d=80, and three reactant concentrations around the cluster c_∞, ranging from c_∞=0.03 mole m^{-3} to c_∞=0.3 mole m^{-3}. The symbol δ represents the film thickness around the cluster.

Figure 4 shows the profiles for three flow averaged concentrations around the cluster, c_∞, in the range from c_∞=0.03 to 0.3 mole m^{-3} (0.2 to 2 vol.%). Similar to figure 1, over the cluster boundary film δ, a linear concentration profile is assumed. For all c_∞-values applied (and Bi_p=10), the concentration decreases significantly inside the particle.

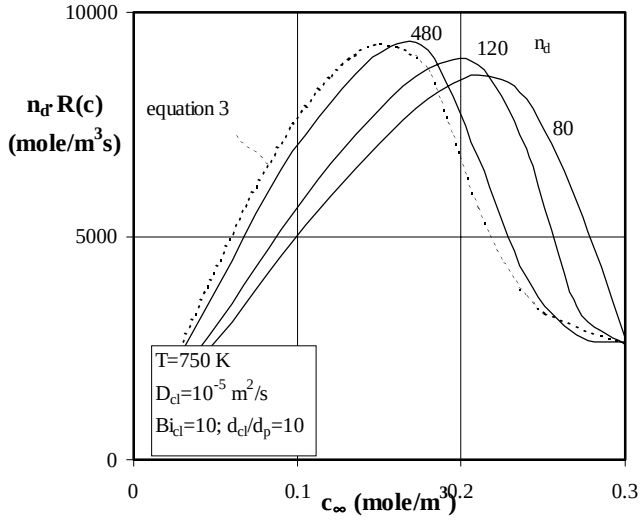

Figure 5. Numerically calculated reaction rate R(c), corrected for n_d, for the particle cluster as a function of the CO bulk concentration c_∞ for the kinetics of equation 3, a temperature T=750 K, n_d=80 to 480, and Bi_p=10. Indicated as a dashed line is also the curve for the fitted reaction rate, equation 3.

On the scale of clusters, the conversion rate is controlled only to a small extent by the gas-to-cluster mass transfer resistance, and mainly by the internal diffusion resistance inside the cluster. The apparent conversion rate R(c), derived from the cluster model, is plotted versus the concentration around the cluster in figure 5. Similar to figure 3, the conversion rate first increases with c_∞, reaches a maximum, and then levels off. The curve for the apparent reaction rate of the individual particles (equation 3), taking into account the dilution ratio n_d, has been plotted also. Compared to this fitted reaction curve, the maximum in the conversion rate curve shifts towards a higher c_∞-value at a lower dilution ratio. The height of the maximum in the cluster reaction rate decreases. The latter effect is due to the increased effect of diffusional resistances at the higher dilution ratios. The shift in the maximum towards the higher c_∞-values is due to the propagation of reaction in the cluster, causing the reactant concentration at a local position in the cluster to decrease. For a certain concentration range a higher conversion rate is derived than can be derived on basis of equation 3.

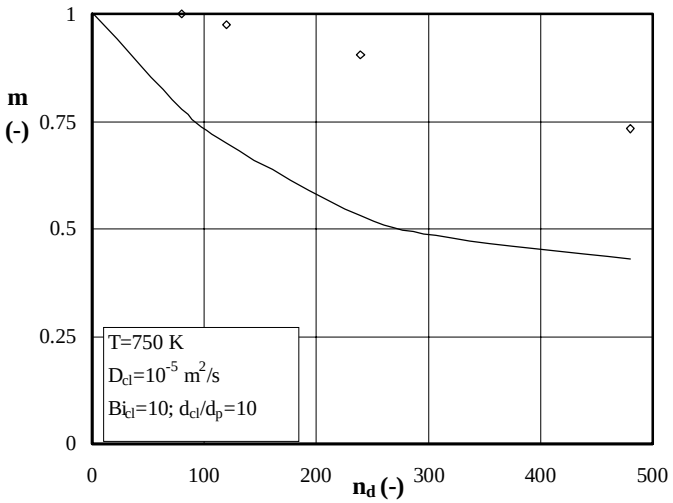

Figure 6. The numerically derived apparent order in the CO concentration, m, $R(c)=kc^m$, over $0.05<c_\infty<0.2$ mole/m^3 versus the dilution ratio n_d for effective cluster size $d_{cl}/d_p=10$ and $Bi_{cl}=10$. The symbols represent the experimentally observed order ($0.05<c_\infty<0.2$ mole/m^3) for u_g=0.6 m/s (chapter 2).

In chapter 1, it was already indicated that, when the intrinsic reaction and mass transfer resistances are interfering, (particle or cluster) effectiveness factors >1 can be calculated. For the extreme situation of $n_d=\infty$ (only a single catalyst particle), the calculated reaction rate curve approximates the particle reaction rate derived by equation 3. Figure 5 again shows that for the individual particles, the apparent reaction order is +1 for low bulk concentrations, while it becomes negative for the higher c_∞-values (> 0.15 mole/m^3). The apparent order of the reaction strongly depends on the concentration range over which it is evaluated, and can now be plotted versus the dilution ratio in figure 6, together with the experimental values reported in the chapter 2 for the concentration interval $0.05<c_\infty<0.15$ mole/m^3.

For a dilution ratio $n_d=1$, an effective order $m\approx1$ can be derived. For the higher dilution ratio, the apparent order decreases, because the intrinsic reaction rate affects the cluster reaction rate. The experimentally derived values for m are much higher than the calculated ones. From the results of the single particle simulations, it was already concluded that the reaction rate expression of equation 1 most probably underestimates the intrinsic reaction rates at T=750 K. Then, the influence of the mass transfer rate on the conversion is larger than predicted in figures 1 to 3, and the reaction rate expressions of equation 1 and 3 are conservative estimates for the particle reaction rate. The reaction rate curve plotted in figure 6, is mainly dominated by reaction kinetics, yielding values for m<1. It is expected that the difference between the experimental data points and the calculated model curve in figure 6 vanishes if the correct reaction rate expression (at T=750) would be available for the modelling.

CONCLUSIONS

In chapter 2, the presence of clusters in the packed bed were proposed to explain the increase in the apparent rate constant, k_{ov}, and the decrease in the reaction order, m, at higher dilution ratios, n_d. In the present calculations, the reaction rate expression derived in chapter 1 for 450<T<525 K, is extrapolated towards higher temperatures (T=750 K) to simulate the conversion on particle scale and on cluster scale. It is shown that the effect of dilution on the rate constant and on the reactant order can not be explained on the scale of the particle. It is caused by the formation of particle clusters.

APPENDIX II

INFLUENCE OF CLUSTER FORMATION ON MASS TRANSFER

ABSTRACT

A possible explanation for the strong decrease in mass transfer coefficients in various gas-solids contactors at low molecular Péclet numbers $Pé_m$ may be the formation of particle clusters. In this appendix a model is developed, based on the assumption that a packed or fluidized bed consists of particle clusters, surrounded by a flowing fluid. The transport of reactant inside such clusters is supposed to occur by molecular diffusion only. Its important parameters are the equivalent cluster diameter d_{cl} and n_d, the dilution of the active material with inert particles. The various effect of cluster formation on the apparent reaction rate constant are discussed. According to the model, dilution of the active material results in an increased apparent rate constant per unit volume of active material, which is due to the reduction of the intra-particle diffusional resistance caused by the decreased cluster reactivity. The apparent rate constant k_{ov} decreases for larger clusters, that is at higher values for the ratio of cluster-over-particle diameter d_{cl}/d_p. This can be partially explained by the decreased mass transfer rate to the cluster-surface, but mainly due to the higher internal diffusional resistance inside the cluster. The cluster model is able to predict the dramatic decrease in mass transfer numbers up to a factor of 10 to 20, observed in experimental studies at low $Pé_m$-numbers.

INTRODUCTION

Based on the observations by Moulijn and van Swaaij, and on the assumption that Sherwood and Nusselt numbers for the individual particle approach a constant value in the limiting case that the molecular Péclet number $Pé_m=0$, the following hypothesis is developed. In a system with only one active particle, surrounded by an inactive matrix, the observed mass transfer number might approach a constant value, close to the one, which can be calculated by the Ranz-Marshall equation (Ranz and Marshall, 1952). However, for an undiluted system in which all particles are active, the measured values for the mass transfer number (at low molecular Péclet) appears to be decades lower than the Ranz-Marshall values. Consequently, dilution of the active particles with inert material should result in higher values for the observed mass transfer number. In other words, the observed value for an apparent rate constant should be dependent on the dilution ratio n_d, defined as the total volume of inert particles over the volume of active particles.

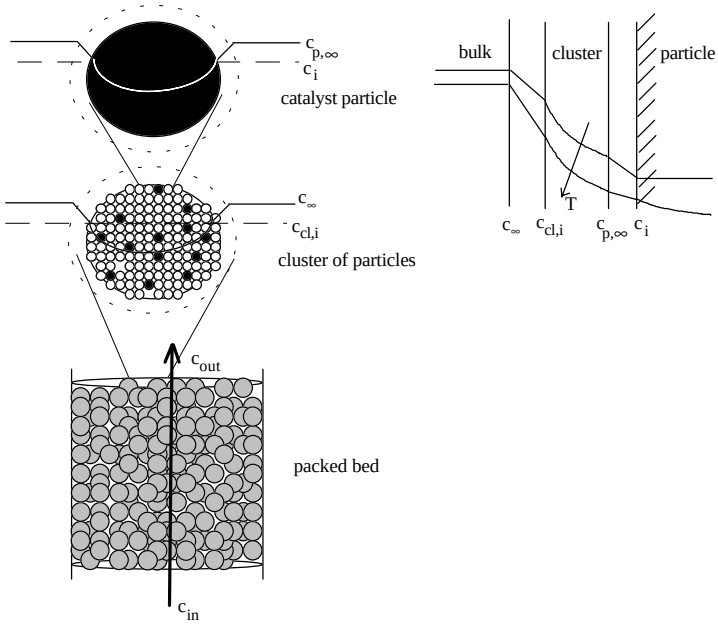

Figure 1. Schematic representation of the cluster model.

In our opinion, the strong decrease in mass and heat transfer coefficients in packed and/or fluidized beds could be caused by the formation of clusters of particles. To test this concept, a cluster model has been developed more or less similar to the agglomeration model proposed by Kunii and Suzuki (1967) and to the later models by Moulijn and van Swaaij (1976) and Verver (1984). It is schematically represented in figure 1. Due to the formation two additional resistances will become important: the gas-to-cluster mass transfer coefficient, and the intra-cluster diffusional resistance. Both will be introduced in the underlying model.

THEORY

In the following the equations for the cluster model will be derived.

For a single spherical particle with a specific conversion rate, R(c), the volume average pseudo-homogeneous concentration equation can be written as:

$$\frac{\partial}{\partial r}\left(r^2 D_p \frac{\partial c}{\partial r}\right) - r^2 R(c) = 0 \qquad (1)$$

where D_p is the effective diffusion coefficient inside a solid particle and r the intra-particle radial position.

With the appropriate boundary conditions and first order kinetics equation 1 can be integrated, yielding the particle effectiveness factor, or the degree of catalyst utilization η_p (see also Westerterp *et al.*, 1987). This parameter, defined as the ratio between the observed reaction rate and the reaction rate when all intra-particle and external concentration gradients are absent, can be given as:

$$\eta_p = \frac{\int_0^{V_p} R(c)dV_p}{R(c_\infty)} = \frac{Bi_p}{3\phi_p^2}\left(\frac{3\phi_p - \tanh(3\phi_p)}{3\phi_p + (Bi_p - 1)\tanh(3\phi_p)}\right) \qquad (2)$$

which, analogous to Froment and Bischoff (1990), can be rewritten as:

$$\frac{1}{\eta_p} = \frac{1}{\eta_p^*} + \frac{3\phi_p^2}{Bi_p} \text{ with } \eta_p^* = \frac{1}{3\phi_p^2}\left(\frac{3\phi_p - \tanh(3\phi_p)}{\tanh(3\phi_p)}\right) \qquad (3)$$

On basis of equation 2 or 3 the relation between the Thiele modulus ϕ_p and the effectiveness factor η_p can be plotted.

In chapter 1, equation 1 is numerically solved for power law and Langmuir-Hinshelwood kinetics.

Similar to the derivation of this single particle equations, the relations for a single (spherical) cluster can be derived, assuming that the active material is homogeneously distributed over the cluster volume. For a cluster containing n_d inert particles per active one, and assuming first order kinetics, it then follows that the reaction rate constant per unit volume of cluster equals:

$$k_{cl} = k_p \eta_p \frac{(1-\varepsilon_{cl})}{(1+n_d)} \qquad (4)$$

Here $(1-\varepsilon_{cl})$ is the solids volume fraction of the cluster, and n_d the dilution ratio, that is the ratio of the volume of inert solids over the volume of active material. The overall kinetic rate constant for the single particle $k_p\eta_p$ can be derived from equations 1 to 3. A similar result is obtained as for the single particle model:

$$\frac{1}{\eta_{cl}} = \frac{1}{\eta_{cl}^*} + \frac{3\phi_{cl}^2}{Bi_{cl}} \text{ with } \eta_{cl}^* = \frac{1}{3\phi_{cl}^2}\left(\frac{3\phi_{cl} - \tanh(3\phi_{cl})}{\tanh(3\phi_{cl})}\right)$$

$$\text{and } \phi_{cl} = \frac{d_{cl}}{6}\sqrt{\frac{k_{cl}}{D_{cl}}} \quad Bi_{cl} = \frac{k_{g,cl} d_{cl}}{2D_{cl}} \qquad (5)$$

After some rearrangements the relation for the apparent reaction rate constant is obtained as:

$$k_{ov} = \left(\frac{1}{\eta_{cl}^*} + \frac{3\phi_{cl}^2}{Bi_{cl}}\right)^{-1}\left(\frac{1}{\eta_p^*} + \frac{3\phi_p^2}{Bi_p}\right)^{-1} k_p = \eta_{cl}\eta_p k_p \qquad (6)$$

with $R(c)= k_{ov}c_\infty=\eta_{ov}k_pc_\infty$ taken as the overall production rate, the overall effectivity of the cluster, η_{ov}, can be written as:

$$\eta_{ov} = \left(\frac{1}{\eta_{cl}^*} + \frac{3\phi_{cl}^2}{Bi_{cl}}\right)^{-1}\left(\frac{1}{\eta_p^*} + \frac{3\phi_p^2}{Bi_p}\right)^{-1} \qquad (7)$$

If external mass transfer resistances are neglected (Bi_{cl}»1 and Bi_p»1) equation 7 becomes equal to the relation proposed by Örs and Dogu (1979) for the effectiveness factor in case of an isothermal first-order reaction taking place in a catalyst particle with a bidisperse pore structure.

Table I. Relations and constants used in the model.

parameter	expression
particle diameter	65 μm
bulk diffusion coefficients, Fuller *et al.* (1966)	$D = 3.16\cdot 10^{-8}\dfrac{T^{1.75}}{P\left(\nu_{CO}^{1/3}+\nu_{air}^{1/3}\right)^2}\left(\dfrac{1}{M_{CO}}+\dfrac{1}{M_{air}}\right)^{1/2}$
Knudsen diffusion coefficient	$D_{Knudsen} = 97\cdot r_{pore}\left(\dfrac{T}{M_{CO}}\right)^{1/2};\ r_{pore} = 2\cdot 10^{-8}\,m$
particle diffusion coefficient	$D_p = \dfrac{D_{Knudsen}\varepsilon_p}{\tau_p};\ \varepsilon_p = 0.54;\ \tau_p = \sqrt{2}$
cluster diffusion coefficient	$D_{cl} = \dfrac{D(1-\beta_{cl})}{\tau_{cl}};\ \tau_{cl} = \sqrt{2}$
particle mass transfer coefficient	$k_g = \dfrac{Sh_p D}{d_p};\ Sh_p = 2$
cluster mass transfer coefficient	$k_{g,cl} = \dfrac{Sh_{cl}D}{d_{cl}};\ Sh_{cl} = 2 + 1.8\left(\dfrac{\rho_g d_{cl} u_{cl}}{\eta_g}\right)^{1/2}\left(\dfrac{\eta_g}{\rho_g D}\right)^{1/3}$
reaction rate constant	$k_p = 2.75\cdot 10^{10}\exp\left(-\dfrac{91.5\cdot 10^3}{RT}\right)$
effective gas velocity	$u_{cl} = \dfrac{u_g}{\varepsilon} = \dfrac{u_g(1-\varepsilon_{cl})}{(\varepsilon-\varepsilon_{cl})}$

CLUSTER MODEL SIMULATIONS

To illustrate the effect of cluster formation on the apparent reaction rate constant k_{ov}, results of model simulations will be shown hereafter for such a first order reaction. The kinetic values and relations for additional parameters, such as Sherwood numbers and diffusion coefficients are already presented in table I. The gas-to-particle mass transfer rate to the particles in the clusters is estimated from Sh_p=2 (the minimum value in the Ranz-Marshall equation), although values much lower and slightly higher (up to Sh_p=3.89) have also been reported in the literature (Rexwinkel *et al.*, 1997).

All simulation are carried out by using an experimentally obtained expression (listed in table I) for the oxidation reaction of CO over a CuO/γ-alumina catalyst. The kinetics were determined in previous work by the present author (not reported in this thesis), but could be represented by a (simple) first-order reaction, in contrast to the kinetics of the oxidation reaction over a platinum catalyst.

As explained with the previous formulation of the cluster model, the total mass transfer resistance is composed of a contribution around and inside the individual particle plus a contribution around and inside the cluster of particles. All the figures 2 to 4 contain, as two base cases, the rate curve for complete reaction rate control ($k_{ov}=k_p$), and the one for the reaction and mass transfer in series, for a single (active) particle ($k_{ov}=k_p\eta_p$). Besides, a number of other curves are included which additionally account for the effect of cluster related mass transfer resistances.

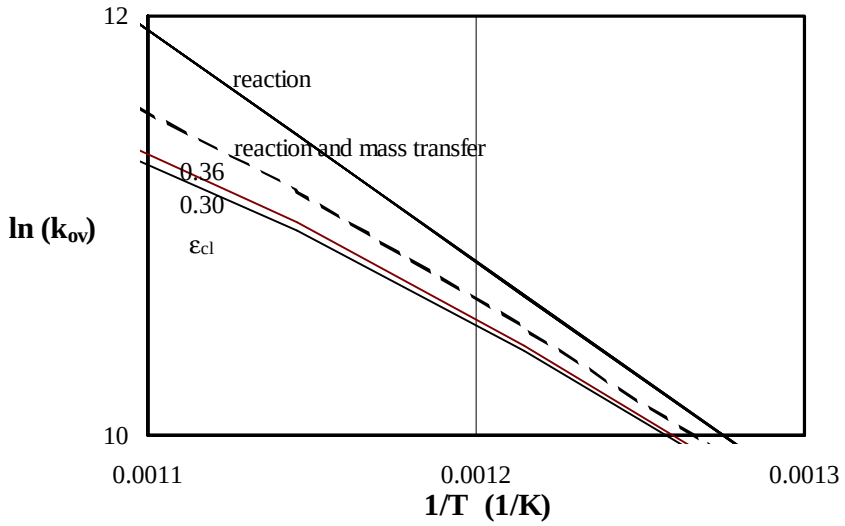

Figure 2. Cluster model simulation: dependence of the apparent rate constant k_{ov} on the inverse temperature T for two cluster porosities ε_{cl}=0.30 and ε_{cl}=0.36. The solid and dashed lines represent the intrinsic kinetics of a model reaction, ln(k_p), and the apparent rate constant for the mass transfer and reaction kinetics in series model, ln($k_p\eta_p$), respectively. Conditions: d_{cl}/d_p=10; n_d=100; u_g=0.6 m/s.

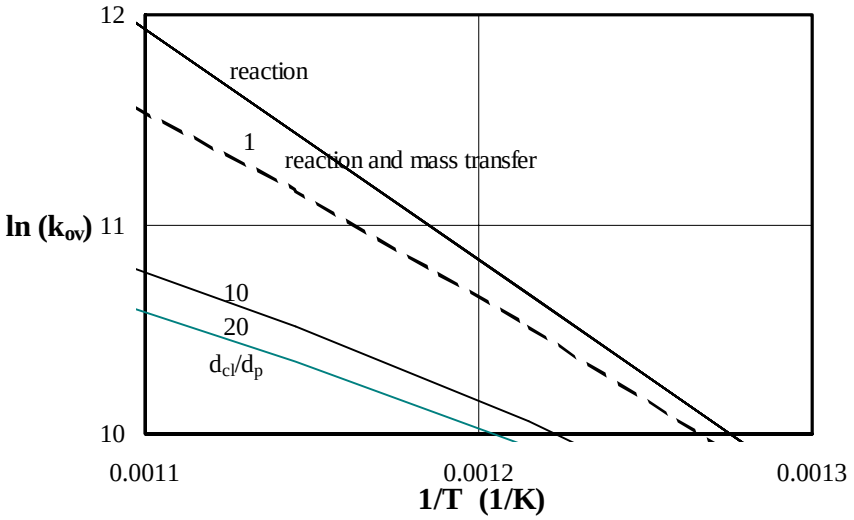

Figure 3. Cluster model simulation: dependence of the apparent rate constant k_{ov} on the inverse temperature T and three cluster-over-particle diameter ratios d_{cl}/d_p. The solid and dashed lines represent the intrinsic kinetics of the model reaction, ln(k_p), and the apparent rate constant for the mass transfer and reaction kinetics in series model, ln($k_p\eta_p$), respectively. Conditions: ε_{cl}=0.36; n_d=100; u_g=0.6 m/s.

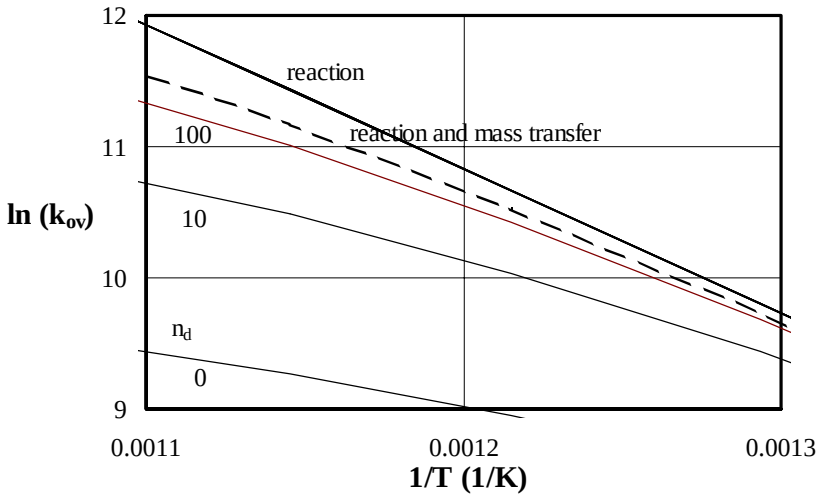

Figure 4. Cluster model simulation: dependence of the overall apparent rate constant k_{ov} on the operating temperature T for different dilution ratios n_d. The solid and dashed lines represent the intrinsic kinetics of the model reaction, $\ln(k_p)$, and the apparent rate constant for the mass transfer and reaction kinetics in series model, $\ln(k_p\eta_p)$, respectively. Conditions: d_{cl}/d_p =10; ε_{cl}=0.36; u_g=0.6 m/s.

These curves are meant especially to illustrate the effects of cluster porosity (figure 2), cluster-to-particle diameter ratio (figure 3) and the dilution ratio (figure 4).

Similar to mass transfer and reaction in series for an individual particle, the logarithmic value of the apparent rate constant, k_{ov}, plotted as a function of the inverse operating temperature, can show an increasing effect of mass transfer limitation at higher operating temperatures. Whereas all curves in figures 2 to 4 approach the intrinsic kinetics at low temperatures, at high temperatures they diverge, depending on the cluster porosity ε_{cl}, the cluster-to-particle diameter d_{cl}/d_p, and the dilution ratio n_d. Figure 2 illustrates the effect of ε_{cl} on the apparent rate constant. It shows that the influence of cluster porosity is of minor importance, because the possible variation in ε_{cl} is limited; the overall mass transfer number is affected only slightly by the cluster porosity. On the basis of these calculations a constant value for ε_{cl} of 0.36 has been assumed in the rest of this study.

The influence of the cluster size on the overall apparent rate constant is shown in figure 3. Mass transfer limitation starts at lower temperatures if the cluster-over-particle diameter ratio d_{cl}/d_p increases. The effect of increasing intra-cluster mass transfer limitation at higher temperatures is clearly visible, especially for larger cluster diameters.
The same explanation can be given for the effect of the dilution ratio n_d on the overall apparent rate constant illustrated in figure 4. An increase in the dilution ratio n_d results in smaller values for ϕ_{cl}, due to the decrease in k_{cl}. Consequently higher values for the cluster effectivity are obtained. The apparent rate constant calculated per unit volume of catalyst becomes higher, and this effect is illustrated in figure 5 and 6, where this rate constant is plotted as a function of the dilution ratio n_d and the cluster-over-particle diameter ratio d_{cl}/d_p, respectively. Obviously, an undiluted bed of particles (n_d=0) can yield much lower values for the apparent rate constant: observed mass transfer numbers can be more than a factor 10 to 20 lower than those that can be derived from ideal gas-solids contacting (d_{cl}/d_p=20). This factor is comparable with the decrease in observed mass transfer numbers in undiluted packed beds.
The experimental part of future work on gas-solids contacting is now aimed at determining values for the apparent rate constant k_{ov} as a function of n_d, and to present them in a way similar to figure 6.

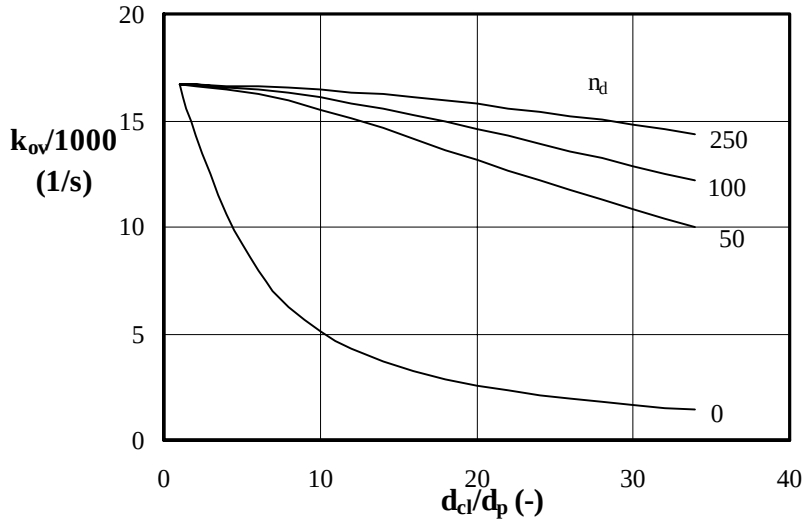

Figure 5. Cluster model simulation: dependence of the overall apparent rate constant k_{ov} on the cluster-over-particle diameter ratio d_{cl}/d_p for various dilution ratios n_d. Conditions: ε_{cl}=0.36; u_g=0.6 m/s; T=775 K.

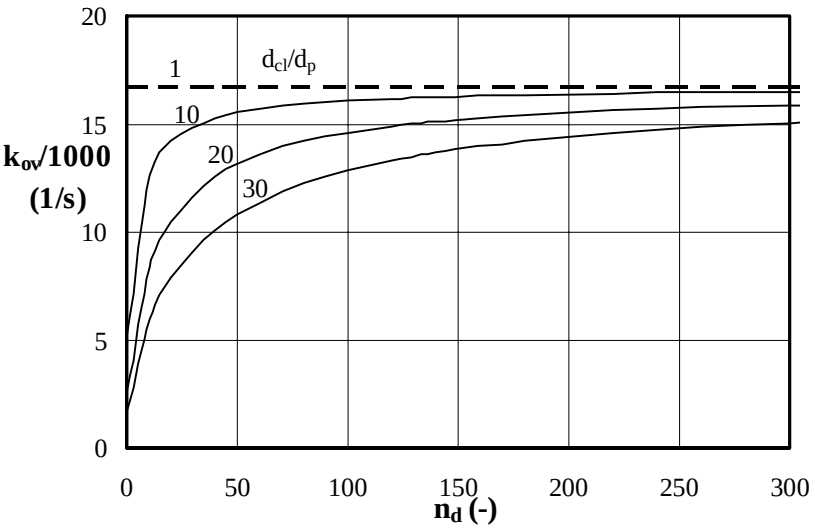

Figure 6. Cluster model simulation: dependence of the overall apparent rate constant k_{ov} on the dilution ratio n_d for different cluster-over-particle diameter ratios d_{cl}/d_p. Conditions: ε_{cl}=0.36; u_g=0.6 m/s; T=775 K.

As a general conclusion, the cluster model predicts that the overall rate constant, k_{ov} (defined per unit volume of active catalyst) increases at higher dilution ratios. This is due to the decrease in cluster reactivity. The effectivity of the cluster approaches 1 in the extreme case of infinite dilution.

Furthermore, the influence of the dilution ratio on k_{ov} becomes more pronounced for larger clusters, that is at higher values for the ratio of cluster-over-particle diameter d_{cl}/d_p. This can be explained by the increasing effect of limitation of mass transfer from reactant to the cluster-surface.

CONCLUSIONS

The strong decrease in mass and heat transfer numbers in gas-solids systems at low molecular Péclet numbers could be caused by the formation of clusters of particles. In this appendix a cluster model has been developed to test this concept. It is based on a homogeneously distribution of the active particles in an inert matrix, takes into account the agglomeration of particles, and is presented for first-order kinetics. Its important parameters are the equivalent cluster diameter d_{cl} and the dilution ratio n_d, the ratio of the volume of inert particles over the volume of active ones.

The model predicts that the apparent rate constant k_{ov}, defined per unit volume of catalyst, increases at higher dilution ratios. This is due to the reduction of the intra-particle diffusional resistance caused by the decreased cluster reactivity. In the extreme case of infinite dilution, the cluster effectivity approaches the value of 1. Another outcome of the model is concerned with the size of the clusters. The apparent rate constant k_{ov} decreases for larger clusters, that is at higher values for the ratio of cluster-over-particle diameter d_{cl}/d_p. This can be partially explained by the decreased mass transfer rate to the cluster-surface, but mainly to the increased diffusional resistances inside the cluster. In an undiluted bed (n_d=0), the apparent rate constant can be drastically reduced, up to a factor of 20 (d_{cl}/d_p=20), which is comparable with the decrease in mass transfer numbers observed in literature at low molecular Péclet numbers.

ACKNOWLEDGEMENT

We acknowledge the financial support of the Dutch Ministry of Economic Affairs through the Netherlands Energy Research Foundation ECN. We also acknowledge M.G.B. Bloem for his assistance in the theoretical and experimental work.

NOTATION

a	thermal diffusivity	$m^2\ s^{-1}$
Bi_{cl}	Biot number cluster $k_{g,cl}d_{cl}/(2D_{cl})$	-
Bi_p	Biot number particle $k_g d_p/(2D_p)$	-
c	reactant concentration	mole m^{-3}
c_∞	reactant concentration at bulk conditions	mole m^{-3}
c_i	reactant concentration at particle surface conditions	mole m^{-3}
D	bulk diffusion coefficient component	$m^2\ s^{-1}$
D_{cl}	effective diffusion coefficient in cluster	$m^2 s^{-1}$
d_{cl}	equivalent cluster diameter	m
$D_{Knudsen}$	Knudsen diffusion coefficient	$m^2\ s^{-1}$
d_p	average particle diameter	m
D_p	effective intra-particle diffusion coefficient	$m^2 s^{-1}$
k_{cl}	reaction rate constant per unit volume of cluster	s^{-1}
$k_{g,cl}$	mass transfer coefficient cluster	$m\ s^{-1}$
k_g	mass transfer coefficient particle	$m\ s^{-1}$
k_{ov}	apparent reaction rate constant	s^{-1}
k_p	intrinsic reaction rate constant	s^{-1}
M_i	molecular mass of component i	kg $mole^{-1}$
n_d	dilution ratio	-
P	operating pressure	N m^{-2}
$Pé_m$	molecular Péclet number $u_g d_p/D$	-
R	gas constant	J $mole^{-1}K^{-1}$
r	radial position inside the spherical particle	m

$R(c)$	molar rate of reaction per unit volume of catalyst	mole $m^{-3} s^{-1}$
Re	Reynolds number $\rho_g u_g d_p/\eta_g$	-
r_{pore}	radius of catalyst pore	m
Sc	Schmidt number $\eta_g/(\rho_g D)$	-
Sh_i	Sherwood number $k_{g,i} d_i/D$	-
T	operating temperature	K
u_{cl}	interstitial gas velocity around cluster of particle	m s^{-1}
u_g	superficial gas velocity	m s^{-1}
V_p	volume of particle	m^3
$\bar{\varepsilon}$	porosity accounting for existence of clusters	-
ε	porosity packed bed	-
ε_{cl}	cluster porosity	-
ε_p	particle porosity	-
ϕ_{cl}	Thiele modulus of a spherical cluster in equation 5	-
ϕ_p	particle Thiele modulus	-
η_{cl}	cluster effectiveness factor, defined by equation 5	-
η_{cl}^*	cluster effectiveness factor, defined by equation 5	-
η_g	gas viscosity	Pa s
η_p	particle effectiveness factor, defined by equation 2	-
η_p^*	particle effectiveness factor, defined by equation 3	-
ν_i	diffusional volume of component i	m^3mole^{-1}
ρ_g	gas density	kg m^{-3}
τ_{cl}	cluster phase tortuosity	-
τ_p	particle tortuosity	-

REFERENCES

Froment G.F., Bischoff K.B., 1990, *Chemical reactor analysis and design*, John Wiley & Sons, New York

Fuller E.N., Schettler P.D., Giddings J.C., 1966, A new method for predicting of binary gas phase diffusion coefficients, *Ind. Engng. Chem.*, **58**, 18

Hermann E., 1991, *Katalysierte Stickoxidreduktion in der stationären und zirkulerenden Wirbelschicht*, thesis University of Karlsruhe.

Hsiung T.H., Thodos G., 1977, Mass-transfer in gas-fluidized beds: measurement of actual driving forces, *Chem. Engng. Sci.*, **32**, 581

Kunii D., Suzuki M., 1967, Particle-to-fluid heat and mass transfer in packed beds of fine particles, *Int. J. Heat Mass Trans.*, **10**, 845

Kunii D., Levenspiel O., 1990, *Fluidization Engineering*, J. Wiley & Sons, New York

Langer G., Roethe A., Roethe K.P., Gelbin D., 1978, Heat and mass transfer in packed beds-III. Axial mass dispersion, *Int. J. Heat Mass Transfer*, **21**, 751

Martin H., 1978, low Péclet number particle-to-fluid heat and mass transfer in packed beds, *Chem. Engng. Sci.*, **33**, 913

Moulijn J.A., van Swaaij W.P.M., 1976, The correlation of axial dispersion data for beds of small particles, *Chem. Engng. Sci.*, **31**, 845

Örs, N., Dogu T., 1979, Effectiveness of bidisperse catalysts, *A.I.Ch.E.J.*, **25**, 723

Ranz W.E., Marshall Jr. W.R., 1952a, Evaporation from drop: part I, *Chem. Eng. Prog.*, **48**, 141

Ranz W.E., Marshall Jr. W.R., 1952b, Evaporation from drop: part II, *Chem. Eng. Prog.*, **48**, 173

Resnick W., White R.R, 1949, Mass transfer in systems of gas and fluidized solids, *Chem. Eng. Prog.*, **45**, 377

Rexwinkel G., Heesink A.B.M., Van Swaaij W.P.M., 1997, Mass transfer in packed beds at low Peclet numbers-wrong experiments or wrong interpretations ?, *Chem. Engng. Sci.*, **52**

Rietema K., 1991, *The dynamics of fine powders*, Elsevier Science, London

Turton R., Levenspiel O., 1989, An experimental investigation of gas-particle heat transfer coefficients in fluidized beds of fine particles, in *Fluidization VI*, edited by Grace J.R., Shemilt L.W., Bergougnou M.A., Engineering Foundation, 669

Verver A.B., 1984, *The catalytic oxidation of hydrogen sulphide to sulphur in a gas-solid trickleflow*, thesis

University Twente
Westerterp K.R., van Swaaij W.P.M., Beenackers A.A.C.M., 1987, *Chemical reactor design and operation*, John Wiley & Sons, New York
Yerushalmi J., Turner D.H., Squires A.M., 1976, The fast fluidized bed, *Ind. Engng. Process Des. Dev.*, **15**, 47
Yerushalmi J., Cankurt N.T., 1979, Further studies of the regimes of fluidization, *Powder Technol.*, **24**, 187

APPENDIX III

SIZE AND DENSITY ESTIMATION FOR PARTICLE CLUSTERS IN THE RISER OF A CFB SYSTEM

ABSTRACT

Clustering of the particles causes a serious by-passing of the reactant gas and a reduced accessibility of the catalyst particles. In this appendix, the results of hydrodynamic measurements and of conversion measurements for the oxidation of carbon monoxide over a Pt/γ-alumina catalyst (both obtained with a small scale riser set-up; ID 0.015 m, L=1.17 m), are interpreted by a combination of a terminal falling velocity approach and a proposed cluster model, to derive values for the apparent cluster size and its density.
Generally, the derived cluster diameter d_{cl} (varying from 30 to 70 times the particle diameter) does not depend very much on the average solids concentration β in the riser. The cluster density β_{cl} ($0.05<\beta_{cl}<0.5$) increases linearly at increasing average solids concentration, and the cluster then obviously becomes denser.
The above observations are confirmed by the results of conversion experiments for ozone decomposition, reported in the literature by Ouyang and co-workers.

INTRODUCTION

The differences between the gas and solids velocity (the so-called slip velocity) in riser systems can be over more than a decade higher than the terminal falling velocity of the individual particle. It is also recognized that the rate of gas-to-particle mass transfer in riser systems is much lower than expected if one assumes that the solids are transported as individual particles. In chapters 3 and 4, these observations were confirmed by measurements in a small scale riser set-up (ID 0.015 m, L=1.17 m). The measurements included both, the hydrodynamics and the mass transfer controlled conversion for CO oxidation over a Pt/γ-alumina catalyst. For example, the results presented in chapter 4 demonstrated that derived values for the non-dimensional mass transfer number Sh^0 were decades lower than those obtained when the particles are supposed to be contacted individually. In this chapter, it was noticed additionally that the local catalyst activity (varied by mixing highly active catalyst particles with similar but inert ones in ratios in between 150 and 2500) is an important parameter in the gas-solids contacting process. At a high local activity, the conversion rate per unit volume of (active) catalyst decreases significantly. This observation was confirmed by the analysis of data reported by Ouyang *et al.* (1995) for the kinetically controlled ozone decomposition reaction. The latter authors varied the local catalyst activity by changing the operating temperature.

The observed conversions are even lower than calculated for the extreme case of ideal gas phase mixing, and this shows that the reduced conversion could not be attributed solely to axial back-mixing of the gas. Another cause is responsible for this bad gas-solids contacting. It is quite reasonable that cluster formation is the essential feature of the suspension in the riser set-up. Several authors visualized clusters of 50 to 60 μm FCC particles in risers operated at low gas velocities and very low solids fluxes (Arena *et al.*, 1989; Zou *et al.*, 1994; Horio and Kuroki, 1994; Kuroki and Horio, 1994; Tsukada *et al.*, 1997).

Local gas by-passing as a result of the specific hydrodynamic conditions in a riser reactor affects the chemical conversion of a gaseous reactant as well. From a hydrodynamic point of

view, the momentum is transferred from the bulk gas to particle agglomerates instead of to the individual particles; high slip velocities are then likely to occur. For the special case of riser systems, momentum transfer takes place in the same direction as gas-to-particle mass (or heat) transfer, and therefore conversion processes are also subject to the consequences of cluster formation. In effect, two additional transfer resistances may arise, apart from any possible mass transfer limitation over the gas film around each individual particle. One is related to the transfer of reactant from the main gas bulk to the cluster surface, and the other to transport by diffusion inside such a cluster. Figure 1 illustrates a situation of gas-to-cluster mass transfer, and subsequent diffusion through the cluster in parallel with a) single particle conversion controlled by the catalyst reactivity or b) single particle conversion controlled by particle boundary layer diffusion.

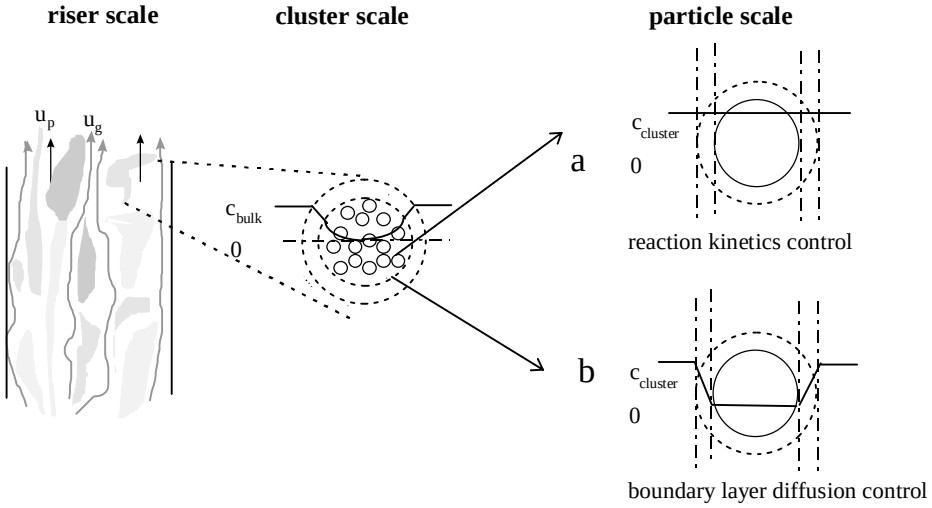

Figure 1. Possible local concentration profiles due to cluster formation for a) particle reaction controlled by the intrinsic reaction kinetics, and b) particle reaction controlled by boundary layer diffusion.

Both, our data in chapter 4 as well as those of Ouyang and co-workers (1995), can be interpreted analogous to the Thiele modulus analysis for a single catalyst particle which is characterized by a particle effectiveness factor. A cluster Thiele modulus ϕ_{cl} can be defined on basis of the cluster properties, together with the belonging cluster effectiveness factor η_{cl}. The local reaction rate constant k_{cl} required in the cluster Thiele modulus is then equal to $k_{cl}=k_p\eta_p\beta_{cl}/(1+n_d)$. For the conditions applied by Ouyang et al. n_d is taken to be zero (undiluted system), while η_p is one (complete particle utilization) and k_p represents the catalyst reactivity. For our own work at the highest temperatures applied, the value of $k_p\eta_p$ can be derived from the theoretical value of $Sh_p=2$ according to the conditions of mass transfer controlled conversion rates on the scale of the individual particle.
Obviously, values for a cluster Thiele modulus and for the gas-to-cluster mass transfer coefficient $k_{g,cl}$ require a precise knowledge of both the cluster size and density; they are expected to be influenced by the superficial gas velocity through the riser and the average solids concentration.

If only hydrodynamical data are analyzed, either the cluster density or the cluster diameter can be derived. Yerushalmi (1978) overcame the closure of this problem by assuming that the solids concentration in a cluster is equal to the solids concentration at minimum fluidization conditions. Horio and Ito (1996) developed a model in which gas around the cluster was supposed to form bubbles moving upwards. The size of these virtual gas bubbles were calculated with a correlation which was similar to the one derived for the

bubbling fluidization regime. The cluster diameter could then be estimated on basis of geometrical considerations, and the cluster density on the hydrodynamic conditions.

In this appendix, both, the cluster diameter and density are estimated by a combination of results of hydrodynamic measurements and those of conversion experiments carried out in the same experimental facility. By assuming that the clusters have a uniform structure (which is supported by visual measurements of Horio and Ito, 1996), it is then possible to derive simultaneously values for the cluster diameter and its density. The momentum and mass balances over a cluster are applied to interpret the hydrodynamic and conversion rate data of the own measurements concerning the oxidation of carbon monoxide (mass transfer controlled particle conversion; see figure 1a), as well as the data of the ozone decomposition measurements by Ouyang and co-workers (kinetically controlled particle conversion see figure 1b).

THEORY

A consistent estimation of the size and density of clusters in a riser is possible by combining an analysis of the hydrodynamic situation with a Thiele modulus evaluation (the 'cluster model') of conversion measurements. First, the formulation of the relevant equations needed to construct a cluster-diameter versus cluster-solids-concentration curve on basis of the results of hydrodynamic measurements is presented in section 2.2. Then, in section 2.3, it will be explained how a second d_{cl} versus β_{cl} curve can be derived from the interpretation of the CO conversion measurements with the cluster model. The intersection of both curves obtained should then yield the unique values of d_{cl} and β_{cl} aimed at.

Cluster flow hydrodynamics

The formation of cluster in risers causes channelling of gas through the riser. Following Yerushalmi *et al.* (1978), the gas-solids interaction can be represented by a configuration in which the particles are segregated in spherical clusters of a certain diameter, d_{cl}, with a cluster solids concentration, β_{cl} (it was assumed by these authors that β_{cl} = 0.4). Representing the volumetric concentration of clusters in the reactor by ~~β~~, its value can be calculated on basis of the average solids concentration and the cluster solids concentration: ~~β~~=β/β_{cl}. The slip velocity of the clusters is then given by

$$u_s = \frac{u_g}{(1-\beta)} - \frac{G_s}{\rho_p \beta} \qquad (1)$$

This slip velocity is directly related to the drag force, C_d, that is exerted by the gas upon the clusters, and the following relation can be derived for the terminal falling velocity of such a cluster:

$$u_{t,cl} = \sqrt{\frac{4 g_x d_{cl} \rho_{cl}}{3 \rho_g C_d}} \qquad (2)$$

In this equation ρ_{cl} represents the cluster density $\rho_{cl}=\rho_p\beta_{cl}+\rho_g(1-\beta_{cl})$ and C_d the cluster drag coefficient. A relation for the drag coefficient for spherical particles, $C_{d,0}$, is provided by Schiller and Naumann (1935):

$$C_{d,0} = \frac{24}{Re_{cl}}\left[1 + 3.6 \cdot Re_{cl}^{0.687}\right] \qquad (3a)$$

However, it seems unreasonable to assume that clusters in a riser are spherical; sphericities far from 1 are more likely (strand-like clusters). This has been noticed in the literature as

well. Ishii *et al*. (1989), for example, suggested the occurrence of spherical nose clusters, while Zou *et al*. (1994) defined a 'roundness factor' for the cluster as the ratio of its perimeter over the perimeter of a sphere with the same surface area. From visual observations, they derived roundness factor values ranging from below 2 for small clusters, up to values higher than 10 for the larger ones. According to Li *et al*.'s (1991) visual observations, most clusters in the central part of the riser column are strand-like, while clusters near the wall are essentially spherical. The non-sphericity of the cluster structure has a strong effect on the drag force exerted by the gas on the cluster. Usually, the sphericity is defined as the ratio between the surface of the sphere and the actual surface of the particle with the same volume. Following this approach, and taking the cluster diameter d_{cl} as the diameter of a sphere which has the same volume as the particle cluster, Haider and Levenspiels (1989) equation for the drag coefficient of a non-spherical (smooth) particle can be applied:

$$C_d = \frac{24}{Re_{cl}}\left[1 + (8.17e^{-4.07\psi_s}\right] \cdot Re_{cl}^{0.096+0.557\psi_s} + \frac{73.7\,Re_{cl} \cdot e^{-5.07\psi_s}}{Re_{cl} + 5.38 \cdot e^{6.21\psi_s}} \qquad (3)$$

with Re_{cl} being the Reynolds number based on the cluster diameter and the cluster slip velocity, and ψ_s representing the sphericity of the cluster. In effect, for constant size and density particles a larger terminal velocity is calculated for the non-spherical particle than for the spherical ones. Similar to Yerushalmi (1978), the Richardson-Zaki equation (1954) is now introduced to account for the hindered settling effects due to the proximity of other clusters.

$$u_s = u_{t,cl}(1-\beta)^m \qquad (4a)$$

Here, m is the Richardson-Zaki index, which is a function of the Reynolds number based upon the terminal velocity of the cluster:

$$m = \begin{cases} 4.65 & Re_{t,cl} < 0.2 \\ 4.4 \cdot Re_{t,cl}^{-0.03} & 0.2 < Re_{t,cl} < 1 \\ 4.4 \cdot Re_{t,cl}^{-0.1} & 1 < Re_{t,cl} < 500 \\ 2.4 & Re_{t,cl} > 500 \end{cases} \qquad (4b)$$

Cluster model interpretation of conversion measurements

Conversion data can be interpreted by equations derived from the mass balances over the cluster and catalyst particle (see figure 1). These equations have originally been derived for the interpretation of CO conversion measurements in a small packed bed reactor (chapter 2 and appendix I of this thesis). In riser systems, the remaining unknown parameters are the cluster diameter d_{cl} and its solids concentration β_{cl}. Unfortunately, the interpretation of conversion data requires the assumption of particles and clusters to be spherical, due to the absence of any relations for coefficients of mass transfer to non-spherical particles. For the case of catalyst dilution it is further assumed that the active material is homogeneously distributed over the cluster volume. The following equation for the apparent reaction rate constant can then be obtained for an intrinsically first order reaction:

$$k_{ov} = \left(\frac{1}{\eta_{cl}^*} + \frac{3\phi_{cl}^2}{Bi_{cl}}\right)\left(\frac{1}{\eta_p^*} + \frac{3\phi_p^2}{Bi_p}\right)k_p = \eta_{cl}\eta_p k_p \qquad (5)$$

k_{ov} represents the experimentally observed reaction rate constant *per unit volume of active catalyst*, and η_p and η_{cl} are defined in appendix II.

The contact efficiency in a reactor, η, can be defined as the ratio of the observed conversion rate over the theoretical maximum one, both defined per unit volume of catalyst (see the introduction of this thesis). If the conversion rate is dominated by the presence of clusters, like in a riser reactor, this contact efficiency is derived as the product of the cluster efficiency and the particle efficiency, $\eta=\eta_{cl}\eta_p$. For spherical clusters, the expression for the cluster efficiency is presented in equation. The application of these equations for riser systems can be justified by the interpretation of the experimental results published in the literature by approximate calculations. For simplicity, it is then assumed that the cluster diameter d_{cl} is constant and independent of the average solids concentration in the riser, while the cluster density increases linearly with the solids concentration in the riser $\rho_{cl}\propto\beta$. The effective cluster diffusivity, D_{cl}, is further related to the gas diffusion coefficient by $D_{cl}\propto D\cdot(1-\beta)$. These assumptions are validated by the experimental results to be discussed later. The following rough simplifications can be derived for ϕ_{cl} and Bi_{cl}:

$$\phi_{cl} = K_1\sqrt{\frac{k_p\beta}{(1-\beta)}} \quad \text{and} \quad Bi_{cl} = \frac{K_2}{(1-\beta)} \tag{6}$$

Here, K_1 and K_2 are then supposed to be approximately constant. Two asymptotic values can now be derived. At low values for the local reactivity (equal to $k_p\eta_p\beta/(1+n_d)$ for our mass transfer controlled CO conversion experiments), that is when $\phi_{cl}=(d_{cl}/6)\sqrt{(k_{cl}/D_{cl})}\ll 1$, the cluster effectiveness factor η_{cl} approaches a value of 1. If the cluster efficiency is correlated to the solids concentration in the riser in an empirical way, according to $\eta\propto\beta^m$, the value of m approaches 0 in case of low values for the local catalyst activity. Such low activities are obtained at low local catalyst activities (catalyst dilution, or low operating temperatures) or by conducting the experiments at very low solids concentrations. On the other hand, when $\phi_{cl}\gg 1$ (and $Bi_{cl}\gg 1$), and $\eta_{cl}\approx 1/\phi_{cl}$, m will approach the value of -0.5. This is exactly what has been derived for the CO conversion experiments reported in chapter 4. The value for m shifted from -0.37 to -0.5 when going from high to low dilution ratios. For the literature data of Ouyang *et al.*, a similar observation has been noticed. The value for m decreases down to m=-0.5 for the experiments conducted at the higher temperatures. Other literature data provide additional support for this conclusion. Van der Ham *et al.* (1991) and later Vollert and Werther (1994) observed that their mass transfer coefficients (which can also be directly related to η) depend on β with a power m ranging from -0.48 to -0.57 (the smallest value belonging to the lower gas velocities). This is expected if high conversion rates are considered. On the other hand, for the low reactivity experiments of Pagliolico *et al.* (1992), the conversion could be well described by the plug flow model, and $m\approx 0$. Clearly, the dependency of the contact efficiency on the solids concentration in the riser can be reasonably explained by the existence of clusters.

Coupling of hydrodynamic with conversion data

If the intrinsic kinetics and the conversion rate are known, the combination of equations 1 to 4 for the hydrodynamic model with equation 5 for the cluster model should yield a unique solution for d_{cl} and β_{cl}. The aim of this work is to derive values of the cluster solids concentration and the cluster diameter on basis of the hydrodynamics and conversion results. Before this can be done properly, additional parameters (such as the diffusion coefficients, and the intrinsic kinetics or the intrinsic mass transfer rate) should be known on beforehand. In table I, the values and relations for these additional parameters as used in this work are summarized.

Table I. Relations and constants used in particle and cluster model. All parameters are calculated for the oxidation of carbon monoxide as the model reaction.

parameter	expression
bulk diffusion coefficients Fuller *et al.* (1966)	$D = 3.16 \cdot 10^{-8} \frac{T^{1.75}}{P\left(\nu_{CO}^{1/3} + \nu_{air}^{1/3}\right)^2} \left(\frac{1}{M_{CO}} + \frac{1}{M_{air}} \right)^{1/2}$
Knudsen diffusion coefficient	$D_{Knudsen} = 97 \cdot r_{pore} \left(\frac{T}{M_{CO}} \right)^{1/2}$; $r_{pore} = 2 \cdot 10^{-8}\,m$
particle diffusion coefficient	$D_p = \frac{D_{Knudsen} \varepsilon_p}{\tau_p}$; $\varepsilon_p = 0.54$; $\tau_p = \sqrt{2}$
cluster diffusion coefficient	$D_{cl} = \frac{D(1-\beta_{cl})}{\tau_{cl}}$; $\tau_{cl} = \sqrt{2}$
particle mass transfer coefficient	$k_g = \frac{Sh_p D}{d_p}$; $d_p = 65\mu m$; $Sh_p = 2$
cluster mass transfer coefficient	$k_{g,cl} = \frac{Sh_{cl} D}{d_{cl}}$; $Sh_{cl} = 2 + 0.6 \left(\frac{\rho_g d_{cl} u_g}{\eta_g} \right)^{1/2} \left(\frac{\eta_g}{\rho_g D} \right)^{1/3}$

The procedure for the estimation of the cluster size and density proposed here is as follows: if the solids concentration in the riser is known, equations 1 to 4 are used to derive a first relationship between the cluster diameter d_{cl} and its density (or β_{cl}). Then, knowing the conversion rate (or k_{ov}) and the intrinsic reaction kinetics, equation 5 yields a second relation between the two unknown cluster properties. The intersection of these two curves eventually yield unique values.

RESULTS

Figure 2 is a diagram of the cluster diameter versus the cluster's solids concentration for a base case conversion experiment with β=0.02, u_g=3.5 m/s and n_d=250. For this particular experiment a conversion corresponding to a value of Sh^0=0.40 was observed:

$$\frac{\partial u_g A C_A}{\partial x} = -k_{ov} C_A \frac{\beta A \Delta L}{(1+n_d)} \Rightarrow k_{ov} = -\frac{u_g (n_d+1)}{\beta \Delta L} \ln\left(\frac{c_{out}}{c_{in}} \right) \Rightarrow Sh^0 = \frac{k_{ov} d_p^2}{6D} \qquad (7)$$

The experimental details are described in chapter 4. Two curves are derived from the hydrodynamics of the riser (equations 1 to 4), viz. for two different cluster sphericities, ψ_s=0.5 and ψ_s=1.0 respectively.

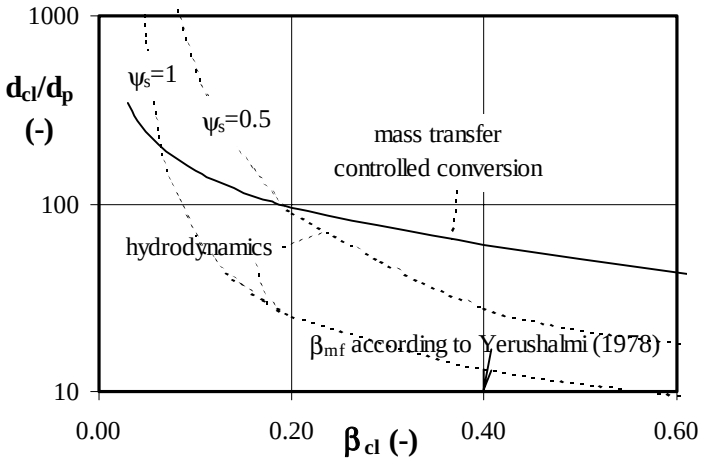

Figure 2. The calculated cluster over particle diameter, d_{cl}/d_p, as a function of the cluster solids concentration, β_{cl} for a base case conversion experiment. The solid line represents equation 5 for the interpretation of the conversion rate, and the dotted lines are derived from equation 1 to 4 of the hydrodynamics evaluation for two cluster sphericities, ψ_s=0.5 and ψ_s=1.0; experimental conditions: u_g=3.5 m/s; β=0.02; T=773 K; n_d=2500; Sh^0=0.40.

The third one represents the result derived from the cluster model interpretation for the case of single particle conversion controlled by particle boundary layer diffusion (Sh^0=0.4, see figure 1b). As expected, figure 2 shows for all three curves that d_{cl}/d_p decreases with increasing β_{cl}. This is in agreement with the result achieved by by Horio and Ito (1996) who published a similar curve for the relation between d_{cl} and β_{cl}. If only the results of hydrodynamic measurements are used to derive d_{cl}, while assuming that β_{cl} equals the solids concentration at minimum fluidization conditions, relatively low values for d_{cl} will be derived (Yerushalmi *et al.*, 1978; $d_{cl}\approx$1 mm). In this appendix, β_{cl} and d_{cl} are obtained from the point of intersection of the curve from the hydrodynamic evaluation, with the one of the cluster model interpretation of CO conversion. As a result, considerably lower values for β_{cl} and higher values for d_{cl}/d_p are derived (for ψ_s=0.5: $\beta_{cl}\approx$0.20 and $d_{cl}\approx$5 mm). This point of intersection shifts towards unrealistic (high) values for d_{cl} and (low values) for β_{cl} if the sphericity of the cluster is taken to be one. A value for d_{cl} in the order of 5 mm is in accordance with earlier observations (see for example Ishii *et al.*, 1989). However, in comparison with the applied reactor diameter (0.015 m), this value seems to be quite high. One should realize, however, that clusters with a sphericity considerably lower than one can be quite elongated. For example, for a particle cluster with d_{cl}=2 mm and a length of 10 cm, an apparent cluster diameter d_{cl}=8 mm with a sphericity of ψ_s=0.36 can be calculated. In a 0.2 m I.D riser Tsukada *et al.* (1997) visualized cluster chains of more than 0.2 m, even at very low solid fluxes. For a 0.05 m ID riser set-up, Horio and Ito (1996) calculated values for d_{cl}= 5 to 12 mm, with β_{cl}=0.05 to 0.15 respectively. They state that clusters of roughly several centimeters can still exist in a very dilute suspension. As a conclusion, the values for d_{cl}/d_p calculated in the present work are not unrealistic.

In our approach, it is assumed that the decrease of the effective Sherwood number, reported in the earlier papers, is due to the mutual shielding of active particles. In case of extremely high dilution ratios, this shielding effect was shown to disappear, and at the higher n_d-values higher corresponding Sherwood numbers were derived.
The effect of the interpretation of the experiments conducted at similar operating condition but with different catalyst dilution ratios, is illustrated in figure 3. Similar to the results

presented in figure 2, the calculated cluster over particle diameter, d_{cl}/d_p, is plotted as a function of the cluster solids concentration, β_{cl} for various dilution ratios (with their corresponding experimental Sh^0-value).

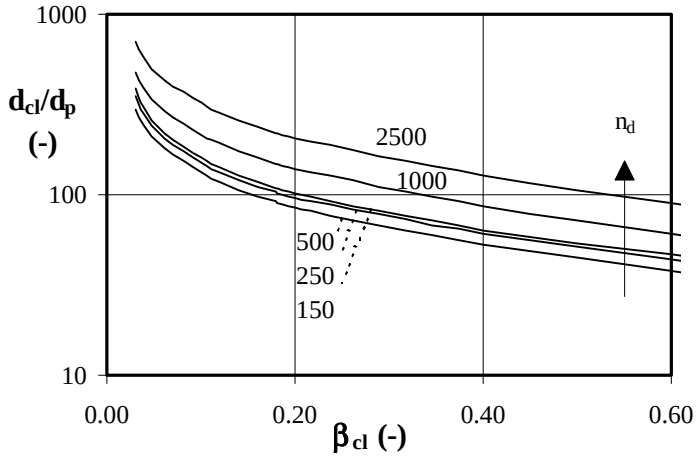

Figure 3. The calculated cluster over particle diameter, d_{cl}/d_p, as a function of the cluster solids concentration, β_{cl} for the CO conversion experiments at different dilution ratios. The lines represent equation 5 with the experimental conditions of u_g=3.5 m/s, β=0.02 and T=773 K and various dilution rations n_d.

All the lines in figure 3 again represent equation 5, which has been used to interpret the results of the experiments performed at different dilution ratios (n_d=150 to 2500), but otherwise the same base-case conditions of β=0.02, u_g=3.5 m/s. The observed values for Sh^0, belonging to the lines presented in figure 3, range from 0.4 to 0.7 for n_d=150 to n_d=2500 respectively. Plotted in a single figure, it was expected that all the solids lines would coincide, because theoretically, the plot of d_{cl} versus β_{cl} should be independent on n_d. At the dilution ratios n_d<500 this is approximately the case. The interpretation of the mass transfer controlled conversion data then yield a more or less unique line, confirming the validity of the cluster model. Unfortunately, for the higher dilution ratios, the deviation with the line calculated for n_d<500 is significant. Obviously, for n_d>500, the model is not valid anymore, perhaps because the averaging of the conversion rate constant over the entire cluster is then incorrect.

The analysis presented in this paper provides a qualitative rather than a quantitative picture on the formation of clusters in riser systems. Uncertainties in the derived cluster properties are caused by one or more of the following reasons:

- the diffusional shielding on particle level is not taken into account, which results in an overestimation of the particle Sherwood numbers. In the next parts of this paper, this diffusional shielding on particle scale has been taken into account by assuming that the value for k_g can be calculated from:

$$Sh_p=Sh_{p,0}\cdot(1-\beta_{cl})/\tau_{cl}=2\cdot(1-\beta_{cl})/\tau_{cl}\approx 2\cdot(1-\beta_{cl})^{1.5} \qquad (8a)$$

- for the interpretation of the CO conversion measurements with the cluster model, it has been assumed that the clusters are spherical. This is obviously not the case; in the present work, hereafter, a correction factor is introduced for the gas-to-cluster mass transfer coefficient $k_{g,cl}$ namely:

$$Sh_{cl}=C_d/C_{d,0}\cdot Sh_{cl,0} \qquad (8b)$$

- a constant value for the cluster sphericity is assumed, although it is likely that ψ_s depends on the solids concentration in the riser as well.

- due to experimental errors, there is quite some scatter in the data obtained.

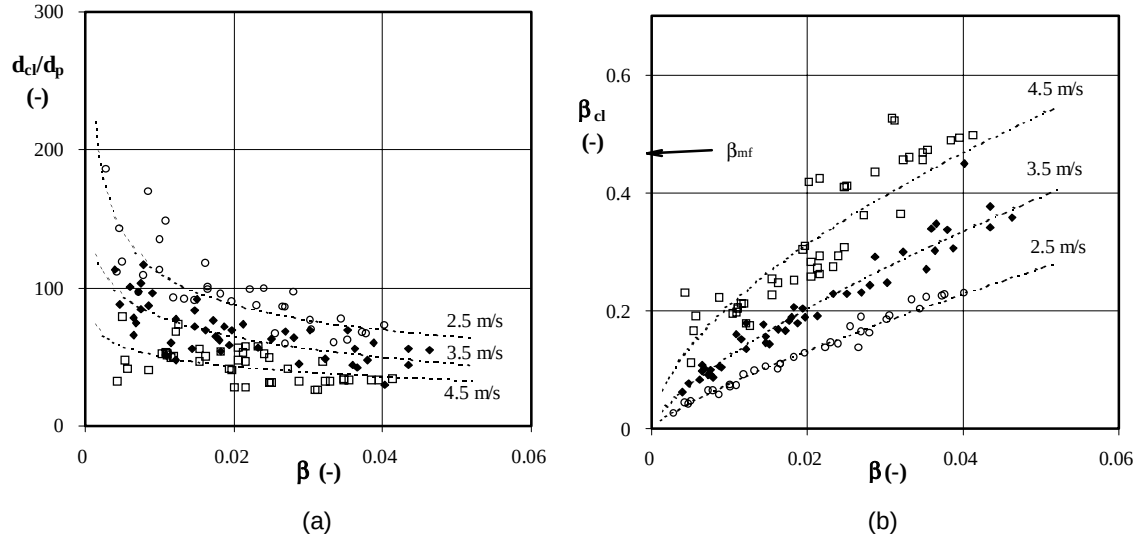

Figure 4. The apparent cluster diameter, d_{cl}, (a) and the cluster solids concentration, β_{cl}, (b) at different reactor solids concentrations, calculated by combination of equations 1 to 5 for the experimental conversion experiments at a dilution ratio of n_d=250. A cluster sphericity of ψ_s=0.7 is assumed. The dashed lines only represent the trends in the results

Upon introduction of the above corrections according to equations 8a and 8b, the intersection of the hydrodynamical curve and the one for mass transfer controlled conversion of CO shifts towards lower values for the cluster diameter, and higher values for the cluster solids concentration. On basis of all the experimental data obtained for n_d=250, the cluster diameter, d_{cl}, and the cluster solids concentration, β_{cl}, have been calculated by combination of equations 1 to 8, with ψ_s=0.5. The result is presented in figure 4, where these parameters have been plotted against the average solids concentration in the riser. Figure 4a shows that, initially, the size of the cluster strongly decreases with the solids concentration in the riser, but then approaches an almost constant value, which depends on the gas velocity. The d_{cl}-values range from 4 mm a gas velocity of 2.5 m/s, to 2 mm at u_g=4.5 m/s. At increasing gas velocities, smaller (figure 4a) but also denser (figure 4b) clusters are calculated. Figure 4b further shows that, at the low riser solids concentrations, the cluster porosity, β_{cl}, is significantly smaller than the solids concentration at minimum fluidization velocity ($\beta_{mf}\approx$0.45). It is then almost linearly dependent on the solids volume fraction, β. At the higher solids concentration in the riser, the cluster solids concentration levels off to a more or less constant value.

Apparently, at low solids concentration (or lower gas velocities), the clusters are larger but more diluted; at increasing solids concentrations (or higher gas velocities) the clusters become smaller, but denser. The influence of the riser solids concentration on the cluster size found in the present work is in close agreement with the visual observation of clusters by Tsukada *et al.* (1997). Defining the cluster size as the distance between the outer surface of the tails, they showed that average cluster sizes have a tendency to decrease with increasing riser solids concentration. However, and contrary to our calculations, these authors observed larger clusters at the higher gas velocities.

The trends in figure 4 are only indicative, since the absolute values of these parameters are strongly dependent on the assumptions concerning the values of Sh and ψ_s. Nevertheless, two interesting phenomena can be observed:

- According to the model, clusters are shown to exist already at very low values of β. This is exactly what has been observed in hydrodynamic and mass transfer studies reported in the literature. Already at very low values for the riser hold-up, large slip velocities and very low values for the mass transfer coefficients were observed. Apparently, even at low values for the hold-up, the particles are still not transported individually.
- From the analysis in the previous section, concerning the dependency of the contact efficiency on the solids concentration according to $\eta \propto \beta^m$, it appeared that the value for m ranges from 0 down to -0.5 This conclusion was derived by assuming that i) the cluster diameter is independent on solids flux and ii) the cluster solids concentration is linearly dependent on the average hold-up in the riser. Figure 4 shows that these assumptions are indeed valid at riser solids concentration β>0.02.

INTERPRETATION OF THE RESULTS OF OUYANG *et al.*

In studies where chemical reactions are considered, overall conversion rates are usually compared with the ones calculated from a reactor model taking into account the intrinsic reaction kinetics, reactor geometry, and operating conditions. Ouyang and co-workers performed conversion experiments for the ozone decomposition reaction in a 0.254 m ID riser, applying similar particles. The data of Ouyang *et al.* can also be analyzed on basis of the presented cluster model. Similarly to figure 4, the cluster diameter, d_{cl}, and the cluster solids concentration, β_{cl}, can then be plotted as a function of the solids concentration β in the reactor for different gas velocities. Unfortunately, the experimental data of Ouyang and co-workers are widely spread. To avoid most of the scatter, their data were first analyzed with respect to the effect of various operating parameters, by which a correlation could be derived as a best fit of the experimental results:

$$\eta = \frac{k_{ov}}{k_p} = 0.103 \cdot \beta^{-0.491} \cdot k_p^{-0.295} \cdot u_g^{0.389} \qquad (9)$$

Figure 5 shows the results obtained by reanalysis of Ouyang *et al.*'s data on basis of the theory presented in this paper. A cluster sphericity of ψ_s=0.70 has been used although a larger reactor (diameter) was applied by Ouyang *et al.* Their data for the lowest gas velocities (viz. u_g=2 m/s) are not included in this plot, because it seems that the belonging experiments are conducted in the turbulent fluid bed regime, rather than the riser regime.

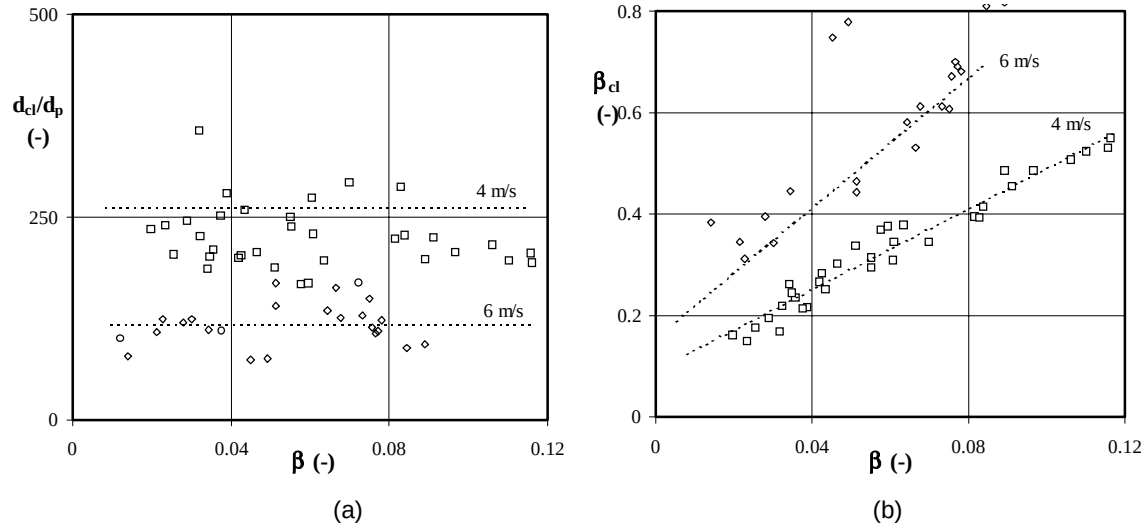

Figure 5. The calculated cluster over particle diameter, d_{cl}/d_p (a) and the cluster solids concentration, β_{cl}, (b) for different reactor solids concentrations, calculated by combining equation 1 to 5 for the data provided by Ouyang and Potter (1995), ψ_s=0.70. The dashed lines only represent the trends. Legend: □ 4 m/s; ◊ 6 m/s

The results of figure 5 show that the apparent cluster diameter is almost independent of the solids concentration. The value for d_{cl} is in the range of 1 to 2 cm, values which are approximately 4 times those derived from the analysis of our own data. Evidently, this is caused by the smaller riser set-up used in our work. However, such high values are still in good agreement with earlier publications. The cluster solids concentration increases almost linearly as a function of the average solids concentration in the reactor, and values ranging from 0.1 up to 0.6 are calculated. The conclusions derived from these calculation are in close agreement with our own results (for comparison see figure 4).
Again it should be emphasized state that the trends are only indicative, since the absolute values of the cluster parameters are strongly dependent on the assumptions for Sh^0 and ψ_s. It should be noticed further that Ouyang *et al.* conducted their ozone decomposition experiments without distinguishing between the developed region or the acceleration region, which leads to high values for the apparent cluster diameters.

CONCLUSIONS

Both, the present work concerning the CO conversion in a small riser set-up, and the Ouyang *et al.*'s data for the ozone decomposition in a much larger riser set-up, can be well interpreted by the cluster model. The results from the applied interpretation method are in close agreement. The following conclusions can be summarized:

- Clusters are likely to be the main causes for the strong decrease in gas-solids contacting in fast fluidized bed reactors.
- The cluster model formulated in this work is able to predict the relation between the gas-solids contacting and the solids hold-up in risers of fast fluidized bed systems. From simple calculations it is shown that, assuming $\eta \propto \beta^m$, at low values for the local conversion rate and/or solids concentration m=0, while for higher values m shifts towards -0.5. This observation is supported by data from other authors.
- On basis of this model apparent values for the cluster diameter, d_{cl}, or the cluster solids concentrations, β_{cl}, can be derived as a function of the gas velocity and the riser solids concentration. It is shown that these values are strongly dependent on the sphericity of such clusters. In general the following trends can be found: i) the cluster diameter is roughly independent on the solids concentration for β>0.02, but increases at lower gas velocities, and ii) the cluster solids concentration is linearly dependent on solids concentration; its values increase with gas velocity. The (relatively) high values derived for the cluster diameter can be explained by the high value of the sphericity. The cluster sphericity remains an important parameter in the interpretation of contact efficiency.

NOTATION

c	concentration	mole m^{-3}
Bi_{cl}	Biot number cluster $k_{g,cl}d_{cl}/(2D_{cl})$	-
Bi_p	Biot number particle $k_g d_p/(2D_p)$	-
C_d	drag coefficient for an isolated particle	-
$C_{d,0}$	drag coefficient for an isolated spherical particle	-
D	molecular diffusion coefficient	$m^2 s^{-1}$
$D_{Knudsen}$	Knudsen diffusion coefficient	$m^2 s^{-1}$
d_{cl}	effective cluster diameter	m
D_{cl}	effective intra-cluster diffusion coefficient	$m^2 s^{-1}$
d_p	average particle diameter	m
D_p	effective intra-particle diffusion coefficient	$m^2 s^{-1}$
g	gravitational constant	m s^{-2}
G_s	solids flux	kg m^{-2} s^{-1}

K_1, K_2	constants in equation 6	-
k_{cl}	reaction rate constant per unit volume of cluster	s^{-1}
k_g	gas-to-particle mass transfer coefficient	m s^{-1}
$k_{g,cl}$	gas-to-cluster mass transfer coefficient	m s^{-1}
k_p	reaction rate constant based on catalyst volume	s^{-1}
k_{ov}	measured reaction rate based on catalyst volume	s^{-1}
m	dependency of contact efficiency on solids hold-up or the Richardson-Zaki index in equation 4a	-
M_i	molecular weight of component i	kg $mole^{-1}$
n_d	dilution ratio	-
P	pressure	Pa
Pr	Prandtl number $\eta_g/(\rho_g a)$	-
Re	Reynolds number based on slip velocity $\rho_g u_s d_p/\eta_g$	-
$Re_{t,cl}$	Reynolds number based on cluster velocity $\rho_g u_{t,cl} d_{cl}/\eta_g$	-
r_{pore}	radius of catalyst pore	m
Sc	Schmidt number $\eta_g/(\rho_g D)$	-
Sh^0	experimentally observed Sherwood number, defined by equation 7	-
Sh_i	particle Sherwood number $k_g d_i/D$	-
$Sh_{i,0}$	particle Sherwood number according to the Ranz-Marshall equation	
T	operating temperature	K
u_g	superficial gas velocity	m s^{-1}
u_s	slip velocity	m s^{-1}
$u_{t,cl}$	terminal falling velocity of a cluster	m s^{-1}
$\bar{\beta}$	average cluster hold-up	-
β	average solids concentration	-
β_{cl}	average solids concentration of a cluster	-
ε_p	particle porosity	-
ϕ_{cl}	Thiele modulus of a spherical cluster	-
ϕ_p	particle Thiele modulus	-
η	contacting efficiency	-
η_{cl}	cluster effectiveness	-
η_{cl}^*	cluster effectiveness	-
η_g	gas viscosity	Pa s
η_p	particle effectiveness	-
η_p^*	particle effectiveness	-
λ	heat conductivity	$Wm^{-1}K^{-1}$
ν_i	diffusional volume of component i	m^3 $mole^{-1}$
ψ_s	sphericity of the particle or cluster	-
ρ_g	gas density	kg m^{-3}
ρ_p	particle density	kg m^{-3}
ρ_{cl}	cluster density	kg m^{-3}
τ_{cl}	cluster phase tortuosity	-
τ_p	particle tortuosity	-
subscript		
cl		cluster
p		particle

REFERENCES

Arena U., Cammarota A., Marzocchella A., Massimila L., 1989, Solids flow structures in a two-dimensional riser of a circulating fluidized bed, *J. Chem. Engng. Japan*, **22**, 236

Fuller E.N., Schettler P.D., Giddings J.C., 1966, A new method for predicting of binary gas phase diffusion coefficients, *Ind. Engng. Chem.*, **58**, 18

Haider A., Levenspiel O., 1989, Drag coefficient and terminal velocity of spherical and non-spherical particles, *Powder Technol.*, **58**, 63

Horio M., Ito M., 1996, Prediction of cluster size in circulating fluidized beds, in: *Preprints of the 5th international Conference on Circulating Fluidized Beds*, Beijing, P.R. China, DGS22

Horio M., Kuroki H., 1994, Three-dimensional flow visualization of dilutely dispersed solids in bubbling and circulating fluidized beds, *Chem. Engng. Sci.*, 49, 2413

Ishii H., Nakajima T., Horio M., 1989, The clustering annular flow model of circulating fluidized beds, *J. Chem. Engng. Japan*, **22**, 484

Kuroki H., Horio M., 1994, The flow structure of a three-dimensional circulating fluidized bed observed by the laser sheet technique, in: *Proceedings of the 4th international Conference on Circulating Fluidized Beds* (edited by Avidan A.A.), Hidden Valley, USA, 77

Li H., Xia Y., Tung Y., Kwauk M., 1991, Micro-visualization of clusters in a riser, *Powder Technol.*, **66**, 231

Ouyang S., Li X.-G., Potter O.E., 1995a, Circulating fluidized bed as a catalytic reactor: experimental study, *A.I.Ch.E.J.*, **41**, 1534

Ouyang S., Li X.-G., Potter O.E., 1995b, Investigation of ozone decomposition in a circulating fluidized bed on the basis of a core-annulus model, in *Preprints of the international symposium of the engineering foundation: Fluidization VIII*, 457

Ouyang S., Potter O.E., 1993a, Consistency of circulating fluidized bed experimental data, *Ind. Engng. Chem. Res.*, **32**, 1041

Ouyang S., Lin J., Potter O.E., 1993b, Ozone decomposition in a 0.254 m I.D. diameter circulating fluidized bed reactor, *Powder Technol.*, **74**, 73

Ouyang S., Potter O.E., 1994, Modelling chemical reaction in a 0.254 m I.D. circulating fluidized bed, in *Circulating Fluidized Bed Technology IV*, Pennsylvania, Engineering Foundation, 422

Pagliolico S., Triprigan M., Rovero G., Gianetto A., 1992, Pseudo-homogeneous approach to CFB reactor design, *Chem. Engng. Sci.*, **47**, 2269

Ranz W.E., Marshall Jr. W.R., 1952a, Evaporation from drop: part I, *Chem. Eng. Prog.*, **48**, 141

Ranz W.E., Marshall Jr. W.R., 1952b, Evaporation from drop: part II, *Chem. Eng. Prog.*, **48**, 173

Richardson J.F., Zaki W.N., 1954, Sedimentation and Fluidisation: Part I, *Trans. Instn Chem. Engng.*, 32, 35

Schiller L., Naumann A., 1935, Uber die grundlegenden Berechnungen bei der Schwerkraftaufbereitung, *Z. Ver. Dtsch. Ing.*, **77**, 318

Tsukada M., Ito M., Kamiya H., Horio M., 1997, Three-dimension imaging of particle-clusters in dilute gas-solid suspension flow, *Can. J. Chem. Engng.*, **75**, 466

Van der Ham A.G.J. Prins W., van Swaaij W.P.M., 1991, Hydrodynamics and mass transfer in a regularly packed circulating fluidized bed, in *Circulating Fluidized Bed Technology III*, Pergamom Press, Oxford, 605

Vollert J., Werther J., 1994, Mass transfer and reaction behaviour of a circulating fluidized bed reactor, *Chem. Engng. Technol.*, **17**, 201

Westerterp K.R., van Swaaij W.P.M., Beenackers A.A.C.M., 1987, *Chemical reactor design and operation*, John Wiley & Sons, New York

Yerushalmi J., Cankurt N.T., Geldart D., Liss B., 1978, Flow regimes in vertical gas-solid contact systems, *A.I.Ch.E.Symp.Ser.*, **176**, 1

Zou B., Li H., Xia Y., Ma X., 1994, Cluster structure in a circulating fluidized bed, *Powder Technol.*, **78**, 193

SUMMARY

Cleaning (like desulfurization) of the coal gas in a IGCC power plant is required to avoid harmful emissions, and protect the gas turbine against damage by corrosion. It is usually done by means of wet gas cleaning. However, the application of a hot dry gas cleaning process (> 623 K) improves the overall efficiency of the IGCC plant significantly. Iron oxide (deposited on for example FCC), is shown to be a suitable sorbent material for high-temperature removal of H_2S and COS. It is mechanically strong and can easily be regenerated with (diluted) air. Due to the fact that the desulfurization and regeneration reactions are very fast, the sorbent particles should be small for a complete utilization. In a continuous process including H_2S/COS absorption and sorbent regeneration, two reactor vessels are required between which an exchange of sorbent must be maintained. On basis of the above conditions, it is interesting to consider a fluid bed reactor system like being used in FCC. The solids are then a.o. circulated through a riser reactor (absorber), cyclones, a stand pipe, a turbulent fluid bed (regenerator) and a return leg.

For the design of such reactors, or for the interpretation of experimental results by theoretical models, it is important to know the degree of contact between the reactant gas and sorbent particles. Especially in case of cleaning processes like the considered desulfurization, when the concentration of an undesired component in a large gas flow (short contact times) must be reduced to an extremely low level, the contact efficiency is a critical factor which must be carefully controlled.
Unfortunately, the literature does not provide a consistent picture with respect to this issue. On the one hand it has been observed for conventional bubbling fluid bed reactors that the contact efficiency can be quite poor. At the same time, it is often stated that the exchange of mass and heat between gas and solids is high in fast fluidization.

This PhD-work is meant to determine the contact efficiency experimentally for fluidization of fine particles over a wide range of superficial gas velocities (d_p<200 μm and 0.1<u_g<4.5 m/s) in bench scale units. A special measuring method has been developed based on the application of rapid oxidation of carbon monoxide over a Pt-catalyst, as a model reaction. For this reaction, it can be recognized immediately whether the conversion is determined by the intrinsic reaction kinetics or by any mass transfer processes. A change of the conversion rate controlling mechanism corresponds to a large change in the reaction order of CO, viz. from minus one to plus one.
As a second tool of this study, dilution of the active catalyst with similar but inert particles has been used to investigate the influence of the local reaction rate on the contact efficiency.

First, the CO oxidation has been carried out in a small fixed bed of fine particles to verify the reaction kinetics, but also to estimate the contact efficiency for various conditions. Subsequently, the CO oxidation measurements have been carried out in a fluid bed (operated at various superficial gas velocities, just below and within the turbulent regime) and in a riser reactor (above the acceleration zone). As final part of this work a series of desulfurization experiments have been performed for an improved iron-oxide based sorbent developed by ECN.

The basic idea is that the observed reduced contact between gas and solids is caused by segregation phenomena (due to hydrodynamical factors and inter-particle forces) leading to the formation of particle agglomerates. While the reactant gas passes through the void space between these agglomerates, embedded catalyst particles can only be reached by

mass transfer to, and diffusive transport through the agglomerates.
In risers, agglomerates or particle clusters have indeed been observed visually. As a part of this thesis, their existence has been demonstrated also on basis of hydrodynamic measurements and tracer particle experiments.

The results of CO conversion experiments have, for all considered reactor types, been interpreted by a so-called 'cluster model', which allows to estimate the size of the clusters relative to the particle diameter. Additionally, for the fluid bed experiments, the usual two-phase model has been applied as well. Herein, the influence of enhancement of the mass transfer rate from bubbles to the dense phase by the subsequent chemical reaction has been taken into account.

An important conclusion of the present work is that, for small particles, the contact efficiency in all three reactor types considered is generally much lower than expected. It has been shown that axial dispersion can hardly have any influence on the observed conversions. The contact efficiency between the reactant gas and the catalyst particles appears to be highly dependent on the local rate of the reaction used to measure it, which could be varied by the degree of catalyst dilution. In case of completely mass transfer controlled conversion for a very diluted catalyst system, transfer coefficients can be derived which appear to be of the same order of magnitude as those predicted by the Ranz-Marshall equation for a single particle. In that case the contact is restored and has become maximal again.

Obviously, the cluster size is decisive for the value of the contact efficiency. As mentioned before, the ratio of cluster over particle diameter could be evaluated by applying the cluster model. The results are summarized in the following table.

With respect to the desulfurization experiments for the sorbent developed by ECN, it has been found that the reaction rates are extremely high, especially for the fresh, unloaded

Table I. Experimental conditions and cluster sizes for various reactor types

gas velocity (m/s)	reactor type	d_p (μm)	d_{cl}/d_p (-)	applied reaction
0.3 - 0.6	fixed bed	42 - 75	7 - 18	CO oxidation
0.4 - 1.3	fluid bed	169	200 - 300	H_2S absorption
0.1 - 0.9	fluid bed	65	200 - 700	CO oxidation
2.5 - 4.5	riser	65	30 - 70	CO oxidation

sorbent material. This means that in future pilot or commercial installations the contact efficiency will certainly be a critical parameter. Besides, in a continuous desulfurization process variation in sorbent loading will occur, by which very reactive sorbent particles will be present in the reactor together with deactivated ones. This situation is similar to the CO oxidation experiments in which the active catalyst was diluted with inert material.
As an additional result, it has been shown by a number of cyclic fluid bed experiments that the ECN sorbent is sufficient strong for fluid bed application and well regenerable.

The strength of the experimental methodology applied for this thesis is that it can be applied at all scales and for the actual process conditions of desulfurization.

SAMENVATTING

Kolengas, dat geproduceerd wordt in een IGCC electriciteitscentrale, moet worden gereinigd om nadelige zijdelingse effecten, zoals beschadigingen van de gas turbine, en de uitstoot van schadelijke componenten in het milieu, te voorkomen. Deze ontzwaveling wordt meestal uitgevoerd door middel van een natte gaswassing. The totale efficiency van zo'n IGCC centrale kan echter aanmerkelijk worden verhoogd als de gasreinigingsstappen, waaronder de ontzwaveling, worden uitgevoerd bij hoge temperaturen (T>600 K), en met vaste absorbentia. IJzer-oxide, bijvoorbeeld geïmpregneerd op een inert dragermateriaal, is een geschikt sorbent gebleken voor de verwijdering van H_2S en COS. Het is mechanisch sterk en met lucht of zuurstof goed te regenereren.
Omdat de ontzwavelings- en regeneratie-reacties erg snel blijken te zijn, is het gebruik van kleine deeltjes aan te bevelen. Om het gesulfideerde materiaal ook te kunnen regenereren, moeten in een continu proces twee reactoren worden gebruikt, een absorber en een regenerator, waartussen een voortdurende stroom van sorbent materiaal wordt uitgewisseld. Het zou interessant kunnen zijn om een wervelbed-systeem te beschouwen zoals toegepast is in het FCC proces: het sorbent materiaal wordt dan gecirculeerd tussen verschillende reactoren, waaronder een riser reactor (als absorber), cyclonen, standpijpen, een (turbulente) wervelbed (als regenerator) en terugvoerlijnen.

Voor het ontwerp van de hierboven genoemde reactoren, of voor de interpretatie van experimenten met theoretische modellen, is het van belang dat de graad van contact tussen het gas (met de reactant) en de sorbentdeeltjes bekend is. Met name in het geval van gasreinigingsprocessen, zoals de ontzwaveling, moet de concentratie van het ongewenste product in een grote gasstroom zeer snel worden gereduceerd tot een extreem laag niveau, en is de contact effectiviteit een kritische factor.
Helaas is de literatuur niet eenduidig met betrekking tot het contact effectiviteiten in wervelbedden. Enerzijds is aangetoond dat in conventionele wervelbedden door de aanwezigheid van bellen de contact effectiviteit zeer laag kan zijn. Tegelijkertijd wordt aangenomen dat de uitwisseling van stof en warmte tussen het gas en de vaste stof zeer goed is in zogenaamde snelle wervelbedden.

Een belangrijke doelstelling van dit promotieproject is om de contact effectiviteit te bepalen voor kleine proefopstellingen door middel van een experimenteel onderzoek. Het gaat hierbij om fluïdisatie van fijne deeltjes over een breed gebied van gassnelheden (d_p<200 μm en 0.1<u_g<4.5 m/s). Hiervoor is een speciale meetmethode ontwikkeld, die gebaseerd is op het gebruik van de zeer snelle oxidatie-reactie van koolmonoxide over een platina-katalysator als modelreactie. Met behulp van deze reactie kan onmiddellijk worden aangetoond of de conversie bepaald wordt door de intrinsieke reactie-kinetiek of door een stofoverdrachtsweerstand. Een verandering van de snelheidsbepalende stap komt overeen met een grote verandering in de orde van de koolmonoxide; deze gaat dan van min één naar plus één.
Tevens is in dit promotieproject de techniek van de verdunning van de actieve katalysator met identieke, maar inerte deeltjes, die gebruikt zijn om de invloed van de lokale reactiesnelheid op de contact effectiviteit te onderzoeken.

De oxidatie van CO is onderzocht voor een klein gepakt bedje van kleine deeltjes om de intrinsieke reactie-kinetiek, en om de contact effectiviteit te bepalen onder verschillende condities. Daarna is de CO oxidatie-reactie toegepast in een wervelbed bij verschillende gassnelheden tot in het turbulente wervelbed-regime, en in een riser reactor boven de versnellingszone. Uiteindelijk is een serie van ontzwavelingsexperimenten uitgevoerd met

een sorbent materiaal, dat ontwikkeld is door het ECN.

Het vermoeden bestond, dat de experimenteel gevonden lage contact effectiviteit wordt veroorzaakt door segregatie, als gevolg van zowel hydrodynamische factoren als krachten tussen de deeltjes, resulterend in de vorming van deeltjes agglomeraten. Als het gas met de reactant voornamelijk door de lege ruimte tussen de agglomeraten stroomt kan de actieve katalysator alleen in contact komen met de reactant door stofoverdacht naar, en diffusie in die agglomeraten. In riser reactors zijn zulke deeltjes agglomeraten visueel waargenomen. In dit promotie-onderzoek is hun bestaan echter ook aangetoond door hydrodynamische metingen en door experimenten met tracer deeltjes.
De CO oxidatie metingen zijn voor ieder reactor type geïnterpreteerd aan de hand van een zogenaamd 'cluster model', waarmee de effectieve diameter van de agglomeraten kan worden berekend. Daarnaast zijn voor de wervelbed-experimenten de conversie metingen geïnterpreteerd met het bekende twee-fasen model, waarin de invloed van de chemische versnelling op de stofoverdrachtssnelheid van de bellen naar de emulsie-fase is meegenomen.

Een belangrijke conclusie na dit onderzoek is, dat, wanneer kleine deeltjes worden gebruikt, de contact-effectiviteit in de beschouwde reactoren veel lager is dan mag worden verwacht. Er is aangetoond dat axiale dispersie bijna geen invloed heeft op de experimentele conversie. Tevens blijkt dat de effectiviteit van het contact tussen het gas en de deeltjes zeer sterk afhankelijk te zijn van de lokale snelheid van de toegepaste reactie, en die is gevarieerd door verdunning. In het geval van een conversie-snelheid die bij zeer hoge verdunningen volledig wordt bepaald door stofoverdracht, worden stofoverdrachtscoëfficiënten afgeleid die van dezelfde orde van grootte zijn als die berekend kunnen worden met de Ranz-Marshall vergelijking. Het contact tussen het gas en de deeltjes lijkt dan weer hersteld en maximaal.

Tabel I. Experimentele condities en cluster-groottes voor verschillende reactor typen.

gassnelheid (m/s)	reactor type	d_p (μm)	d_{cl}/d_p (-)	reactiesysteem
0.3 - 0.6	gepakt bed	42 - 75	7 - 18	CO oxidatie
0.4 - 1.3	wervelbed	169	200 - 300	H_2S absorptie
0.1 - 0.9	wervelbed	65	200 - 700	CO oxidatie
2.5 - 4.5	riser	65	30 - 70	CO oxidatie

Klaarblijkelijk is de effectieve cluster-grootte, d_{cl}, bepalend voor de contact effectiviteit. Deze kunnen worden afgeschat met het cluster model. De resultaten staan vermeld in de onderstaande tabel. Uit de ontzwavelings-experimenten met het sorbent materiaal dat ontwikkeld is door het ECN zijn zeer hoge reactiesnelheden afgeleid, met name voor het verse, onbeladen materiaal. Dit betekent dat in een toekomstige pilot plant of commerciële installatie de contact effectiviteit zeker een essentiële parameter zal zijn. Daarnaast is er in een continu bedreven ontzwavelingsproces sprake van een variatie in de belading van het sorbent, waardoor zeer reactieve sorbent deeltjes in de reactor kunnen voorkomen, naast een grote hoeveelheid volledig gedeactiveerd materiaal. Deze situatie is enigzins te vergelijken met de CO oxidatie metingen, waarin de katalysator verdund is met inert materiaal.
Door middel van proeven met een cyclisch bedreven wervelbed is tenslotte aangetoond dat het ECN sorbent voldoende sterk is voor gebruik in wervelbedden en bovendien goed is te regenereren.

De beschreven methodologie kan worden toegepast in een breed scala van reactoren op

elke schaal en voor de actuele condities van de ontzwavelings-reactie.